Ministère de l'enseignement Supérieur et de la recherche Scientifique
وزارة التعليم العالي والبحث العلمي

Badji Mokhtar Annaba University
Université Badji Mokhtar – Annaba
Faculté des Sciences

Département de Chimie

جامعة باجي مختار– عنابـــة
كـليـة العلوم
قســم الكيمياء

Thèse

Pour l'obtention du diplôme de doctorat

Filière : Chimie

Spécialité : Chimie Pharmaceutique

Thème :

Étude Théorique Et Expérimentale De Nouvelles Molécules à Intérêt Pharmacologique.

Présenté par : SAYAD RAYENE

Devant le jury composé de :

Mme. MERABET-KHELASSI Mounia	Prof	Université Badji Mokhtar - Annaba	Présidente
Mme. AOUF Zineb	MCA	Université Badji Mokhtar - Annaba	Encadrante
M. BOUZINA Abdeslem	MCA	Université Badji Mokhtar - Annaba	Co-encadrant
Mme. ZERROUKI Rachida	Prof	Université de Limoges - France	Examinatrice
Mme. AMIRA Aicha	MCA	École Nationale Supérieure de Technologie et d'Ingénierie	Examinatrice
M. BOUKACHABIA Mourad	Prof	Université Badji Mokhtar - Annaba	Examinateur
M. AOUF Noureddine	Prof	Université Badji Mokhtar - Annaba	Membre invité

Année 2025

Acknowledgement

*This work was carried out within the Bioorganic Chemistry Group, part of the Laboratory of Applied Organic Chemistry (**LCOA**) at Badji Mokhtar University of Annaba.*

*I would like to express my deepest and most heartfelt gratitude to **Dr. Zineb AOUF**, PhD at Badji Mokhtar University of Annaba. You have been far more than a supervisor: a guiding light in moments of uncertainty and a reassuring presence in times of doubt. Through your endless patience, thoughtful guidance, high standards, and unwavering confidence in my abilities, I have been able to grow, thrive, and achieve goals I never thought possible. Your mentorship has left a lasting impact on me, both scientifically and personally. It is with deep respect and enduring gratitude that I dedicate a significant part of this work to you.*

*I also extend my sincere thanks to **Dr. Abdeslem BOUZINA**, PhD at Badji Mokhtar University of Annaba, for his valuable co-supervision throughout this thesis. His scientific rigor, expertise, and insightful guidance greatly enriched my academic journey. His continuous support, availability, and kindness were essential sources of motivation and confidence in the face of challenges. Working alongside him was a formative and intellectually stimulating experience that significantly enhanced the quality of this research. I am deeply grateful for his involvement and dedication.*

*I am profoundly grateful to **Prof. Nour-Eddine AOUF**, former head of our research team at Badji Mokhtar University of Annaba. He was much more than a teacher to me: a paternal figure, always present, supportive, and attentive, even during the most critical stages of my academic journey. His trust, generosity, and wealth of guidance have profoundly shaped both my academic and personal development. His retirement marks the end of an era, but his legacy continues to live on in each of his students. I offer him my deepest respect and enduring gratitude.*

I am deeply grateful to all members of the jury for the valuable time they devoted to carefully reviewing this work.

*I would like to thank **Prof. Mounia MERABET-KHELASSI** from Badji Mokhtar University of Annaba for the honor she did me by agreeing to preside over the jury of this thesis.*

*My sincere gratitude also goes to **Prof. Mourad BOUKACHABIA**, who is, for me, a leading figure in organic chemistry at Badji Mokhtar University of Annaba. I sincerely thank him for honoring this work through his expertise and engagement as an examiner of this thesis. I*

*would also like to thank **Dr. Aïcha AMIRA**, from the National Higher School of Technology and Engineering **(ENSTI)**, for the honor of participating in the evaluation of this research, and for her valuable support, insightful advice, and continuous guidance in the laboratory, which were instrumental in the progress of my work.*

*I would also like to extend my sincere thanks to **Prof. Rachida ZERROUKI** of the University of Limoges, for giving me the opportunity to join her laboratory during my internship. Her scientific rigor, methodological precision, and attentive supervision were instrumental in enriching my academic journey. I greatly benefited from her expertise and insightful advice, which had a lasting impact on my professional development. Her participation in the jury of this thesis is a great honor, and I express my deep gratitude for her commitment.*

*My sincere thanks go to **Prof. Malika BERREDJEM** for welcoming me to the Laboratory of Applied Organic Chemistry, as well as for her constant availability and the high-quality scientific guidance that greatly contributed to the successful completion of my research.*

*I am also grateful to **Prof. Malika IBRAHIM-OUALI** of Aix-Marseille University for her valuable contribution to the crystallographic characterization, and to **Dr. Chahrazed BENZAID** of Badji Mokhtar University of Annaba for her support with the biological evaluation of the synthesized compounds.*

*I express my profound gratitude to **Prof. Jamil KRAIEM**, Head of the Laboratory for Drug Development (LR12ES09) at the Faculty of Pharmacy of Monastir, University of Monastir (Tunisia), for welcoming me into his laboratory and for the high-quality scientific supervision I received throughout my stay. His expertise and the resources provided greatly contributed to the advancement of my research work.*

*I would like to warmly thank all the PhD students **(Houda, Amina, Yousra, Zineb, Ons, Hanen, Ons)** from the Laboratory **(LR12ES09)** at the Faculty of Pharmacy of Monastir for their valuable assistance, insightful advice, and constant positive spirit throughout my internship.*

*I also extend my gratitude to **Hamza Abbassi**, a PhD student at the University of Limoges, for his availability and support during this experience.*

*I sincerely thank all members of the Laboratory of Applied Organic Chemistry **(LCOA)** as well as everyone who contributed, directly or indirectly, to the completion of this work. Their support has been invaluable to my scientific journey.*

Dedication

***First and foremost**, praise be to Allah, Lord of the worlds. By His grace and generosity, this thesis has been accomplished. With His help and the trust, I placed in Him, I was able to overcome difficulties and face challenges.*

***To my mother**, the pillar of my life, whose unwavering love and support guided me every step of the way. Her wisdom and kindness have been a constant source of strength and comfort, illuminating my path and nurturing my confidence. Her dedication was essential to the success of this journey.*

***To my father**, a man of patience and courage, whose reassuring presence and steadfast support provided a precious refuge during difficult times.*

Whose prayers, sacrifices, and unconditional love have supported me throughout my journey. No words can fully express my deep gratitude, respect, and love for you.

***To my sister Imene**, my best friend, my eternal confidante, my other half, and my pride, who has always stood by my side, never ceasing to support and encourage me. No words can fully convey my heartfelt appreciation for you.*

***To my little brother Mohamed,** my hero and essential guide, for his constant support and encouragement. May God bless you, protect you from all harm, and grant you luck and happiness.*

***To my maternal grandmother,** an admirable woman and a constant source of motivation, who has always been an example of strength and determination, May God grant her a long, happy, and healthy life.*

***To my brother Zakaria, to my uncles, aunts, cousins, and all my family**, I express my deepest gratitude and affection for their support, invaluable help, no words can fully reflect the depth of my feelings for you.*

***To a dear person** whose constant support and precious encouragement have been a guiding light throughout these years. Their presence by my side was a solid pillar in moments of weakness and an inexhaustible source of strength and inspiration throughout my journey.*

***To my best friend Yousra**, who has always supported me both scientifically and personally. Her faithful presence in the laboratory and in life has been a precious source of encouragement and friendship throughout this journey.*

***To my labmates and dear friends, Dounia, Achraf, Meriem**, **Amira**, **Ouafa**, **Chaima, Racha, Rayenne, Rania**, with whom I shared the most beautiful moments of my PhD.*

Abstract

This thesis work encompasses three main research axes, focusing on the synthesis of pharmacologically relevant molecules by combining classical methodologies with approaches inspired by the principles of green chemistry.

Initially, our efforts were directed focused on the development of oxygen and phosphorus-containing heterocyclic systems, including xanthene derivatives synthesized *via* an innovative ultrasound-assisted method, as well as 1,2-oxaphospholane-2-oxides obtained under microwave activation. These environmentally friendly processes, conducted under mild conditions, enabled the efficient and high-yield synthesis of the target compounds.

In parallel, a series of carbamate analogues of nitrosourea-based compounds, particularly carmustine derivatives, were synthesized using conventional methods, with the aim of reducing their toxicity while enhancing their bioactive profile and therapeutic potential.

The *in vitro* evaluation of the synthesized compounds, namely the *N*-(2-chloroethyl) carbamate and 1,2-oxaphospholane-2-oxide derivatives, revealed noteworthy pharmacological potential. Some compounds exhibited promising antibacterial activity, highlighting their relevance as potential anti-infective agents. Furthermore, antioxidant activity assessed via the DPPH assay demonstrated a structure-dependent behaviour: the *N*-(2-chloroethyl) carbamate derivatives, in general, showed superior free radical scavenging capacity, with some being comparable in efficacy to ascorbic acid.

Structural elucidation of the synthesized compounds was thoroughly performed using a range of spectroscopic techniques NMR (^{1}H, ^{13}C, ^{31}P), IR, and LC-MS as well as X-ray crystallographic analysis on derivatives III.8a and III.3h, allowing for precise and detailed structural determination.

Finally, an *in-silico* study was carried out, combining molecular docking simulations, DFT calculations, and ADME property predictions to assess the electronic characteristics and pharmacokinetic profiles of the investigated compounds.

Keywords: Xanthene, 1,2-oxaphospholane-2-oxide, *N*-(2-chloroethyl) (nitroso)carbamate, Biological evaluation, Ultrasound and microwave irradiations, *in silico* study.

Résumé

Ce travail de thèse s'articule autour de trois axes de recherche principaux**,** centrés sur la synthèse de molécules d'intérêt pharmacologique, en combinant des méthodologies classiques et des approches inspirées des principes de la chimie verte.

Dans un premier temps, notre attention s'est portée sur l'élaboration de systèmes hétérocycliques oxygénés et phosphorés, comprenant des dérivés du xanthène obtenus par une méthode innovante assistée par ultrasons, ainsi que des 1,2-oxaphospholane-2-oxydes préparés sous irradiation micro-ondes. Ces procédés, menés dans des conditions douces et respectueuses de l'environnement, ont permis d'obtenir les produits attendus avec de bons rendements.

Parallèlement, une série d'analogues carbamates de composés nitroso-urées, notamment dérivés de la carmustine, a été développée à l'aide de protocoles synthétiques conventionnels, dans l'objectif de réduire leur toxicité tout en optimisant leur profil bioactif et leur potentiel thérapeutique.

L'évaluation *in vitro* des composés issus des deux séries étudiées les dérivés *N*-(2-chloroéthyl) carbamate et 1,2-oxaphospholane-2-oxyde a mis en évidence un potentiel pharmacologique notable. Certains composés ont révélé une activité antibactérienne prometteuse, suggérant leur intérêt en tant qu'agents anti-infectieux. En parallèle, l'activité antioxydante, évaluée par le test DPPH, a montré une dépendance à la structure moléculaire : les dérivés *N*-(2-chloroéthyl) carbamate se sont globalement distingués par une capacité de piégeage des radicaux libres supérieure, certains affichant une efficacité comparable à celle de l'acide ascorbique.

L'élucidation structurale des composés synthétisés a été rigoureusement assurée par diverses techniques spectroscopiques RMN (^{1}H, ^{13}C, ^{31}P), IR, spectrométrie de masse (LC-MS) ainsi que par une analyse cristallographique en diffraction des rayons X, réalisée sur les dérivés **III.8a** et **III.3h**, permettant une détermination précise et approfondie de leur structure moléculaire.

Enfin, une étude *in silico* a été menée, intégrant des simulations de docking moléculaire, des calculs DFT et la prédiction des propriétés ADME, afin d'évaluer les caractéristiques électroniques et pharmacocinétiques des composés étudiés.

Mots clés : Xanthène, 1,2-oxaphospholane-2-oxyde, *N*-(2-chloroethyl)(nitroso)carbamate, Évaluation biologique, Irradiations par ultrasons et micro-ondes, Étude *in silico*

الملخص

يرتكز هذا العمل البحثي على ثلاثة محاور رئيسية، تهدف إلى تحضير مركبات ذات قيمة علاجية واعدة، وذلك من خلال الجمع بين المناهج التقليدية والأساليب المستوحاة من مبادئ الكيمياء الخضراء.

في المرحلة الأولى، تركّز العمل على تطوير أنظمة حلقية غير متجانسة تحتوي على عنصري الأكسجين والفوسفور، من بينها مشتقات الزانثين التي تم تحضيرها باستخدام طريقة مبتكرة بمساعدة الموجات فوق الصوتية، بالإضافة إلى مركبات 1،2-أوكسافوسفولان-2-أوكسيد المحضّرة تحت تأثير الموجات الدقيقة (الميكروويف). وقد أتاحت هذه الأساليب، التي تعتمد شروطًا تفاعلية معتدلة وصديقة للبيئة، إنتاج المركبات المنشودة بمردودات جيدة.

وفي محور موازٍ، تم تطوير سلسلة من مركبات النيتروزوكاربامات، نظائر النيتروزويوريا، خصوصًا مشتقات الكارموستين، باستخدام بروتوكولات تركيبية تقليدية، وذلك بهدف تقليل سميتها وتحسين خصائصها البيولوجية وإمكاناتها العلاجية.

كشفت التقييمات المخبرية (*in vitro*) للمركبات المحضّرة من السلسلتين، أي مشتقات *N*-(2- كلوروإيثيل) كاربامات و1،2-أوكسافوسفولان-2-أوكسيد، عن نشاط دوائي ملحوظ. حيث أظهر عدد من المركبات فعالية مضادة للبكتيريا، مما يدل على إمكانيتها المحتملة كمضادات للعدوى. وفي الوقت نفسه، أظهر اختبار النشاط المضاد للأكسدة باستخدام طريقة DPPH اختلافًا مرتبطًا بالبنية الجزيئية: حيث تميّزت مشتقات *N*-(2-كلوروإيثيل) كاربامات بقدرة عالية على تثبيط الجذور الحرة، وقد أبدى بعضها فعالية مماثلة لحمض الأسكوربيك.

تمت دراسة البنية الجزيئية للمركبات المحضّرة بدقة باستخدام تقنيات طيفية متعددة، مثل الرنين المغناطيسي النووي (H^1، C^{13}، P^{31})، والأشعة تحت الحمراء، ومطيافية الكتلة (LC-MS) ، بالإضافة إلى التحليل البلوري بالأشعة السينية للمشتقات III.8a و III.3h، مما سمح بتحديد دقيق ومتكامل لبنيتها الجزيئية.

أُجريت في نهاية المطاف دراسة حاسوبية شاملة (*in silico*)، تضمنت محاكاة الالتحام الجزيئي(docking) ، وحسابات نظرية الكثافة الإلكترونية (DFT)، والتنبؤ بخواص الامتصاص والتوزيع والتمثيل الحيوي والإطراح (ADME) ، بهدف تقييم الخصائص الإلكترونية والحركية العلاجية للمركبات المدروسة.

الكلمات المفتاحية :الزانثين، 1،2-أوكسافوسفولان-2-أوكسيد، -*N*-(2-كلوروإيثيل)نتروزوكاربامات، التقييم البيولوجي ، التنشيط بالأمواج فوق الصوتية والميكروويف ، دراسة حاسوبية.

Table of contents

List of abbreviations

✓ **Chemicals, reagents, and solvents**

Ac	Acetyl.
CAN	Acetonitrile.
ACNU	1-(4-amino-2-methyl-5-pyrimidinyl) methyl-3-(2-chloroethyl)-1-nitrosourea, nimustine.
AK10	Amikacin.
AM-B	Amphotericin B.
AMC30	Amoxicillin-clavulanic acid.
Ar	Aromatic.
BCNU	1,3-bis(2-chloroethyl)-1-nitrosourea, carmustine.
BGCNU	*N*-(2-chloroethyl)-*N′*-2-(O6-benzyl-9-guanine)ethyl-N-nitrosourea
[Bmim][HSO_4]	1-Butyl-3-methylimidazolium hydrogen sulfate.
Bu	Butyl.
CAN	Ceric ammonium nitrate.
CCNU	1-(2-chloroethyl)-3-cyclohexyl-1-nitrosourea, lomustine.
ccPA	Carbocyclic phosphatidic acid.
CENC	Chloroethylnitrosocarbamates.
CENS	2-Chloroethylnitrososulfamides.
CENUs	Chloroethylnitrosoureas.
CEUs	*N*-aryl-*N′*-(2-chloroethyl)ureas.
CSI	Chlorosulfonyl isocyanate.
DABCO	1,4-diazabicyclo[2.2.2]octane.
DCC	Dicyclohexylcarbodiimide.
DCM	Dichloromethane.
DIAD	Diisopropyl azodicarboxylate.
DMF	Dimethylformamide.
DMSO	Dimethyl sulfoxide.
DPPH	2,2-diphenyl-1-picrylhydrazyl.
EtOH	Ethanol.
Fe^{3+}-MT	Fe^{3+}-montmorillonite.

[Hmim]TFA	1-methylimidazolium trifluoroacetate.
Me	Methyl.
MeOH	Methanol.
MNNG	1-methyl-2-nitro-1-nitrosoguanidine.
MNU	1-methyl-1-nitrosourea.
NBS	*N*-bromosuccinimide.
NDEA	*N*,*N*-diethylnitrous amide.
NDMA	*N*,*N*-dimethylnitrous amide.
[NMP]H_2PO_4	N-methyl-2-pyrrolidone phosphoric acid.
O^6-BG	O^6-Benzylguanine.
PANI	Polyaniline.
Ph	Phenyl.
PMA	Phosphomolybdic acid.
PPA	Polyphosphoric acid.
PPh_3	Triphenylphosphine.
***p*-TSA**	*Para*-Toluenesulfonic acid.
STZ	Streptozotocin.
TBAHS	Tetrabutylammonium hydrogen sulfate.
TBN	*Tert*-butyl nitrite.
TEA	Triethylamine.
TFA	Trifluoroacetic acid.
THF	Tetrahydrofuran.
[TMPSA]HSO_4	N, N, N-trimethyl-N-propanesulfonic acid ammonium hydrogen sulfate.
TMS	Tetramethylsilane.
TMSBr	Bromotrimethylsilane.
TNUs	nitrosoureas containing tyrosine derivatives.
TsOH	Toluenesulfonic acid.
$Zn(OAc)_2$	Zinc acetate.

✓ **<u>Other abbreviations</u>**

*****	Asymmetric carbon.
ADME	Absorption, Distribution, Metabolism and Excretion.
AGT	O^6-alkylguanine-DNA alkyltransferase.
AMP	Adenosine monophosphate.

AMPK	AMP-activated protein kinase.
BBB	Blood-Brain Barrier.
CCD	Charge-coupled device.
CCDC	Cambridge Crystallographic Data Centre.
CCR1	C-C chemokine receptor type 1.
CI	Chemical ionization.
CV	Crystal violet.
d	doublet.
dd	doublet of doublets.
DEPT	Distortionless Enhancement by Polarization Transfer.
DHPS	Dihydropteroate synthase.
DLS	Drug likeness score.
DNA	Deoxyribonucle$_{ic}$ acid.
DFT	Density Functional Theory.
EC_{50}	Half maximal effective concentration.
EMC	Encephalomyocarditis.
eq	Equivalent.
ESI	Electrospray Ionization.
FDA	Food and Drug Administration.
FLEX	Flexibility.
FMOs	Frontier Molecular Orbitals.
FT-IR	Fourier Transform Infrared spectroscopy.
GI	Gastrointestinal.
HIV	Human immunodeficiency virus.
HMPA	Hexamethylphosphoramide.
HMQC	Heteronuclear Multiple Quantum Coherence.
HOMO	Highest Occupied Molecular Orbital.
IC_{50}	Half maximal inhibitory concentration.
ID	Identifier.
INSATU	Insaturation.
INSOLU	Insolubility.
IR	Infrared.
IZD	Inhibitory zone diameter.

J	Coupling constant.
LIPO	Lipophilicity.
LUMO	Lowest Unoccupied Molecular Orbital.
m/z	Mass-to-charge ratio.
M	Molecular weight.
m	multiplet.
MEP	Molecular electrostatic potential.
MGMT	O^6-methylguanine-DNA methyltransferase.
MICs	Minimum inhibitory concentrations.
MIP-1α	Macrophage Inflammatory Protein-1 alpha.
MW	Microwave.
NCCSC	National Cancer Chemotherapy Service Center.
NCDs	Non-communicable diseases
NCI	National Cancer Institute.
NMR	Nuclear magnetic resonance.
no.	Number.
OD	Optical density.
ORTEP	Oak Ridge Thermal Ellipsoid Plot Program.
PDB	Protein Data Band.
pH	Potential of hydrogen.
POLAR	Polarity.
q	quartet.
R	Resistance.
RCSB	Research Collaboratory for Structural Bioinformatics.
Ref	Reference.
R_f	Retention Factor.
Rint	Independent reflections.
RMSD	Root Mean Square Deviation.
RNA	Ribonucleic acid.
rt	Room temperature.
s	singlet.
SAR	Structure–activity relationship.
SP	Standard precision.

SRI	Southern Research Institute.
t	triplet.
TLC	Thin Layer Chromatography.
TPSA	Topological polar surface area.
TR	Trypanothione reductase.
US	Ultrasound.
uHPLC/MS	Ultra-high performance liquid chromatography–mass spectrometry.
UV	Ultra-violet.
VEGFR-2	Vascular Endothelial Growth Factor Receptor 2.
XRD	X Ray Diffraction.
δ	Chemical shift.
λ	Wavelength.

Units

%	Percent.
°	Degrees.
°C	Degrees Celsius.
µL	Microliters.
Å	Angstrom.
cm	Centimeters.
D	Debye.
Da	Dalton.
eV	Electronvolts.
g	Grams.
h	Hours.
Hz	Hertz.
K	Kelvin.
kcal	Kilocalories.
kg	Kilograms.
kHz	Kilohertz.
mg	Milligrams.
min	Minutes.
mL	Milliliters.

mm	Millimeters.
mM	Millimolar.
mmol	Millimoles.
mol	Moles.
N	Normal.
nm	Nanometers.
nM	Nanomolar.
ppm	parts per million.
s	Seconds.
W	Watt.
µg	Micrograms.
µm	Micrometers.
µM	Micromolar.Isobutyl

List of schemes

Chapter I Overview on heterocyclic compounds

Chapter II Overview on *N*-nitroso compounds

Chapter III Results and discussion

List of figures

Introduction

Chapter I Overview on heterocyclic compounds

Chapter II Overview on *N*-nitroso compounds

Chapter III Results and discussion

Chapter IV *In vitro* and *in silico* studies of synthesized

Conclusion

List of tables

Chapter III Results and discussion

Chapter IV *In vitro* and *in silico* studies of synthesized

Chapitre V Experimental data

Introduction

Research in chemistry and medicine is continuously evolving, driven by the need to develop new bioactive molecules capable of addressing the emergence of complex diseases and the growing resistance to existing treatments.**[1]** This ongoing pursuit relies heavily on heterocyclic chemistry, a fundamental area of organic chemistry owing to the ubiquitous presence of heterocycles in biological systems and their crucial role in pharmacology and industry.**[2]**

Among these structures, oxygenated heterocycles stand out for their structural diversity and broad applications, making them a key focus in the development of novel synthetic strategies. Numerous approaches have been developed to optimize their accessibility and explore their therapeutic potential.**[3]** In parallel, phosphorus-containing compounds have gained significant attention due to their unique chemical and biological properties, as well as the synthetic challenges they present.**[4]** The incorporation of phosphorus atoms into oxygenated heterocycles offers promising new avenues, particularly for enhancing their pharmacological profiles and developing innovative therapeutic candidates.**[5]**

One of the most prominent oxygenated heterocyclic frameworks is the xanthene core, which, due to the presence of an oxygen atom within its conjugated tricyclic structure, facilitates extensive electron delocalization. This characteristic endows xanthenes with remarkable chemical stability and optoelectronic properties, making them valuable in various scientific domains.**[6]** The structural diversity of xanthene derivatives arises from the numerous substitution possibilities at both aromatic and heterocyclic positions, allowing for the synthesis of a wide range of functionalized compounds. This chemical versatility establishes xanthenes as key scaffolds in medicinal chemistry, where they exhibit a broad spectrum of biological activities, including antitumor **(0.1)**, **[7]** antimicrobial **(0.2)**, **[8]** and antioxidant **(0.3)** properties. **[9]** As a result, the xanthene core serves as a versatile pharmacophore, providing a robust structural framework for designing new bioactive molecules with optimized therapeutic properties, thus reinforcing its crucial role in the development of innovative therapeutic entities.**[10]**

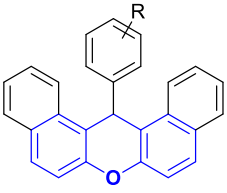

(0.1)

Antitumor agent

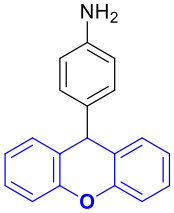

(0.2)

Antimicrobial agent

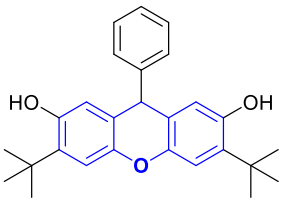

(0.3)

Atioxidant agent

Figure 0.1. Structure of biologically active xanthene-containing compounds.

Another heterocyclic system of interest is the 1,2-oxaphospholane-2-oxide core, a five-membered framework that incorporates both oxygen and phosphorus atoms. These compounds have garnered growing interest due to their unique chemical properties and structural versatility, making them promising candidates for various scientific applications, particularly in the design of novel therapeutic agents. **[11]** Numerous studies have highlighted their remarkable biologically activities, including anti-inflammatory **(0.4), [12]** and antitumor **(0.5)** effects, **[13]** further supporting their potential in the development of innovative bioactive molecules.

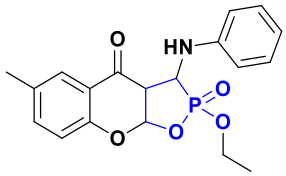

(0.4)

Anti-inflammatory agent

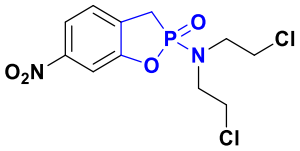

(0.5)

Antitumor agent

Figure 0.2. Structures of biological active 1,2-oxaphospholane-2-oxide derivatives.

On the other hand, non-communicable diseases **(NCDs)** currently pose a major global health challenge, accounting for over 70% of deaths worldwide.**[14]** Among them, cancer is particularly notable due to its high complexity, arising from the progressive transformation of healthy cells into malignant ones under the influence of genetic and environmental factors. Various agents, such as tobacco, alcohol, radiation, and certain chemical substances,**[15]** can disrupt cellular regulatory mechanisms, leading to tumor development. To combat this disease, several therapeutic strategies are employed, including surgery, radiotherapy, and chemotherapy.**[16]**

Among chemotherapeutic agents, nitrosoureas, particularly chloroethylnitrosoureas **(CENUs)**, are widely used due to their ability to induce irreversible DNA damage, thereby blocking cell replication and triggering cancer cell death.**[17]** However, their clinical application is significantly limited by severe hematological toxicity and the release of isocyanates, which contribute to additional adverse effects. To address these limitations, research has focused on designing novel analogues that retain the cytotoxic efficacy of CENUs while minimizing their toxicity.**[18]** In this context, our work aims to synthesize and evaluate new *N*-nitrosocarbamate analogues, structurally inspired by Carmustine, with the goal of optimizing their therapeutic potential.

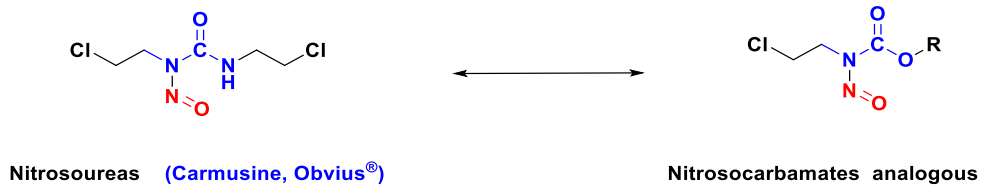

Figure 0.3. Structures of synthesized analogues of carmustine.

This thesis is structured into five chapters, exploring both the development of efficient synthetic protocols and the study of the properties of the synthesized compounds. It highlights the design of novel xanthene derivatives, oxaphospholane-based compounds, and carbamate analogues of Carmustine, while evaluating their potential in medicinal chemistry. Each chapter provides a significant contribution to this research, from the bibliographic study to the experimental and theoretical evaluation of the synthesized compounds.

The first chapter presents a comprehensive literature review on oxygenated heterocycles, with a particular focus on xanthenes and oxaphospholanes. It begins by examining the main synthetic strategies reported in the literature, emphasizing methodological advancements that enable efficient access to these structures. Their significance in organic and medicinal chemistry is also highlighted, particularly in relation to their biological activity. This bibliographic study lays the groundwork for the subsequent research, offering a broad perspective on these heterocyclic systems and their implications.

Chapter II is dedicated to a literature review on *N*-nitroso compounds, emphasizing their synthetic methodologies and applications. Special attention is given to nitrosoureas and their nitrosocarbamate analogues, which have been extensively studied for their anticancer properties and their application in chemotherapy, particularly for the treatment of brain tumors and leukemias. The key synthetic strategies reported in the literature are analyzed, showcasing the methodological advancements that have facilitated access to these structures. This study aligns with the objective of developing novel carbamate analogues of Carmustine, aiming to enhance their therapeutic activity and pharmacological profile while reducing their toxicity.

The third chapter presents and analyzes the experimental results obtained throughout this research. It focuses on the synthesis of three series of compounds: xanthene derivatives, oxaphospholanes, and novel carbamate analogues of Carmustine. The optimization of synthetic protocols is detailed, highlighting the most suitable reaction conditions. The structural characterization of the final products is carried out using various spectroscopic and spectrometric techniques, including **IR, ^{1}H NMR, ^{13}C NMR, ^{31}P NMR, ^{19}F NMR,** and **LC-**

MS. Additionally, X-ray diffraction **(XRD)** crystallographic analysis is conducted for selected compounds to confirm their structures. This chapter provides an in-depth analysis of the implemented strategies and obtained results, forming a solid foundation for the evaluation of the properties of the synthesized compounds.

In the fourth chapter, an *in-silico* study of the synthesized compounds is presented, particularly through molecular docking, which will highlight key interactions between the active compounds and the binding sites of target enzymes. Furthermore, a density functional theory (DFT)-based study will provide additional insights into the structural properties of the investigated compounds. Pharmacokinetic properties can also be predicted using the SwissADME online server.

Complementary *in vitro* assays are conducted to evaluate the antioxidant and antibacterial activity of the synthesized oxaphospholanes and chloroethylcarbamates. A comparative analysis between *in vitro* and *in silico* results is carried out using molecular docking studies to predict the binding mode of these compounds with the respective target enzymes involved in antioxidant and antibacterial mechanisms of action.

The final chapter is dedicated to a detailed description of the experimental protocols implemented for the synthesis of the target compounds, as well as their structural characterization. All relevant information regarding reagents, materials, and reaction conditions is specified. General procedures for obtaining each series of compounds are presented, along with the physicochemical, spectroscopic, and crystallographic data of the obtained products.

Chapter I

Overview on heterocyclic compounds

1. Chemistry of heterocyclic compounds

Heterocyclic compounds represent a major class of organic compounds, characterized by the presence of at least one heteroatom (such as nitrogen, oxygen, sulfur or phosphorus) integrated within a carbon ring. **[19]** Their widespread occurrence in biological systems, along with their significance in various industrial **[20]** and pharmaceutical applications, **[21]** makes them a key area of study in organic chemistry **(Figure I.1).[22]**

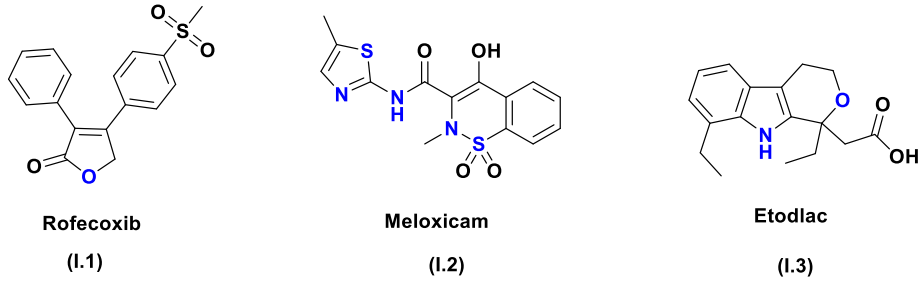

Figure I.1. Heterocyclic drug compounds

The study of heterocyclic compounds spans more than two centuries, paralleling the advancements in organic chemistry. Foundational discoveries include the isolation of alloxan **(I.4)** from uric acid in 1818 by Brugnatelli **[23]** and the production of furfural **(I.5)** in 1832 by Döbereiner. **[24]** More recently, Chargaff's work in 1951 highlighted the importance of purine **(I.6)** and pyrimidine **(I.7) bases** in DNA, emphasizing the essential role of heterocycles in biological systems **(Figure I.2)**. **[25]**

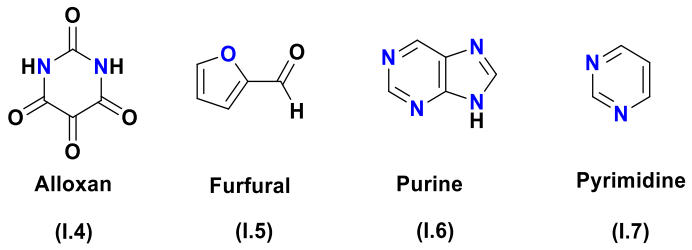

Figure I.2. Historical development of key heterocyclic compounds in organic chemistry

Heterocyclic compounds play a central role in the development of therapeutic agents. They serve as the backbone of numerous bioactive molecules found in essential structures such as DNA, RNA, hemoglobin, and chlorophyll. **[26]** Their pharmacological properties are extensive, including antifungal **(I.8)**, **[27]** anti-inflammatory **(I.9)**, **[28]** antibacterial **(I.10)**, **[29]** anticonvulsant **(I.11) [30]** and anticancer activities **(I.12) (Figure I.3)**. **[31]**

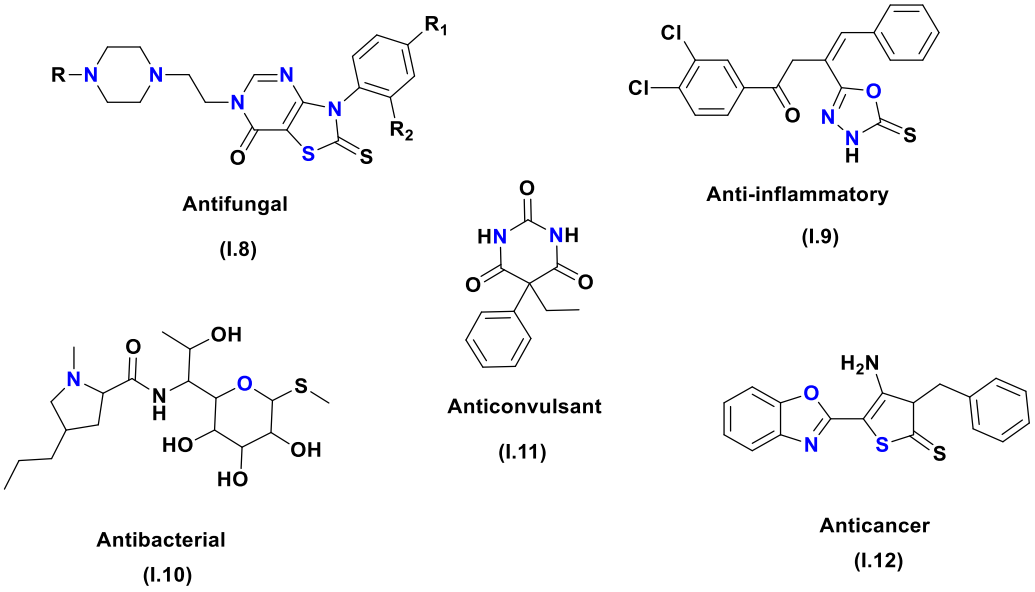

Figure I.3. Structures of pharmacologically active heterocyclic compounds

The classification of heterocyclic compounds is based on the nature and number of heteroatoms present within the ring. **[32]** The most common structures include five- and six-membered heterocycles, such as pyrrole **(I.13)**, furan **(I.14)**, and thiophene **(I.15)**, each containing a single heteroatom. More complex structures, including morpholine **(I.16)** and thiazole **(I.17)**, are essential in medicinal chemistry **(Figure I.4)**. **[33]**

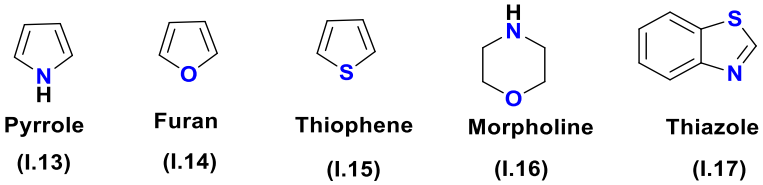

Figure I.4. Examples of heterocyclic compounds classified by ring structure and heteroatoms

Various strategies are employed in the synthesis of heterocyclic compounds, depending on the ring's characteristics and intended applications. The most common methods include intramolecular cyclization of functionalized precursors, condensation of bifunctional compounds, and the use of specific catalysts to facilitate ring formation. **[34]** Furthermore, recent advancements in green chemistry have encouraged the development of environmentally friendly processes, such as microwave irradiation or aqueous-phase chemistry, reducing the ecological impact of heterocyclic synthesis. **[35]**

Heterocycles are characterized by their chemical reactivity, which directly results from the presence of heteroatoms that influence their electronegativity and behavior in chemical reactions. **[36]** Aromatic heterocycles, such as pyridine and indole, exhibit electronic stability, making them particularly valuable in organic synthesis. **[37]** In contrast, saturated

heterocycles are more reactive and are often used in chemical transformations to produce new bioactive molecules. **[38]**

Beyond the pharmaceutical field, heterocyclic compounds have widespread applications. They play a key role in the agrochemical industry, particularly in the development of pesticides **(I.18)**, **[39]** herbicides **(I.19)**, and fungicides **(I.20)**. **[40]** They are also used in the manufacture of dyes, polymeric materials, antioxidants, and corrosion inhibitors **(I.21)**. **[41]** Due to their remarkable chemical versatility, they meet the specific needs of various industrial sectors, explaining the ongoing interest of researchers in their study and development. **(Figure I.5)**

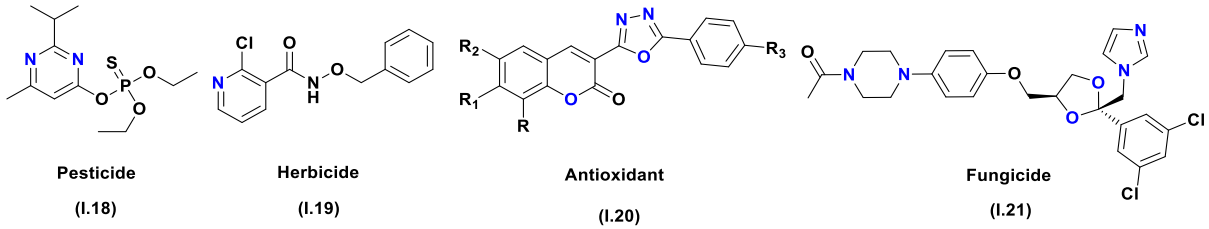

Figure I.5. Structures of heterocyclic compounds used in the agrochemical industry

1.1. Classification of heterocyclic compounds

Heterocyclic compounds are cyclic structures that incorporate at least one heteroatom, such as nitrogen, oxygen, sulfur, or phosphorus within their framework. **[42]** Their structural diversity allows them to be classified according to several criteria, primarily based on the heteroatoms they contain. These include ***N*-heterocycles** (containing nitrogen), ***O*-heterocycles** (containing oxygen), ***S*-heterocycles** (containing sulfur), as well as hybrid systems such as ***N, O*-heterocycles**, ***N, S*-heterocycles**, and ***O, P*-heterocycles**. Additionally, heterocycles can be classified based on their ring size, with distinct categories for saturated and unsaturated heterocycles. **[43]**

Oxygen-containing heterocycles represent a fundamental class of compounds in organic and medicinal chemistry due to their presence in numerous essential biomolecules. **[44]** They are found in sugars **(I.22)**, nucleosides **(I.23)**,**[45]** where their structural features directly influence biological activity and molecular interactions. **(Figure I.6)**

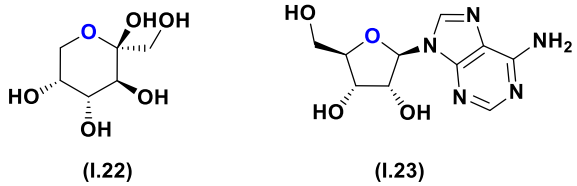

Figure I.6. Structures of biomolecules based on *O*-heterocyclic rings

In this context, this chapter focuses on two specific classes of *O*-heterocycles: xanthenes and oxaphospholanes. These compounds have attracted considerable interest due to their promising medicinal applications, particularly their pharmacological properties. Exploring their various synthetic pathways and investigating the reactivity of selected derivatives will provide valuable insights into their potential as structural frameworks for the development of new bioactive molecules.

2. Overview of *O*-heterocyclic compounds

The chemistry of oxygen-containing heterocycles has advanced significantly due to the unique properties imparted by these structural motifs when incorporated into organic and pharmaceutical compounds, including solvents **(e.g., tetrahydrofuran) (I.24)** and flavoring agents **(lactones) (I.25, I.26) (Figure I.7)**. **[46]**

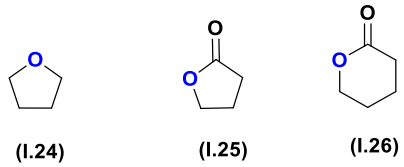

Figure I.7. Structures of organic compounds based on *O*-heterocyclic rings

Many natural and semi-synthetic oxygen containing heterocycles have emerged as promising therapeutic agents. Notable examples include Taxol (anticancer) **(I.27)**, **[47]** Digoxin (used in heart failure treatment) **(I.28)**, **[48]** and Lovastatin (hypolipidemic) **(I.29)**, **[49]** all of which are well recognized for their medical applications **(Figure I.8)**.

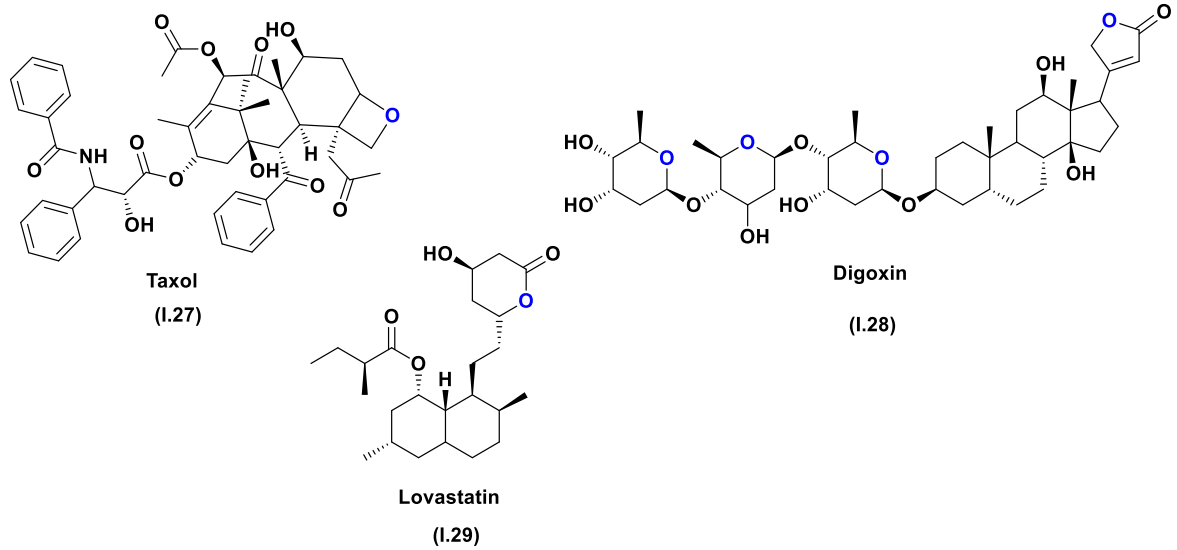

Figure I.8. Structure of natural and semi-synthetic *O*-heterocycle as therapeutic agents.

The presence of oxygen within a heterocyclic system profoundly influences its physicochemical and biological properties. **[50]** Fusion with aromatic rings alters the electronic density of the system, affecting its reactivity and requiring tailored synthetic

strategies. **[51]** Specifically, oxygen substitution in an aromatic ring induces an electron-donating effect in five-membered rings, whereas it exerts an electron-withdrawing effect in six-membered rings. These electronic variations modulate nucleophilic reactivity and govern the balance between addition and substitution reactions. **[52]**

2.1. Classifications of *O*-heterocyclic compounds

Oxygen heterocycles exhibit structural diversity that directly affects their chemical behavior. Their classification is based on several criteria, including the number of oxygen atoms, the degree of saturation, and aromaticity, all of which are closely linked to their reactivity. **[53]** Saturated heterocycles, being more reactive than their stabilized aromatic counterparts, undergo transformations influenced by interactions between oxygen and the molecular framework. **[54]** Likewise, non-aromatic heterocycles often resemble their acyclic analogues in reactivity, though some, such as oxirane and oxetane, display high reactivity due to ring strain. Among the various classes of oxygen-containing heterocycles, pyrans hold a central position due to their role in the synthesis of numerous bioactive molecules, such as pheromones and natural pigments. **[55]** These structures serve as key scaffolds in the development of compounds exhibiting a broad spectrum of pharmacological activities, including HIV protease inhibition **(I.30)**, **[56]** antifungal **(I.31)**, **[57]** anticonvulsant **(I.32)**, **[58]** antimicrobial **(I.33)**, **[59]** and antitumoral activity **(I.34) (Figure I.9)**. **[60]**

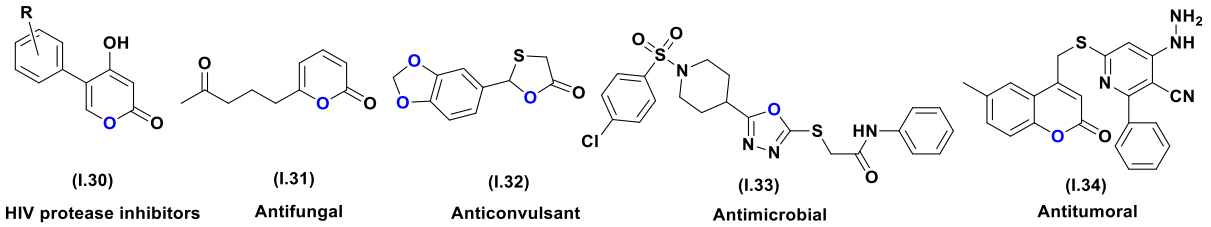

Figure I.9. Structures of bioactive *O*-heterocyclic compounds

The pyran ring is also a predominant structural motif in numerous natural products, including xanthenes, coumarins, and flavonoids, **[61]** which are recognized for their biological properties and significance in medicinal chemistry. Among these derivatives, 9H-dibenzopyrans, commonly referred to as xanthenes, **[62]** represent a distinct class of tricyclic heterocycles that incorporate an oxygen atom within their carbon framework. **[63]** These structures are found in both natural products and synthetic compounds with diverse applications, particularly as pharmacological agents and fluorescent probes. **[64]**

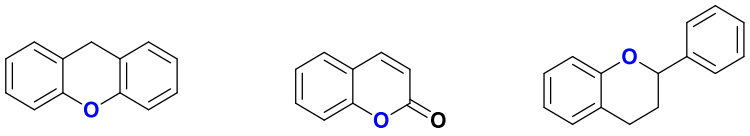

(I.35) (I.36) (I.37)

Figure I.10. Structure of natural products containing a pyran ring

In recent decades, xanthene derivatives have attracted increasing interest in organic and medicinal chemistry due to their unique reactivity and wide range of therapeutic applications. **[65]**

2.2. Chemistry of xanthene

Xanthene represents a versatile and multifunctional heterocyclic system characterized by a tricyclic structure comprising fused aromatic ethers and a dibenzo[b,e]pyran core. **[66]** This unique chemical framework exhibits significant electronic delocalization facilitated by the conjugation of its aromatic rings. Such delocalization enhances chemical stability and enables the formation of excited states, making xanthene particularly suitable for applications in medicinal chemistry and optoelectronic materials. **[67]**

The reactivity and functionality of xanthene derivatives are largely determined by substitutions at their aromatic and heterocyclic positions. **[68]** These substitutions strongly influence their chemical and electronic properties, enabling xanthene compounds to act as nucleophilic or electrophilic agents in diverse chemical reactions. This adaptability highlights the importance of xanthenes as a highly valuable and versatile class of compounds across a broad spectrum of scientific and industrial applications. **[69]**

2.3. Applications of xanthene

Xanthene derivatives, particularly 1,8-dioxo-octahydroxanthenes, represent an important class of oxygen-containing heterocycles, characterized by an aryl-substituted pyran ring fused to two cyclohexanone rings. Due to broad and expanding range of applications, their synthesis has gained significant interest in recent years, especially in medicinal chemistry and materials science. **[70]** These compounds have diverse applications in biodegradable agrochemicals, **[71]** cosmetics, pigments, fluorescent materials, **[72]** and advanced technologies such as photodynamic therapy, **[73]** luminescent sensors, **[74]** and laser technologies. **[75]**

2.4. Pharmacological effects of xanthenes

Xanthenes, a class of tricyclic dibenzopyrans, are distinguished by their diverse physicochemical and pharmacological properties. **[76]** Although numerous natural products belonging to this class have been isolated and characterized, the development of therapeutic agents leveraging their unique heterocyclic structure remains limited **(Figure I.11). [77]** This therapeutic potential is further reinforced by the broad biological activities of derivatives from this family, driven by their ability to interact with multiple protein receptors. **[78]** In addition to the aforementioned properties, these derivatives have been reported to possess antitumoral **(I.38)**, antimicrobial **(I.39)**, antidiabetic **(I.40)**, antioxidant **(I.41)**, antiviral **(I.42)** and anti-inflammatory activities **(I.43)**. **[79]** Recent studies have further deepened the understanding of these biological activities, emphasizing their increasing relevance for the development of novel therapeutic applications. **[80]**

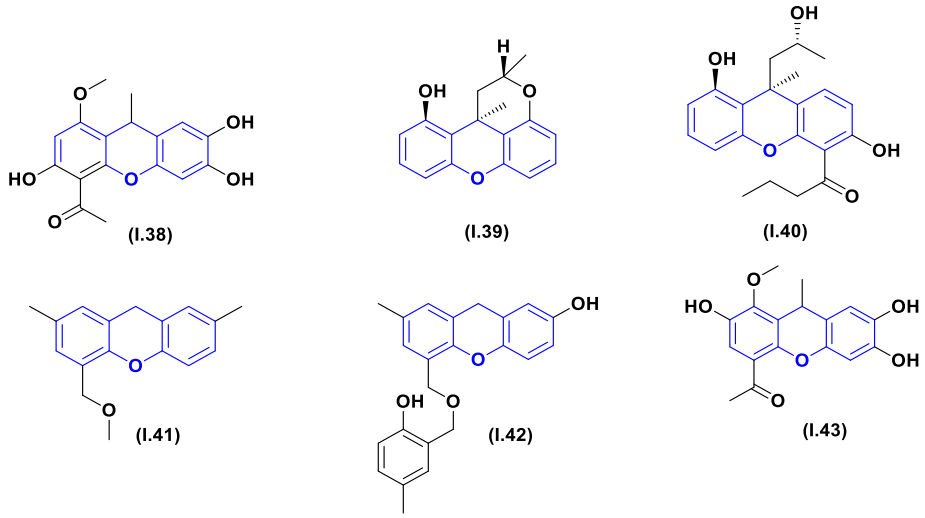

Figure I.11. Structures of natural xanthenes.

2.4.1. Xanthenes as antitumor agents

The annual increase in cancer-related deaths highlights the urgent need to develop active, selective, and efficient anticancer drugs. Among existing therapies, heterocyclic structures represent a common feature of most anticancer agents due to their diverse biological activities. Human DNA topoisomerases, key enzymes involved in resolving DNA topological issues during replication and transcription, have been identified as promising molecular targets for anticancer drug development. **[81]**

In 2010, Giri et *al*. **[82]** synthesized and evaluated a series of substituted xanthene derivatives for their anticancer activity against DU-145, MCF-7, and HeLa cancer cell lines. Among these compounds, ([*N*, *N*-diethyl]-9-hydroxy-9-(3-methoxyphenyl)-9H-xanthene-3-carboxamide) **(I.44)** emerged as the most potent, exhibiting cancer cell growth inhibition with IC_{50} values ranging from 36 to 50 µM across all tested cell lines. **(Figure I.12)**

Structure–activity relationship **(SAR)** studies indicated that further modifications of the lead compound, such as incorporating of a 7-fluoro substituent, **(I.45)** could enhance its potency. Additionally, the results suggested that these compounds operate through a unique mechanism of action, distinct from related acridine and xanthene derivatives, which are known to intercalate into DNA and inhibit topoisomerase II activity.

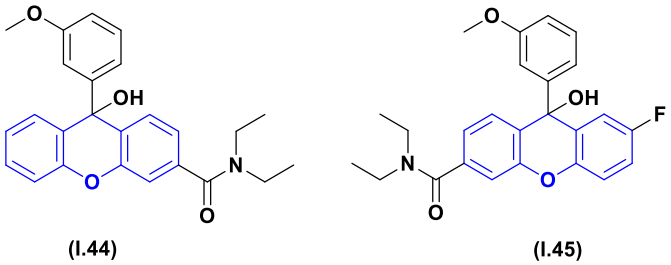

Figure I.12. Structures of antitumor xanthenes derivatives.

2.4.2. Xanthenes as antimicrobial agents

Among the various studies conducted on the antimicrobial properties of natural and synthetic compounds, the evaluation of derivatives has attracted considerable attentionfrom plant and fungal sources has attracted considerable attention. In particular, research on xanthene-based compounds has revealed promising biological activities. In 2015, a study isolated compounds **(I.46)** and **(I.47)** from foliar fungal endophytes of *Pinus strobus* (Eastern white pine) and tested their antimicrobial properties **(Figure I.11). [83]** These compounds notably inhibited the growth of *Microbotryum violaceum* and demonstrated significant antibacterial activity against the Gram-positive bacterium *Bacillus subtilis*. Building on these findings, Yunnikova et *al.* **[84]** further explored the antimicrobial potential of xanthene derivatives by designing and synthesizing a series of *N*-arylmethyl-4-(xanthene-9-yl)anilines **(I.46)** and *N*-arylmethylene-4-(xanthene-9-yl)anilines **(I.47)**. Among these, the compound *N*-(4-(9H-xanthen-9-yl) benzyl)-*N*, *N*-dimethylbenzene-1,4-diamine exhibited a bacteriostatic effect against *Staphylococcus aureus* at a concentration of 500 µg/mL **(Figure I.13)**.

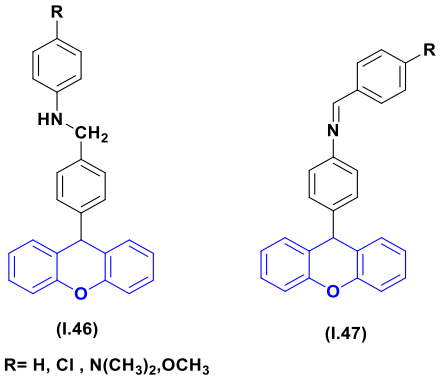

Figure I.13. Structures of antimicrobial xanthenes derivatives.

2.4.3. Xanthenes as antiviral agents

Carr et *al*. **[85]** explored the antiviral potential of xanthenes, particularly against encephalomyocarditis **(EMC)**, a severe viral infection affecting various mammals and causing myocarditis, encephalitis, and neurological disorders. Their study identified several compounds, including compound **(I.48)** as particularly effective in prolonging the survival of infected mice. This compound exhibited antiviral activity through both oral and subcutaneous administration, demonstrating broad-spectrum efficacy. **(Figure I.14)**

Structure-activity relationship **(SAR)** studies revealed that the introduction of carbonyl or alkenyl functions conjugated to the xanthene nucleus, along with the reduction of side-chain length and substituent molecular weight, enhances antiviral activity. Beyond their efficacy against EMC virus, these compounds also showed promising results against other viruses, such as the *Semliki Forest virus* and *Vaccinia virus*.

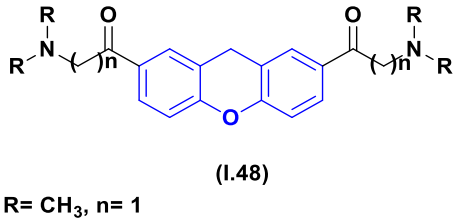

Figure I.14. Structure of antiviral xanthene derivative.

2.4.4. Xanthenes as antiparasitic agents

The antiparasitic activity of xanthene derivatives has garnered increasing attention due to their potential against various parasitic infections. Research has particularly focused on the use of these compounds to inhibit essential targets in parasites responsible for human African trypanosomiasis, Chagas disease, and leishmaniasis, mainly by disrupting their redox systems. For instance, derivatives of 9,9-dimethylxanthene have been evaluated for their activity against trypanothione reductase **(TR)**, a key target for these diseases, showing that structural

modifications, such as the addition of methylene groups, can influence the effectiveness of inhibitors. **[86]**

In another study conducted by Wu et *al*. a series of 9H-xanthene derivatives **(Figure I.15)** were tested for their antimalarial activity against chloroquine-sensitive and chloroquine-resistant strains of *Plasmodium falciparum*. Among these compounds, derivative **(I.49)** exhibited remarkable antimalarial activity, with a mechanism of action distinct from that of chloroquine, particularly in resistant strains. This compound also demonstrated a strong synergistic effect, increasing chloroquine accumulation in a resistant strain, offering promising prospects for more effective treatments. **[87]**

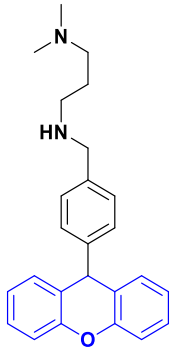

(I.49)

Figure I.15. Structure of antiparasitic xanthene derivative.

2.4.5. Xanthenes as anti-inflammatory agents

The anti-inflammatory potential of xanthene derivatives has been extensively studied, yielding promising results across various models. One notable study evaluated the anti-inflammatory effects of 9-aryl-9H-xanthene-3,6-diol derivatives **(I.50)** using a carrageenan-induced rat paw edema model. These compounds demonstrated significant activity, particularly during the second phase of the edema response (180-360 min), at doses of 30, 60, and 90 mg/kg, suggesting that prostaglandin pathways likely mediate their mechanism of effects. **[88]**

In parallel, research by Naya et *al*. **[89]** focused on the modulation of chemokine receptors, particularly **CCR1**, which is implicated in chronic inflammatory conditions such as rheumatoid arthritis and multiple sclerosis. By targeting MIP-1α, a ligand for **CCR1**, Naya et *al*. identified xanthene-9-carboxamide derivatives, such as **(I.51)**, which exhibited an IC_{50} value of 510 nM for human **CCR1** receptors. Further structural modifications, including the replacement of the *n*-pentyl group with cycloalkyl or arylmethyl groups resulted in enhanced receptor binding. Notably, the compound with a cyclooctyl group, exhibited a threefold

improvement in affinity compared to the parent compound. These findings underscore the therapeutic potential of xanthene derivatives in modulating inflammatory pathways, offering new avenues for the treatment of chronic inflammatory diseases **(Figure I.16)**. **[90]**

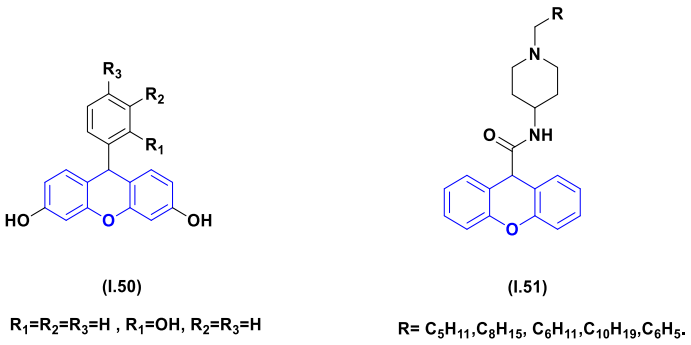

(I.50)

R_1=R_2=R_3=H , R_1=OH, R_2=R_3=H

(I.51)

R= C_5H_{11},C_8H_{15}, C_6H_{11},$C_{10}H_{19}$,C_6H_5.

Figure I.16. Structures of anti-inflammatory xanthenes derivatives.

2.4.6. Xanthenes as antidiabetic agents

AMP-activated protein kinase **(AMPK)** is a key enzyme that regulates cellular energy balance and plays a crucial role in responding to low energy levels. Its activation induces insulin-sensitizing effects, making it a promising therapeutic target for the treatment of type 2 diabetes. In this context, Kwon et *al*. **[91]** investigated xanthene derivatives **(I.52)** as AMPK activators. **(Figure I.17)** These compounds were selected due to their structural similarity to mangiferin, a secondary metabolite used in Southeast Asia to manage diabetes. *In vitro* studies on L6 myotubes showed that these compounds had a low effective concentration (EC_{50}) of approximately 1.5 mM for AMPK phosphorylation, which is approximately 6000 times lower than metformin's EC_{50}. Furthermore, *in vivo* studies in high-fat diet-induced diabetic mice demonstrated that administering 3 mg/kg of xanthene derivatives produced results similar to those of 50 mg/kg of metformin, indicating comparable efficacy at significantly lower doses. These findings highlight the potential of these xanthene derivatives as promising therapeutic candidates for type 2 diabetes.

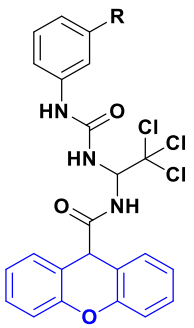

(I.52)

R= NO_2, CN

Figure I.17. Structures of antidiabetic xanthenes derivatives.

2.4.7. Xanthenes as antioxidant agents

Various series of xanthene derivatives have been evaluated for their antioxidant activity, particularly their ability to scavenge free radicals and inhibit oxidative processes. Studies revealed that compounds such as 9H-xanthene-2,7-diols **(I.53)** act as hydrogen donors, effectively suppressing the oxidation of tetralin and linoleic acid. Further research on these derivatives in soybean phosphatidylcholine liposomal membranes demonstrated that their antioxidant properties depend not only on the initial hydrogen abstraction from the xanthene molecule but also on a secondary abstraction from the phenolic OH group of the oxidation product. **[92]** Additionally, other xanthene derivatives, such as benzo[kl]xanthene lignans **(I.54**, **I.55)**, were investigated for their radical-scavenging activities, with compound **(I.54**) exhibiting the highest activity. These findings highlight the potential of xanthene-based compounds as effective antioxidants **(Figure I.18)**. **[93]**

Furthermore, a SAR study revealed that compounds substituted with a free OH group acted as better scavengers compared with those bearing a protected OH group.

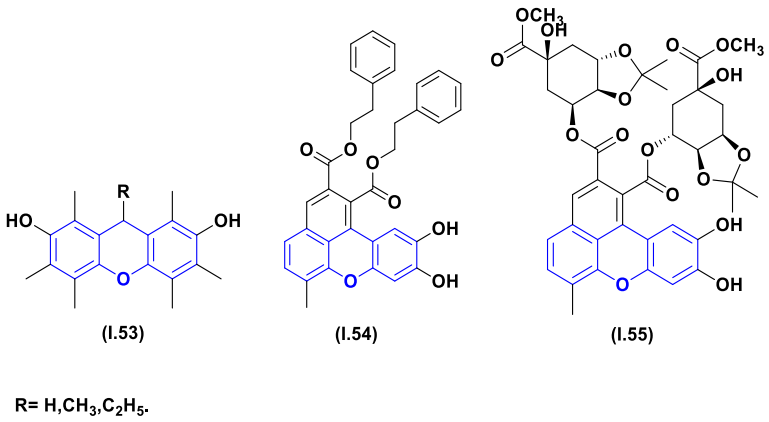

Figure I.18. Structures of antioxidant xanthenes derivatives.

2.4.8. Xanthenes as antipsychotic agents

The potential antipsychotic activity of xanthene derivatives has been widely studied, particularly due to their structural similarities with phenothiazine-based compounds, known for their ability to suppress dopamine activity in the brain. **[94]** Among these, xanthene analogs of diphenylmethane-type chlorpromazine have attracted attention. Compounds **(I.56, I.57)**, or their corresponding salts (HCl, 2HCl, citrate, maleate, or dimaleate), were investigated through several pharmacological tests. **[95]** Notably, the aminoalkyl derivative **(I.57)** (**R**=$N(Me)_2$, **Y**= CF_3) was found to be nearly as potent as chlorpromazine. Interestingly, xanthene **(I.56)** (**R**=$N(Me)_2$, **Y**= CF_3) exhibited even greater potency than chlorpromazine in several animal tests, where many neuroleptic agents are typically active. These findings

underline the potential of xanthene-based compounds as candidates for the development of novel antipsychotic drugs **(Figure I.19)**. **[96]**

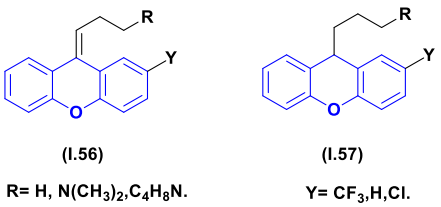

Figure I.19. Structures of antioxidant xanthenes derivatives.

2.5. Synthesis of xanthene

Driven by the biological and pharmacological interest in xanthenes, several synthetic strategies have been developed and reported in the literature for their preparation. Historically, one of the first syntheses of the xanthene core was reported in 1925, when 3-hydroxyxanthene was obtained through the condensation of saligenin **(I.58)** and resorcinol **(I.59) (Scheme I.1)**. **[97]**

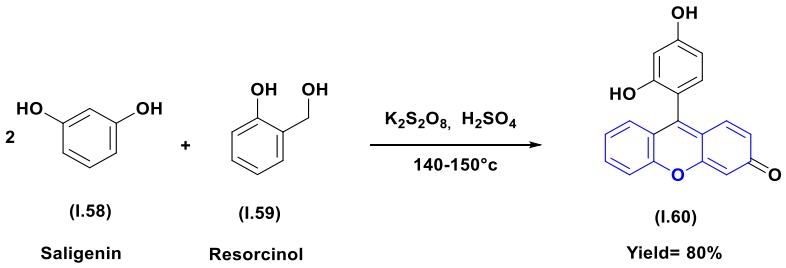

Scheme I.1. First synthesis of xanthene from saligenin and resorcinol

These pioneering works laid the foundation for a variety of modern synthetic approaches. These methods provide great flexibility in modifying substitution patterns on the core while incorporating environmentally friendly procedures, aligning with green chemistry principles. **[98]** In this context, we present a compilation of the most commonly used methods as well as recent approaches, for the synthesis of xanthene derivatives.

2.5.1. Condensation of aldehydes and dimedone

The condensation reaction between diketones, such as dimedone and cyclohexanedione, with various aromatic aldehydes is one of the most commonly described methods for the synthesis of xanthenes. Numerous scientific studies have explored this reaction, ranging from conventional methods to more optimized and environmentally friendly conditions. The application of acid- or base-catalyzed condensation of aldehydes **(I.61)** with 5,5-dimethyl-1,3-cyclohexanedione **(I.62)** has been described several times in solvent-free conditions, aqueous media, or ionic liquids, leading to the generation of 1,8-dioxo-octahydroxanthene derivatives

(I.63). Among these studies, the work by Borah et *al*. **[99]** reported the synthesis of xanthenedione derivatives from aromatic aldehydes **(I.61)** and 5,5-dimethyl-1,3-cyclohexanedione **(I.62)** under reflux and solvent-free conditions, using reusable supported solid acid catalysts such as **(**PANI-TsOH, PANI-$FeCl_3$ and Clayfen**)**. Furthermore, Paramasivam et *al*, developed an economical method for the synthesis of 1,8-dioxo-octahydroxanthene *via* a one-pot synthesis catalyzed by ceric ammonium nitrate (CAN) supported on HY-zeolite as an efficient catalyst **(Scheme I.2). [100]**

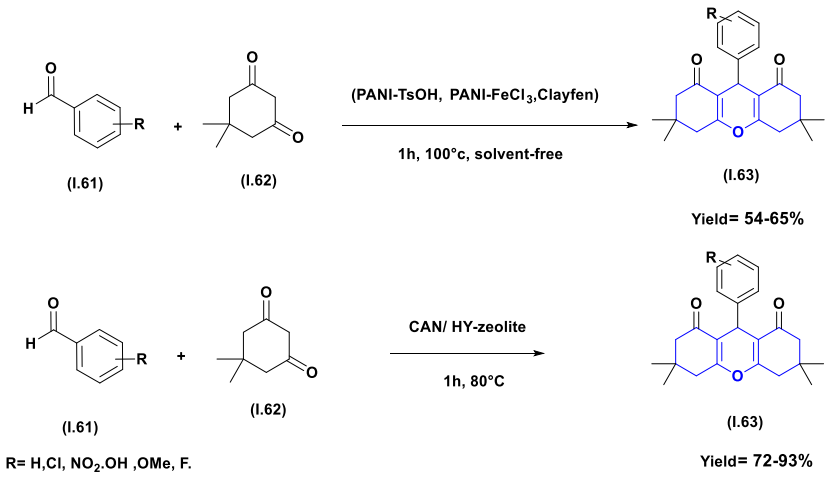

Scheme I.2. Xanthene synthesis from aldehydes and dimedone.

Several other methods have been reported in the literature for the synthesis of 1,8-dioxo-octahydroxanthene compounds, which involve a variety of catalysts. These include metal oxides, resins, carbon-based materials, silicon-based materials, ionic liquids, heteropoly-acids, and metal sulfides. Specifically, Lewis acids such as $InCl_3 \cdot 4H_2O$, **[101]** $FeCl_3 \cdot 8H_2O$, **[102]** $NaHSO_4$,**[103]** and tetrabutylammonium hydrogen sulfate **(TBAHS) [104]** have been employed.

Moreover, various heterogeneous catalysts have been explored, including silica sulfuric acid **[105]**, polyaniline *p*-toluene sulfonate, **[106]** PPA-SiO_2, **[107]** TiO_2/SO_4,**[108]** amberlyst-15, **[109]** Fe^{3+}-MT, **[110]** alumina-sulfuric acid, **[111]** silica-bonded *N*-propyl sulfamic acid, **[112]**, as well as ZnS-Fe_2O_3-Ag, **[113]** PMA-SiO_2,**[114]** NBS,**[115]**[Bmim][HSO_4]**[116]**[Hmim]TFA, **[117]** and[TMPSA]HSO_4.**[118]**

2.5.2. Condensation of aromatic aldehydes, 2-naphthol and cyclic 1,3-dicarbonyl

Another family of xanthene derivatives was synthesized through the condensation of 2-naphthols, aldehydes, and cyclic 1,3-dicarbonyl compounds in the presence of ionic liquids, which served as efficient, homogeneous, and reusable catalysts.

In 2013, Moosavi-Zare et *al*. **[119]** described the use of a novel ionic liquid, sulfonic acid-functionalized pyridinium chloride [Pyridine–SO_3H]Cl, for the one-pot three-component synthesis of 12-aryl-8,9,10,12-tetrahydrobenzo[a]xanthen-11-ones **(I.65)**. Similarly, Singh et *al*. **[120]** employed task-specific acidic ionic liquid [NMP]H_2PO_4 to catalyze the preparation of 12-aryl-8,9,10,12-tetrahydrobenzo[a]xanthen-11-ones **(I.65)** at 80 °C **(Scheme I.3).**

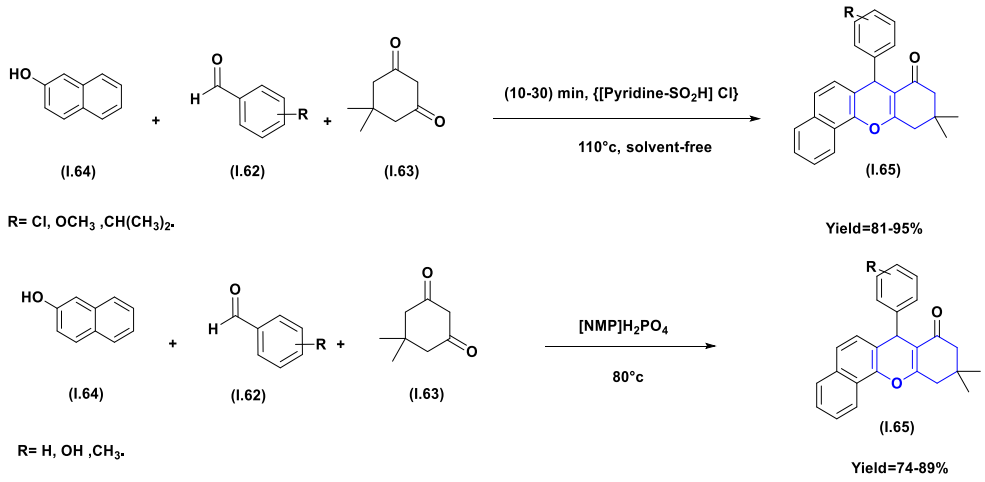

Scheme I.3. Xanthene synthesis from 2-naphthol**,** aldehydes and dimedone

2.5.3. *Via* oxa-Michael aldol reaction

The domino oxa-Michael–aldol reactions, studied by Emilie et *al*. **[121]** as model reactions, represent an efficient approach for the synthesis of tetrahydroxanthenones **(I.68)**. These reactions offer a simple and rapid method using ball milling, a mechanochemical technique, starting from salicylaldehyde **(I.66)** and cyclohexanone **(I.67) (Scheme I.4)**. Emilie and her collaborators conducted a systematic study to optimize this transformation by focusing on key parameters, including the stoichiometric ratio of reactants, the rotational frequency of the mill, the number of balls used, and the milling time. The aim of their work was to make this transformation, which is already highly efficient under solution-phase conditions, even more effective. They also investigated in detail the influence of various factors, such as equivalents of salicylaldehyde, the amount of cyclohexanone, and the milling time. Furthermore, they demonstrated that the number of balls used plays a significant role in the reaction outcome, enabling improved yields under optimized conditions.

Scheme I.4. Xanthene synthesis *via* oxa-michael aldol reaction performed in a ball mill.

2.5.4. From 2-amino-1,1,3-tricyanopropene

2-amino-1,1,3-tricyanopropene has been used as a key precursor for the synthesis of new xanthene derivatives, particularly 2,4-diamino-5H-chromeno[2,3-b]pyridine-3-carbonitriles **(I.71)**. Shaabani et *al*. **[122]** reported an innovative method based on a one-step, three-component condensation reaction, involving 2-amino-1,1,3-tricyanopropene **(I.69)**, salicylaldehyde **(I.66)**, and secondary cyclic amines **(I.70)** (**Scheme I.5**). This reaction, carried out in ethanol at room temperature, afforded the desired products in good to excellent yields **(80-94%)**. In this study, the authors demonstrated that this method relies on simple, readily available precursors, offering a novel approach for the preparation of heterocyclic systems of synthetic and pharmaceutical relevance.

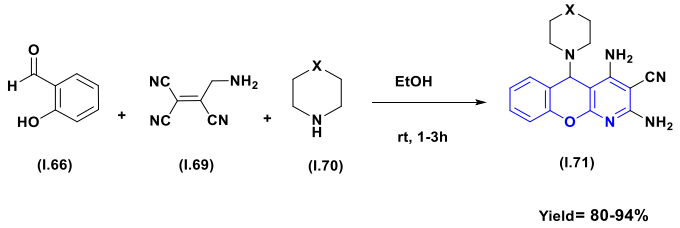

Scheme I.5. Synthesis of 2,4-diamino-5H-chromeno[2,3-b] pyridine-3-carbonitriles.

2.5.5. Via a cycloaddition

Cycloaddition reactions have proven to be a powerful strategy for the efficient synthesis of xanthene derivatives, which are of significant interest in pharmaceutical chemistry. One promising method for preparing these compounds is through a **[3+3]** cycloaddition, as demonstrated by Narayana et *al*. **[123]** In their study, they successfully employed a one-pot reaction combining Knoevenagel condensation and **[3+3]** cycloaddition to synthesize 1,8-dioxo-octahydroxanthenes **(I.74)** under mild conditions, using the SO_4^{2-}/SnO_2 catalyst. The reaction proceeds *via* the Knoevenagel condensation between the enol derivatives of *α*, *β*-unsaturated aldehydes **(I.72)** and *β*-diketones **(I.73)**, followed by the electrocyclization to yield the desired product. **(Scheme I.6)**.

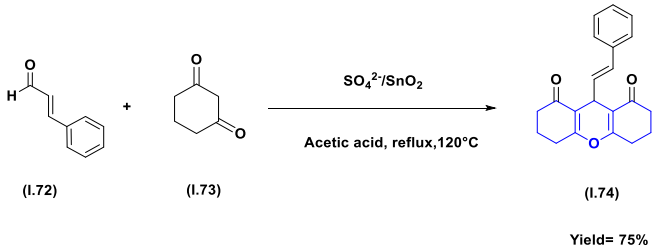

Scheme I.6. Xanthenes derivatives synthesis *via* a cycloaddition reaction.

2.5.6. From 2-hydroxynaphthalene-1,4-dione

Xanthene derivatives can be synthesized from 2-hydroxynaphthalene-1,4-dione **(I.75)** through various multicomponent condensation reactions. These synthetic routes can proceed either *via* a $Bi(OTf)_3$-catalyzed condensation or through a cyclocondensation in an aqueous medium, offering efficient and versatile approaches for the construction of these valuable heterocyclic structures. One of the earliest efficient approaches was reported by Bazgir et *al.* in 2008, **[124]** who described the synthesis of spiro[dibenzo[b,i]xanthene-13,30-indoline]pentaones **(I.77)** and 5H-dibenzo[b,i]xanthene-tetraones **(I.78)** through the condensation of 2-hydroxynaphthalene-1,4-dione **(I.75)** with isatins **(I.76)** or aldehydes **(I.61)** in an aqueous medium or under solvent-free conditions. More recently, Turhan et *al.* **[125]** proposed a method involving 2-hydroxy-1,4-naphthoquinone **(I.80)**, dimedone **(I.62)**, and aromatic aldehydes **(I.61)** for the synthesis of 3,4-dihydro-12-aryl-1H-benzo[b]xanthene-1,6,11-(2H,12H)triones **(I.79)**. Catalyzed by bismuth triflate $Bi(OTf)_3$, this green and reusable catalyst enables the preparation of the target compounds with high yields under mild conditions **(Scheme I.7).**

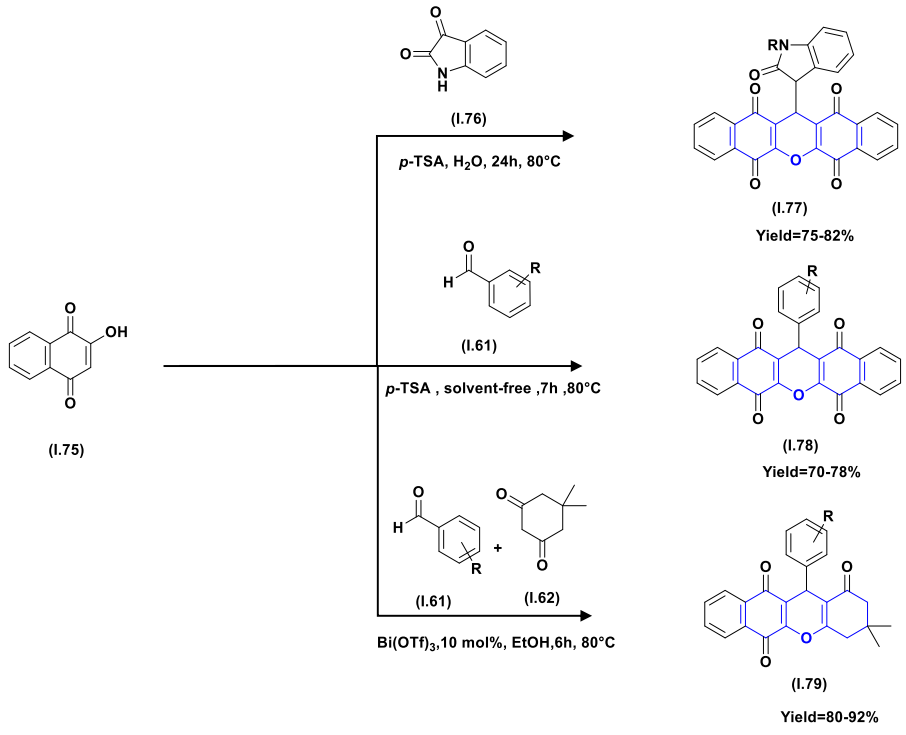

Scheme I.7. Xanthenes derivatives synthesis from 2-hydroxynaphthalene-1,4-dione.

3. *O, P*-heterocyclic compounds

Hybrid oxygen heterocycles can also formed by incorporating a second heteroatom, such as phosphorus, into their ring structure. **[126]** Compounds that simultaneously incorporate these two elements have attracted significant interest due to their unique structural and chemical properties. **[127]** The ring size of these systems typically ranges from five to nine members, providing remarkable structural diversity. **[128]** Since the first synthesis of phosphorus-containing heterocycles in the 20th century, their study has experienced renewed interest, particularly in pharmaceutical chemistry. **[129]** These compounds represent an exceptionally important class of heterocycles, found in a wide variety of drugs, including antihypertensives **(I.80)**, **[130]** anticancer agents **(I.81)**, **[13]** enzyme inhibitors (acetylcholinesterase inhibitors) **(I.82) [131]** antimicrobial agents **(I.83) (Figure I.20)**. **[132]**

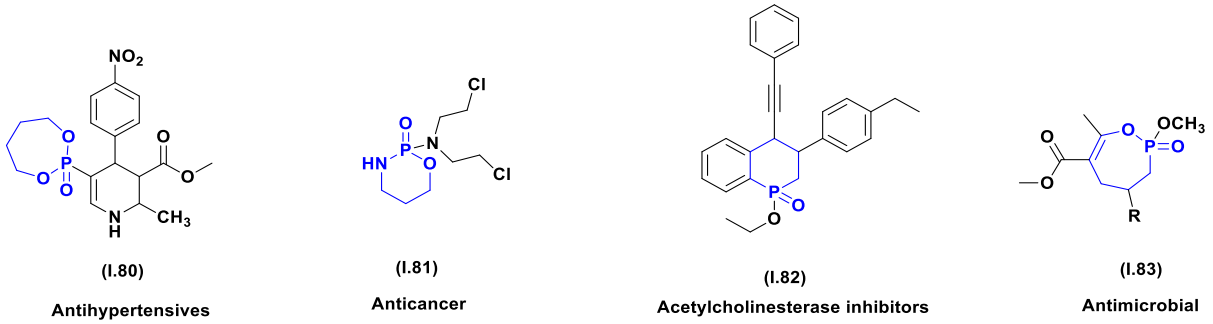

Figure I.20. Structures *O*, *P*-heterocyclic compounds as therapeutic agents.

Four major families of compounds stand out due to their broad spectrum of biological activities: 1,2-oxaphospholane-2-oxides **(I.84)**, 1,2-oxaphosphinane-2-oxides **(I.85)**, 1,2-oxaphosphepane-2-oxides **(I.86)**, and 1,2-oxaphosphocane-2-oxides **(I.87) (Figure I.21)**.

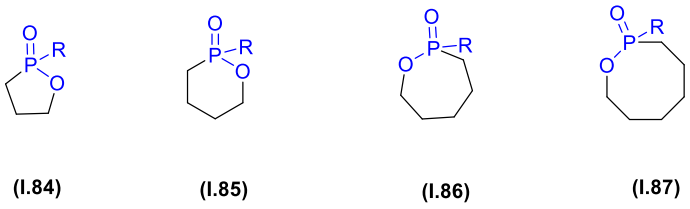

Figure I.21. Main classes of 1,2-oxaphospholane-2-oxides

In this context, our work focuses on the synthesis of a new family of five-membered *O*,*P*-heterocycles, specifically 1,2-oxaphospholane-2-oxides, in order to explore their properties and potential applications.

3.1. Chemistry of 1,2-oxaphospholane-2-oxides

The 1,2-oxaphospholane-2-oxides are five-membered heterocycles incorporating both phosphorus and oxygen atoms, which have garnered increasing interest due to their distinctive

chemical properties and potential applications across diverse scientific domains. **[133]** These characteristics make them particularly attractive scaffolds for the development of novel therapeutic agents. **[134]** Several studies have demonstrated promising biological activities, **[135]** including anti-inflammatory **(I.88)** and **[136]** antitumor **(I.89)** properties. **[137]** Furthermore, their unique structure imparts interesting properties for materials science applications, particularly as precursors for the synthesis of functional polymers and composite materials **(Figure I.22)**. **[138]**

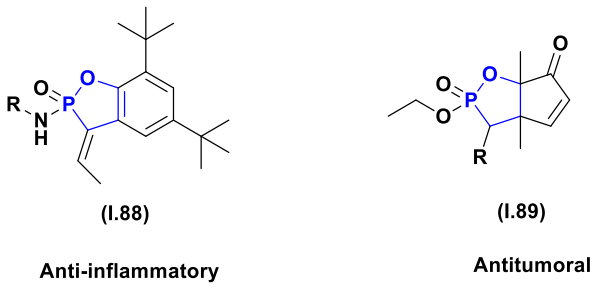

Figure I.22. Anti-inflammatory and antitumor activities of 1,2-oxaphospholane-2-oxides.

3.2. Synthesis pathways of 1,2-oxaphospholane-2-oxides

3.2.1. From 1-alkyl-1-fluoro-3,4-dihydroxybutyl) phosphonic acid

Xu et *al*. **[139]** prepared novel cyclic phosphonate derivatives, analogues of carbocyclic phosphatidic acid (ccPA), in four steps under ambient temperature conditions. Initially, (1-alkyl-1-difluoro-3,4-dihydroxybutyl) phosphonic acid **(I.91)** was obtained by treating the corresponding diethyl phosphonate **(I.90)** with TMSBr in dichloromethane (DCM) for 5h. Since intramolecular cyclization of phosphonates can be challenging, the authors employed dicyclohexylcarbodiimide (DCC), a reagent known to efficiently promote such transformations under high-dilution conditions. The cyclization of compound **(I.91)** was therefore performed in the presence of DCC in DMF**,** followed immediately by esterification of the remaining hydroxyl group, performed under basic medium, also in DMF, for 16h **(Scheme I.8)**.

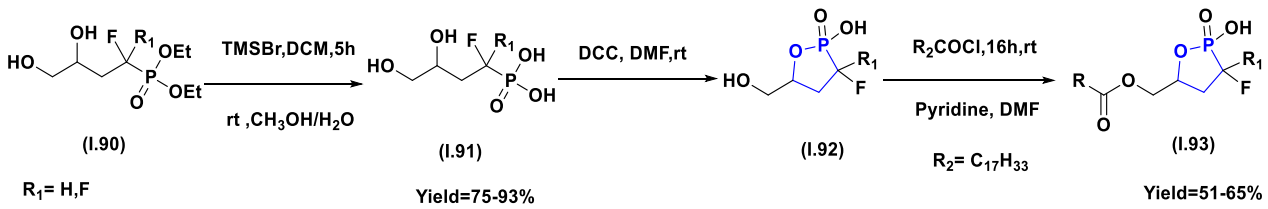

Scheme I.8. Synthesis of 1,1-difluoro-3-hydroxyl-4-oleoyloxylbutane analogues of ccPA.

3.2. 2. *Via* phospha-Michael addition

A selective phospha-Michael addition of diethyl phosphite to chalcones represents an efficient method for generating oxaphospholanes as reported by Zhang et *al*, **[140]** this reaction is carried out in a toluene/HMPA mixture in the presence of lanthanide salts, facilitating the process under mild conditions. Lanthanide catalysts $[(Me_3Si)_2N]_3La(\mu\text{-}Cl)Li(THF)_3$ predominantly produce 1,2-oxaphospholane-5-phosphonates **(I.101)** in moderate to good yields. This methodology provides a simple and practical approach to synthesizing organophosphorus compounds with potential biological applications **(Scheme I.9)**.

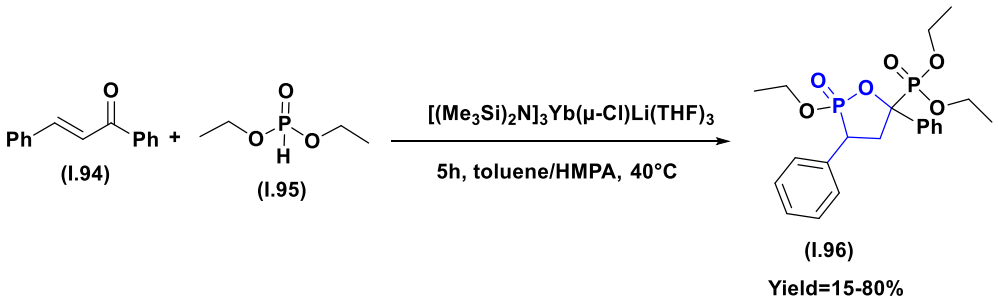

Scheme I.9. Lanthanide-catalyzed phospha-Michael addition for the synthesis of 1,2-oxaphospholane-phosphonates.

3.2.3. Via the condensation of *o*-hydroxybenzyl alcohol with trialkyl phosphite

Ageeva et *al*. **[141]** reported the one-step synthesis of a new series of 2-oxo-2-alkoxy-1-oxa-2-phosphaindanes **(I.100)**. This transformation involves an exothermic condensation reaction between *o*-hydroxybenzyl alcohol **(I.97)** and various trialkyl phosphites **(I.98)**. To ensure complete conversion, an equimolar mixture of the reagents was heated at 150-160 °C for approximately 3h in a suitable solvent, such as dimethylformamide (DMF) or tetrahydronaphthalene. During the process, an alcohol is released as a by-product, and a low-boiling volatile compound is eliminated. **(Scheme I.10)**

The efficiency and cleanliness of the synthesis are closely influenced by both the nature of the trialkyl phosphite and the reaction conditions. While triethyl phosphite enables a clean conversion without significant tar formation, the use of trimethyl or tripropyl phosphites results in the production of considerable amounts of tar (**30–50%** of the reaction mass), complicating purification. Furthermore, performing the reaction without a solvent leads to a spontaneous temperature increase of **45–50 °C**, yet the yields remain lower than those obtained in solution, highlighting the crucial role of the solvent in optimizing the reaction outcome.

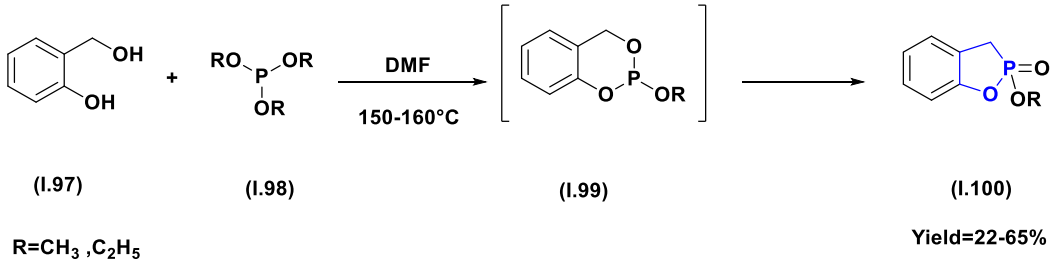

(I.97) (I.98) (I.99) (I.100)

$R=CH_3, C_2H_5$ Yield=22-65%

Scheme I.10. Synthesis of novel 1,3-dihydro-2,1-benzoxaphosphole-1-oxide

3.2.4. From *o*-tolylphosphonate

The synthesis of 1-alkyl-1,3-dihydro-2,1-benzoxaphosphole 1-oxide **(I.104)** was achieved from *o*-tolylphosphonate **(I.101)**, as reported by Miles et *al*.**[142]**, through an efficient multistep procedure yielding excellent results. The process begins with the hydrolysis of *o*-tolylphosphonate **(I.101)** under refluxing hydrochloric acid to afford the corresponding phosphinic acid **(I.102)**. This is followed by halogenation *via* either photolytic chlorination or *N*-bromosuccinimide (NBS) bromination, generating the halogenated intermediate **(I.103)**. Finally, solvolysis in perchloric acid promotes intramolecular cyclization, leading to the formation of the desired heterocyclic compound, 1-*O*-alkyl-1,3-dihydro-2,1-benzoxaphosphole 1-oxide **(I.104)**. **(Scheme I.11)**

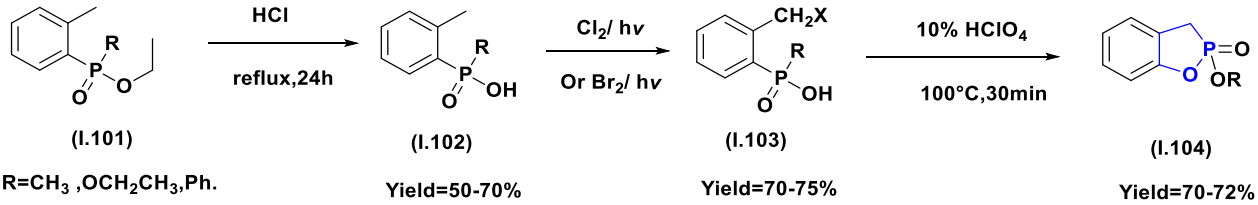

(I.101) (I.102) (I.103) (I.104)

$R=CH_3, OCH_2CH_3, Ph.$ Yield=50-70% Yield=70-75% Yield=70-72%

Scheme I.11. Synthesis of 1-alkyl-1,3-dihydro-2,1-benzoxaphosphole-1-oxide catalyzed by nickel (II) chloride.

4. Conclusion

Heterocyclic compounds play a fundamental role in various fields owing to their chemical diversity and wide range of applications, particularly in the pharmaceutical domain. These structures are frequently used as intermediates in drug synthesis, highlighting their growing importance in the development of new bioactive agents. This chapter provides an overview of two specific classes of heterocycles, xanthenes and oxaphospholanes, emphasizing their scientific and clinical relevance.

Initially, the focus is placed on xanthenes, exploring their key role in pharmacology. We detailed various synthetic methods used to obtain these structures from diverse reagents, while highlighting their chemical reactivity and potential in various medical applications.

In the second part, the discussion focuses on oxaphospholanes, which remain underexplored in the literature. Although they have been studied infrequently so far, these compounds exhibit promising potential that warrants further investigation.

In conclusion, this chapter emphasizes the need to continued research on xanthenes and oxaphospholanes, both in terms of their synthesis and their therapeutic applications. Exploiting these heterocycles in innovative strategies represents a critical research avenue for the future.

Chapter II

Overview on N-nitroso compounds

1. Chemistry of *N*-nitroso compounds

N-nitroso compounds are characterized by the presence of an NO group attached to a nitrogen atom, forming an *N*-NO bond. This structure is stabilized by the delocalization of the nitrogen lone-pair electrons into the π-system of the oxygen atom of NO group, resulting in two major resonance forms **(Figure II.1)**.**[143]** This electronic delocalization imparts specific chemical reactivity to these compounds, explaining their significance in organic and medicinal chemistry.**[144]** Due to their unique electronic and structural properties, they take part in various biological processes and have diverse applications in pharmaceutical chemistry, agro-chemistry, and materials science.**[145]**

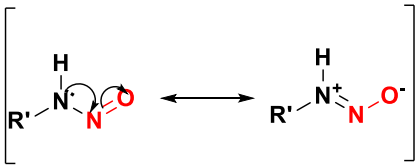

Figure II.1. Resonance forms of *N*-nitroso compounds.

From a biological and pharmacological perspective, these compounds exhibit a wide range of activities **(Figure II.2)**, including anticancer **[146]** and antimicrobial properties. **[147]** Their involvement in oxidative stress regulation and other essential biochemical mechanisms makes them promising candidates for novel therapeutic agents. However, their use must be carefully controlled, as certain classes present toxicological and environmental risks, particularly due to their mutagenic potential and their occurrence in various food products. **[148]**

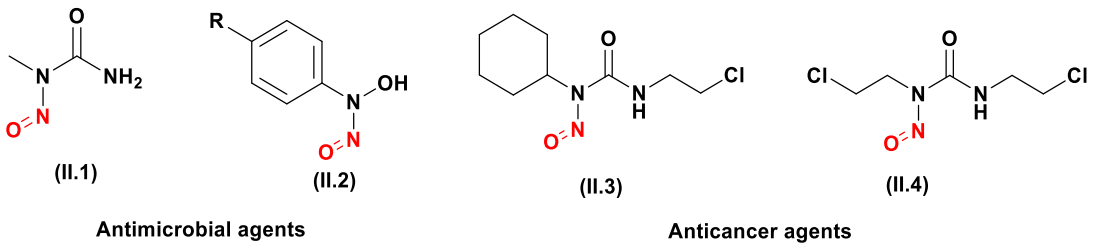

Figure II.2. Structures of some anticancer and antimicrobial agents derivatives of *N*-nitroso compounds

Based on their structure and chemical properties, *N*-nitroso compounds can be classified into several categories **(Figure II.3)**.**[149]** ***N*-nitrosamines (II.5)** have been extensively studied due to their toxicity and potential role in disease development.**[150]** ***N*-nitrosoamides (II.6)** are widely used in organic synthesis and exhibit interesting pharmacological properties. **[151]** Another important class, ***N*-nitrosoureas (II.7)**, is well known for its applications in anticancer chemotherapy. **[152]** Finally, ***N*-nitrosocarbamates (II.8)** have attracted increasing attention due to their biological potential in pharmaceutical and agrochemical research.**[153]**

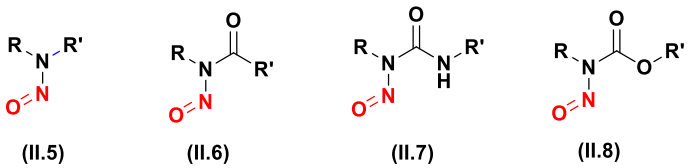

Figure II.3. Types of *N*-nitroso compounds

2. Applications of *N*-nitroso compounds

N-nitroso compounds are defined by the presence of the nitroso functional group (-NO) and encompasses several distinct subclasses, including *N*-nitrosamines, *N*-nitrosamides, *N*-nitrosoureas, and *N*-nitrosocarbamates. **[154]** Each category exhibits specific chemical and biological properties that influence their reactivity, formation mechanisms, and diverse applications. Their molecular structure also determines their therapeutic potential and toxicological effects, highlighting their significance in pharmaceutical chemistry, agrochemistry, and materials science. **[155]**

2.1. Applications in pharmaceutical chemistry

In the pharmaceutical field, *N*-nitroso compounds hold dual significance. On one hand, the surveillance of *N*-nitrosoamines is essential due to their unintentional presence in certain drugs and food products, raising significant health concerns because of their carcinogenic potential. Extensive research has elucidated the mechanisms governing their formation, prompting the implementation of regulatory measures to limit their occurrence. **[156]** These compounds, such as NDMA **(II.9)** and NDEA **(II.10)**, can undergo metabolic activation, primarily by cytochrome P450 enzymes, generating reactive intermediates capable of inducing DNA modifications. **[157]** This biochemical transformation can result in mutations that contribute to cancer development. **[158]** This structured organization clarifies the diverse roles of *N*-nitroso compounds while eliminating redundancies, ensuring better scientific coherence and fluidity.

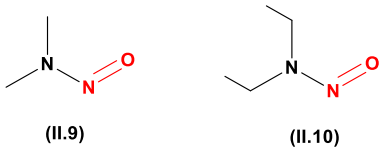

Figure II.4. Structures of *N*-nitroso compounds with carcinogenic potential.

Conversely, specific subclasses such as *N*-nitrosoureas and *N*-nitrosocarbamates are exploited in chemotherapy for their antitumor properties. **[159]** Their mechanism of action involves DNA alkylation, inhibiting cancer cell proliferation, a principle applied in the treatment of brain tumors and certain lymphomas like streptozocin **(II.11)** and fotemustine **(II.12)**, **[160]**

illustrating the dual nature of these compounds, both toxic and therapeutic **(Figure II.5)**. **[161]**

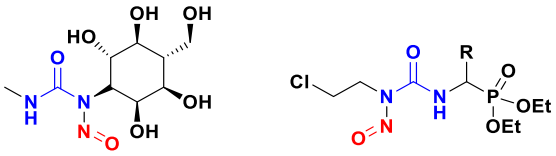

(II.11) (II.12)

Figure II.5. Structures of *N*-nitroso compounds as anticancer agents

2.2. Applications in agrochemistry

In agrochemistry, *N*-nitrosamines are primarily studied for their unintentional formation during industrial processes and their impact on food safety and environmental health. **[162]** Their presence in certain pesticides, particularly dinitroanilines (e.g., pendimethalin) **(II.13)**, has been detected at concerning concentrations, increasing the risk of human exposure. These mutagenic compounds are formed through a side reaction between a nitrosating agent and secondary amines **(II.14)** during manufacturing **(Scheme II.1)**. Some studies suggest that they may exhibit higher genotoxicity than other *N*-nitrosamines already classified as probable human carcinogens. **[163]**

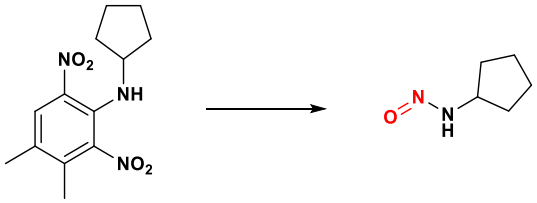

(II.13) (II.14)

Scheme II.1. Dinitroanilines (pendimethalin) and their associated *N*-nitrosamine impurities

3. Pathways for the preparation of *N*-nitroso compounds

N-nitroso compounds are molecules characterized by a functional group NO attached to nitrogen**.** This structure results from a reaction called ***N*-nitrosation (scheme II.2)**, in which a compound containing an NH group **(II.15)**, such as a secondary amine, reacts with a nitrosating agent. **[164]** The latter, acting as an electrophilic source of nitrosonium ions **(NO^+)**, induces the formation of an **N−NO** bond, thereby creating an *N*-nitroso compound. Amines **(II.16)**, as well as other compounds such as ureas **(II.17)**, carbamates **(II.18)** and amides **(II.19)**, are susceptible to undergoing this reaction.**[165]**

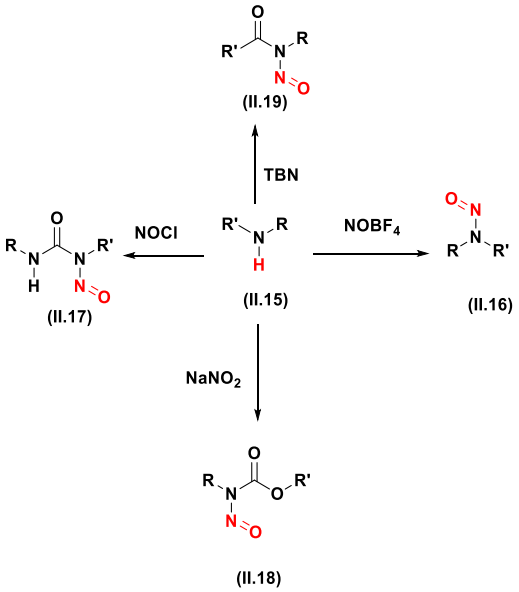

Scheme II.2. Synthetic pathways leading to *N*-nitroso compounds

3.1. *N*-nitrosation reaction

The *N*-nitrosation reaction is the most widely described synthetic route in the literature for the preparation of *N*-nitroso compounds. **[166]** This reaction involves the use of nitrosating agents**,** which are reagents capable of introducing an NO group to the nitrogen atom of the substrate. Nitrosating agents, by generating nitrosonium ions **(NO^+)**, react with the NH group via nucleophilic attack. Among the most commonly used agents are nitrosonium ions, nitrosyl halides, alkyl nitrites, and nitrogen oxides such as dinitrogen trioxide and dinitrogen tetroxide. **[167]**

The effectiveness of these nitrosating agents varies depending on their nature and the reaction conditions. Some agents, such as alkyl nitrites or nitrosyl halides, are directly active, while others, like nitrogen oxides, require the *in situ* formation of an active nitrosating agent. The choice of the latter, as well as the substrate, thus allows for control over the reactivity and targeted synthesis of nitroso compounds based on specific needs. **[168]**

3.1.1. *N*-nitrosation reaction using sodium nitrite

Sodium nitrite in acidic aqueous solution is one of the most commonly used reagents for the *N*-nitrosation of compounds containing an NH group. However, the active nitrosating agent does not originate directly from the NO_2^- anion or nitrous acid **(HNO_2)** but results from a rapid equilibrium between protonated HNO_2 and a nucleophilic species X^-. **[169]**

Various strategies have been reported in the literature for the synthesis of *N*-nitroso compounds using the $NaNO_2$/aqueous acid system, which enables the nitrosation of secondary amines as well as other substrates such as (hetero)amides, carbamates, hydroxylamines, hydroxylamine ethers, hydrazines, hydrazones, hydrazides, and ureas. **[170]**

Among these strategies, Aouf et *al*.**[171]** investigated the nitrosation of a urea analogue of fotemustine **(CENU)**. The target compound, *N*-nitroso-2-chloroethylureidophosphonate **(II.23)**, was obtained by treating 2-chloroethylureidophosphonate **(II.22)** with three equivalents of sodium nitrite, using formic acid at 0 °C in dichloromethane for two hours **(Scheme II.3)**.

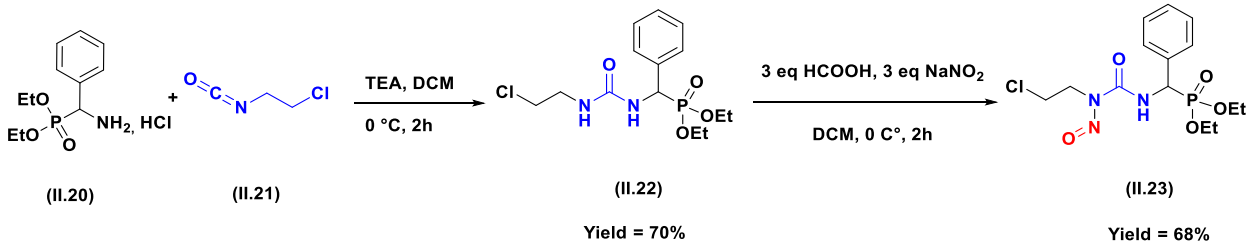

Scheme II.3. Synthesis of N-nitroso-2-chloroetylureidophosphonate.

In 2010, Gupta et *al*. **[172]** reported the nitrosation of novel nitrosourea derivatives as bifunctional anticancer agents using sodium nitrite and acetic acid. This approach afforded 3-methyl-5,7-alkyl-4-(*N*-propyl-*N*-nitrosoamido)-2-(3,4-dichlorobenzoyl)-4H-1,4-benzothiazine **(II.25)** in quantitative yield at 0 °C **(Scheme II.4)**.

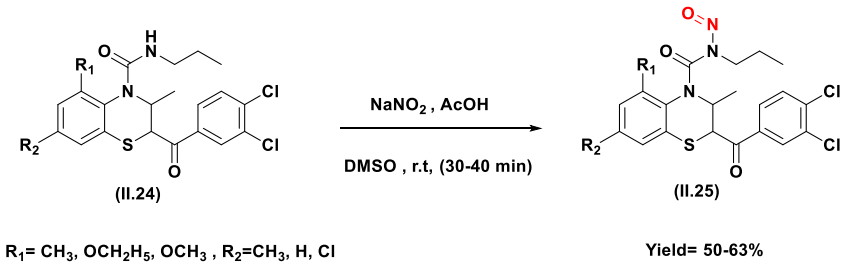

Scheme II.4. Synthesis of nitrosourea derivatives of 3- methyl- 5/7-alkyl-2-(3,4-dichloro)benzoyl-4H-l,4-benzothiazines.

3.1.2. *N*-nitrosation reaction using nitrosyl halides and nitrosonium salts

Due to their higher reactivity, NOX-type nitrosating agents, including nitrosyl halides and nitrosonium salts, have been employed for the synthesis of challenging *N*-nitroso compounds, particularly those derived from sterically hindered secondary amines. Compared with other NO^+ donors, such as sodium nitrite/acid or alkyl nitrites, these reagents offer enhanced efficiency. **[173]**

Most *N*-nitrosation reactions involving nitrosyl halides have been carried out using nitrosyl chloride **(NOCl)**. Meanwhile, the most commonly used nitrosonium salts include tetrafluoroborate **($NOBF_4$)**, hexafluorophosphate, and hydrogen sulfate. These salts can be directly employed as nitrosating agents in organic media. **[174]**

Nitrosyl chloride **(NOCl)** has been utilized for the *N*-nitrosation of sulfamoyloxazolidinones **(II.26)** and sulfamoylperhydrooxazinones **(II.27)** using aqueous LiOH in dichloromethane at 0 °C, as reported by Dewynter et *al*. yielding five new novel *N*-nitrososulfamoyloxazolidinones **(II.28)** and *N*-nitrososulfamoylperhydrooxazinones **(II.29)** derivatives **(Scheme II.5)**. **[175]**

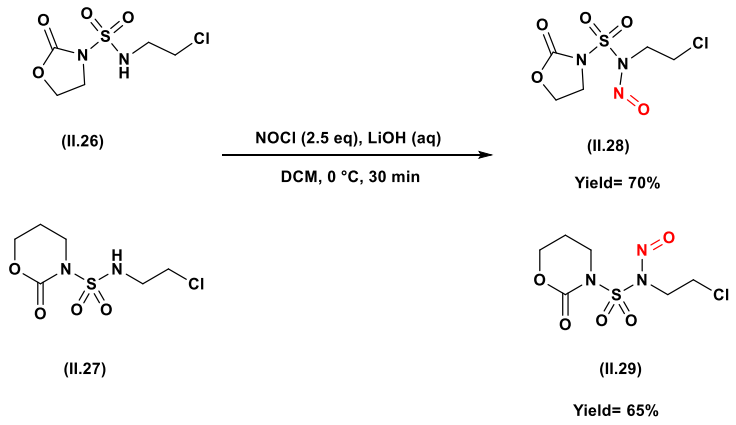

Scheme II.5. Synthesis of new 2-chloroethylnitrososulfamides derivatives.

Following on this strategy, Domarkas et *al*. **[176]** reported the synthesis of analogues of 1-(2-chloroethyl)-1-nitroso-3-(4-(phenylamino)quinazolin-6-yl)urea **(II.31)**, which are also structurally analogous to CENU derivatives. In their approach, nitrosonium tetrafluoroborate **($NOBF_4$)** in acetonitrile, together with a moderate amount of glacial acetic acid at 0 °C, was used for the nitrosation of 1-(2-chloroethyl)-3-(4-(phenylamino) quinazolin-6-yl)urea **(II.30)** **(Scheme II.6)**.

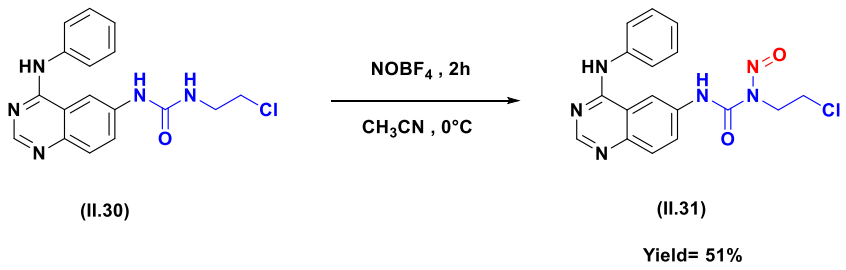

Scheme II.6. Synthesis of a novel combi-nitrosourea analogue.

Other nitrosation methods leading to the formation of *N*-nitroso compounds involve the use of alkyl nitrites, specifically *tert*-butyl nitrite **(TBN)**, **[177]** and organic nitro compounds, including: bromonitromethane, **[178]** trichloronitromethane, **[179]** and

tetranitromethane.**[180]** Additionally, several nitrogen oxides, such as nitrogen monoxide **(NO)**, nitrogen dioxide **(NO_2)**, dinitrogen trioxide **(N_2O_3)**, **[181]** and di-nitrogen tetroxide **(N_2O_4)** are also used as nitrosating agents **(Scheme II.7).[182]**

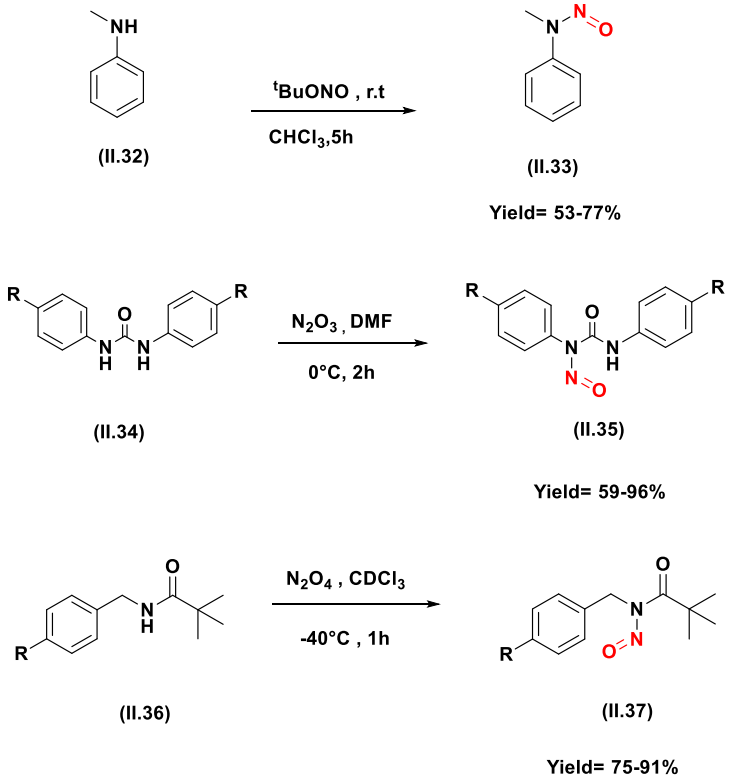

Scheme II.7. Other nitrosation reaction used in the synthesis of *N*-nitroso compounds.

3. Derivatives of *N*-nitroso compounds

N-nitroso compounds, which encompass a wide range of chemically diverse species, are of considerable interest in organic chemistry, pharmacology, and toxicology due to their unique structural characteristics. **[183]** These compounds are primarily classified based on their functional groups and their roles in various fields, with the most studied classes being: ***N*-nitrosamines**, ***N*-nitrosoamides**, ***N*-nitrosoureas**, ***N*-nitrosocarbamates** and ***N*-nitrososulfamides**.

The synthesis of *N*-nitroso derivatives has gained substantial attention due to their significant pharmacological potential, particularly in the development of novel therapeutic agents. **[184]** Among these, *N*-nitrosocarbamates, which are structural analogues of *N*-nitrosoureas, hold great promise due to their bioactivity and ability to act as alkylating agents. The pharmacological implications of these compounds are manifold, making them pivotal not only for therapeutic purposes but also for toxicological assessments. **[185]**

Our research, presented herein, aims to advance the synthetic methodologies for these critical *N*-nitroso derivatives, particularly *N*-nitrosocarbamates, to explore their potential applications in medicinal chemistry.

3.1. *N*-nitrosoureas

Nitrosoureas were identified in the 1950s as a crucial class of alkylating agents with promising anticancer properties, particularly for the treatment of brain tumors and leukemias **(Figure II.6). [186]** Their high lipophilicity allows them to effectively penetrate the blood-brain barrier, making them particularly effective against central nervous system malignancies. **[187]**

Interest in these compounds was reinforced by the discovery of 1-methyl-2-nitro-1-nitrosoguanidine **(MNNG) (II.38)**, whose anticancer activity laid the foundation for the development of nitrosourea-based drugs. **[188]** In this context, the National Cancer Chemotherapy Service Center **(NCCSC)** in the United States, in collaboration with the Southern Research Institute **(SRI)** and the Sloan-Kettering Cancer Center, conducted extensive research that led to the synthesis of 1-methyl-1-nitrosourea **(MNU) (II.39)** in 1961. This compound demonstrated significant efficacy against L1210 murine leukemia and exhibited potential for the treatment of brain tumors.**[189]** However, its limited chemical stability and pharmacological drawbacks prompted the development of a more stable and potent analogue, 1,3-bis(2-chloroethyl)-1-nitrosourea **(BCNU, carmustine) (II.40)**. In 1963, T.P. Johnston and J.A. Montgomery at **SRI** replaced the methyl group of **MNU** with a 2-chloroethyl moiety, significantly enhancing its anticancer efficacy. **[190]** Following clinical trials conducted by the National Cancer Institute **(NCI)** in 1965, carmustine was approved by the **FDA** in 1977 as a treatment for brain tumors and remains a key therapeutic agent in this field. **[191]**

To improve bioavailability and reduce adverse effects, several derivatives have been developed, including lomustine **(CCNU) (II.41)** and streptozotocin **(STZ) (II.42)**. **[192]** The latter, being more hydrophilic and less toxic to the bone marrow, has demonstrated promising efficacy against pancreatic islet cell tumors. **[193]** Among the third-generation nitrosoureas, fotemustine **(Muphoran®) (II.43)** was designed for the treatment of disseminated malignant melanoma. However, its clinical application is somewhat restricted due to its toxicity and the acquired resistance of cancer cells. **[194]**

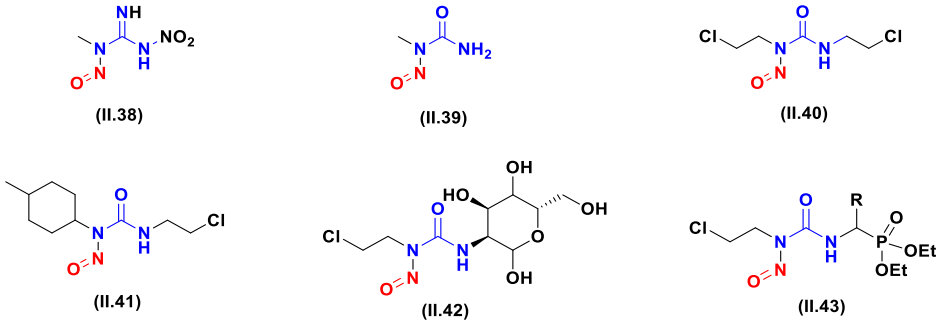

Figure II.6. Structures of *N*-nitrosourea drugs.

3.1.1. Mechanism of action of 2-chloroethylnitrosoureas as alkylating agents

Nitrosoureas exert their antitumor activity through a spontaneous decomposition process that generates two highly reactive electrophilic intermediates: 2-chloroethyldiazene hydroxide **(II.45)** and isocyanate **(II.46) (Scheme II.8). [195]**

2-chloroethyldiazene hydroxide plays a crucial role in DNA alkylation by forming adducts with several nucleobases, specifically, alkylation at the O^6 position of guanine **(II.49)** leads to the formation of a monoalkylated product that undergoes rearrangement to create interstrand cross-links between O^6-guanine and a complementary cytosine residue **(II.52)**. **[196]**

This cross-linking process occurs relatively slowly, allowing the activation of DNA repair mechanisms, particularly the O^6-alkylguanine alkyltransferase enzyme, which counteracts the cytotoxic effects of nitrosoureas. **[197]**

Additionally, nitrosoureas containing a 2-chloroethyl moiety function as DNA cross-linking agents, inducing structural damage that disrupts replication and transcription. Concurrently, the decomposition of nitrosoureas releases isocyanates, which react with lysine residues in proteins **(II.54)**, leading to carbamoylation and inhibition of key enzymes involved in DNA repair and RNA processing. **[198]**

Furthermore, isocyanates **(II.46)** contribute to a reduction in glutathione levels, potentially enhancing cellular sensitivity to DNA damage caused by alkylation. The combined effects of DNA alkylation and protein carbamoylation underlie the cytotoxic and anticancer properties of 2-chloroethyl nitrosoureas. **[199]**

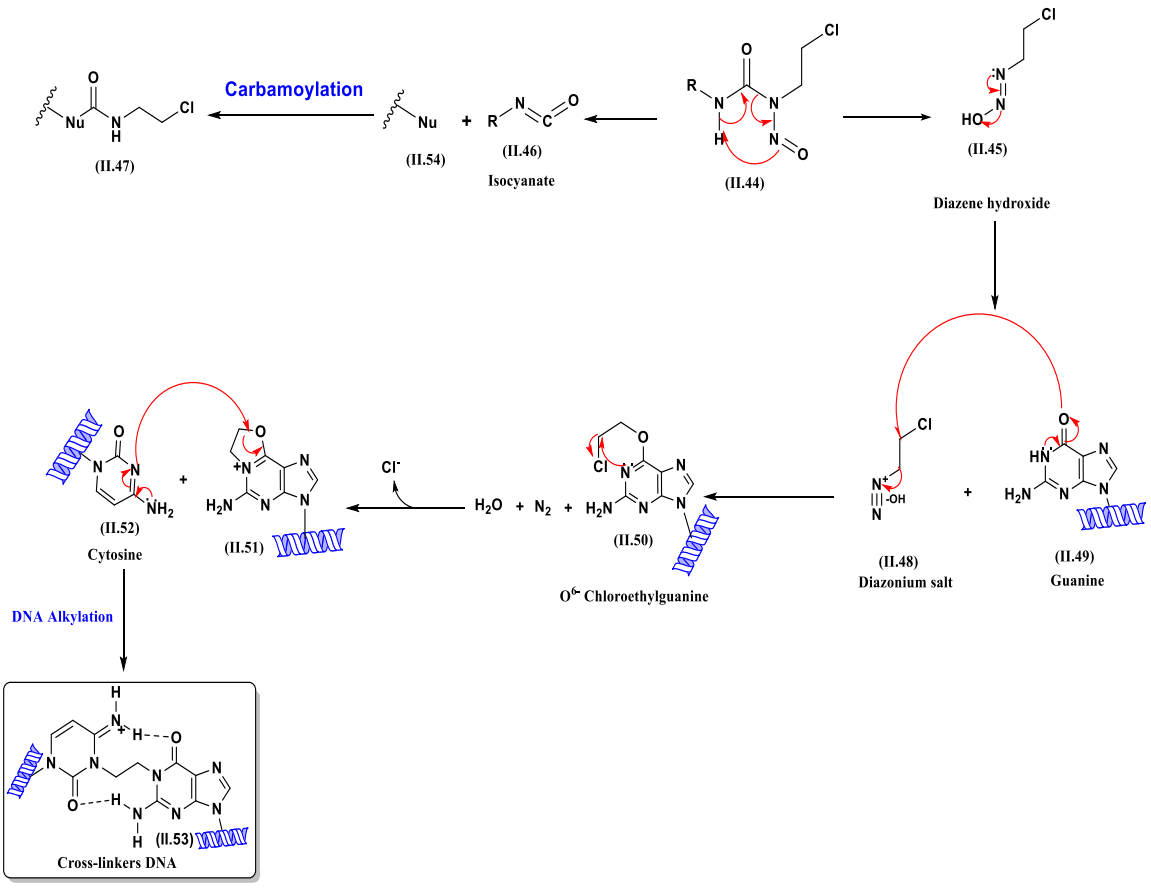

Scheme II.8. DNA cross-linking by nitrosoureas.

3.1.2. Synthetic pathways of nitrosourea and analogues

3.1.2.1. Synthesis of chloroethyl-nitrosoureas (CENU)

Chloroethyl-nitrosoureas **(CENU)** represent a crucial class of alkylating agents extensively studied for their therapeutic potential, particularly in the treatment of brain tumors and lymphomas. **[200]** Jaman et *al.* **[201]** developed an innovative approach for the synthesis of lomustine **(II.57)** using a continuous-flow methodology. This strategy was optimized through desorption electrospray ionization mass spectrometry **(DESI-MS)**, enabling rapid screening of reaction conditions and their efficient translation into continuous production. As a result, lomustine **(II.57)** was obtained with an overall yield of 63% in just 9 minutes, compared to over two hours under conventional batch conditions, while also improving the product's purity **(Scheme II.9).**

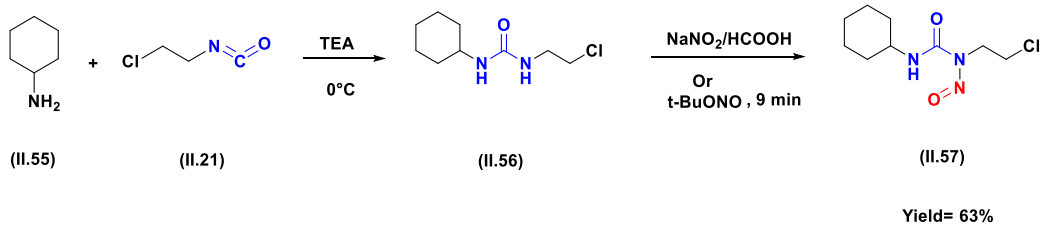

Scheme II.9. Synthesis of chloroethyl-nitrosoureas (CENU) analogues of lomustine.

3.1.2.2. Synthesis of new nitrosoureas containing tyrosine derivative (TNUs)

Tyrosine, a non-essential amino acid derived from phenylalanine, plays a crucial role in various biological processes, including the biosynthesis of neurotransmitters and melanin. **[202]** Its structural versatility makes it an attractive scaffold for the design of bioactive molecules. In particular, the incorporation of tyrosine derivatives into nitrosourea compounds has gained interest due to their potential as selective alkylating agents with improved therapeutic profiles.

In this context, Gadjeva et *al*. **[203]** synthesized a novel series of nitrosoureas containing tyrosine derivatives **(TNUs) (II.61)** using two distinct synthetic pathways. In the first approach, tyrosine-derived amino esters **(II.58)** were condensed with 2-chloroethylisocyanate **(II.21)** in tetrahydrofuran **(THF)** at **0°C**, followed by nitrosation of the resulting urea intermediates, yielding the target **TNUs** with a yield of **72%**. The second strategy involved a regioselective transfer method, where the nitroso-functionalized chloroethyl moiety was directly introduced onto the tyrosine ester using *N*-hydroxysuccinimide-*N*-(2-chloroethyl)-*N*-nitrosocarbamate **(II.60)** as a transfer reagent. This alternative route provided high yields and improved selectivity. The synthesized **TNUs** were subsequently subjected to biological evaluation, demonstrating potent *in vitro* activity with enhanced selectivity and reduced toxicity toward melanoma and lymphocyte cells compared to lomustine, the reference compound **(Scheme II.10).**

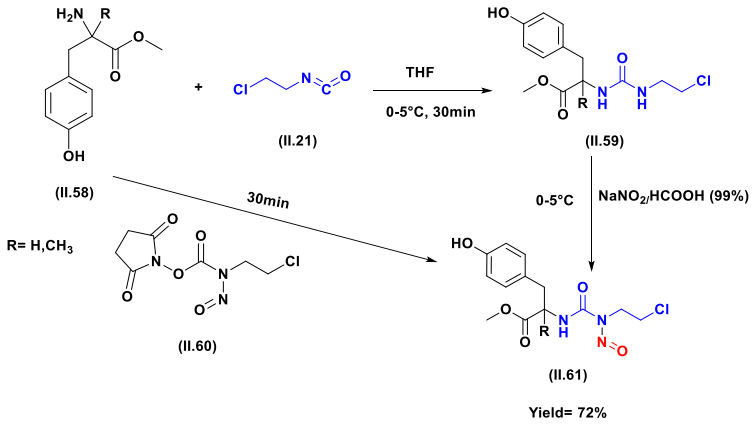

Scheme II.10. Synthesis of nitrosoureas containing tyrosine derivatives.

3.1.2.3. Synthesis of a new combi-nitrosourea (BGCNU)

Combi-nitrosoureas represent a promising class of alkylating agents designed to enhance anticancer efficacy by simultaneously targeting **DNA** and key repair mechanisms. Among

these, **BGCNU** has garnered significant attention due to its dual action, combining a **DNA** cross-linking moiety with an inhibitor of O^6-alkylguanine-DNA alkyltransferase **(AGT)**, a key enzyme involved in **DNA** repair that often confers resistance to nitrosourea-based treatments. **[204]**

In this context, Sun et *al*. **[205]** reported the synthesis of a novel combi-nitrosourea prodrug, 3-(3-(((2-amino-9H-purin-6-yl)oxy)methyl)benzyl)-1-(2-chloroethyl)-1-nitrosourea **(II.68)**, designed to simultaneously release a **DNA** cross-linking agent and an **AGT** inhibitor. This compound demonstrated enhanced cytotoxicity against mer^+ glioma cells compared to conventional nitrosoureas such as **ACNU** and **BCNU**, as well as their respective combinations with O^6-benzylguanine (**O^6-BG**) **(Scheme II.11).**

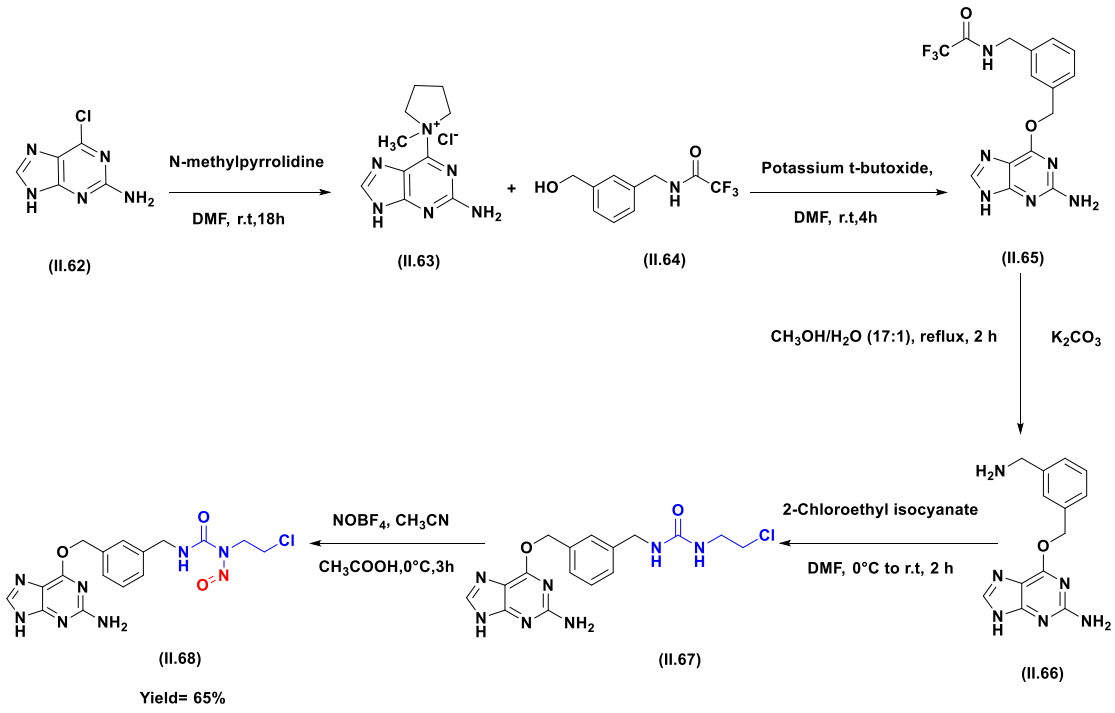

Scheme II.11. Synthesis a novel combi-nitrosourea as an inhibitor of O^6-alkylguanine-DNA alkyltransferase.

Similarly, Wang et *al*. **[206]** synthesized and evaluated **BGCNU**, a novel combi-nitrosourea incorporating an **O^6-BG** pharmacophore **(II.75)**. This modification significantly increased its cytotoxic potency and DNA interstrand cross-linking efficiency by effectively inhibiting **AGT** activity in **AGT^+** cells, thereby overcoming a major resistance mechanism associated with traditional nitrosourea-based chemotherapies. These findings highlight the potential of combi-nitrosoureas as next-generation chemotherapeutic agents with improved efficacy against resistant tumor cells **(Scheme II.12).**

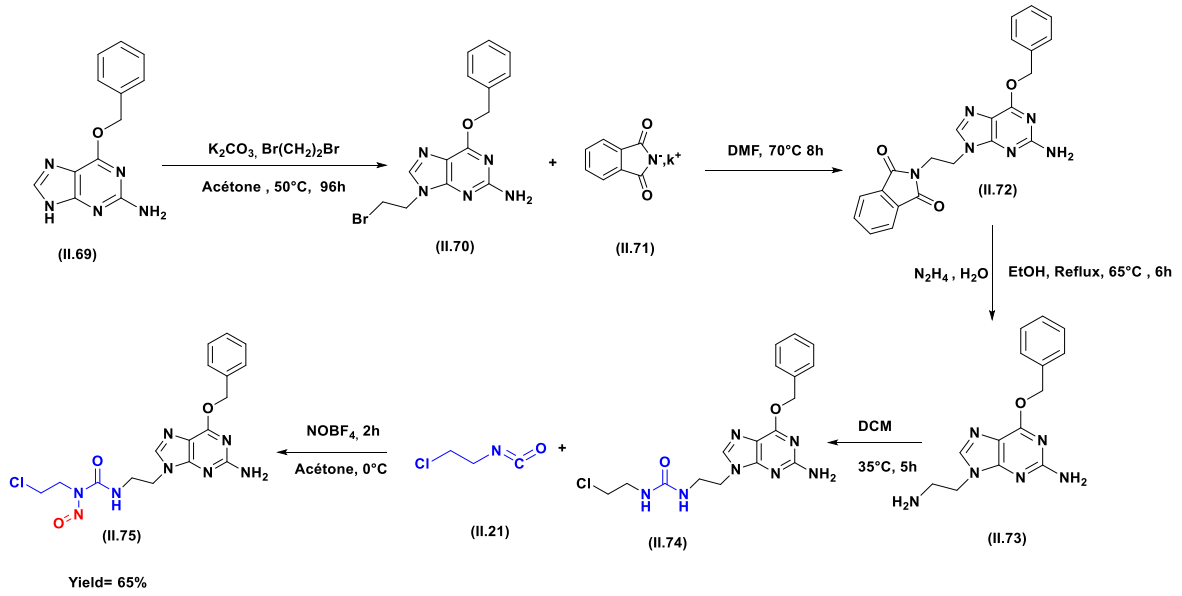

Scheme II.12. Synthesis of a novel combi-nitrosourea incorporating an O^6-BG pharmacophore

3.1.2.4. Synthesis of chloroethylnitrososulfamide analogs (CENS)

N-nitrososulfamide analogues, particularly 2-chloroethylnitrososulfamides (CENS), have garnered increasing interest due to their promising antitumor properties. Their unique hybrid chemical structure, which combines the characteristics of nitrosoureas and sulfamides, offers significant therapeutic potential, particularly in the treatment of various cancer types. **[206]** The first reported synthesis of **CENS** compounds was reported by Dewynter et *al*. in 1991, marking a key milestone in their exploration for therapeutic applications .**[207]** Over the following years, nearly twenty publications described the synthesis, biological evaluation, kinetic studies, and chemical decomposition of various **CENS** compounds.

In 1996, Abdaoui et *al*. **[208]** improved this synthesis by introducing a four-step method using CSI **(II.76)** as the starting reagent. This approach, which involved carbamoylation, sulfamoylation, Mitsunobu alkylation, deprotection, and finally nitrosation, enabled the production of **CENS (II.83)** compounds with yields ranging from **71%** to **88% (Scheme II.13)**.

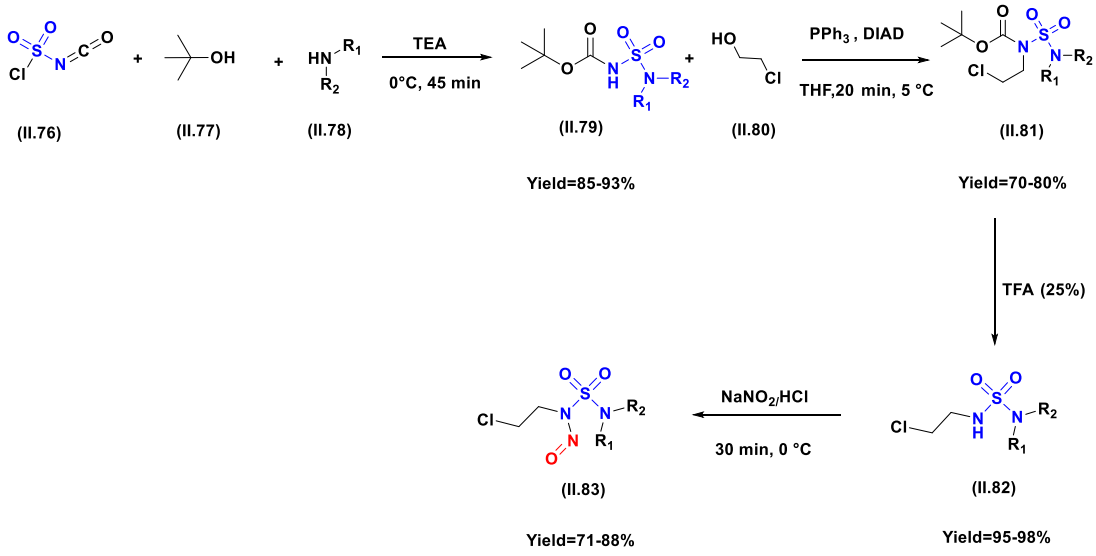

Scheme II.13. Synthesis of new family of 2-chloroethylnitrososulfamides (CENS).

In 2003, Winum et *al*. **[209]**synthesized new CENS analogues and evaluated their antitumor activity against melanoma cell lines. These compounds demonstrated superior efficacy compared to fotemustine, particularly against the **A375** cell line, known for its chemoresistance due to **MGMT** expression. Subsequently, diethyl aminomethylphosphonate **(II.84)**, obtained by reduction of the corresponding 1-hydroxyiminophosphonate, was subjected to sulfamoylation with *tert*-butoxysulfamoyl chloride to give compound **(II.85)**, which then reacted with 2-chloroethanol under Mitsunobu conditions to yield a mixture of compounds **(II.86)** and **(II.88)**. From compound **(II.88)**, Boc-deprotection afforded an intermediate sulfamide that, upon nitrosation, led to compound **(II.90)**, unstable and difficult to isolate; to improve its stability, N-methylation of **(II.88)** was performed to provide compound **(II.89)**, which, after Boc-deprotection and nitrosation, furnished compound **(II.91)** as a yellow oil. In parallel, compound **(II.86)** afforded the target compound **(II.87)** as a single product after Boc deprotection and nitrosation **(Scheme II.14)**.

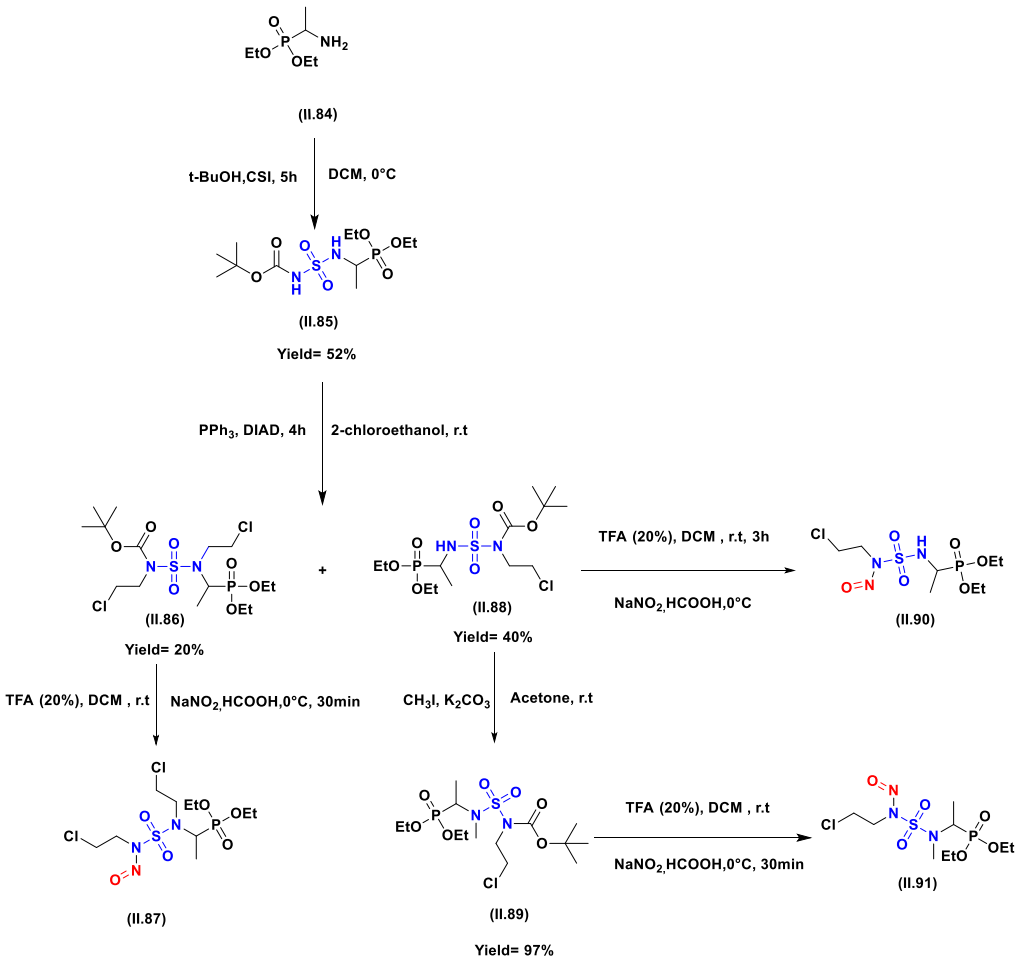

Scheme II.14. Synthesis of new analogues of Fotemustine

3.2. *N*-Nitrosocarbamates

Chloroethylnitrosoureas **(CENU)** are widely used alkylating agents in anticancer chemotherapy due to their ability to induce irreversible DNA damage, primarily through inter- and intra-strand cross-linking mediated by the chloroethyl cation. **[210]** However, their clinical application is limited by significant hematological toxicity, including cumulative thrombocytopenia and leukopenia. **[211]** Additionally, their spontaneous degradation in aqueous solution releases isocyanates, leading to protein carbamoylation, which further contributes to their adverse effects. To overcome these limitations, research has focused on developing novel analogues that retain the cytotoxic efficacy of **CENU** while minimizing toxicity. **[212]** In this context, our work aims to synthesize and evaluate new *N*-nitrosocarbamates analogues inspired by carmustine and fotemustine to optimize their therapeutic potential.

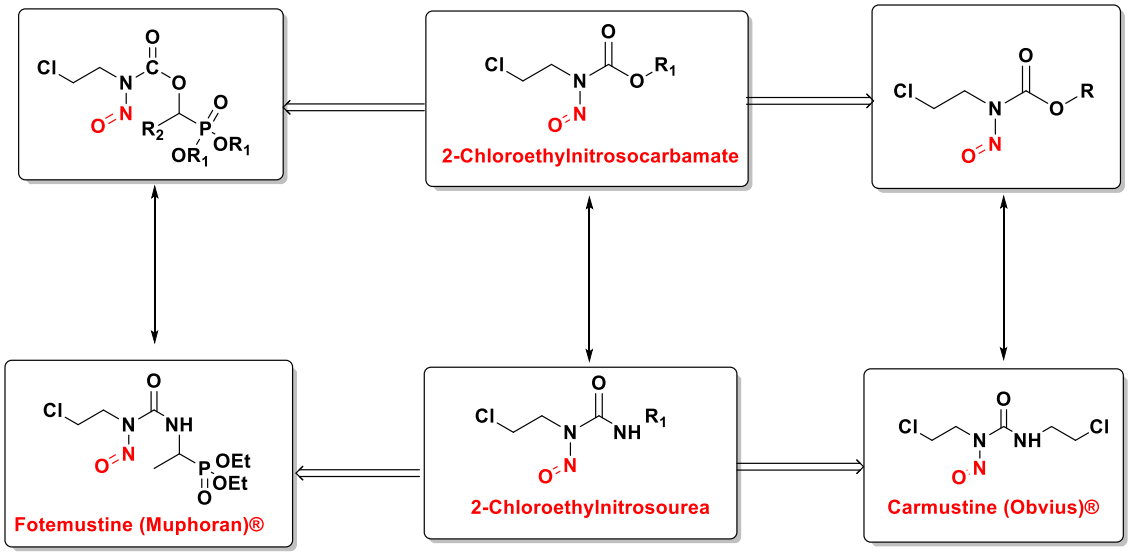

Figure II.7. Structural analogies between Chloroethylnitrosoureas (CENU) and Chloroethylnitrosocarbamates (CENC)

3.2.1. Synthetic methods for *N*-nitrosocarbamate derivatives

On the one hand, the potential to develop analogues with pharmacological effects similar to those of well-established nitrosourea drugs, such as fotemustine and carmustine, and on the other hand, to reduce the associated toxicity, remains a major area of interest. In this regard, several synthetic strategies have been described in the literature to access *N*-nitrosocarbamates.

A promising approach involves replacing the urea moiety with a carbamate group, yielding several analogues of 2-chloroethylnitrosocarbamates **(CENS)**. **(II.94, II.97)** These compounds generate the same alkylating species *in vivo*, responsible for their anticancer activity, while preventing the release of isocyanates, thereby reducing protein-associated toxicity as reported by Reynolds et *al*.**[213]** These compounds were designed to incorporate functional groups that enhance aqueous solubility or act as prodrugs, thereby improving their bioavailability. Among them, ethyl (2-chloroethyl)-*N*-nitrosocarbamate **(II.94, II.97)** demonstrated significant activity against multiple human tumor cell lines, with IC_{50} values ranging from 1 to 10 µg/mL. Furthermore, the structural similarities between these analogues and clinically established nitrosourea-based drugs underscore the continued interest in this class of compounds.

From a synthetic perspective, Reynolds et *al*. proposed two distinct approaches to access (2-chloroethyl)-nitrosocarbamate analogues **(II.94, II.97)**. The first strategy involves the selective acetylation of the phenol group in 4-hydroxybenzyl alcohol **(II.92)** using the method developed

by Paradisi et *al*,**[214]** followed by a reaction with 2-chloroethyl isocyanate **(II.21)** and subsequent nitrosation, yielding the target compound with high overall efficiency **(Scheme II.14)**.

The second approach utilizes commercially available nitrobenzyl alcohols **(II.95)** and heterocyclic bases such as 5-hydroxypyrimidine and 3-hydroxypyridine. These intermediates undergo carbamoylation followed by nitrosation, leading to a series of conjugated (2-chloroethyl)-*N*-nitrosocarbamate analogues **(II.97)**. This methodology has expanded the structural diversity of the synthesized compounds, enabling further evaluation of their potential anticancer activity **(Scheme II.15)**.

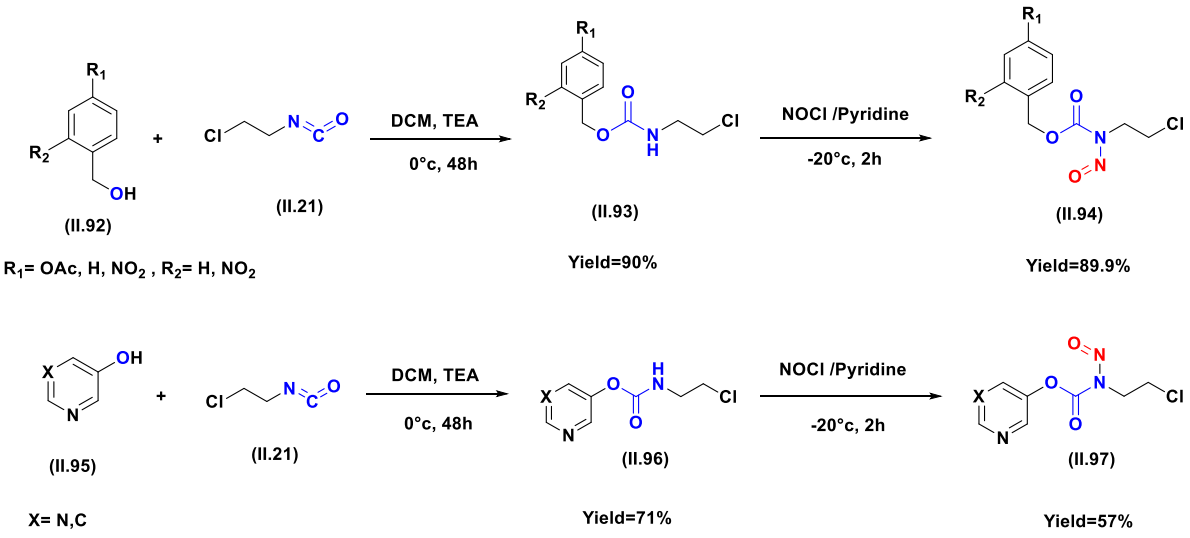

Scheme II.15. Pathways for the synthesis of several new *N*-(2-chloroethyl) nitrosocarbamates.

4. Conclusion

This chapter provides a comprehensive review of *N*-nitroso compounds, with a particular focus on nitrosoureas and *N*-nitrosocarbamates. We explore their chemical properties, reactivity, and applications as alkylating agents in chemotherapy, particularly in the treatment of brain tumors and leukemias. The analysis of their mechanisms of action highlights their ability to induce DNA cross-linking, a key feature underlying their anticancer activity.

Additionally, we examined the main synthetic strategies for these compounds, emphasizing recent advancements aimed at enhancing their selectivity and reducing toxicity. The development of novel analogues, such as nitroso-carbamates, reflects the ongoing pursuit of more effective and better-tolerated structures, optimizing their therapeutic potential.

This scientific analysis serves as a critical foundation for our research, which focuses on the design and synthesis of new nitrosourea and nitroso-carbamates derivatives.

Chapter III

Results and discussion

1. Synthesis and characterization of xanthene derivatives

1.1. Introduction

In the framework of developing a new approach based combining the synergistic effect of sonochemistry and catalysis, the synthesis of xanthene moiety was carried out by the condensation of two equivalents of dicarbonyl compounds **(**1,3-cyclohexanedione or dimedone**)** with various aromatic aldehydes in the presence of zinc acetate $Zn(OAc)_2$ as a heterogeneous catalyst in ethanol. The reaction mixture was then subjected to ultrasound irradiation to enhance molecular activation and reaction efficiency. These reaction conditions were achieved after optimizing a model reaction **(**dimedone **(I.61)** and benzaldehyde **(I.62))** as indicated in the table **(III.1)**.

1.2. Optimization of reaction conditions

Initially, we aimed to determine the optimal parameters for this reaction, including catalyst loading, solvent influence, and sonochemical effects, to obtain the desired product with the best possible yield in the shortest time. The reaction between benzaldehyde **(I.61)** and dimedone **(I.62) (Scheme III.1)** was selected as a model reaction to optimize the reaction conditions.

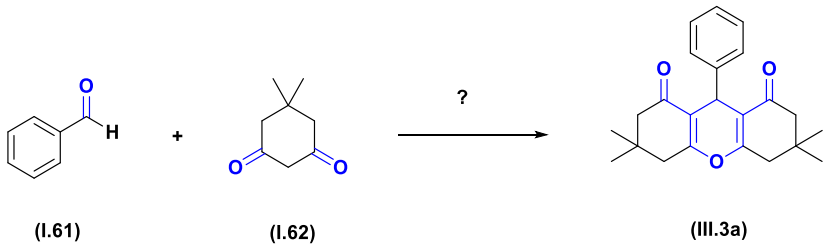

Scheme III.1. Model reaction for the synthesis of xanthene derivatives.

At first, the reaction was conducted without a catalyst or solvent, using ultrasound irradiation **(40 kHz)** at room temperature. Only trace amounts of the desired product **(III.3a)** were obtained after an extended reaction time **(entry 1, Table III.1)**.

Given the growing interest in heterogeneous catalysts, we selected zinc acetate **$Zn(OAc)_2$** due to its commercial availability, low cost, and environmental friendliness. We tested various concentrations of zinc acetate **(2 mol%, 5 mol%, 10 mol%, and 15 mol%)** in our study **(entries 2-5, Table III.1)**. The results indicated that the reaction was less effective at **2 mol%** or **5 mol%** concentration of the catalyst, even with extended reaction times. Conversely,

using **10 mol%** or **15 mol%** catalyst concentrations yielded good results. Therefore, a **10 mol%** concentration of **$Zn(OAc)_2$** is sufficient to effectively promote the reaction.

To examine the effect of the solvent, the model reaction was repeated using **10 mol% $Zn(OAc)_2$** in various solvents such as dichloromethane, tetrahydrofuran, toluene, acetonitrile, water, and ethanol. A significant improvement in yield **(70-87%)** was observed after 30 minutes. Ethanol proved to be the most effective solvent for the reaction, providing the highest product yield.

Additionally, the effect of temperature was investigated under different temperature settings. The results showed that the reaction proceeded efficiently at **60°C** in **15** minutes under ultrasonic irradiation, compared to **40°C** and room temperature.

Finally, to evaluate the impact of ultrasonic irradiation on this reaction, the synthesis of **(III.3a)** was carried out using **10 mol% $Zn(OAc)_2$** in ethanol in the absence of ultrasonic irradiation, both at room temperature and under refluxing **(Entries 14 and 15, table III.1.)**. Without sonication, the yield of product **(III.3a)** at **60°C** was low **(35%)**, and at room temperature, the reaction did not proceed.

Table III.1. Optimization reaction conditions of benzaldehyde and dimedone.

Entry	Catalyst (mol %)	Solvants	Conditions	Times (min) / Yields %
1	Catalyst-free	Neat	US (40 kHz), rt	240/trace
2	$Zn(OAc)_2$ (2 mol %)	Neat	US (40 kHz), rt	120/25
3	$Zn(OAc)_2$ (5 mol %)	Neat	US (40 kHz), rt	120/50
4	$Zn(OAc)_2$ (10 mol %)	Neat	US (40 kHz), rt	120/69
5	$Zn(OAc)_2$ (15 mol %)	Neat	US (40 kHz), rt	120/69
6	$Zn(OAc)_2$ (10 mol %)	DCM (2 mL)	US (40 kHz), rt	30/78
7	$Zn(OAc)_2$ (10 mol %)	THF (2 mL)	US (40 kHz), rt	30/71
8	$Zn(OAc)_2$ (10 mol %)	Toluene (2 mL)	US (40 kHz), rt	30/74
9	$Zn(OAc)_2$ (10 mol %)	ACN (2 mL)	US (40 kHz), rt	30/70
10	$Zn(OAc)_2$ (10 mol %)	Water (2 mL)	US (40 kHz), rt	30/82
11	$Zn(OAc)_2$ (10 mol %)	EtOH (2 mL)	US (40 kHz), rt	30/87
12	$Zn(OAc)_2$ (10 mol %)	EtOH (2 mL)	US (40 kHz), 40 °C	15/90
13	**$Zn(OAc)_2$ (10 mol %)**	**EtOH (2 mL)**	**US (40 kHz), 60 °C**	**15/95**
14	$Zn(OAc)_2$ (10 mol %)	EtOH (2 mL)	Without US (agitation, rt)	120/trace
15	$Zn(OAc)_2$ (10 mol %)	EtOH (2 mL)	Without US (agitation, reflux)	120/35

Based on these results, the synthesis of 1,8-dioxo-octahydroxanthene derivatives was developed under the previously reported conditions, utilizing the efficiency and versatility of the combined $Zn(OAc)_2$/ultrasound system. Numerous aromatic aldehydes with various substituents were reacted with dimedone or 1,3-cyclohexanedione under optimal reaction conditions to produce the desired products **(III. 3a-t)** with excellent yields within **15-45** minutes. The resulting products are detailed in **scheme III.2**.

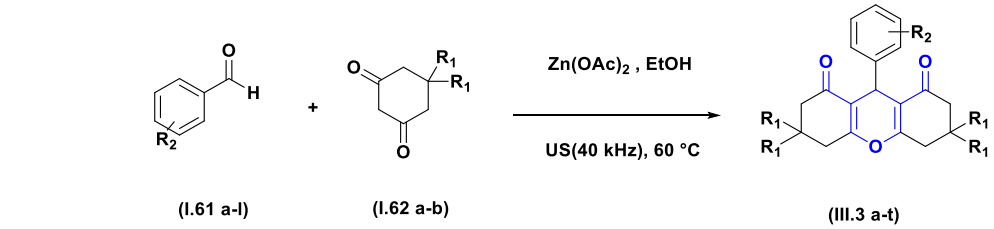

(I.61 a-l) (I.62 a-b) (III.3 a-t)

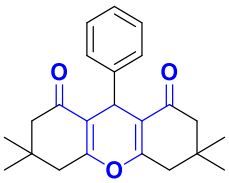

(III.3a)
15min, 95%

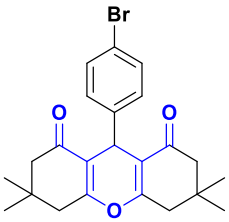

(III.3b)
20min, 93%

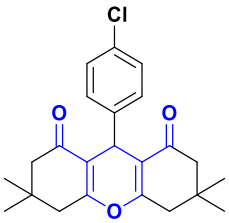

(III.3c)
20min, 94%

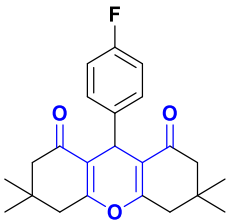

(III.3d)
20min, 92%

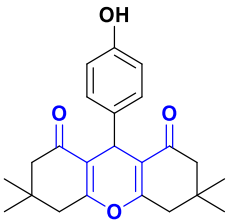

(III.3e)
35min, 88%

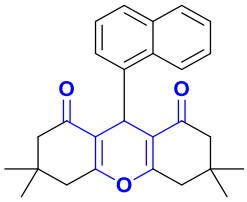

(III.3f)
40min, 89%

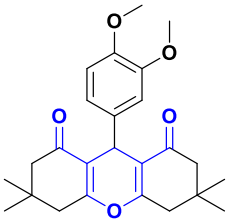

(III.3g)
40min, 86%

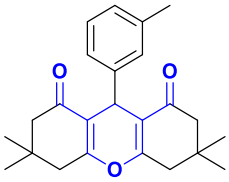

(III.3h)
35min, 89%

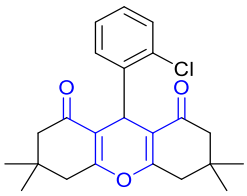

(III.3i)
30min, 87%

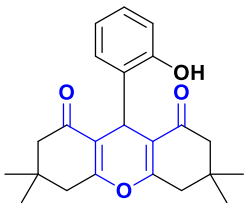

(III.3j)
45min, 84%

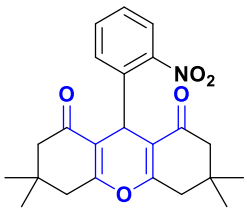

(III.3k)
40min, 85%

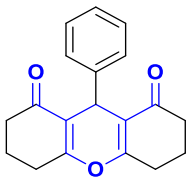

(III.3l)
15min, 94%

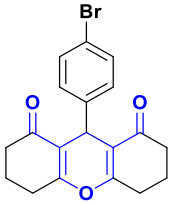

(III.3m)
20min, 91%

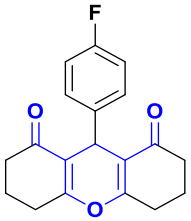

(III.3n)
20min, 92%

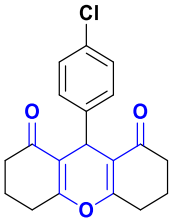

(III.3o)
25min, 93%

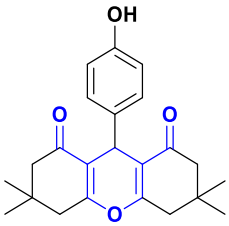

(III.3p)
25min, 89%

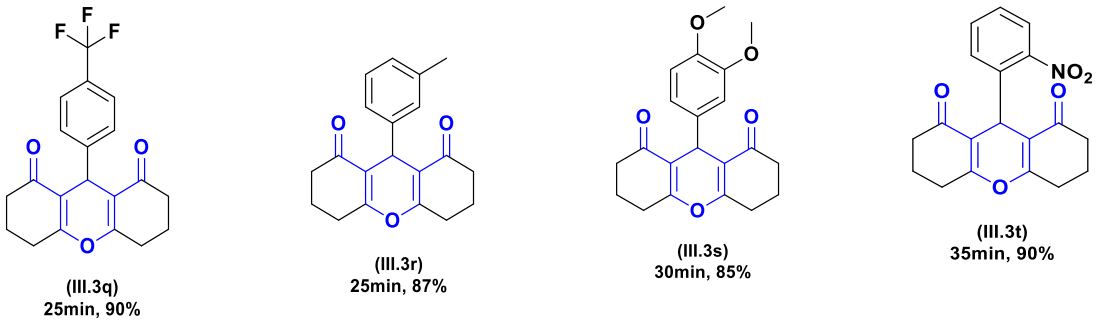

Scheme III.2. Synthesized derivatives of xanthene.

A remarkable influence on the reaction yield was observed because of electron-withdrawing and electron-donating substituents on the aromatic ring of the aldehydes. The highest yields **(90-94%)** were obtained for aldehydes with electron-withdrawing groups compared to those with electron-donating substituents.

Additionally, aldehydes substituted at the *para* position were found to be more reactive than those at the *ortho* and *meta* positions. The highest yield **(95%)** was achieved with benzaldehyde **(III.3a)** after **15** minutes, while the lowest yield **(84%)** was observed with 2-hydroxybenzaldehyde **(III.3j)** after **45** minutes.

1.3. Mechanistic proposal

The proposed mechanism is illustrated in **scheme III.3** for the synthesis of xanthene derivatives using **$Zn(OAc)_2$**. First, acoustic cavitation facilitates the coordination and activation of **$Zn(OAc)_2$** with aldehyde, generating the zinc-aldehyde intermediate **(A)**. This intermediate reacts with dimedone or 1,3-cyclohexanedione to form intermediate **(B)** through dehydration and elimination of **$Zn(OAc)_2$**. Next, intermediate **(B)** undergoes a nucleophilic attack by the **C=C** bond of the second molecule of dimedone or 1,3-cyclohexanedione through a conjugate Michael addition, forming intermediate **(C)**. This intermediate then undergoes intramolecular cyclization with the elimination of **H_2O** and **$Zn(OAc)_2$**, to afford the final products **(D)**.

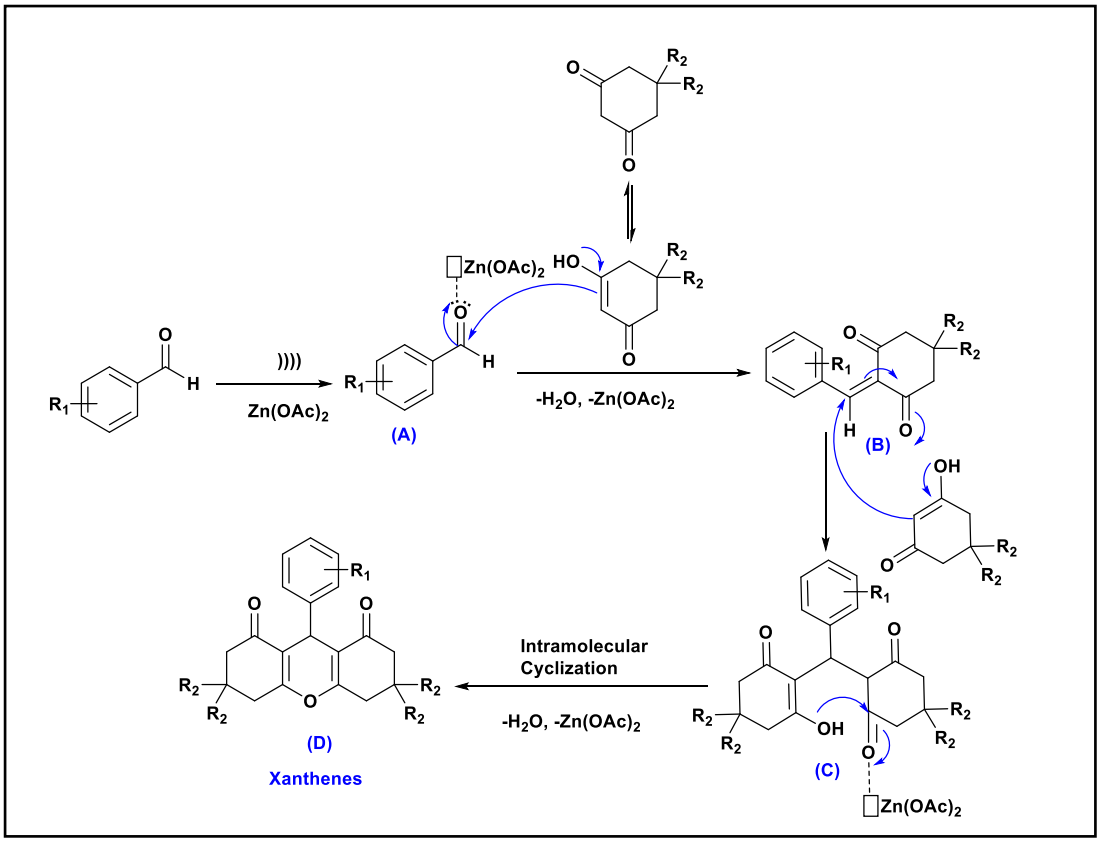

Scheme III.3. Proposed mechanism for the synthesis of xanthene derivatives.

1.4. Spectral characterization of xanthene

The identification of the prepared xanthene structures was carried out using the usual spectroscopic analysis techniques: **^{1}H NMR, ^{13}C NMR, IR.**

In ^{1}H NMR, the spectral analysis of compound **(3a)**, for example, shows the appearance of two singlets corresponding to the methyl protons of dimedone at **0.99** and **1.10** ppm. A quartet and a singlet characteristic of the methylene protons **(2CH$_2$-C=C)**, **(2CH-CO)** with an integration of **4H** resonate between **2.12-2.20** ppm and **2.46** ppm, respectively. The proton of the asymmetric carbon **(*CH)** appears at **4.75** ppm as a singlet, and the aromatic protons are observed in the usual region at **7.09-7.29** ppm.

In ^{13}C NMR, the spectral analysis of compound **(III.3a**) shows that, the methyl carbon appear at **[27.5-29.4]** ppm. Similarly, the methylene carbons resonate at **[31.9-32.3]** ppm. The asymmetric carbon appears at **41.0** ppm, and the signals of the aromatic carbons appear in the usual region at **[126.4-144.2]** ppm. In addition, the carbonyl carbon appears as a distinct peak at approximately **196.4** ppm.

In IR, the structure is confirmed by the presence of the carbonyl group **(CO)** group at **1667** cm^{-1}and **(C=C)** bonds absorbing at **1485** cm^{-1}.

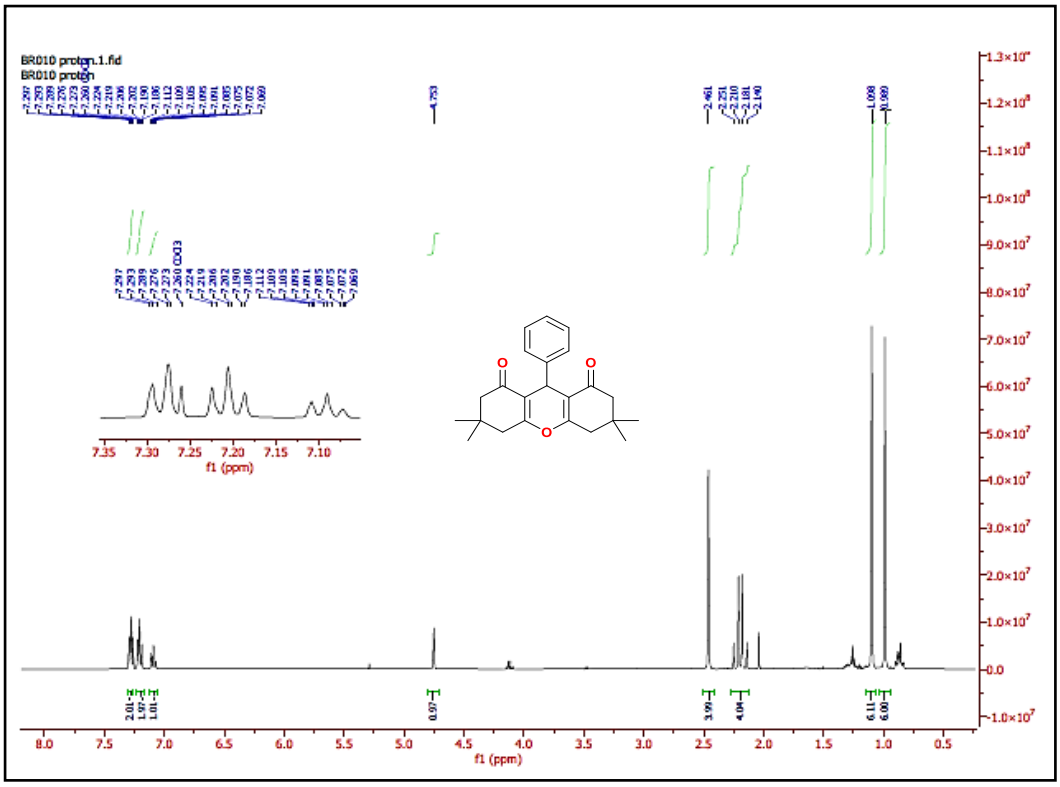

Figure III.1. ^{1}H NMR spectra of 3,3,6,6-tetramethyl-9-phenyl-3,4,5,6,7,9-hexahydro-1H-xanthene-1,8(2H)-dione (III.3a).

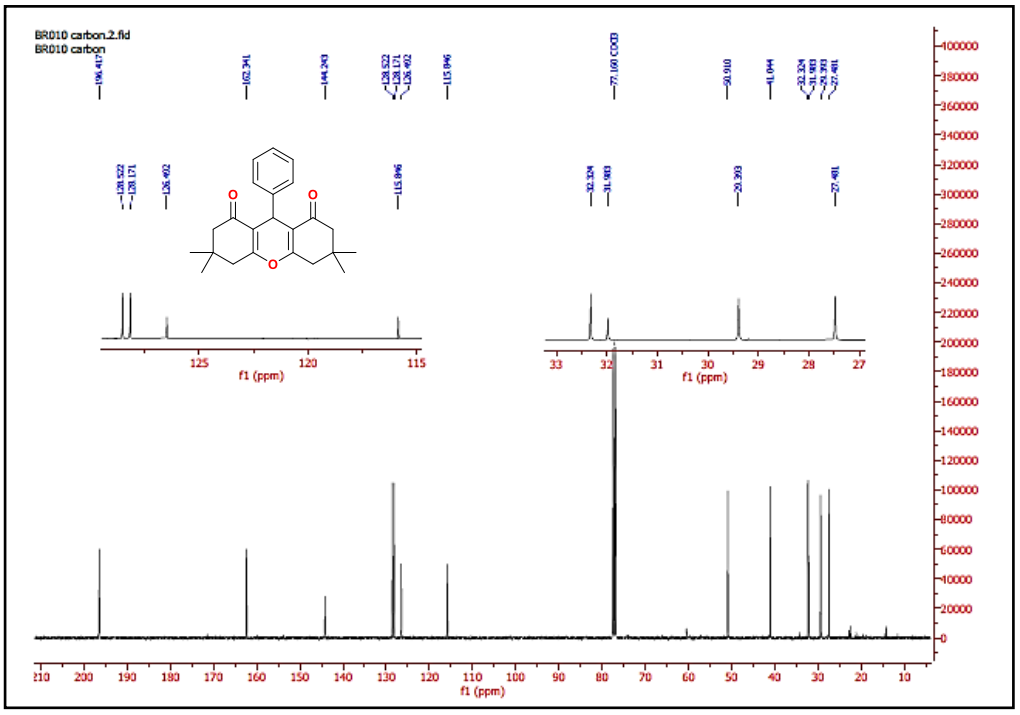

Figure III.2. ^{13}C NMR spectra of (3,3,6,6-tetramethyl-9-phenyl-3,4,5,6,7,9-hexahydro-1H-xanthene-1,8(2H)-dione (III.3a)

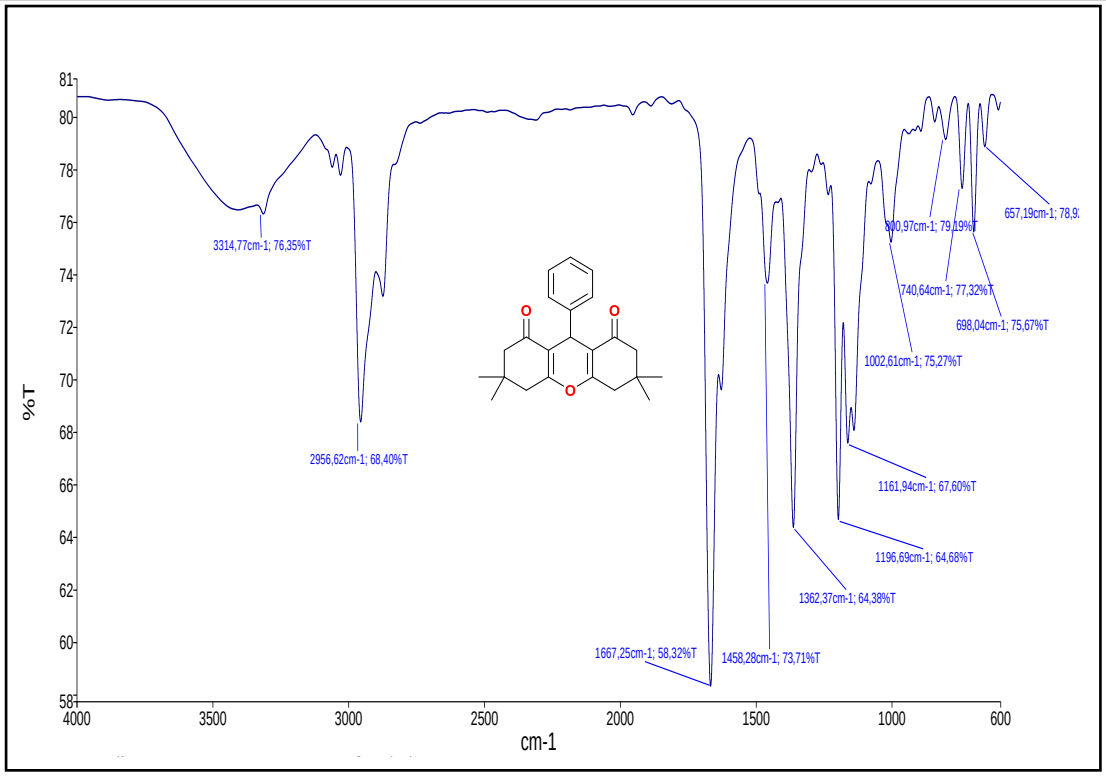

Figure III.3. IR spectra of 3,3,6,6-tetramethyl-9-phenyl-3,4,5,6,7,9-hexahydro-1H-xanthene-1,8(2H)-dione (III.3a).

1.5. Crystallographic study for compound III.3r

Suitable crystals of compound **(III.3r)** were obtained by crystallization in diethyl ether/*n*-hexane and were subjected to X-ray diffraction analysis to fully determine its structural composition.

As displayed in the ORTEP diagram represented in **figure III.4**, the asymmetric unit of the crystal structure comprises one molecule of compound 9-(*m*-tolyl)-3,4,5,6,7,9-hexahydro-1H-xanthene-1,8(2H)-dione, which crystallizes in the orthorhombic system with the Pca21 space group.

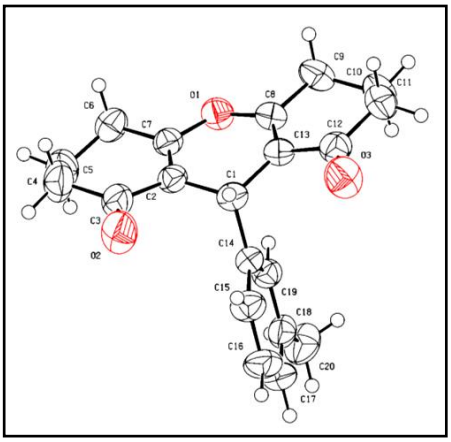

Figure III.4. ORTEP diagram of compound (III.3r).

No conventional hydrogen bonds were observed since there is no hydrogen linked to an electronegative heteroatom. However, several short contacts were noticed **(Table III.2)** in the structure that contribute to the linkage of the crystal components including intermolecular contacts of type C-H…O with lengths ranging between 2.609 and 2.654 Å, and C-H…C with a length of 2.847 Å. A crystal-packing diagram was built using Mercury software **(Figure III.5)**, which shows a general view of the arrangement of the molecules that constitutes the crystal structure.

Table III.2. Short contacts in the crystal structure of compound 3r.

D-H…A	*d*(D-H)	*d*(H…A)	*d*(D-A)	D-H-A	Symmetry
C_9-H_9A…O_2	0.970	2.613	3.416(5)	140.2	x,y,z ; 1-x,1-y,-1/2+z
C_{11}-$H_{11}B$…O_2	0.970	2.654	3.488(5)	144.3	x,y,z ; 1-x,1-y,-1/2+z
C_6-H_6B…O_3	0.970	2.609	3.432(4)	142.8	x,y,z ; 1-x,1-y,-1/2+z
C_{15}-H_{15}…C_{13}	0.930	2.847	3.702(4)	153.2	x,y,z ; 1-x,1-y,-1/2+z

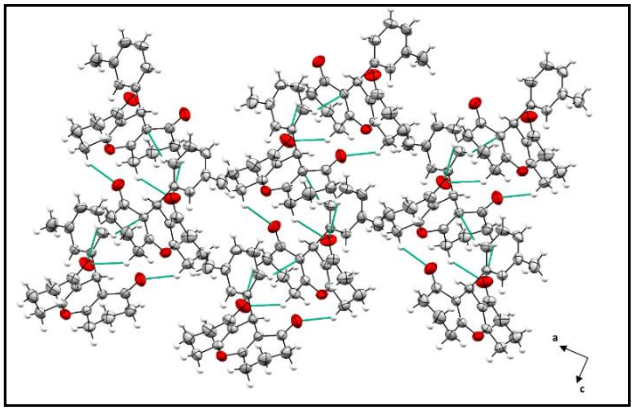

Figure III.5. Crystal packing diagram viewed along (b) axis represented as ellipsoids drawn at 40% probability level. Contacts are represented as green dashed sticks.

A general comparison between the structure of compound **III.3r** and some previously reported xanthene derivatives with different substituents in various positions indicates resemblances in geometry, bond lengths, and bond angles.**[215]** The bond lengths in the structure closely match those of analogous cyclohexanedione and dimedone-based xanthene compounds. For instance, the carbonyl bond lengths of the cyclohexanone ring, C3-O2 and C12-O3, are respectively equal to **1.225** and **1.211 Å**, which is consistent with previous studies that report carbonyl bond lengths in the range of **(1.221-1.229 Å)**. Similarly, the C–O bond lengths of the central pyran heterocycle in compound **III.3r** citing C7-O1 **(1.380 Å)** and C8-O1 **(1.376 Å)** align with literature values ranging from **1.376** to **1.380** Å. Cyclohexanone rings adopt half-chair conformations in which **C5** and **C10** deviate from the planes **A** and **C**

with distances equal to **0.631** and **0.643** Å respectively. While the pyranic ring displays an almost planar geometry, with atom C1 distancing from the plane **B** by a length of **0.287** Å **(Figure III.6)**. These findings are in perfect reliability with crystallographic identifications of similar xanthenedione rings.**[216]** Furthermore, torsions angles compared to the aromatic ring are near to 180°, which suggests an antiperiplanar conformation.

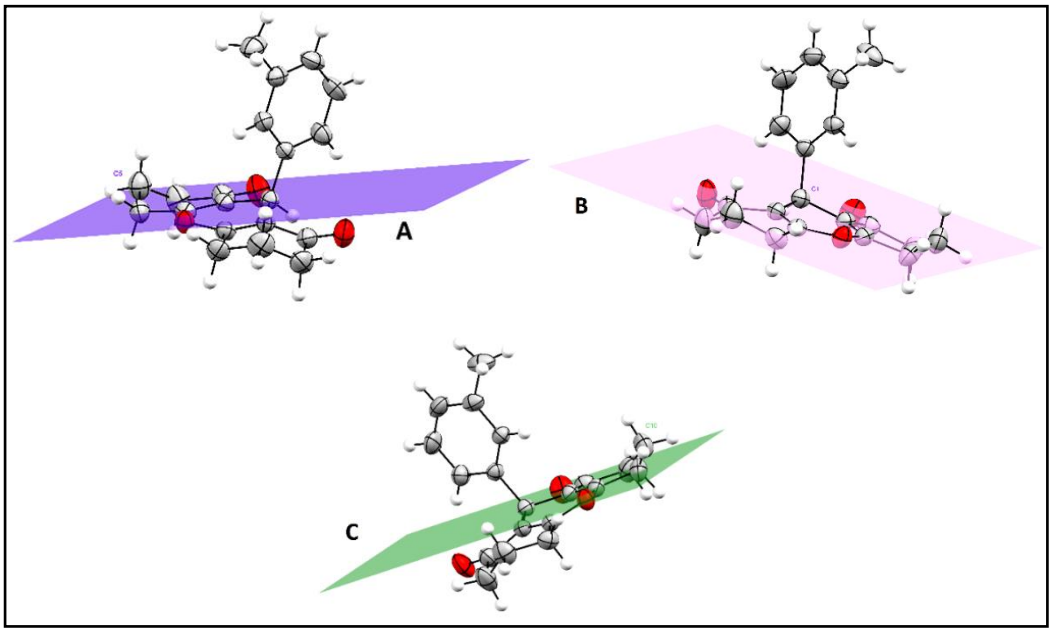

Figure III.6. Graphical representation of planes A, C corresponding to cyclohexanones rings and plane B corresponding to the pyranic cycle. (Plane A: calculated through C2-C3-C4-C6-C7, Plane B: calculated through C2-C7-O1-C8-C13, and Plane C: calculated through C8-C9-C11-C12-C13). Obtain permission and include the acknowledgement required by the copyright holder if a figure is being reproduced from another source.

2. Synthesis and characterization of 1,2-oxaphospholanes-2-oxides derivatives

2.1. Synthesis of 1,2-oxaphospholanes-2-oxides derivatives

"Where there is life, there is phosphorus," as emphasized by Alexander Todd, Nobel Laureate in chemistry (1957) **[217]**. This statement underscores the essential role of phosphorus in living organisms, and its incorporation into heterocycles, often combined with other heteroatoms such as oxygen or nitrogen, has attracted increasing interest due to their bioactivity and importance in drug design **[218]**. Among these compounds, 1,2-oxaphospholane-2-oxides **(III.5)** can be synthesized through a simple and environmentally friendly method **(Scheme III.4)**, involving the condensation of dimedone **(I.62)**, an aromatic aldehyde **(I.61)**, and diethyl phosphite **(III.4)** in ethanol, under microwave irradiation. Purification by column chromatography was required to obtain the desired products in good yield**s (75-82%).**

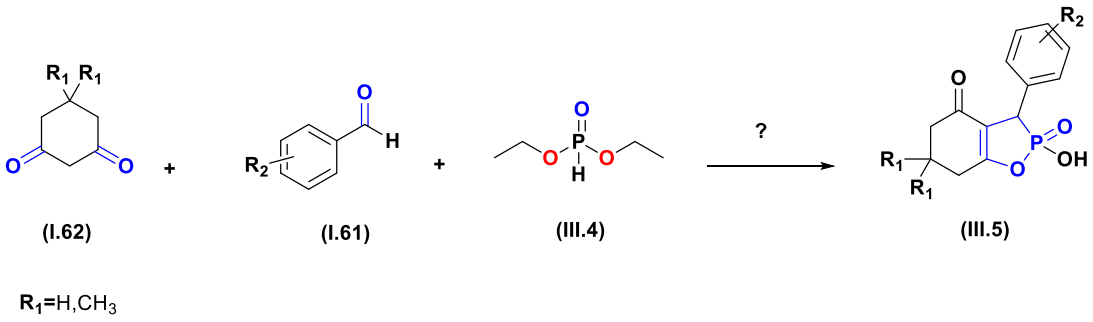

Scheme III.4 synthesis of 1,2-oxaphospholanes-2-oxides derivatives.

2.1.1. Optimization of reaction condition

To determine the optimal reaction conditions, we selected a model reaction involving the condensation of benzaldehyde **(I.61)**, diethyl phosphite **(III.4)**, and dimedone **(I.62)**.

In an initial attempt, we followed the method of Shaabani et *al.*, performing the reaction in an ethanolic solution under reflux at **80** °C. After **48** hours, the formation of a new product was observed, albeit with a moderate yield. **(Entry 1, table III.3)** Subsequently, we attempted the reaction at room temperature under stirring, still using ethanol as the solvent. After **24** hours, a new spot appeared on the TLC plate, indicating product formation. **(Entry 3, table III.2)**

To accelerate the reaction and improve the yield, we explored alternative activation methods. First, ultrasonic irradiation was tested using ethanol as the solvent. After only **30** minutes, the desired product was obtained in good yield. **(Entry 3, table III.3)** Encouraged by these results, we then employed microwave irradiation as an activation source. Under these conditions, and using ethanol as the solvent, the target product was obtained in just **2 min** with an excellent yield. **(Entry 4, table III.3)**

Compared to the other tested methods, microwave activation proved to be the most efficient, providing the highest yield in a significantly reduced reaction time.

Solvent selection is a crucial parameter in the development of a chemical reaction, as it influences reactivity, yield, and reaction time. Under microwave irradiation, polar solvents play a key role in absorbing electromagnetic energy and converting it into heat through the dipolar polarization mechanism. This interaction promotes reactant activation and enhances reaction efficiency.

To assess the influence of the solvent in our study, the model reaction was carried out in ethanol, methanol, and acetone. The results indicate that although the reaction times and yields were relatively similar, noticeable differences remained. **(Entries 5-8, Table III.3)** Ethanol proved to be the most efficient solvent, providing the highest yield in the shortest reaction time, and was therefore selected as the optimal solvent for further experiments. **(Entry 6, Table III.3)**

Table III.3. Optimization of conditions for the synthesis of 1,2-oxaphospholanes-2-oxides derivatives.

Entry	Methods	Solvents	Times (min) /Yields%
1	Refluxing (80°C)	EtOH (1mL)	2880/60
2	Classic stirring (rt)	EtOH (1mL)	1440/45
3	US (40 kHz)	EtOH (1mL)	30/75
4	MW (100W)	EtOH (1mL)	2/82
5	MW (100W)	No solvent	2/75
6	MW (100W)	**EtOH** (1mL)	2/84
7	MW (100W)	Methanol (1mL)	2/80
8	MW (100W)	Acetone (1mL)	2/78

Under these optimized conditions, a variety of substituents was introduced onto the aromatic ring of the aldehyde **(Scheme III.5)**.

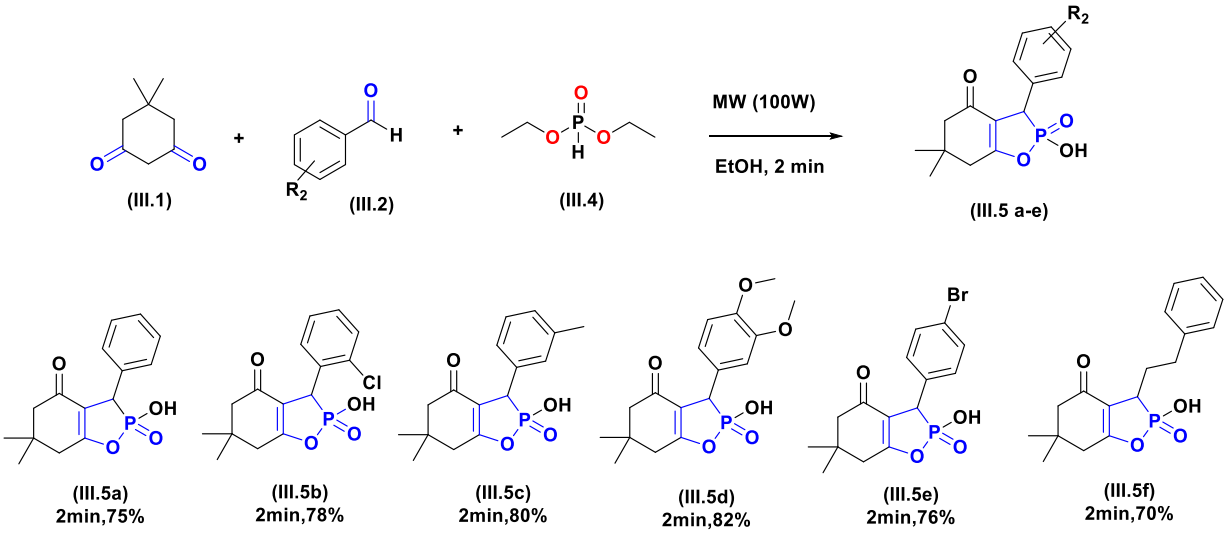

Scheme III.5. Synthesized derivatives of 1,2-oxaphospholanes-2-oxides

The obtained yields were significantly influenced by the nature of the substituents on the aromatic ring. The introduction of electron-donating groups, such as **CH_3** and **OCH_3** at the *meta* and *para* positions **(III.5c, III.5d)**, led to an increase in yields **(70-80%)**. In contrast, the lowest yield was observed for the unsubstituted product **(phenyl)**.

2.1.2. Mechanistic proposal of 1,2-oxaphospholanes-2-oxides derivatives

We propose the mechanism illustrated in scheme (III.6) for the microwave-assisted synthesis of 1,2-oxaphospholane-2-oxides. Initially, microwave irradiation enhances the electrophilicity of the aldehyde, thereby promoting its nucleophilic attack by dimedone and leading, after dehydration, to the formation of intermediate (A). In the reaction medium, diethyl phosphite exists in a tautomeric equilibrium between phosphonate and phosphite forms; the latter, being more nucleophilic, reacts with the C=C double bond of the intermediate through a Phospha-Michael addition (B), affording intermediate (C). This species subsequently undergoes an intramolecular cyclization accompanied by the elimination of an ethanol molecule, yielding product (D). Finally, under microwave irradiation and in the presence of the water released during the first step, hydrolysis occurs, leading to the final formation of 1,2-oxaphospholane-2-oxide derivatives (F).

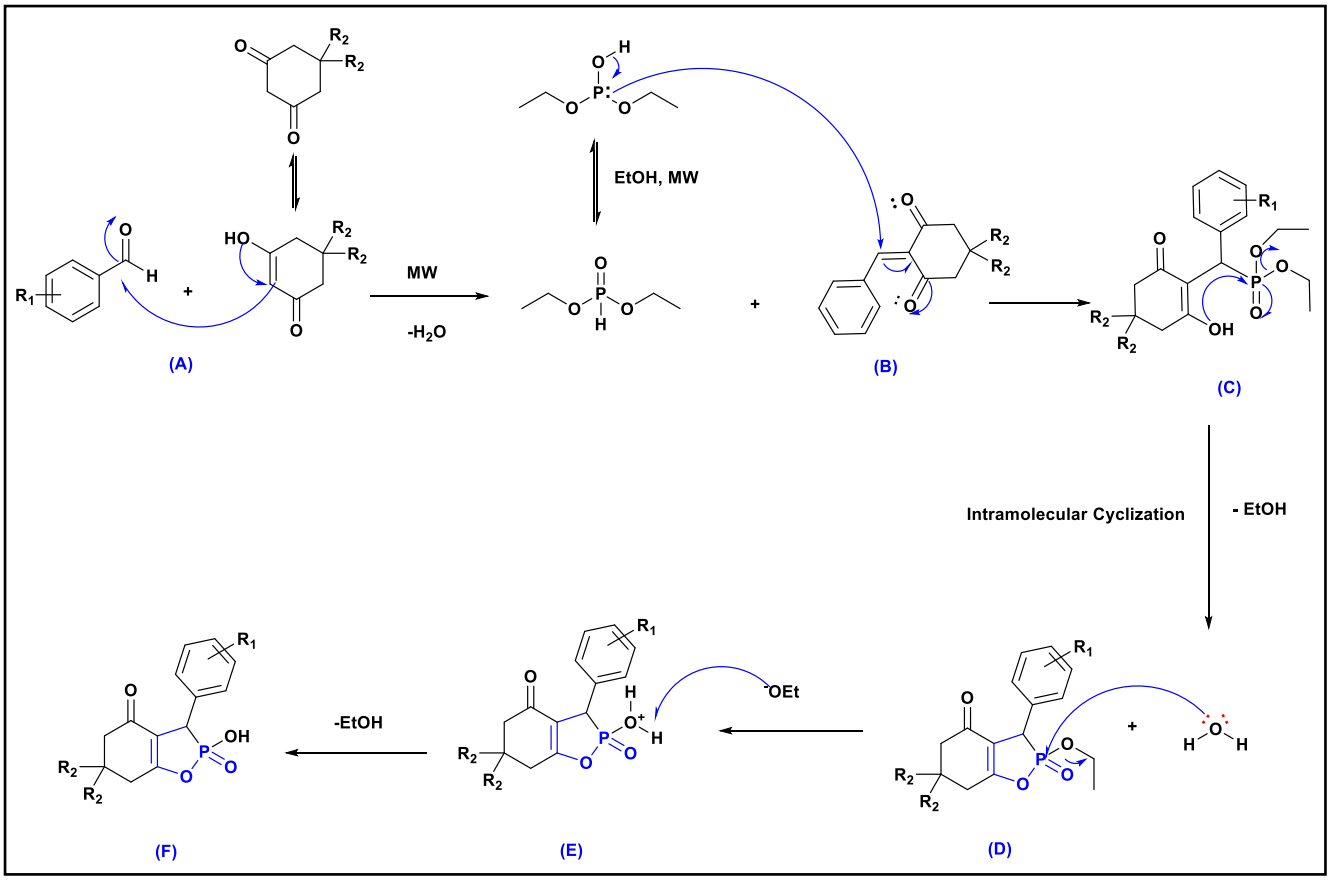

Scheme III.6. Proposed mechanism for the synthesis of 1,2-oxaphospholones-2-oxides derivatives.

2.2. Spectral characterization of 1,2-oxaphospholones-2-oxides

The synthesized molecules were characterized using spectroscopic analysis techniques, including **^{1}H NMR** and **^{13}C NMR**, **IR** and mass spectrometry **(MS)**.

In the **^{1}H NMR** spectra, all synthesized compounds exhibit a singlet around **0.90** ppm, corresponding to the six equivalent protons of the dimedone moiety. The aromatic protons appear as a multiplet in the **7.00–7.25** ppm region. Additionally, two characteristic signals confirm the structure: a doublet at **4.75** ppm, assigned to the proton on the asymmetric carbon, and a singlet around **2.30** ppm, corresponding to the four protons of the two **CH_2** groups in the dimedone units.

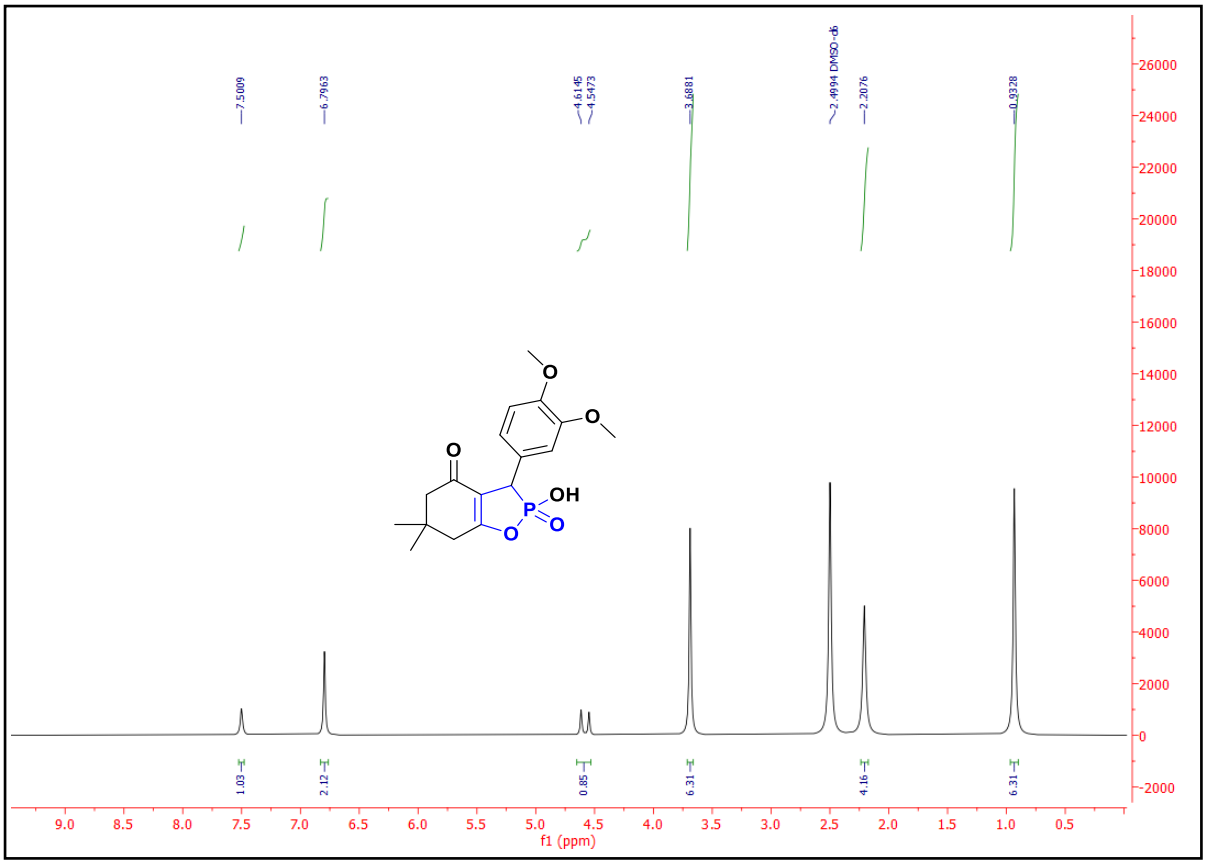

Figure III.7. ^{1}H NMR spectra of 3-(3,4-dimethoxyphenyl)-2-hydroxy-6,6-dimethyl-3,6,7-trihydrobenzo [1,2] oxaphosphol-4(5H)-one 2-oxide (III.5d).

The ^{13}C NMR spectra confirmed the structures of the expected products by the presence of characteristic peaks. The aromatic ring carbons resonate within the range of **125.4-129.7** ppm, whereas the methyl **(CH_3)**, methylene **(CH_2)**, and asymmetric carbons appear between 18 and 55 ppm. Additionally, the carbonyl carbon is observed as a distinct peak around **194.9** ppm.

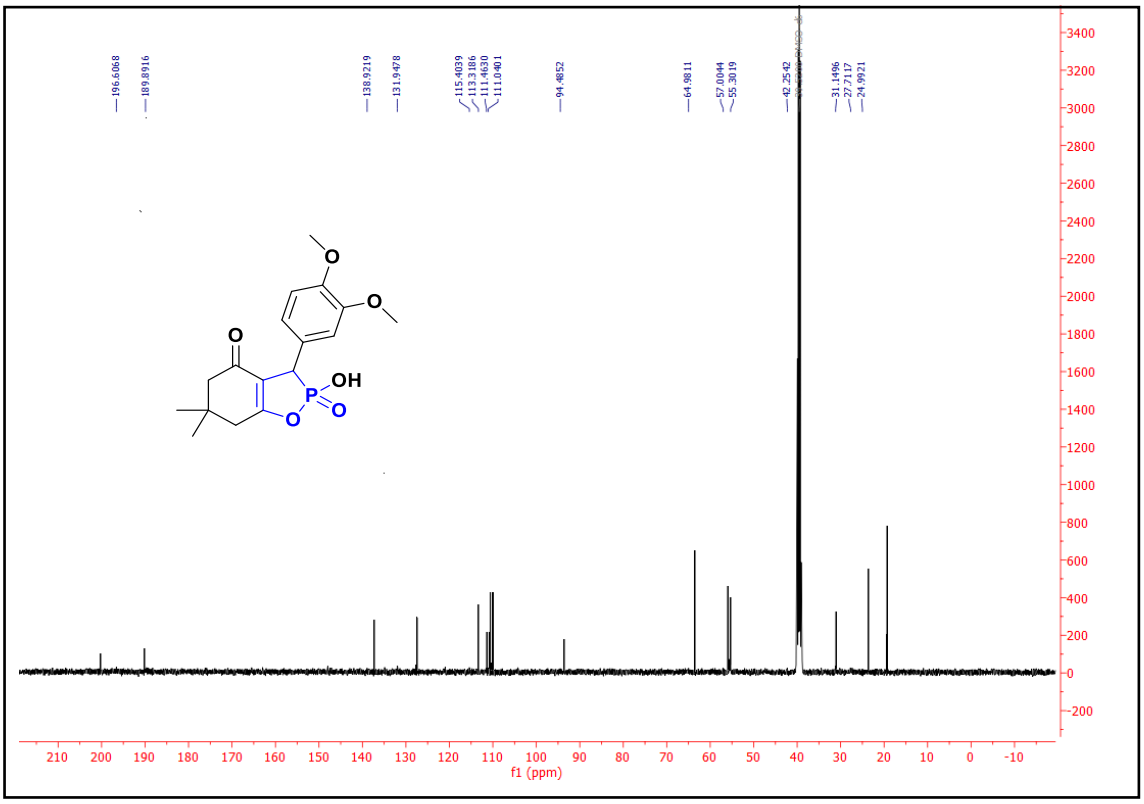

Figure III.8. ^{13}C NMR spectra of 3-(3,4-dimethoxyphenyl)-2-hydroxy-6,6-dimethyl-3,6,7-trihydrobenzo [1,2] oxaphosphol-4(5H)-one 2-oxide (III.5d).

In ^{31}P NMR spectra, the presence of a peak at **26.86** ppm confirms the incorporation of a phosphorus atom into the product.

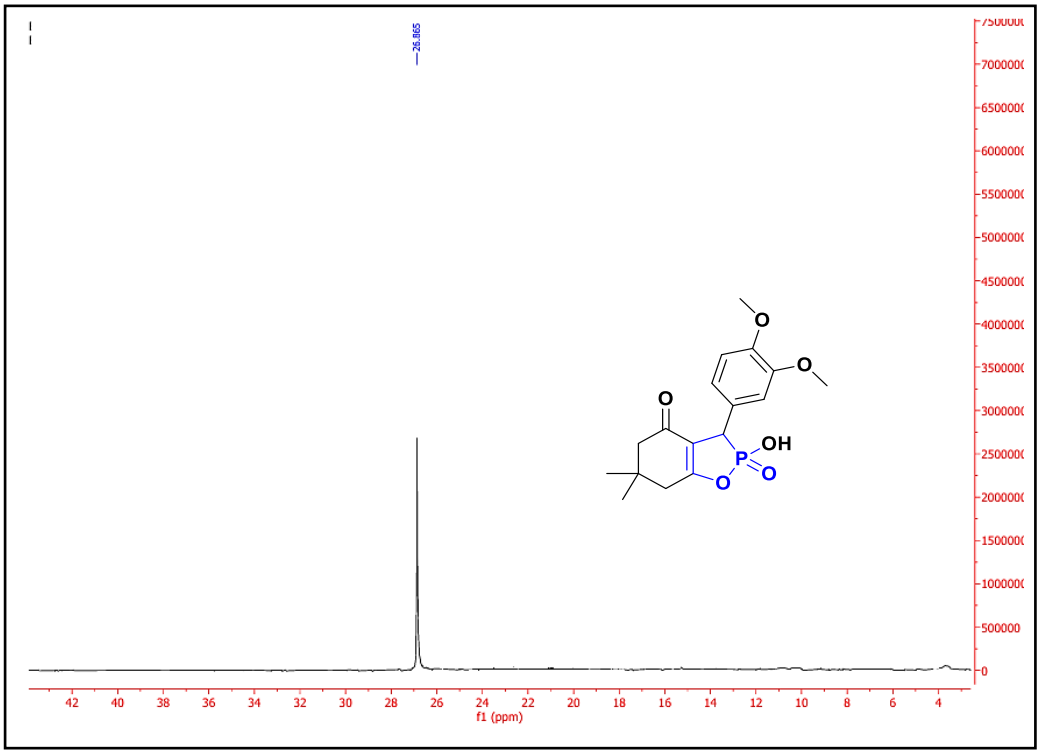

Figure III.9. ^{31}P NMR spectra of 3-(3,4-dimethoxyphenyl)-2-hydroxy-6,6-dimethyl-3,6,7-trihydrobenzo [1,2] oxaphosphol-4(5H)-one 2-oxide (III.5d).

LC-MS, spectra exhibited ion molecular peak that corresponding to $[M+18]^+$.

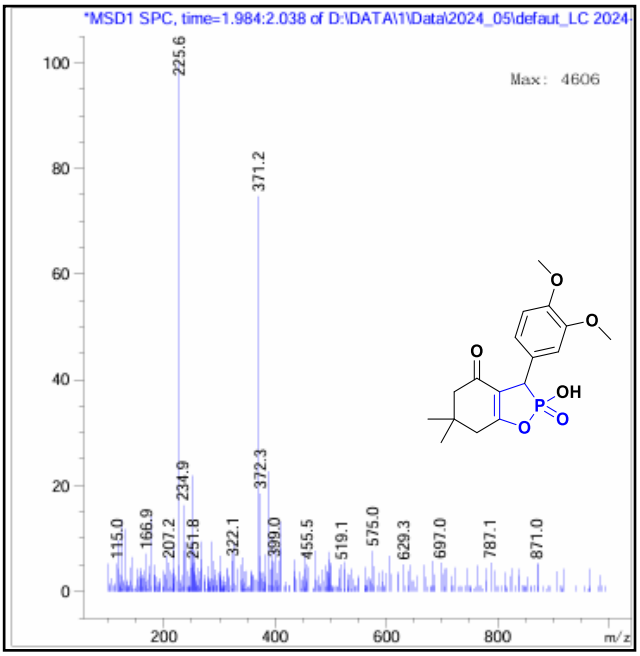

Figure III.10. Mass spectra of 3-(3,4-dimethoxyphenyl)-2-hydroxy-6,6-dimethyl-3,6,7-trihydrobenzo[1,2]oxaphosphol-4(5H)-one 2-oxide (III.5d).

3. Synthesis and characterization of *N*-nitroso-carbamate derivatives

3.1. Introduction

The 2-chloroethylnitrosoureas **(CENU)** represent an important class of alkylating agents employed in cancer chemotherapy. However, this class is also associated with cumulative and damaging side effects.**[219]** The essential cytotoxic effects of the alkylating agents used in antitumor chemotherapy arise from binding to the **DNA** molecule by a bifunctional electrophile (e.g., the chloronium ion) and the release of isocyanates during their decomposition.**[220]**

Consequently, in recent decades, significant efforts have been devoted to synthesizing structurally similar drugs with improved activity and reduced toxicity. **[221]**

In this context, our research has focused on developing a novel series of alkylating agents, the 2-chloroethylnitrosocarbamate **(CENC)**, inspired by the 2-chloroethylnitrosourea scaffold.

Starting from 2-chloroethylisocyanate, a two-step sequence comprising carbamoylation followed by nitrosation allowed the preparation of carmustine analogues, affording the target compounds in overall yields of **32–50%**. Additionally, a three-step synthesis was developed for fotemustine analogues, beginning with the preparation of hydroxyphosphonate via the

Pudovik reaction, followed by a carbamoylation step, and concluding with nitrosation, affording the rearranged product**.**

3.1. Synthesis of carmustine analogues

With the aim of preparing carbamate analogues structurally related to carmustine, potentially exhibiting interesting biological activities with reduced toxicity, we proposed a synthetic strategy primarily based on the specific reactivity of the reagents used and the suitability of the selected reactions.

To this end, we selected 2-chloroethyl isocyanate **(III.6)**, the key reagent in the synthesis of carmustine. This compound displays exceptional reactivity towards hydrogen-bearing functional groups such as alcohols, thiols, phenols, and amines, due to the presence of two electrophilic centers: the carbon of the isocyanate group and the chlorine atom of the chloroethyl moiety. This dual reactivity makes the compound particularly valuable in organic synthesis.

The first step involves the preparation of 2-chloroethyl carbamates by reacting an aromatic alcohol with 2-chloroethyl isocyanate **(III.6)** at **0°C** in anhydrous dichloromethane in the presence of triethylamine. In our case, we selected a series of aromatic alcohols **(III.7)** to obtain a new series of 2-chloroethylcarbamates **(III.8)**. After **2 hours** of reaction, TLC analysis showed the appearance of a new, less polar product. After acidic work-up and crystallization from a **1:1** mixture of *n*-hexane and diethyl ether, the novel carbamate derivatives were obtained with an excellent yields of **(89–95%)** as demonstrated in **(Scheme III.7)**.

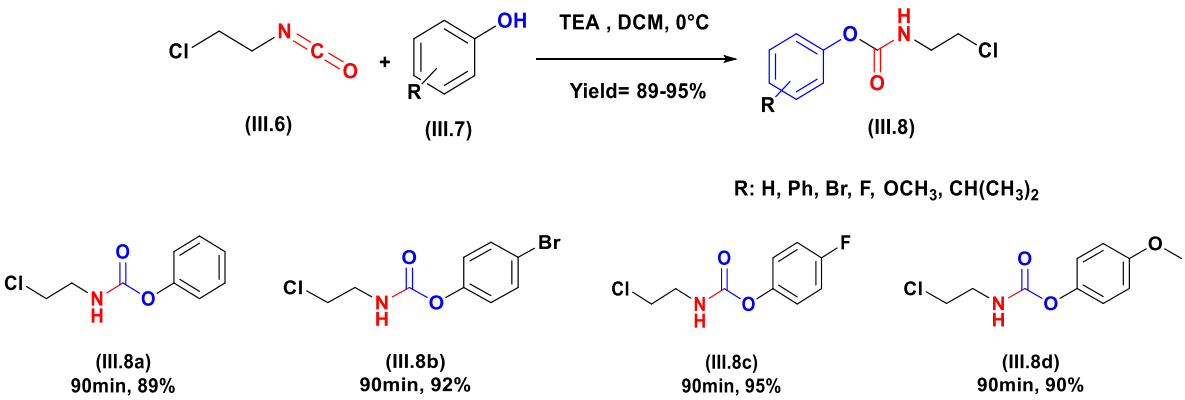

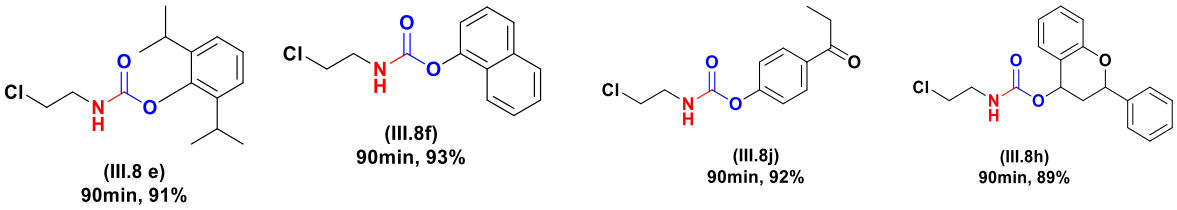

Scheme III.7. Synthesis of *N*-2-chloroetylcarbamate.

The nitrosation step was carried out by adding a nitrosating agent **(sodium nitrite)** to the previously prepared chloroethyl carbamate **(III.8)** in the presence of an acidic medium at **0 °C**, affording the corresponding chloroethylnitrosocarbamate **(Scheme III.8)**.

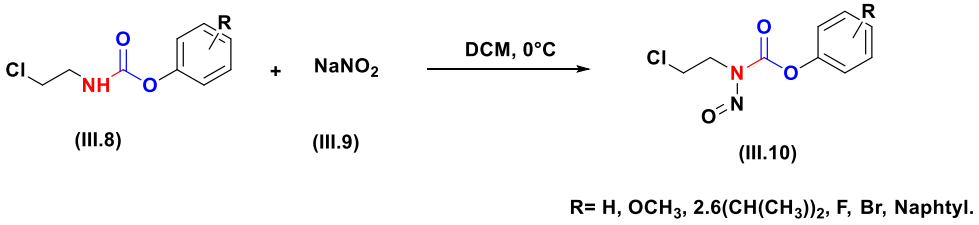

Scheme III.8. Synthesis of *N*-2-chloroetylnitrosocarbamate.

To access 2-chloroethylnitrosocarbamate **(III.10)** derivatives, reaction conditions were optimized by systematic variation of parameters.

We initially attempted to replicate the standard nitrosation conditions described in the literature. For this purpose, we reacted one equivalent of phenyl (2-chloroethyl)carbamate **(III.8)**, three equivalents of **$NaNO_2$ (III.9)**, and three equivalents of **HCOOH** in **2.5** mL of anhydrous **DCM** at **0 °C** for **2** hours. However, under these conditions, degradation of the starting material occurred, without the formation of the expected product. (**Entry 1, Table III.4**).

In a second attempt (**Entry 2, Table III.4**), we maintained the same conditions but replaced concentrated formic acid **(HCOOH, 98%)** with hydrochloric acid **(HCl, 35%)**. Again, we observed complete degradation of the starting material.

Subsequently, we attempted the nitrosation of phenyl (2-chloroethyl) carbamate **(III.8)** with sodium nitrite **(6 eq $NaNO_2$)**. In entries **3** and **4 (Table III.4)**, none of our trials yielded more than trace amounts of the expected product, whether using **HCl** or **HCOOH**, or by extending the reaction time.

Finally, we applied the conditions outlined in entries **5** and **6 (Table III.4)** by adding **10** equivalents of sodium nitrite **($NaNO_2$)** in the presence of **10** equivalents of concentrated **HCl**

or **HCOOH** at **-10 °C** to **0 °C** in DCM. After **90** minutes of stirring at low temperature, a yellow suspension formed, and TLC monitoring indicated the appearance of a new, more polar product compared to the starting compound. The product was obtained with a **10%** yield in the presence of **10** equivalents of hydrochloric acid and a **45%** yield in the presence of **10** equivalents of formic acid.

We then attempted to increase the reaction yield by using **15** equivalents of formic acid (**entry 7, table III.4**), but the yield remained the same as in (**Entry 6, Table III.4**).

Table III.4. Optimization reaction conditions of phenyl(2-chloroethyl) carbamate and nitrite de sodium.

Entry	Reagent	Solvent	Conditions	Times (min) / Yields %
1	$NaNO_2$ (3 eq)	DCM (2.5 mL)	**HCl (3 eq)**	120/--
2	$NaNO_2$ (3 eq)	DCM (2.5 mL)	**HCOOH (3 eq)**	120/--
3	$NaNO_2$ (6 eq)	DCM (2.5 mL)	**HCl (6 eq)**	120/trace
4	$NaNO_2$ (6 eq)	DCM (2.5 mL)	**HCOOH (6 eq)**	120/15
5	$NaNO_2$ (10 eq)	DCM (2.5 mL)	**HCl (10 eq)**	90/10
6	$NaNO_2$ (10 eq)	DCM (2.5 mL)	**HCOOH (10 eq)**	90/45
7	$NaNO_2$ (15 eq)	DCM (2.5 mL)	**HCOOH (15 eq)**	90/45

Consequently, we adopted the optimized conditions to prepare a series of 2-chloroethylnitrosocarbamates **(III.10)** by introducing various substituents onto the aromatic ring of the corresponding alcohols.

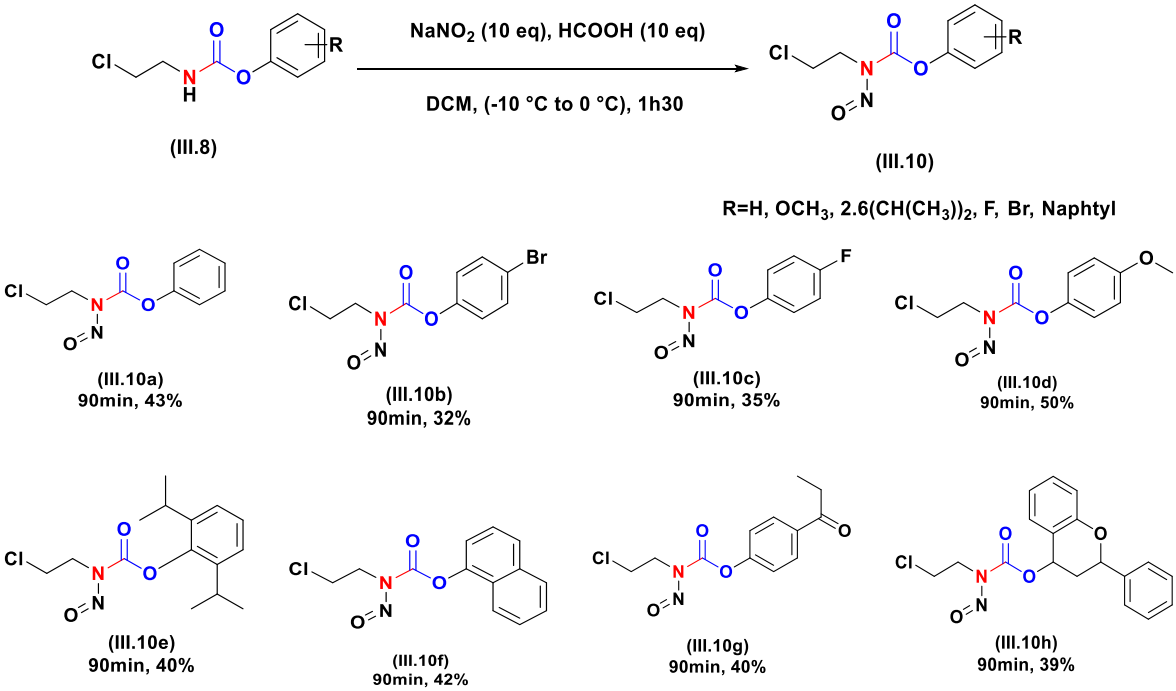

Scheme III.9. Synthesis of 2-chloroethyl(nitroso)carbamates derivatives**.**

As illustrated in scheme **(III.9) (3)**, substituents on the aromatic ring of alcohols, whether electron-donating or electron-withdrawing, influence reaction yields to different extents.

Phenol was initially selected to evaluate the reaction feasibility and efficiency, yielding the desired nitrosocarbamate derivative as a yellow oily product with a moderate yield of **43%**. The method exhibited good tolerance toward various substituents under the given conditions. Alcohols bearing electron-donating groups (e.g., -OMe, isopropyl) produced moderate yields **(50–40%)** compared to those with electron-withdrawing groups (e.g., F, Br). The highest yield **(50%)** was achieved with methoxyphenol **(III.10d)** within **1h 30min**, whereas fluorophenol gave the lowest yield **(35%)**.

3.1.2. Mechanistic proposal

The mechanism for the formation of phenyl 2-chloroethyl(nitroso)carbamates is depicted in **scheme III.10**. Initially, triethylamine activates phenol **(A)** by enhancing its nucleophilicity, thereby promoting its addition to 2-chloroethyl isocyanate, affording the intermediate chloroethyl carbamate **(B)**. Subsequently, sodium nitrite reacts with formic acid to generate the nitrosonium ion, which is then attacked by the lone pair on the nitrogen atom of 2-chloroethyl phenylcarbamate, leading to the formation of the desired nitrosocarbamate product **(Scheme III.10)**.

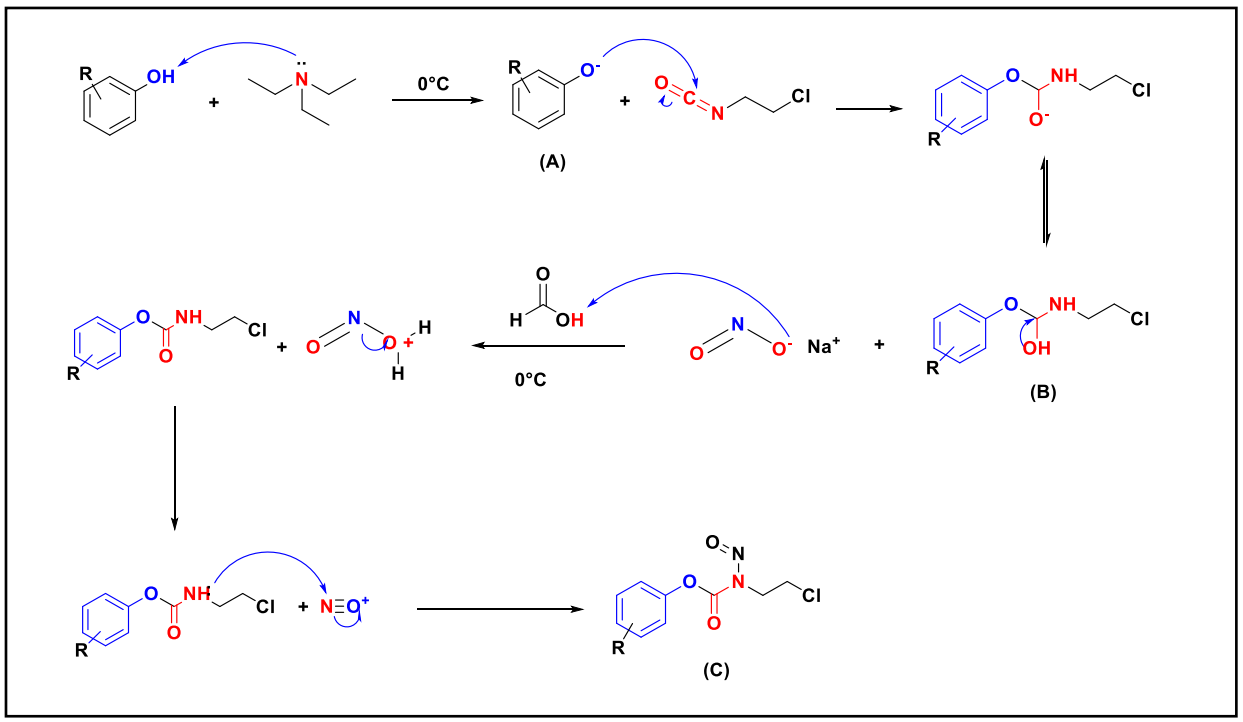

Scheme III.10. Proposed mechanism for the synthesis of phenyl 2-chloroethyl(nitroso)carbamates derivatives.

3.1.3. Spectral characterization

Structural analysis of the obtained products (2-chloroethylcarbamates and *N*-nitrosocarbamates) was carried out using standard spectroscopic methods, including **^{1}H** and **^{13}C NMR**, **IR** and **MS**.

In the **^{1}H NMR** spectrum, compound **(III.8d)** is characterized by the appearance of a quartet corresponding to the two protons of the **CH_2-NH** group **(J_{H-H} =6.0 Hz)** in the range of **[3.36–3.49]** ppm. The protons of the **CH_2-Cl** group resonate as a triplet **(J_{H-H} = 6.1 Hz)** at **3.66** ppm. The aromatic protons resonate in the region **[6.89–7.03]** ppm. Additionally, a signal at **7.92** ppm is observed as a triplet **(J_{H-H} = 5.70 Hz)**, attributed to the proton of the **NH** group.

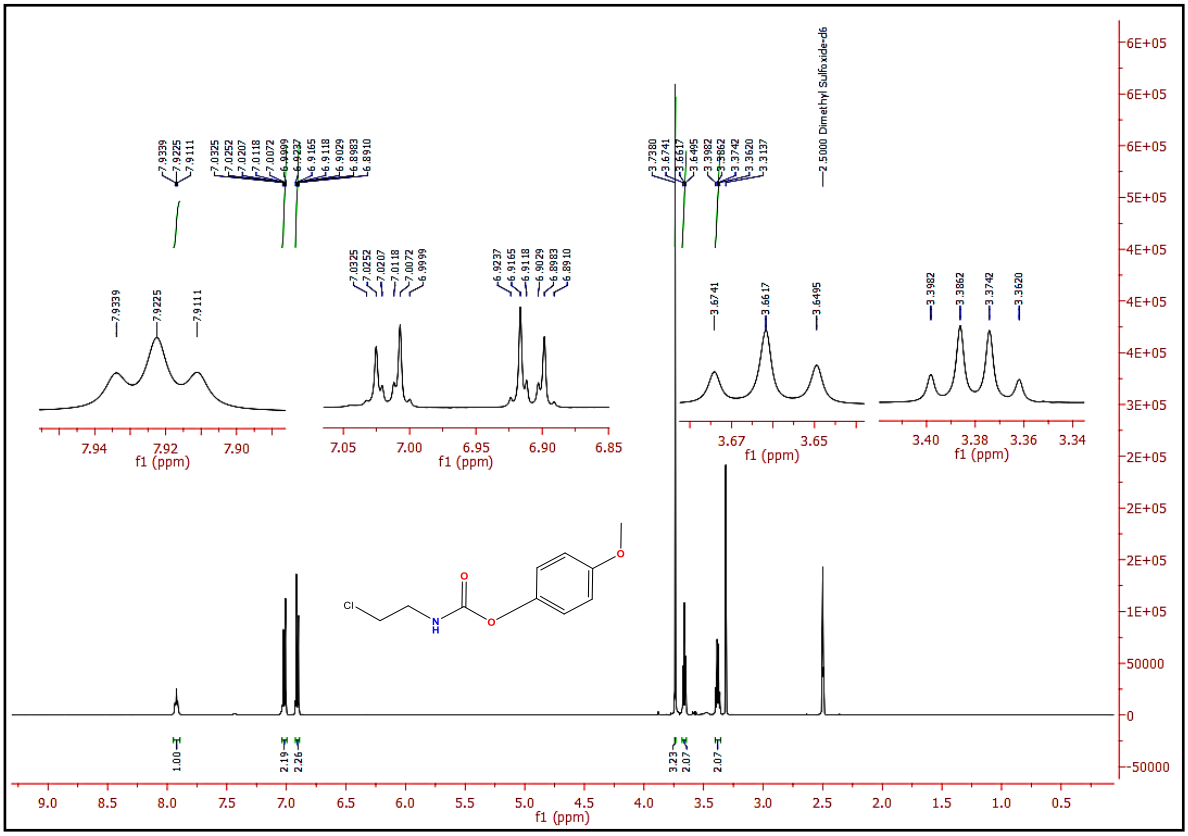

Figure III.11. ^{1}H NMR spectra of 4-methoxyphenyl (2-chloroethyl)carbamate (III.8d).

In the **^{13}C NMR** spectrum, the–analysis of compound **(III.8d)** reveals the appearance of signals for the two methylene carbons at **42.5** and **43.2** ppm. Additionally, the carbonyl carbon resonates at **156.3** ppm. The aromatic carbons appear in the expected region, between **114.1** and **122.5** ppm.

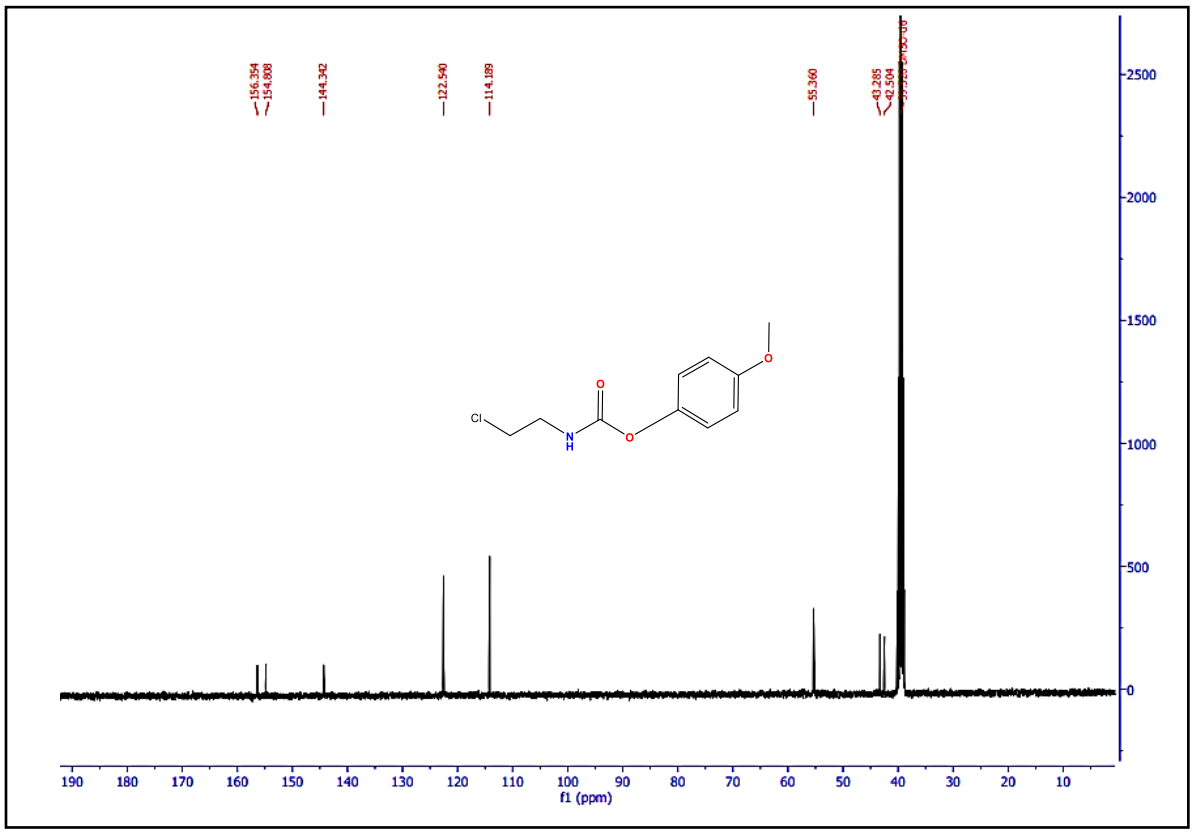

Figure III.12. ^{13}C NMR spectra of 4-methoxyphenyl (2-chloroethyl)carbamate (III.8d).

In the **IR** spectrum, the structure of 4-methoxyphenyl-2-chloroethylcarbamate **(III.8d)** is confirmed by the presence of a characteristic **N-H** stretching band at **3324** cm^{-1} and a **C=O** stretching band at **1710** cm^{-1}.

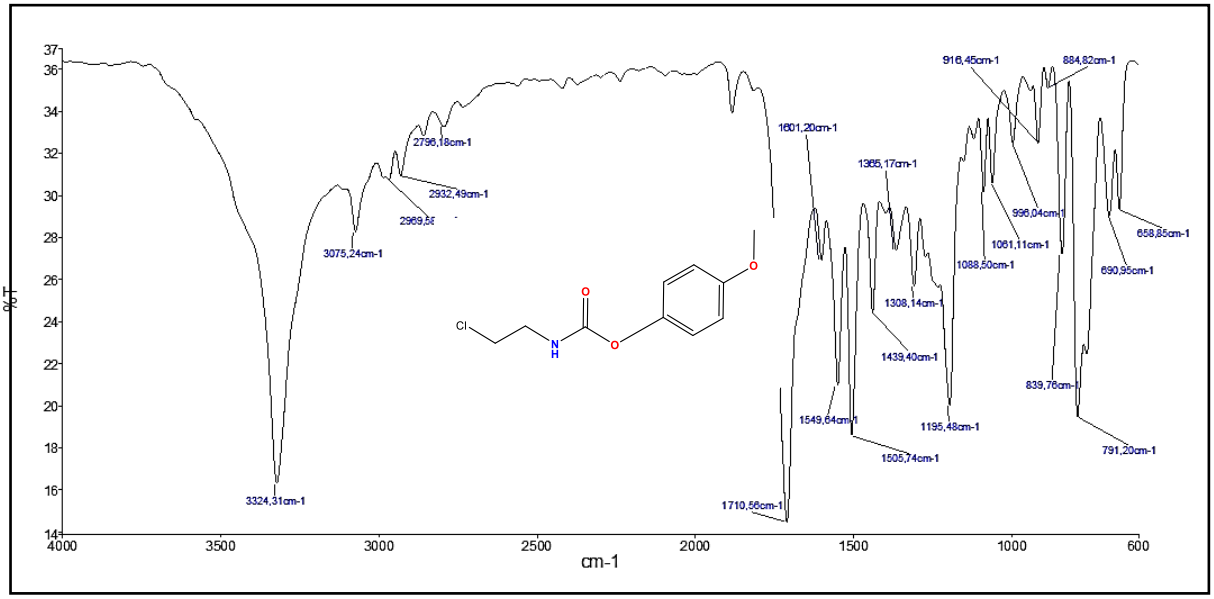

Figure III.13. IR spectra of 4-methoxyphenyl (2-chloroethyl)carbamate (III.8d).

LC-MS, spectra exhibited a molecular ion peak that corresponds to [M+1].

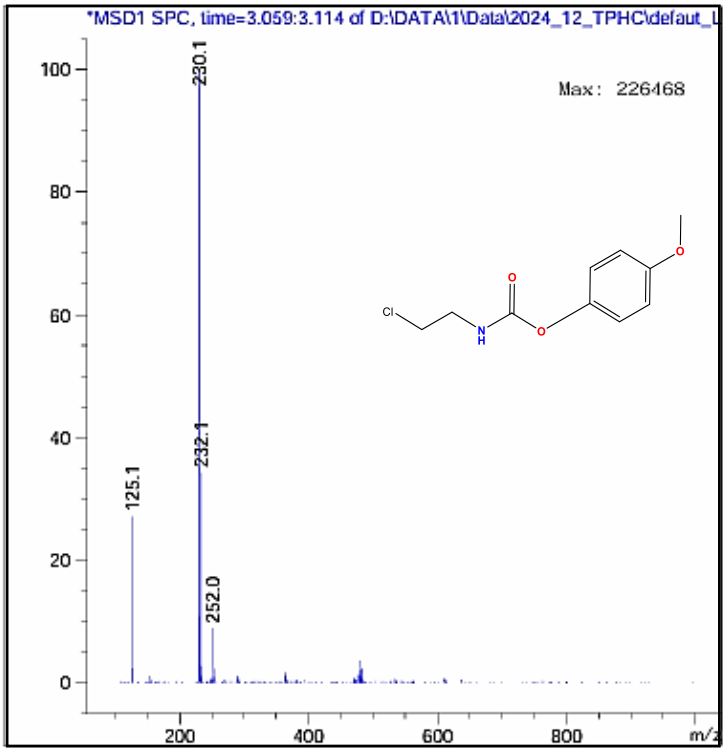

Figure III.14. Mass spectra of 4-methoxyphenyl (2-chloroethyl)carbamate (III.8d).

In the **^{1}H NMR** spectrum, compound **(III.10d)** is primarily characterized by the disappearance of the signal at around **8.10** ppm, which corresponds to the **NH** proton.

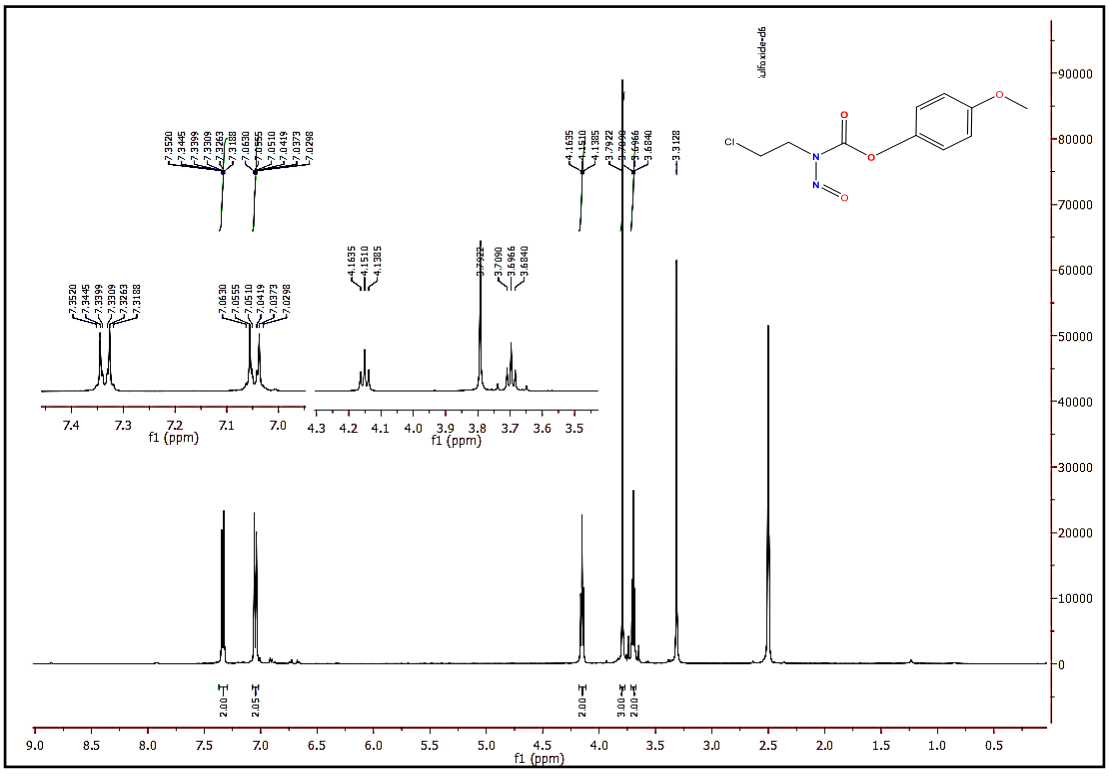

Figure III.15. ^{1}H NMR spectra of 4-methoxyphenyl (2-chloroethyl)(nitroso)carbamate (III.10d).

In the ^{13}C NMR spectrum, compound **(III.10d)** is mainly characterized by the shielding of the signals already observed in the spectrum of compound **(III.8d)**, which is attributed to the presence of nitroso groups.

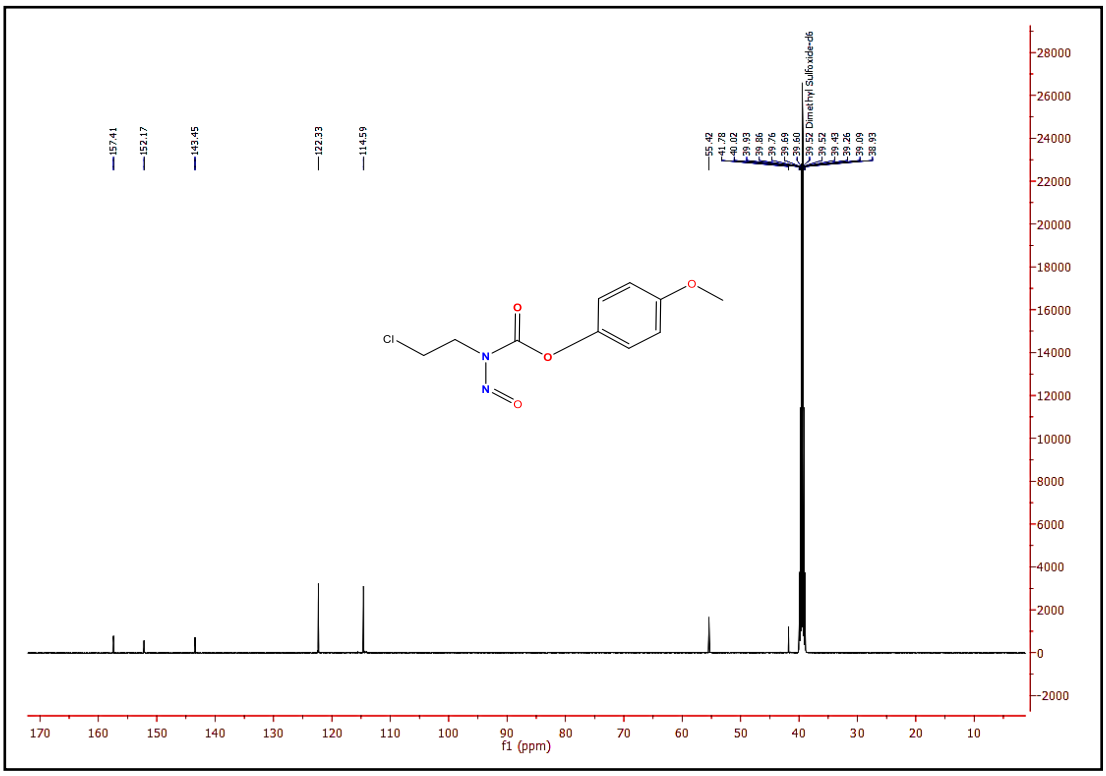

Figure III.16. ^{13}C NMR spectra of 4-methoxyphenyl (2-chloroethyl) (nitroso)carbamate (III.10d).

LC-MS, spectra always exhibited a molecular ion peak that corresponds to [M+18].

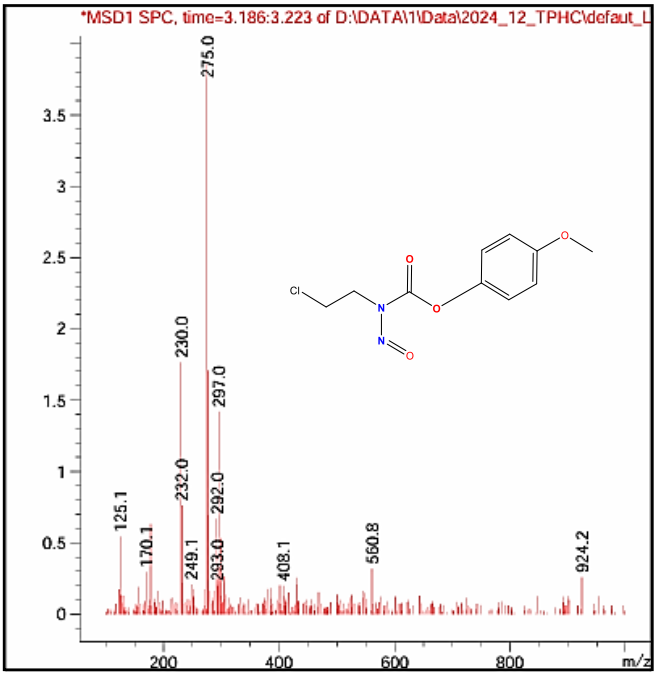

Figure III.17. Mass spectrum 4-methoxyphenyl (2-chloroethyl) (nitroso)carbamate (III.10d).

3.2. Crystallographic study for compound III.8a

Compound **III.8a** was obtained as crystals suitable for a single crystal X ray diffraction analysis allowing a complete structure elucidation of the latter. As shown in the ORTEP diagram drawn at **50%** probability **(Figure III.18)**, the expected structure of the corresponding intermediate **III.8a** was confirmed. Additional, the asymmetric unit encloses one molecule of phenyl (2-chloroethyl) carbamate that crystallizes in the monoclinic crystal system with the P 21/n space group.

The cohesion of the crystal structure was ensured making use of conventional hydrogen bonds as well as additional contacts (**Table III.5**). The presence of the carbamate moiety allowed the formation of an intermolecular hydrogen bond **N_1-H_1…O_2** with a distance of 0.860 Å. Furthermore, two additional intermolecular contacts were noticed including **C_8-H_8…O_2** and **C_1-H_{1B}…C_7** with distances of 0.930 and 0.970 Å respectively keeping the components of the crystal together.

Crystal packing diagrams of compound **III.8a** were constructed and viewed along *a* and *b* axes **(Figure III.19)** enabling a better observation of the crystal structure. Notably, the presence of hydrogen bonds permitted the formation of two infinite chains supporting the cohesion of the structure.

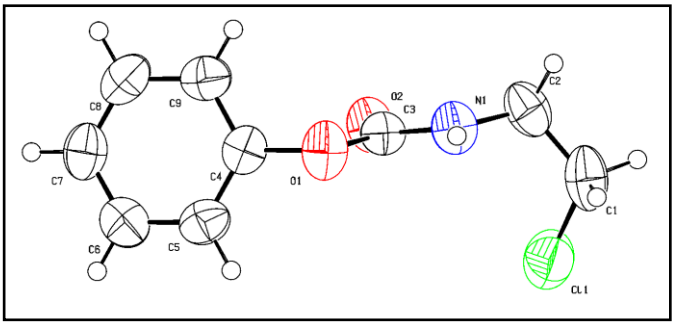

Figure III.18. ORTEP diagram of compound III.8a

Table III.5. Distances (Å) and angles (°) of hydrogen bonds for compound III.8a

D-H…A	***d*(D-H)**	***d*(H…A)**	***d*(D-A)**	**D-H-A**	**Symmetry**
N_1-H_1…O_2	0.860	2.054	2.814(1)	146.83	x,y,z ; -1+x,y,z
C_8-H_8…O_2	0.930	2.696	3.504(2)	145.8	x,y,z ; -x,2-y,1-z
C_1-H_{1B}…C_7	0.970	2.888	3.688(3)	140.4	x,y,z ; -1/2+x,1.5-y,1/2+z

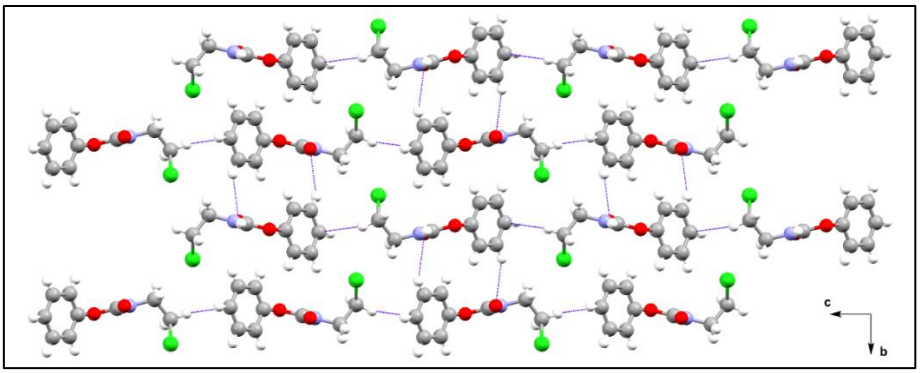

(a)

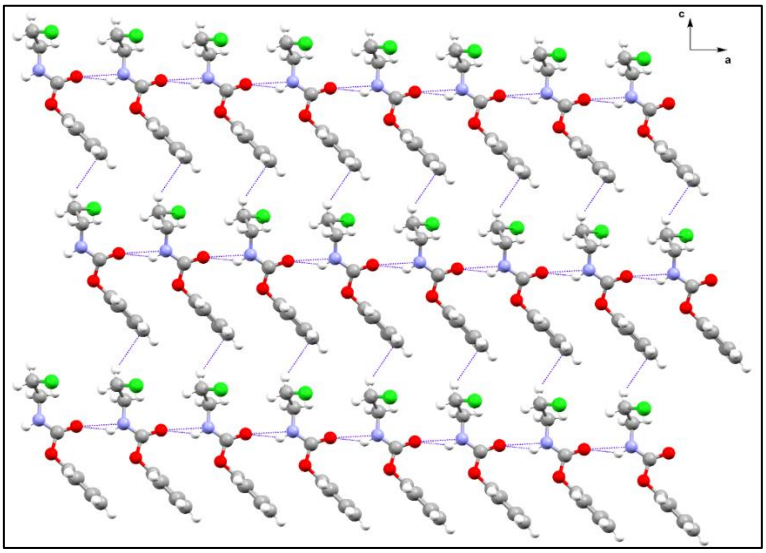

(b)

Figure III.19. Crystal packing of compound III.8a viewed along the *a* axis (a) and the *b* axis (b). H-bonds are shown as blue dashed sticks.

3.2. Attempted synthesis of fotemustine

The structure of fotemustine was developed by the french pharmaceutical company Servier. Its conventional synthesis involves the addition of racemic diethylaminoethylphosphonate (**III.11**) to 2-chloroethyl isocyanate (**III.6**), followed by nitrosation with sodium nitrite **($NaNO_2$) (Scheme III.11).[222]**

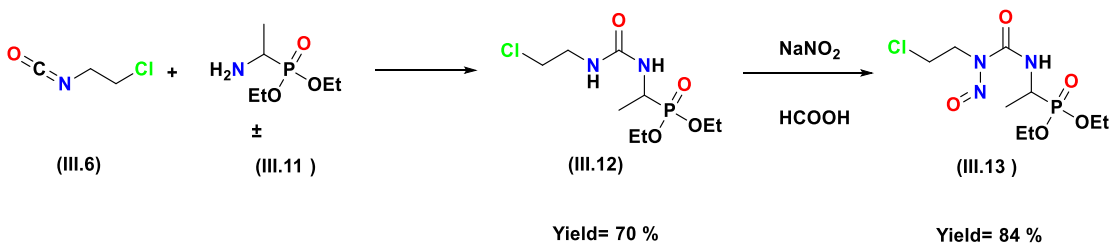

Scheme III.11. Synthesis of Fotemustine by the pharmaceutical company Servier.

As mentioned earlier, to prevent the release of toxic isocyanates during decomposition in aqueous medium, we aimed to develop a new series of compounds, the 2-chloroethylnitrosocarbamates, which are carbamate analogues of fotemustine.

In this context, our efforts focused on the development of a novel 2-chloroethylnitrosocarbamate structure, synthesized from α-hydroxyphosphonate through a three-step process, as outlined in the following scheme **(III.12)**.

The α-hydroxyphosphonate (**III.14**) used in this study were synthesized following the method described by Kaboudin et *al*, *via* the Pudovik reaction between diethyl phosphite (**III.4**) and various aromatic aldehydes (**III.2**) in the presence of **K_2CO_3** as a basic catalyst at room temperature. Based on this approach, we reproduced the same reaction conditions using benzaldehyde (**III.2**) in anhydrous **DCM** for **2h**. TLC analysis confirmed the formation of a new, less polar product. After recrystallization in hexane, the α-hydroxyphosphonate (**III.14**) derivative was obtained with excellent yield **(97%) (Scheme III.13)**.

In the second step, triethylamine **(TEA)** was reacted with the previously synthesized α-hydroxyphosphonate (**III.14**) in anhydrous **DCM** at **0°C** for **30 min**. Subsequently, 1-chloro-2-isocyanatoethane (**III.6**) was added dropwise, and the reaction mixture was stirred overnight at room temperature **(Scheme III.13)**. TLC analysis revealed the formation of a new, less polar product, confirming the progression of the reaction. Completion was verified by the disappearance of the α-hydroxyphosphonate (**III.14**) in the reaction medium. Following acidic workup and recrystallization in diethyl ether/hexane **(1:1)**, the target compound (**III.15**) was obtained as white crystals with a yield of **(80%)**.

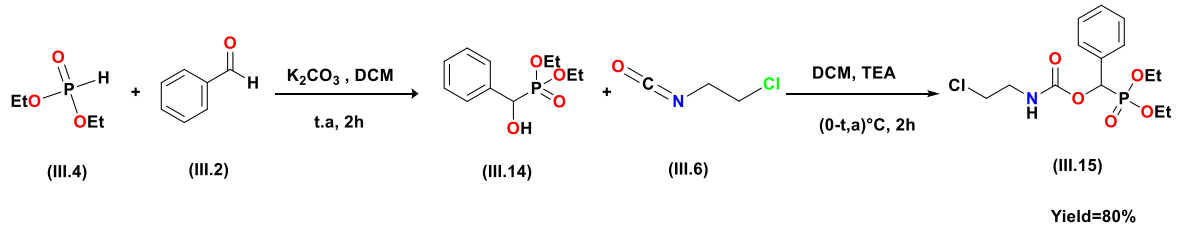

Scheme III.13. Synthesis of (diethoxyphosphoryl)(phenyl)methyl (2-chloroethyl) carbamate.

The nitrosation of (diethoxyphosphoryl)(phenyl)methyl(2-chloroethyl) carbamate **(III.13)** was carried out under the same conditions previously used for the nitrosation of carmustine analogues. The reaction was conducted at **0 °**C in anhydrous dichloromethane **(DCM)** for **2** hours, using **10** equivalents of formic acid **(HCOOH)** and 10 equivalents of sodium nitrite **($NaNO_2$)**, **(Scheme III.14)**.

Thin-layer chromatography **(TLC)** analysis revealed the appearance of a new spot, less polar than the starting material. After filtration of the resulting suspension, the reaction mixture was

treated with 5% aqueous sodium bicarbonate solutionand then washed with water to neutralize the medium. The crude product was subsequently purified by column chromatography (eluent: ethyl acetate/petroleum ether **60:40**).

However, analysis of the product using standard spectroscopic techniques revealed that the nitrosation of **(diethoxyphosphoryl)(phenyl)methyl(2-chloroethyl)** carbamates under these conditions led exclusively to the formation of rearranged products 2-chloroethyl(2-chloroethyl) carbamate **(III.17)**, instead of the expected nitroso derivative **(III.16) (Scheme III.14)**.

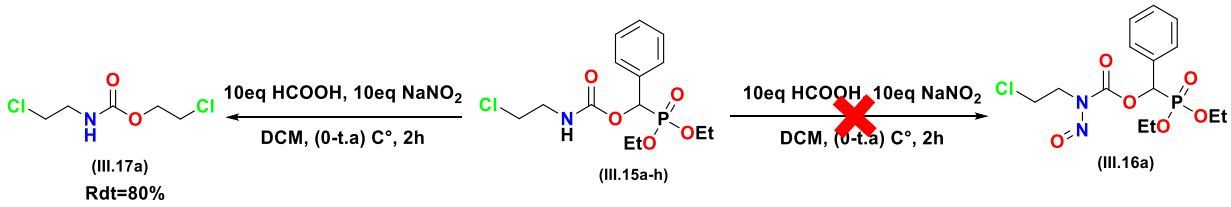

Scheme III.14. Synthesis of (diethoxyphosphoryl)(phenyl)methyl (2-chloroethyl)nitrosocarbamate (III.16).

3.2.2. Spectral characterization of diethoxy phosphoryl (phenyl)methyl (2-chloroethyl) carbamates derivatives

In NMR ^{1}H spectrum, The formation of (diethoxy phosphoryl)(phenyl)methyl(2-chloroethyl) carbamate (**III.15**) is confirmed by the presence of two triplets at **1.18** and **1.29** ppm, with coupling constants of $J_{H\text{-}H}$ **= 7.2 Hz** and $J_{H\text{-}H}$ **= 6.6 Hz,** corresponding to the two methyl groups. Additionally, two multiplets integrating for **4H** each, respectively, are observed in the range **3.50-4.12** ppm, corresponding to the eight methylene protons **(2CH₂N, 2CH₂PO)**.

The proton attached to the asymmetric carbon **(CH)** resonates at **6.04** ppm as a doublet with a coupling constant of $^{1}J_{H\text{-}P}$ **= 14.1 Hz**. Furthermore, a singlet at **5.47** ppm, attributed to the **NH** proton, confirms the presence of the carbamate functionality. Finally, the aromatic protons appear in their expected region, between **7.29** and **7.50** ppm.

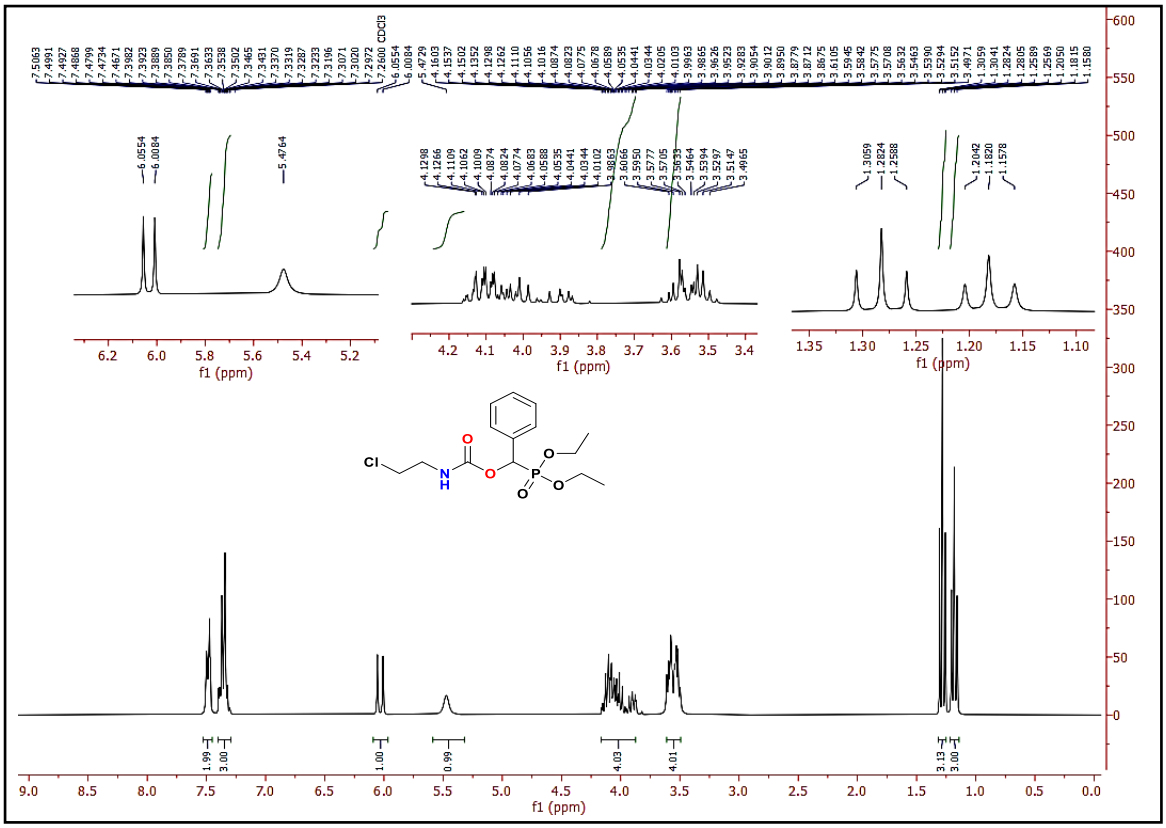

Figure III.20. ^{1}H NMR spectra of (diethoxyphosphoryl)(phenyl)methyl (2-chloroethyl)carbamate (III.15a).

The **^{13}C NMR** spectrum of our compound (**III.15a**) reveals characteristic peaks corresponding to methyl carbons, which appear between **16.2** and **16.5** ppm as doublets with a coupling constant of **(J_{C-P}=7.5 Hz)**. Additionally, three distinct peaks corresponding to methylene carbons **(CH_2Cl, CH_2N, and $2CH_2PO$)** are observed at **43.0, 43.6**, **63.3** ppm respectively. The asymmetric carbon appears at approximately **72.0** ppm as a doublet with a coupling constant of **(J_{C-P}=170.5 Hz)**. Finally, the carbonyl carbon resonates at **154.7** ppm.

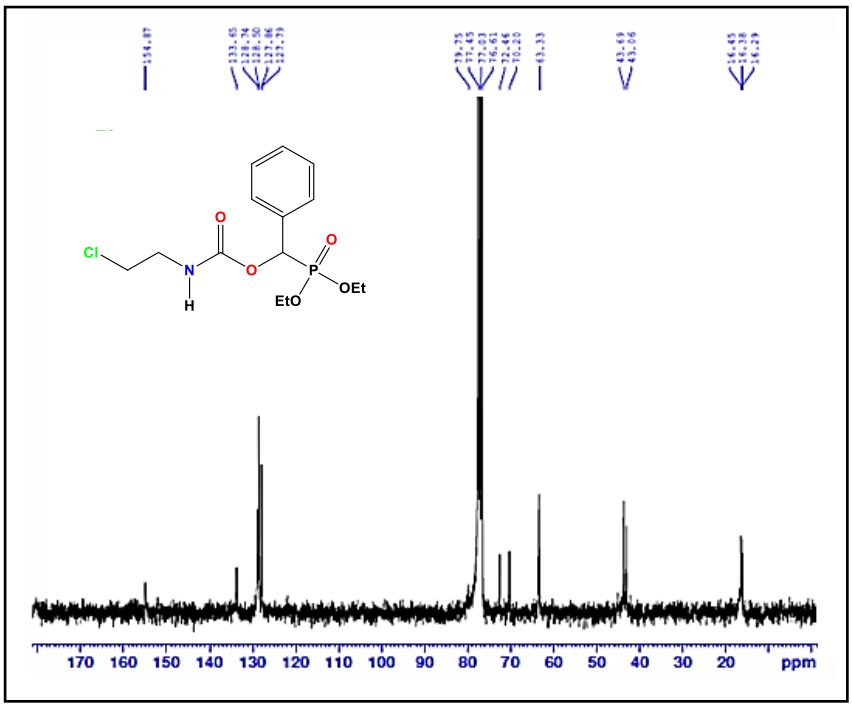

Figure III.21. ^{13}C NMR spectra of (diethoxyphosphoryl)(phenyl)methyl (2-chloroethyl)carbamate (III.15e).

In the infrared spectrum, compound (**III.15a**) is characterized by the presence of an absorption band at **1735 cm^{-1}**, corresponding to the stretching vibration of the carbonyl **(C=O)** functional group. Additionally, a broad absorption band appears at **3310 cm^{-1}**, attributed to the **N–H** stretching vibration. The bands observed at **1246 cm^{-1}** and **1026 cm^{-1}** are assigned to the stretching vibrations of the **P=O** functional group.

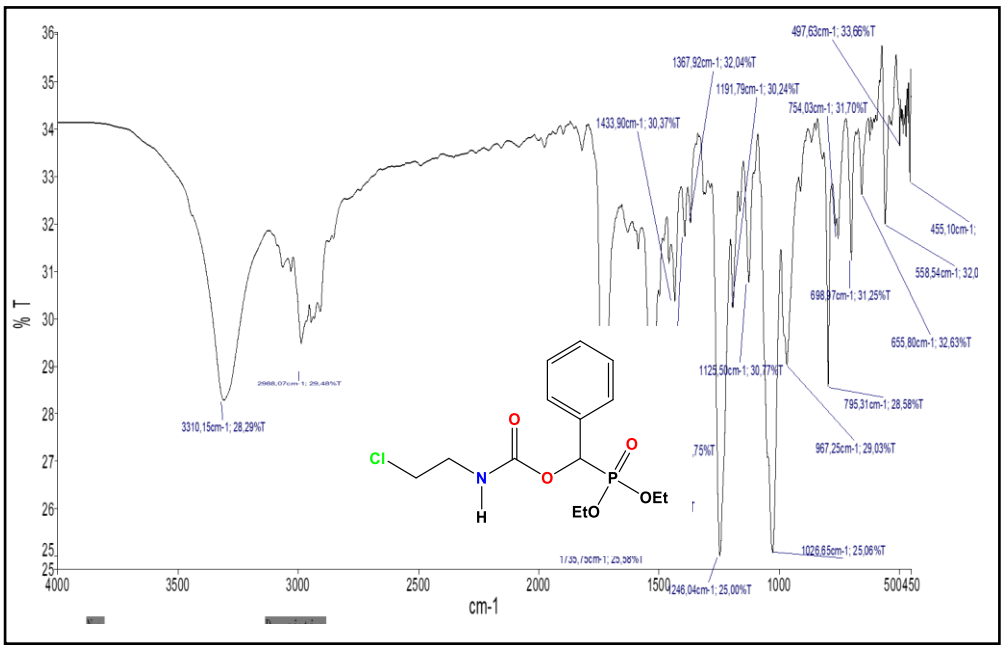

Figure III.22. Infrared spectrum of (diethoxyphosphoryl)(phenyl)methyl (2-chloroethyl) carbamate (III.15a).

In the ^{31}P NMR spectrum, the presence of a singlet at **17.35** ppm confirms the presence of a phosphorus atom in the compound.

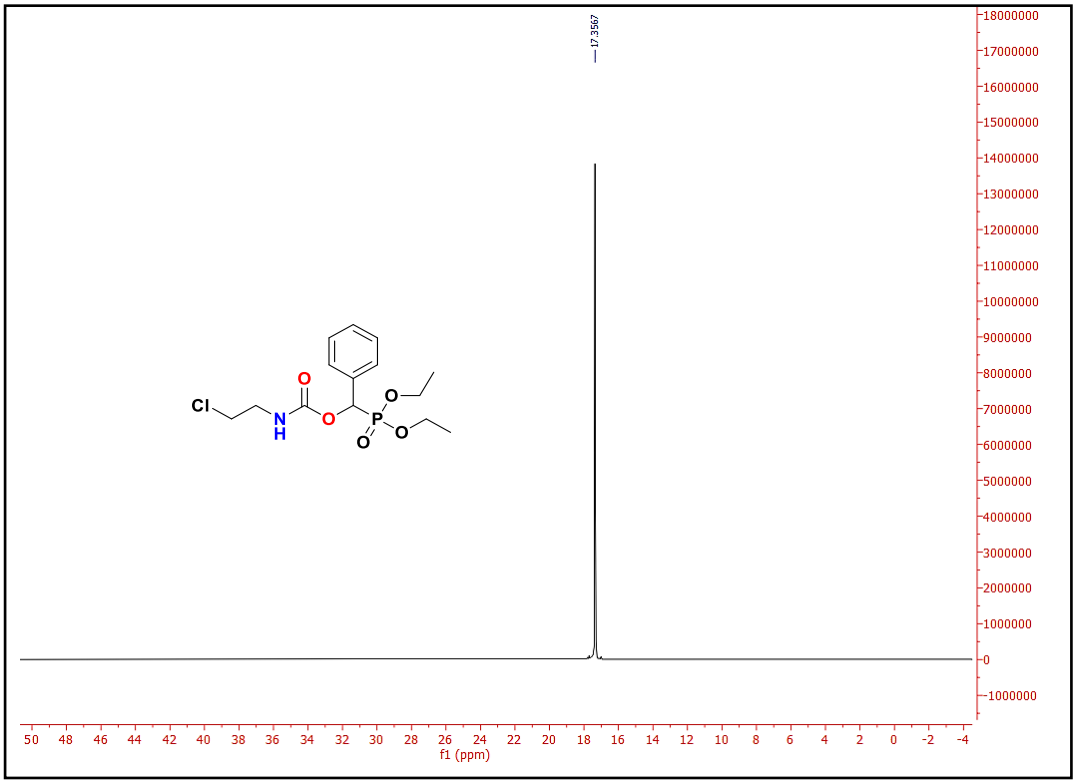

Figure III.23. ^{31}P NMR spectra of (diethoxyphosphoryl)(phenyl) methyl (2-chloroethyl) carbamate (III.15a).

The structure of the rearranged products was confirmed by spectroscopic techniques, including **IR**, **^{1}H NMR**, and **^{13}C NMR** analyses.

The **^{1}H NMR** spectrum of 2-chloroethyl(2-chloroethyl) carbamate **(III.16)** shows two characteristic triplets at δ **3.75** and **4.10 ppm**, with coupling constants of ***J* = 6.0 Hz** and ***J* = 6.5 Hz**, respectively. These signals are assigned to the methylene protons of the NH–**CH₂** and **CH₂**-Cl groups. Additionally, a set of multiplets integrating for four protons appears in the δ **3.60–3.65 ppm** region, corresponding to the two-methylene groups of the **OCH₂CH₂Cl** fragment, A triplet at δ **8.97** ppm, attributed to the proton of the **NH** group adjacent to the methylene groups.

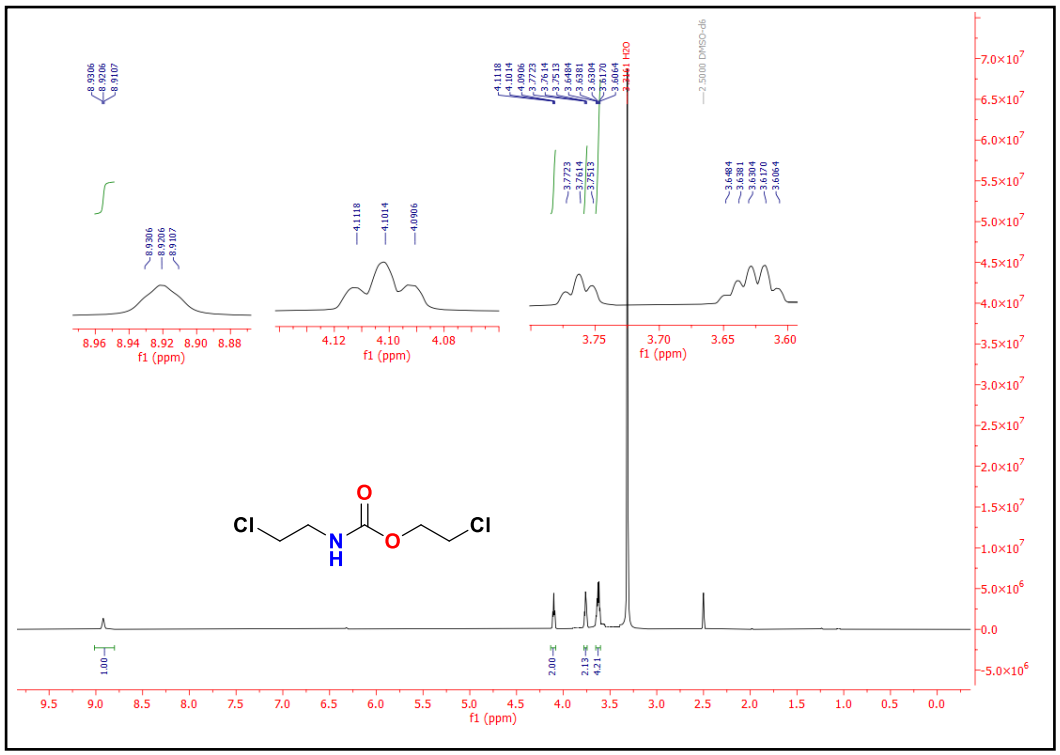

Figure III.24. ^{1}H NMR spectra of (2-chloroethyl(2-chloroethyl) carbamate) (III.16).

The ^{13}C NMR spectrum of compound **III.15e** shows peaks corresponding to the methylene carbons **(CH_2Cl, CH_2N, and OCH_2)** in the region of **42.6-43.2 ppm**. The resonance of the carbamate carbonyl carbon appears at **153.4 ppm**.

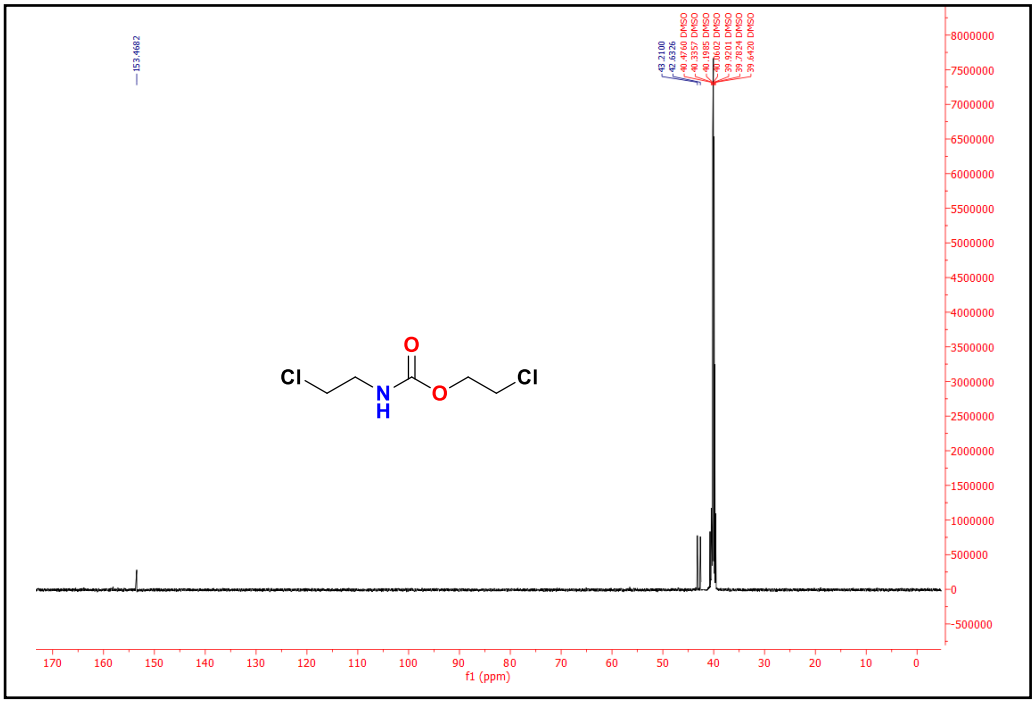

Figure III.25. ^{13}C NMR spectra of (2-chloroethyl(2-chloroethyl) carbamate) (III.15e).

4. Conclusion

The exploration of new chemical entities with high pharmacological potential remains one of the key challenge in medicinal chemistry. Among the approaches employed, the design of structures inspired by known bioactive molecules allows for the optimization of their properties while improving pharmacokinetic and toxicological profiles.

In this chapter, we have explored the synthesis of four distinct series of compounds that may exhibit interesting biological activities.

First, we developed a series of xanthene derivatives, obtained through the condensation of two equivalents of dimedone with an aromatic aldehyde. This reaction, optimized under ultrasonic irradiation in the presence of a heterogeneous zinc acetate-based catalyst, afforded the desired products with excellent yields **(84–95%),** highlighting the efficiency of this approach.

Next, we established the synthesis of 1,2-oxaphospholanes-2-oxides *via* a Phospha-Michael addition followed by an intramolecular cyclization. This methodology, achieved in a single step from dimedone, diethyl phosphite and an aromatic aldehyde, provides an efficient alternative for obtaining these heterocycles.

Furthermore, we designed and synthesized a series of nitrosourea derivatives, relying on 2-chloroethylisocyanate as a key reagent. The series consists of 2-chloroethylnitrosocarbamates, analogues of carmustine, synthesized in two successive steps (carbamoylation followed by nitrosation).

We also used 2-chloroethylisocyanate in the attempted synthesis of carbonylated analogues of fotemustine, involving a three-step sequence (Pudovik reaction, carbamoylation, and nitrosation), which unexpectedly led to a rearranged product rather than the targeted nitroso derivative.

Chapter IV

In vitro and *in silico* studies of synthesized compounds

1. *In silico* study of xanthenes derivatives

1.1. Molecular docking

Molecular docking studies highlight the significance of VEGFR-2 in the design of novel therapeutic agents targeting angiogenesis. Understanding the molecular interactions with VEGFR-2 provides valuable insights for designing innovative therapies against cancer and related disorders.**[223]** By analyzing the interactions between this protein and small molecules, these studies help identify potential pharmacological candidates. In this context, a docking study was conducted using the Schrödinger Suite and ChimeraX to examine the binding modes of the investigated compounds. The molecular docking simulations were performed to evaluate the binding affinity of the synthesized compounds toward the VEGFR-2 active site. For this purpose, the crystallographic structure of the VEGFR-2 enzyme complexed with 4-amino-furo[2,3-d]pyrimidine **(PDB ID: 1YWN)** was retrieved from the RCSB Protein Data Bank.**[224]** The 4-amino-furo[2,3-d]pyrimidine was used as a reference ligand to validate the docking protocol, whose reliability was confirmed through precise redocking **(RMSD = 0.38 Å) (Figure IV.1)**. This approach, based on a standard precision (SP) scoring function and excluding water molecules, provided reliable predictions of ligand–receptor interactions.

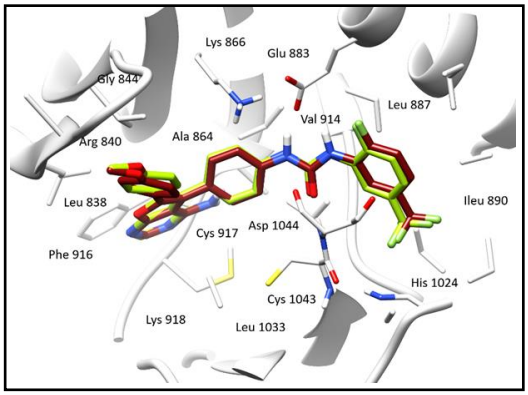

Figure IV.1. Representation of the docked and co-crystallized 4-amino-furo[2,3-d] pyrimidine within the active site of the VEGFR-2 enzyme following self-docking calculations. The co-crystallized ligand is depicted in green sticks, while the docked ligand is shown in brown sticks.

The analysis of molecular docking for the compounds investigated indicates that the majority exhibit favourable stability within the binding pocket. Among these, compounds **III.3t, III.3p, III.3e, III.3i, III.3b, III.3m,** and **III.3c** stand out due to their superior binding affinities, as reflected in their higher glide scores compared to the other tested compounds. These specific compounds displayed average binding scores between **-6.99** and **-6.12** kcal/mol. Conversely, compounds **III.3f**, **III.3a**, and **III.3o** showed diminished stability, with

glide scores of **-4.80, -5.08** and **-5.20** kcal/mol **(Table IV.1)**, respectively. Overall, these findings provide valuable insights into the binding affinity and stability of the examined compounds within the active site of the target protein **(Figure IV.2)**.

Table IV.1 Docking scores (kcal/mol) of synthesized xanthene derivatives (III.3a–III.3t) and the reference ligand (4-amino-furo[2,3-d]pyrimidine) against the VEGFR-2 enzyme, obtained through molecular docking analysis..

Entry	Docking score	Compound code	Docking score
III.3a	-5.08	**3k**	-5.12
III.3b	-6.24	**3l**	-6.10
III.3c	-6.12	**3m**	-6.20
III.3d	-6.02	**3n**	-5.94
III.3e	-6.52	**3o**	-5.20
III.3f	-4.80	**3p**	-6.80
III.3g	-6.01	**3q**	-5.80
III.3h	-5.28	**3r**	-6.05
III.3i	-6.34	**3s**	-5.40
III.3j	-5.80	**3t**	-6.99
	Reference ligand	-13.11	

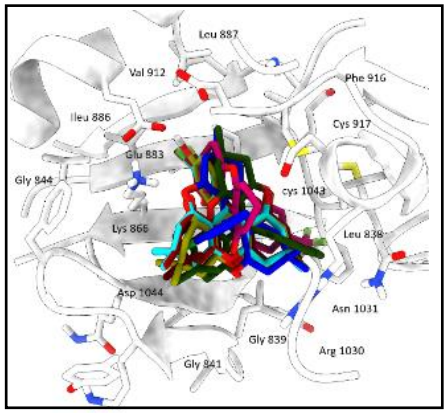

Figure IV.2. Superimposition of the most stable xanthene derivatives in the active site of VEGFR-2 enzyme

Compounds **(III.3e** and **III.3p)** demonstrated remarkable stability within the **VEGFR-2** active site, primarily due to the presence of a hydroxyl group in the para position of their aromatic rings. This functional group forms a key hydrogen bond with the crucial residue Glu803, significantly enhancing ligand stability within the binding pocket. Additionally, compound **III.3e** exhibited further stabilization through an additional hydrogen bond and a cationic interaction with Lys866, a residue known to contribute to enzyme inhibition **(Figure IV.3)**.

Both compounds also engaged in extensive hydrophobic interactions with residues Phe916, Cys917, Val897, Leu1033, and Cys1043, which are recognized for their role in **VEGFR-2** inhibition. These interactions not only support the observed docking scores but also provide insight into the inhibitory mechanisms of these compounds.

Similarly, compound **III.3s** displayed a binding profile comparable to that of **III.3e** and **III.3p**, showing substantial stability within the active site with favorable docking scores. This compound formed a critical hydrogen bond with Asp1044, a key residue involved in **VEGFR-2** inhibition, and an ionic interaction with Glu883. Furthermore, it engaged in significant hydrophobic interactions, including a π-cation interaction with Lys886, further stabilizing its binding within the enzyme pocket.

An analysis of the remaining compounds revealed that the nature of the substituent on the phenyl ring plays a crucial role in determining stability within the active site. Specifically, compounds featuring halogen substitutions or an additional aromatic ring, such as a naphthalene moiety, exhibited moderate stability compared to other derivatives. This trend is exemplified by compound **III.3f**, which serves as a representative case of this structural influence.

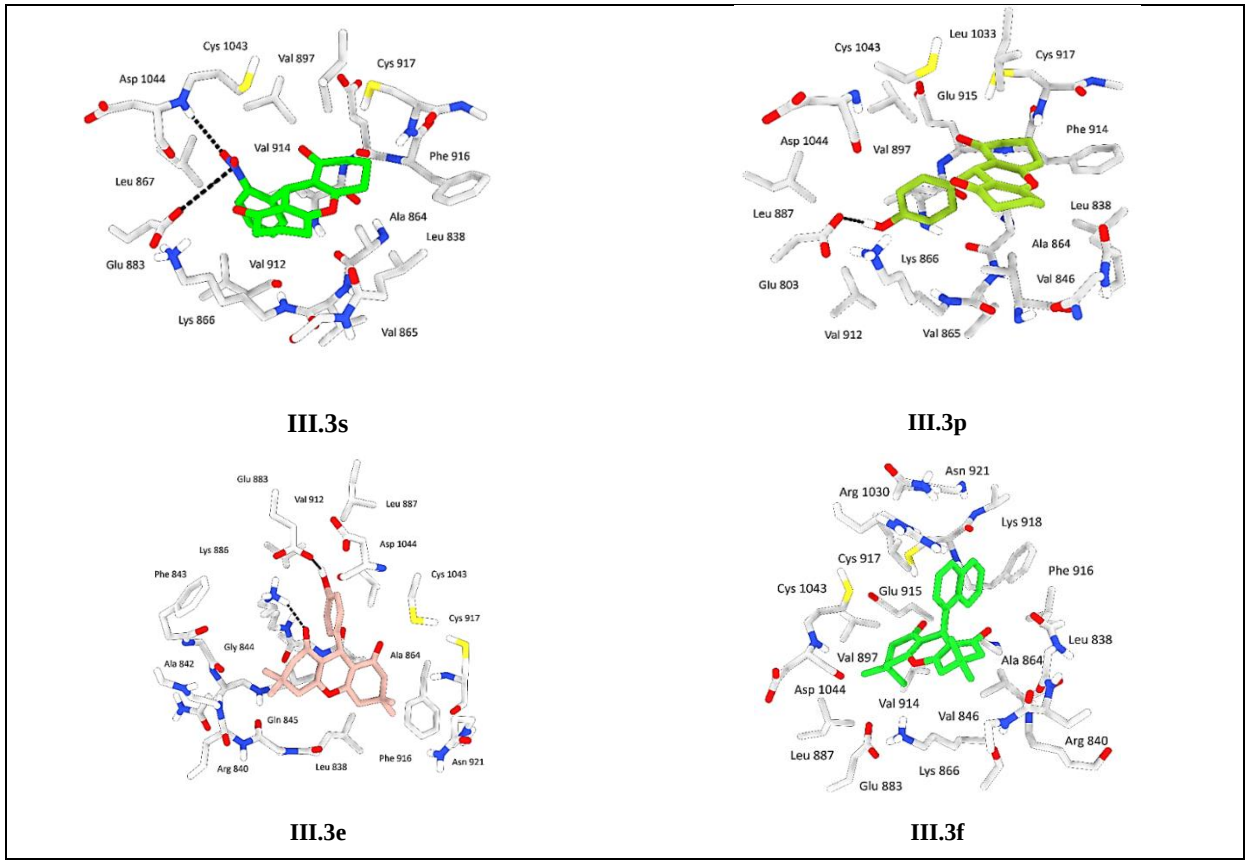

Figure IV.3. 3D binding interactions of compounds 3s, 3p, 3e and 3f after docking calculations in the active site of VEGFR-2 enzyme. The amino acid residues were shown as grey stick model and H-bonds were shown as black lines.

1.2. ADME analysis

To evaluate the drug-likeness potential of the synthesized xanthenes, an *in silico* study was performed using the SwissADME online server.**[225]** This computational analysis provided insights into key pharmacokinetic parameters related to ADME (absorption, distribution, metabolism, and excretion), as summarized in the table below. These properties are critical in drug development, influencing dosage, administration regimen, and safety margins.**[226]** The assessment of molecular suitability was based on Lipinski's rule of five. This rule considers essential criteria such as a molecular weight **≤ 500** Da, an octanol-water partition coefficient (miLogP) **≤ 5**, and a limited number of hydrogen bond acceptors **(≤ 10)** and donors **(≤ 5)**, all of which contribute to a compound's potential as a drug candidate.**[227]**

The results indicate that all studied compounds comply with these criteria, ensuring favorable absorption and bioavailability. The molecular weights of the investigated compounds **(III.3a–III.3t)** range from **294.34** to **442.54** Da, facilitating their transport, diffusion, and absorption. The number of hydrogen bond acceptors varies between **3** and **6 (< 10)**, while hydrogen bond donors remain below 5 in all cases, promoting membrane permeability. Additionally, most derivatives exhibit optimal lipophilicity, with Log P values between **2.83** and **3.81**, well within the recommended threshold **(Log P < 5)**, a crucial factor for passive diffusion across biological membranes and overall pharmacokinetic behaviour **[228] (Table IV.2).**

Solubility, another key factor in drug formulation, was assessed using Log S values, which range from -**3.12** to -**5.79.** These values indicate that the compounds possess adequate aqueous solubility, facilitating drug formulation and absorption. Regarding skin permeability, the Log Kp values vary, with compound **III.3g** exhibiting the lowest permeability **(-6.93 cm/s)** and compound **III.3l** the highest **(-4.13 cm/s)**. Lower permeability is generally advantageous for oral drug candidates. Furthermore, the topological polar surface area **(TPSA)** values range from **43.37** to **89.19 Å** ,**[229]** all falling within the recommended limits for oral bioavailability.

Table IV.2. Pharmacokinetic parameters and drug likeness score (DLS) of compounds **(III.3a–III.3t)** and Rhodomyrtone drug.

Properties	Molecular weight (g/mole)	Rotatable bonds	H-bond donor	H-bond acceptor	Log Po/W iLogP	Log S ESOL	Log Kp	Bioavailability Score	TPSA (Å)	DLS
Rhodomyrtone	442.54	5	2	6	3.76	-6.02	-4.91	0.56	100.90	-0.33
III.3a	350.45	1	0	3	3.40	-4.62	-5.62	0.85	43.37	-1.31
III.3b	429.35	1	0	3	3.81	-5.54	-5.54	0.85	43.37	-1.17
III.3d	368.44	1	0	4	3.54	-4.79	-5.66	0.85	43.37	-0.98
III.3c	384.90	1	0	3	3.71	-5.22	-5.38	0.85	43.37	-0.77
III.3e	366.45	1	1	4	3.16	-4.48	-5.97	0.85	63.60	-0;72
III.3f	400.51	1	0	3	3.61	-5.79	-5.04	0.85	43.37	-1.10
III.3g	410.50	3	0	5	3.85	-4.80	-6.93	0.85	61.83	-0.41
III.3h	364.48	1	0	3	3.44	-4.93	-5.45	0.85	43.37	-0.99
III.3i	384.90	1	0	3	3.62	-5.22	-4.13	0.85	43.37	-0.87
III.3j	366.4	1	1	4	3.02	-4.48	-5.97	0.85	63.60	-0.78
III.3k	395.45	2	0	5	3.07	-4.71	-6.01	0.56	89.19	-1.25
III.3l	310.34	1	1	4	2.40	-3.12	-6.81	0.85	63.60	-0;54
III.3m	373.24	1	0	3	3.09	-4.17	-6.45	0.85	43.37	-0.99
III.3n	312.33	1	0	4	2.83	-3.42	-6.49	0.85	43.37	-0.80
III.3o	328.79	1	0	3	3.00	-3.85	-6.23	0.85	43.37	-0.62
III.3p	294.34	1	0	3	2.70	-3.26	-6.46	0.85	43.37	-1.16
III.3q	362.34	2	0	6	3.06	-5.38	-6.25	0.85	43.37	-1.04
III.3r	308.37	1	0	3	2.88	-3.56	-6.29	0.85	43.37	-0.63
III.3s	354.40	3	0	5	3.15	-3.43	-6.86	0.85	61.83	0.07
III.3t	339.34	2	0	5	2.70	-3.33	-6.86	0.56	89.19	-0.98

The bioavailability radar visualization provides a comprehensive overview of the physicochemical properties of the investigated compounds. Most xanthenes align with the optimal ranges for lipophilicity, size, polarity, flexibility, and solubility, suggesting promising pharmacokinetic profiles. These findings, as presented in **figure IV.4**, highlight their potential for further development as drug candidates.

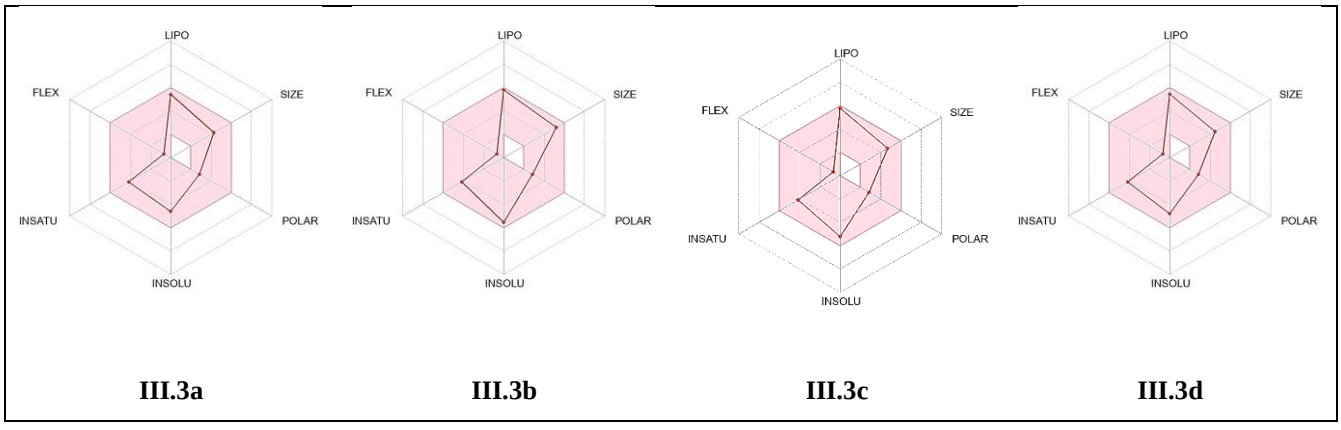

Figure IV.4. Radar related to physicochemical properties of the synthesized molecules.

1.3. Density functional theory

To complement our *in silico* study and establish a correlation between the predicted binding mode of xanthene derivatives and their structural properties, we performed a computational study using density functional theory **(DFT)**. As a fundamental tool in computational chemistry, **DFT** provides a robust framework for calculating molecular properties and elucidating the electronic behavior of a structure in various states. This method is particularly effective in assessing chemical reactivity and stability. In this study, we employed the **B3LYP/6-31G(d,p)** model, implemented in Gaussian **09** to optimize molecular geometries, analyse electron density distributions, and determine key global chemical reactivity descriptors. These descriptors include chemical hardness **(η)**, molecular softness **(s)**, electronic chemical potential **(μ)**, electronegativity **(χ)**, and electrophilicity index **(ω)**.

The dipole moment, which reflects charge separation and molecular polarity, was found to range between **4.7750** and **8.1477** D for the studied xanthene-based derivatives. Among them, compound **III.3j** was the most polar, while **III.3e** was the least. The obtained results are summarized in **table IV.3.**

Table IV.3 Calculated molecular descriptors of the studied xanthene derivatives obtained by DFT B3LYP/6-31G (d,p) method in gas phase.

Molecular descriptors (Gaz phase)									
Entry	**μ (D)**	**E_{HOMO} (eV)**	**E_{LUMO} (eV)**	**ΔEgap**	**(η)**	**(*S*)**	**(μ)**	**(χ)**	**(ω)**
III.3a	6.0432	-6,1471	-1.5445	4.6025	2.3013	0.4345	-3.8458	3.8458	3.2135
III.3b	7.3494	-6.1416	-1.6936	4.4480	2.2240	0.4496	-3.9176	3.9176	3.4505
III.3c	7.4033	-6.2042	-1.6920	4.5122	2.2561	0.4432	-3.9481	3.9481	3.4545
III.3d	6.8678	-6.1149	-1.6262	4.4888	2.2444	0.4456	-3.8705	3.8705	3.3375
III.3e	4.7750	-5.6145	-1.5124	4.1021	2.0511	0.4876	-3.5635	3.5635	3.0955
III.3f	5.7832	-5.5130	-1.5818	3.9312	1.9656	0.5087	-3.5474	3.5474	3.2011
III.7g	7.1153	-5.4768	-1.4887	3.9881	1.9941	0.5015	-3.4828	3.4828	3.0415
III.3h	5.6706	-6.0861	-1.5233	4.5628	2.2814	0.4383	-3.8047	3.8047	3.1725
III.3i	7.1479	-6.1710	-1.6098	4.5612	2.2806	0.4385	-3.8904	3.8904	3.3183
III.3j	8.1477	-5.4975	-1.8278	3.6697	1.8349	0.5450	-3.6627	3.6627	3.6556
III.3k	9.1839	-6,3639	-1,9323	4,4316	2,2158	0,4513	-4,1481	4,1481	3,8827
III.3l	6.0239	-6,1612	-1,5666	4,5946	2,2973	0,4353	-3,8639	3,8639	3,2493
III.3m	7.2722	-6,1509	-1,7173	4,4336	2,2168	0,4511	-3,9341	3,9341	3,4909
III.3n	6.8094	-6.1272	-1.6490	4.4782	2.2391	0.4466	-3.8881	3.8881	3.3758
III.3o	7.3246	-6.2162	-1.7162	4.4999	2.2500	0.4444	-3.9662	3.9662	3.4958
III.3p	7.1185	-5.6295	-1.5350	4.0945	2.0472	0.4885	-3.5822	3.5822	3.1341

III.3q	7.8681	-6.4736	-1.7832	4.6904	2.3452	0.4264	-4.1284	4.1284	3.6337
III.3r	6.1091	-6.0251	-1.5429	4.4823	2.2411	0.4462	-3.7840	3.7840	3.1945
III.3s	7.1539	-5.4820	-1.5075	3.9745	1.9872	0.5032	-3.4948	3.4948	3.0729
III.3t	9.2091	-6,4031	-1,9497	4,4534	2,2267	0,4491	-4,1764	4,1764	3,9166

The optimized molecular geometries, along with the Frontier Molecular Orbitals (FMOs), are illustrated in **Table IV.4**. In **FMO theory**, the energies of the **HOMO** and **LUMO** are essential for understanding molecular reactivity. The **HOMO** represents a molecule's ability to donate electrons, thus acting as a nucleophile, while the **LUMO** reflects its tendency to accept electrons, making it an electrophile.**[230]**The energy gap between these two orbitals, referred to as the energy gap **(ΔE)**, is a key parameter in evaluating chemical stability and reactivity**.** A large energy gap is generally associated with high kinetic stability and low chemical reactivity**,** making the molecule less polarizable and more resistant to electronic interactions.**[231]**

For the studied xanthene derivatives, the calculated energy gaps **range** from **3.6697 to 4.6904 eV**, indicating significant differences in terms of stability and chemical reactivity**.** Compound **III.3q** exhibits the highest energy gap**,** demonstrating its superior stability compared to other analogues. This observation aligns with the importance of **FMOs** in predicting ligand-receptor interactions, where a lower energy gap facilitates electron transfer and enhances reactivity, a key factor in molecular interaction studies.

Furthermore, the graphical representation of optimized structures and the charge density distribution in **HOMO** and **LUMO** orbitals helps identify electrophilic and nucleophilic regions within the molecules, providing qualitative insights into their electronic susceptibility**.** The geometric optimization of these derivatives was performed using **Gaussian 09W software**, where the red and green colors represent the negative and positive phases of the orbitals, respectively, thereby facilitating the interpretation of electronic interactions within the studied structures.

Table IV.4. Optimized structures and HOMO/LUMO orbitals of studied xanthenes.

Code	Optimized structure	HOMO	LUMO
III.3a	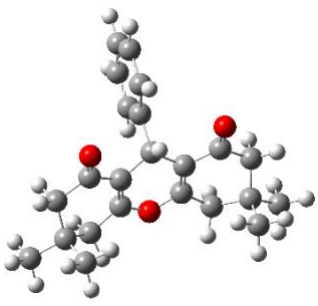	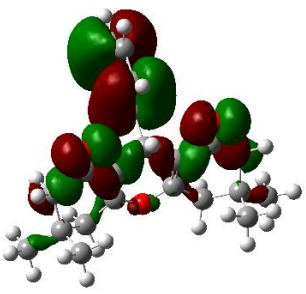	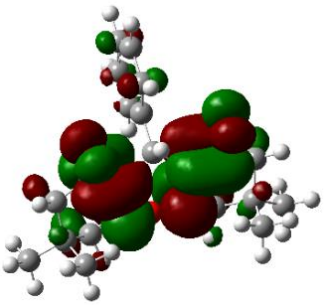

III.3b	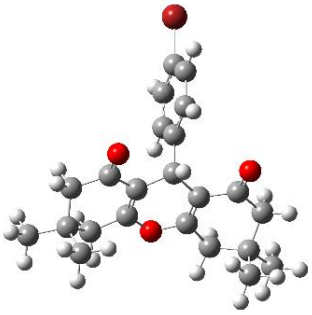	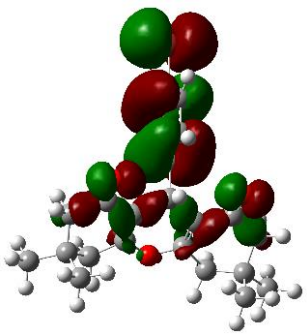	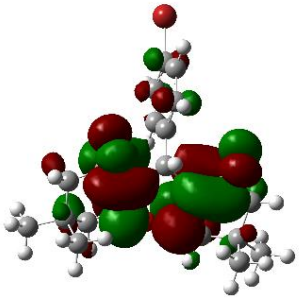
III.3c	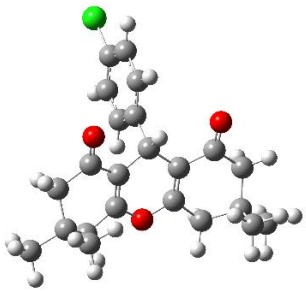	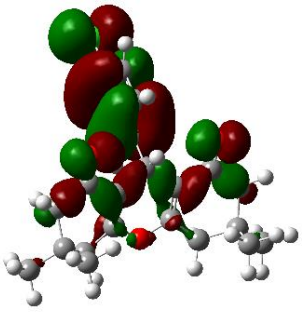	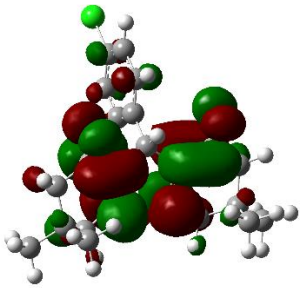
III.3d	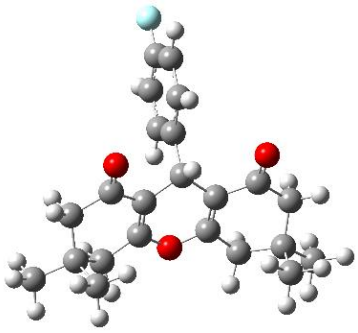	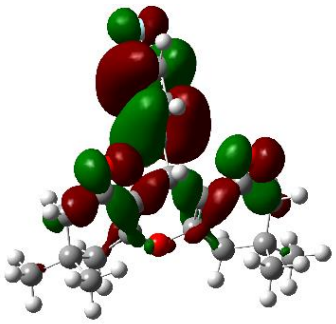	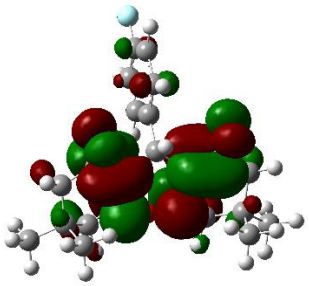
III.3d	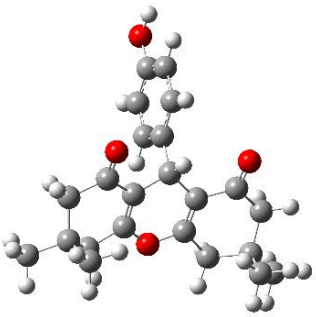	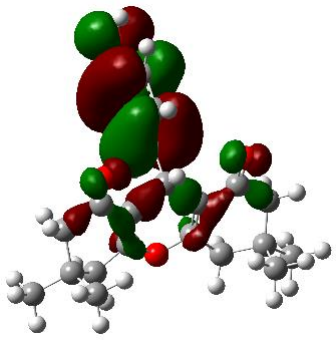	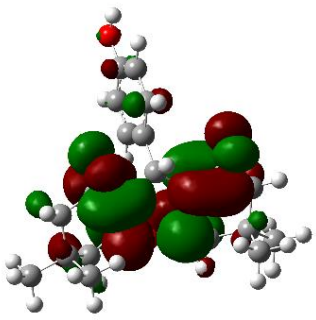
III.3e	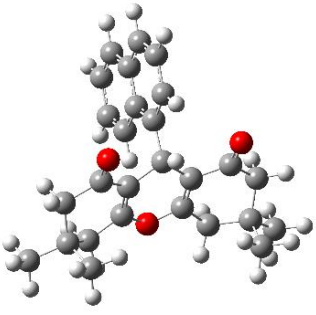	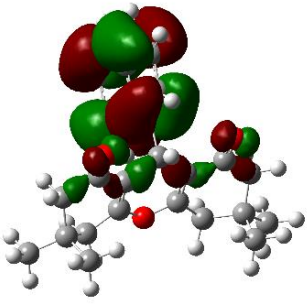	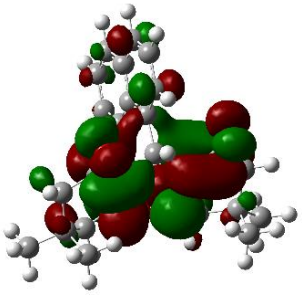

III.3f	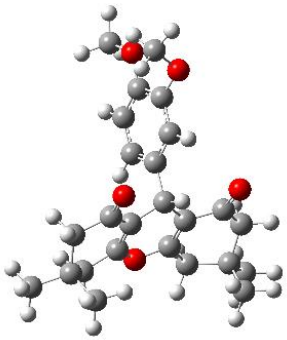	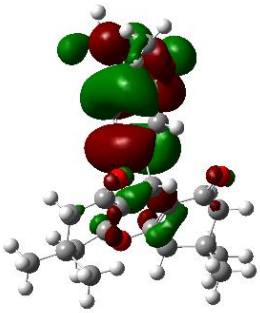	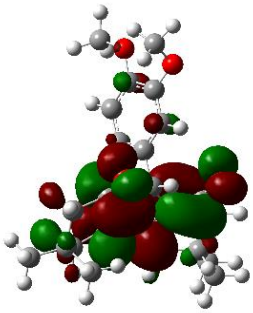
III.3g	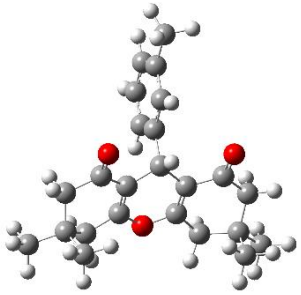	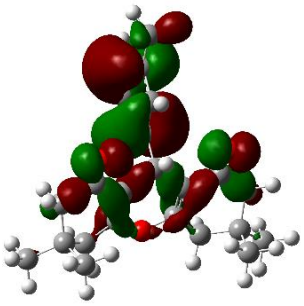	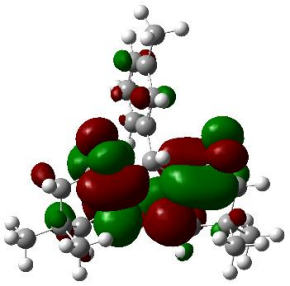
III.3h	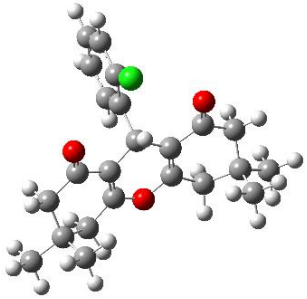	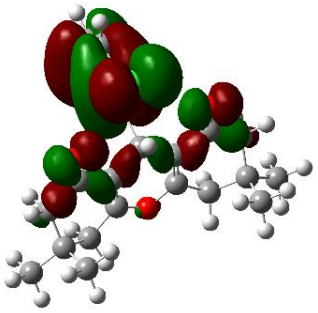	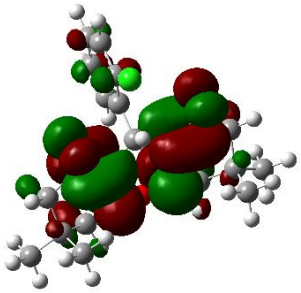
III.3i	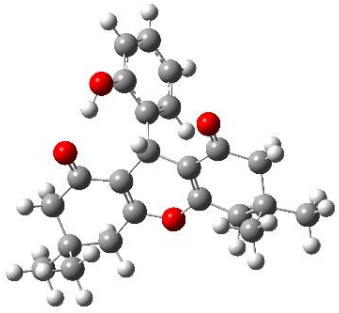	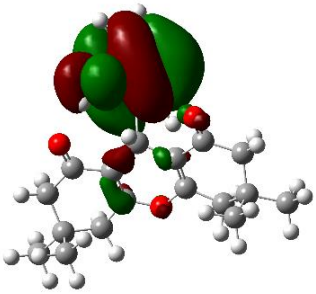	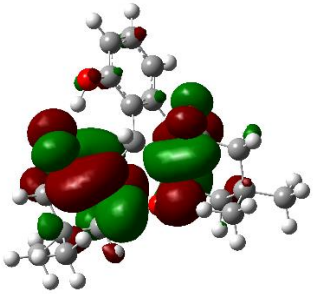
III.3j	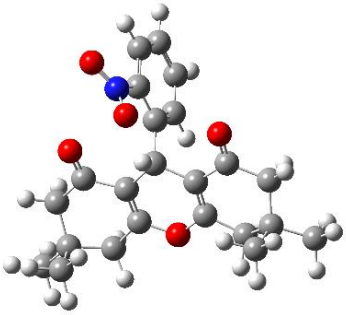	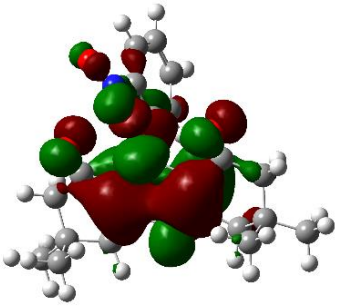	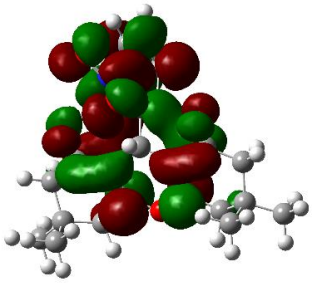

III.3l	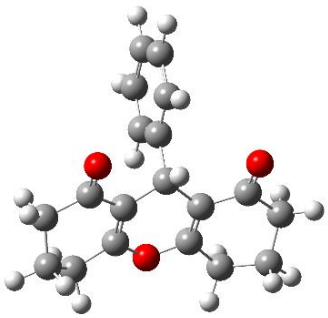	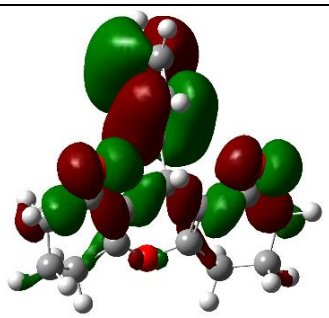	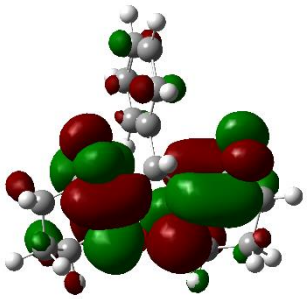
III.3m	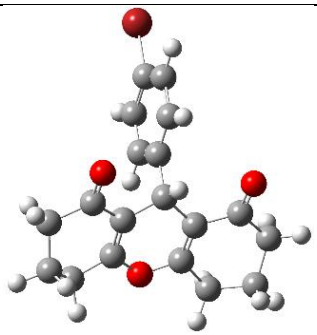	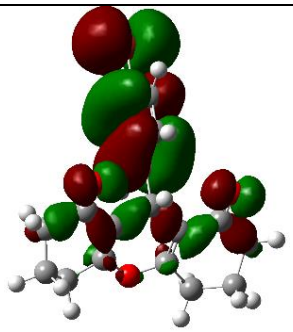	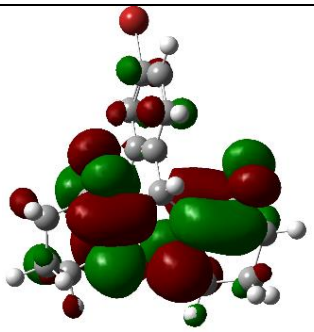
III.3n	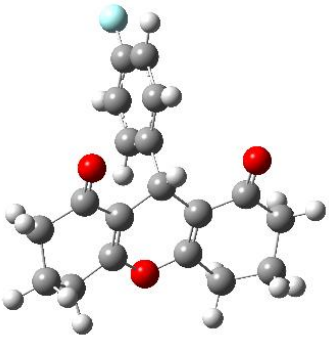	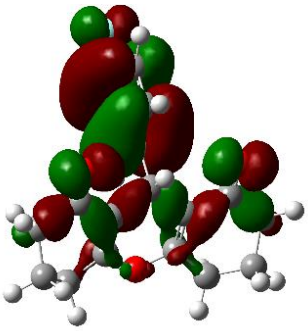	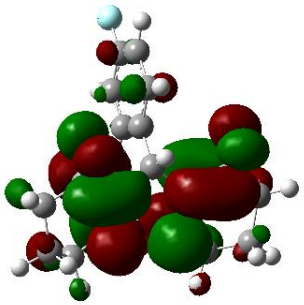
III.3o	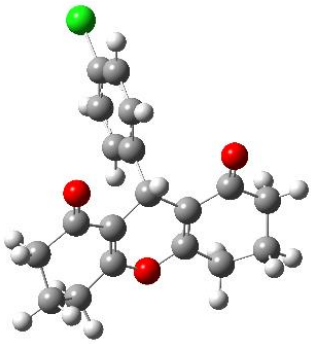	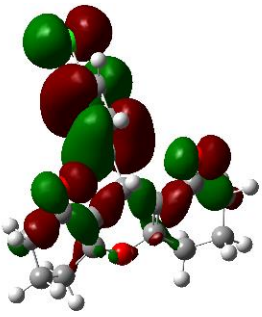	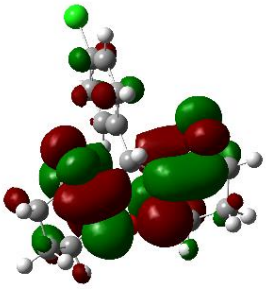
III.3p	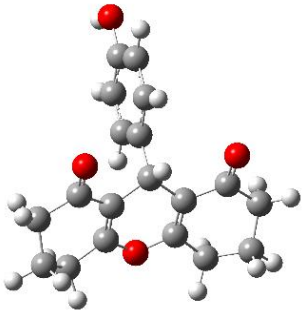	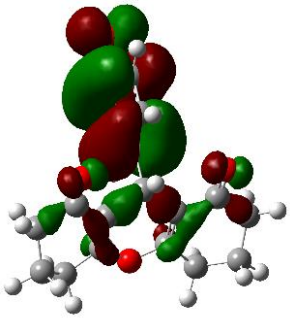	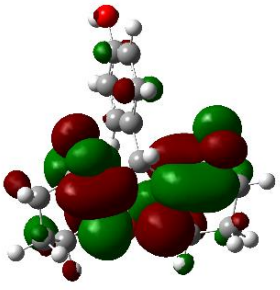

III.3q	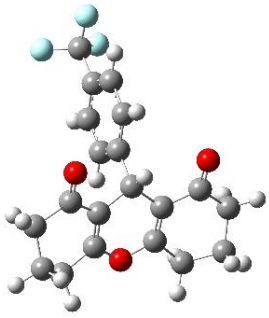	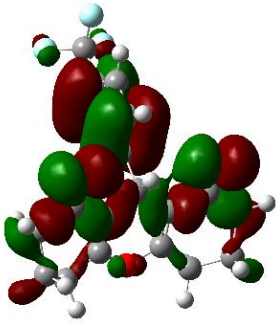	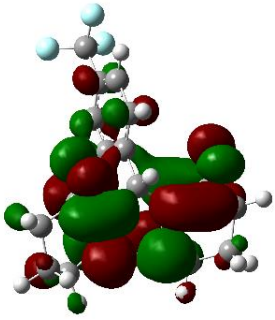
III.3r	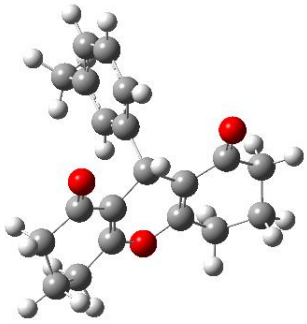	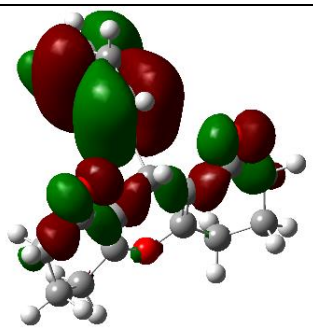	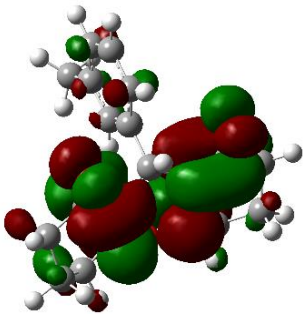
III.3s	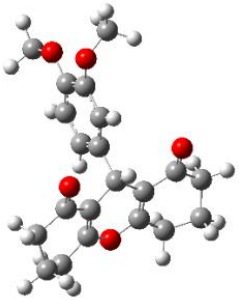	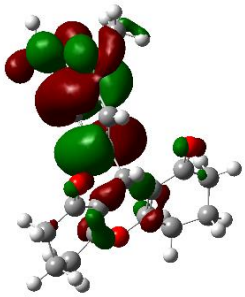	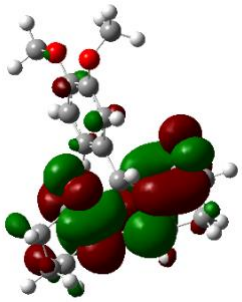
III.3t	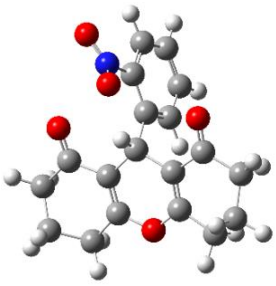	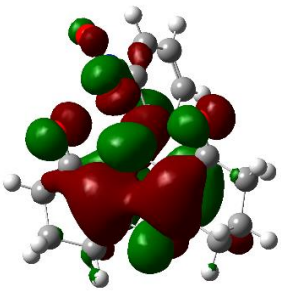	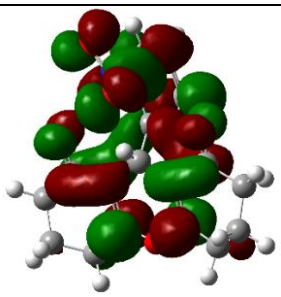

The molecular electrostatic potential **(MEP)** is a powerful computational approach for visualizing the distribution of electron density within a molecule. It plays a crucial role in understanding molecular interactions, chemical reactivity, and the potential for hydrogen bond formation, particularly in biological environments. **[232]**MEP surface mapping enables the identification of regions most susceptible to nucleophilic and electrophilic attacks, where the most electron-rich **(red)** and electron-deficient **(blue)** areas are distinctly highlighted. These visual representations help pinpoint key reactive sites and are essential for predicting ligand-receptor interactions and variations in binding affinity.**[233]**

In this work, MEP surfaces were generated for all studied compounds based on structures optimized using density functional theory **(DFT)** with the **B3LYP** functional and the 6-**31G(d,p)** basis set, as depicted in **figure IV.5**. The results indicate that red regions, corresponding to high electron density, are mainly concentrated on the oxygen atoms of the carbonyl **(C=O)** group, making them favorable sites for electrophilic attack. This charge distribution is in agreement with the frontier molecular orbital **(HOMO-LUMO)** analysis, further reinforcing insights into the chemical reactivity of the molecules.

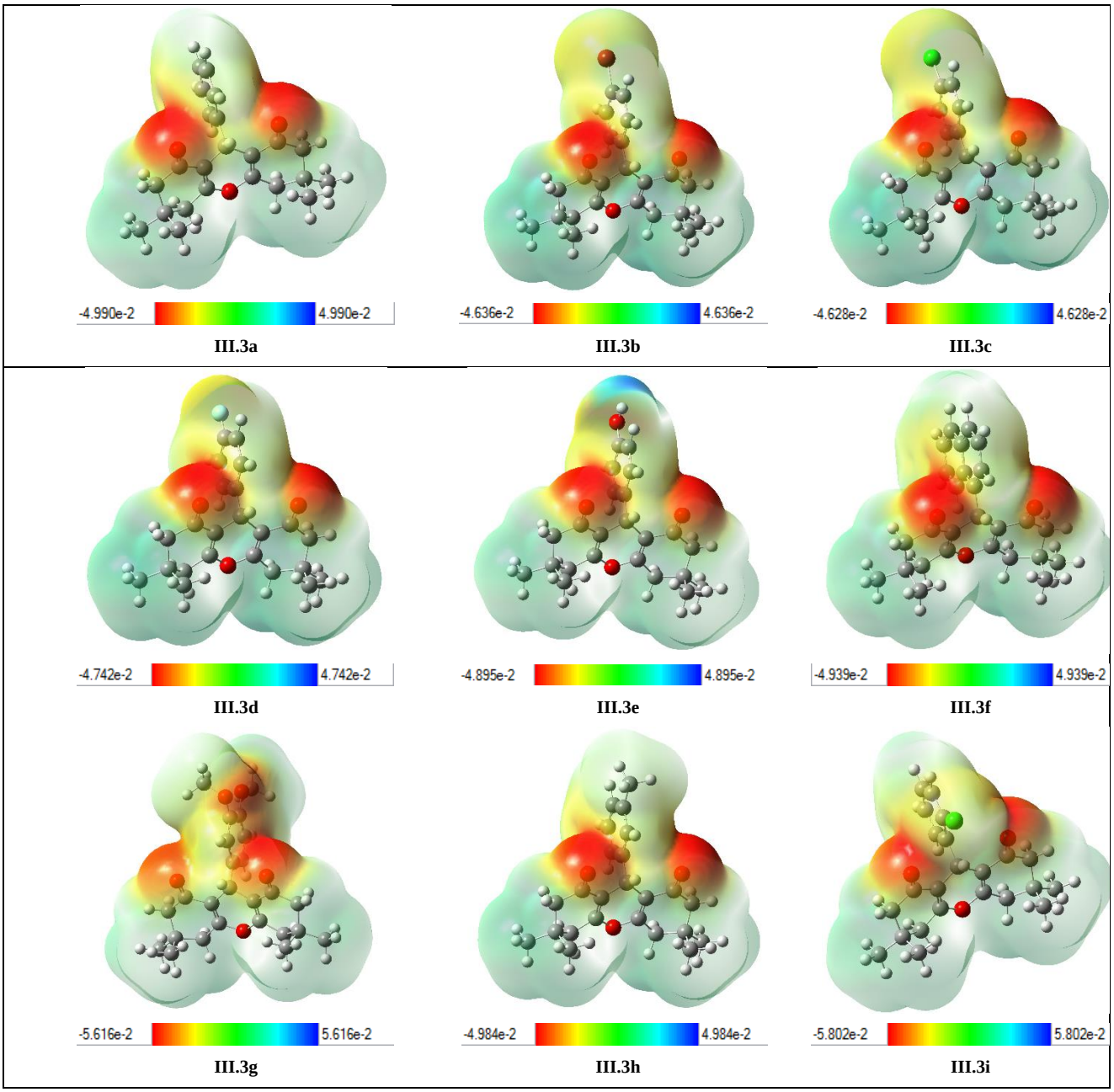

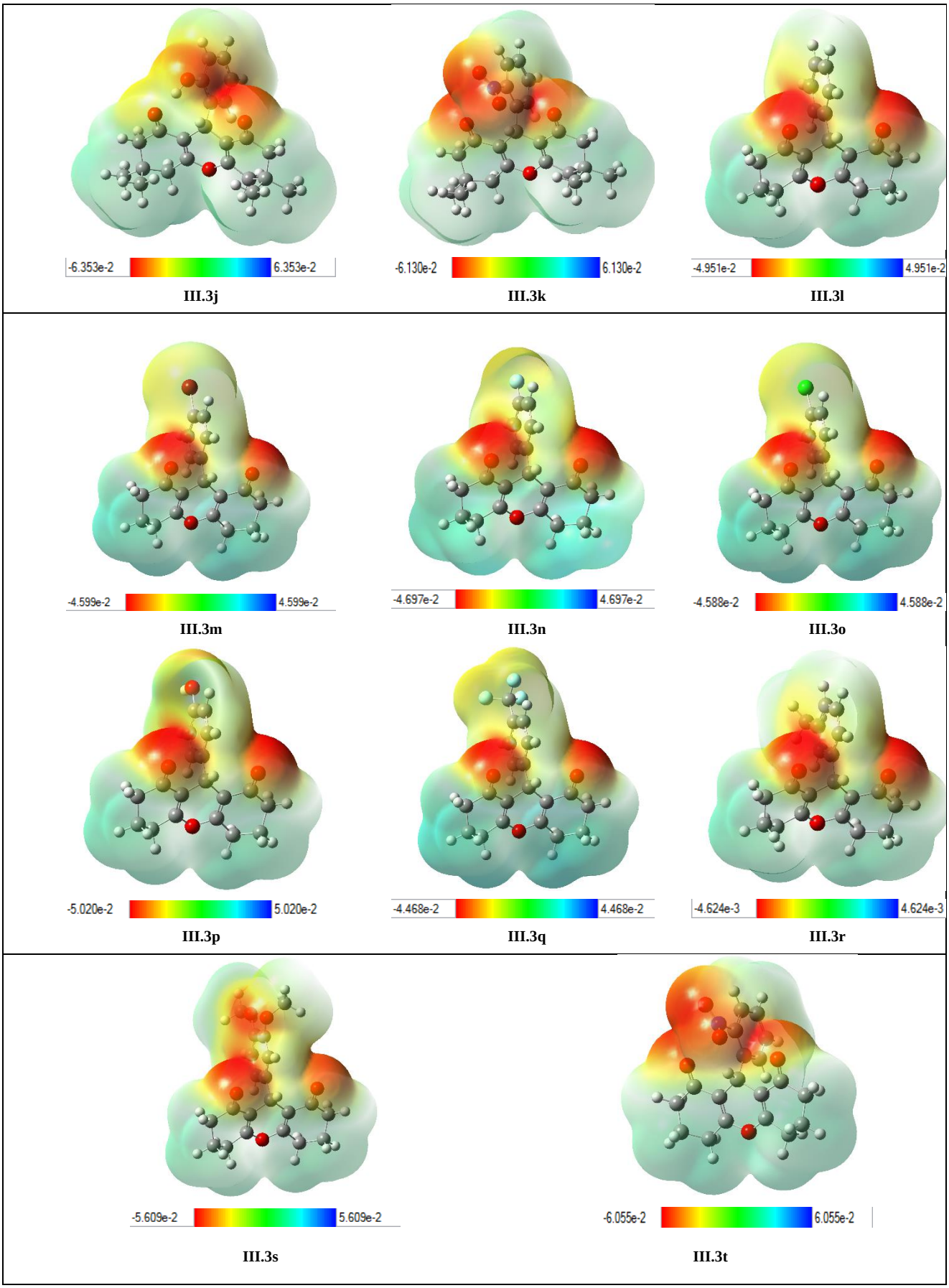

Figure IV.5. MEP maps of synthesized xanthene derivatives.

2. *In vitro* and *in silico* assessment of 1,2-oxaphospholanes-2-oxides derivatives

2.1. Antioxidant activity

The antioxidant potential of the synthesized compounds **III.5** was assessed using the DPPH (2,2-diphenyl-1-picrylhydrazyl) free radical scavenging assay, a widely recognized method for evaluating the ability of compounds to donate protons and neutralize free radicals.**[234]** The antioxidant activity was determined by calculating the **IC_{50}** values, representing the concentration required to inhibit 50% of the DPPH radicals in solution **(Table IV.5)**.

The tested compounds exhibited variable antioxidant activities. Compound **III.5d** demonstrated a relatively good scavenging effect, with an **IC_{50}** of **23.91 ± 0.05 µg/mL** and a **DPPH** inhibition rate of **68.10 ± 0.01%**, although this performance remained inferior to that of ascorbic acid used as a reference.

Conversely, compounds **III.5e**, **III.5f**, **III.5c**, and **III.5a** displayed weak antioxidant responses, with significantly higher **IC_{50}** values of **58.95 ± 1.61 µg/mL**, **53.42 ± 1.43 µg/mL**, **50.43 ± 1.13 µg/mL**, and **46.42 ± 1.48 µg/mL**, respectively. These findings indicate a limited capacity to scavenge free radicals.

In terms of percent inhibition, these same compounds also recorded low values, with **III.5e** showing only **24.20 ± 0.45%**, **III.5f** at **28.13 ± 0.40%**, and **III.5c** at **34.48 ± 1.43%**, thus confirming their weak antioxidant efficacy.

Table IV.5. IC_{50} of molecules and ascorbic acid

Molecules	IC_{50} (µg/mL)	Percentage of DPPH inhibition
Ascorbic acid	11,31 ± 0,32	94.39 ± 0.18
III.5b	21,22 ± 1,01	79,78 ± 0,28
III.5a	46.42 ± 1,48	39,14 ± 0,64
III.5c	50.43 ± 1,13	34,48 ± 1,43
III.5d	23,91 ± 0,05	68,10 ± 0,01
III.5f	53,42 ± 1,43	28,13 ± 0,40
III.5e	58,95 ± 1,61	24,20 ± 0,45

2.2. Evaluation of antimicrobial and biofilm inhibitory properties via *in vitro* and molecular docking approaches

The antimicrobial properties of the chemical compounds were assessed against a range of pathogenic microorganisms, which included two Gram-negative bacteria: *Klebsiella pneumoniae* and *Pseudomonas aeruginosa*; two Gram-positive bacteria: *Staphylococcus aureus* and *Staphylococcus epidermidis*; as well as two yeast species from the genus Candida: *Candida albicans* and *Candida tropicalis.*

According to the results presented in **table IV.6**, the strains tested showed variable sensitivity to the six molecules evaluated.

Regarding Gram-negative bacteria, *Klebsiella pneumoniae* was susceptible to all of the compounds analyzed, with inhibition zones ranging from **12** to **18 mm**, particularly with **III.5d (18 mm)** and **III.5e (17 mm)**, which corresponded to minimum inhibitory concentrations **(MICs)** of **125** and **62.5 µg/mL**, respectively. Conversely, *Pseudomonas aeruginosa*, recognized for its inherent resistance, displayed sensitivity only to the reference treatments **AK10 (19 mm)** and **AMC30 (25 mm)**, with **MICs** of **250** and **125 µg/mL**, respectively, thereby confirming a resistance profile against the compounds that were investigated.

In the context of Gram-positive bacteria, *Staphylococcus epidermidis* exhibited moderate sensitivity to the **III.5b** and **III.5a** compounds **(12 mm)**, accompanied by comparatively high **MICs (1000** and **500 µg/mL)**. In contrast, *Staphylococcus aureus* was resistant to all the compounds examined, including standard controls, indicating a profile of multidrug resistance.

Simultaneously, regarding yeasts, *Candida albicans* demonstrated notable sensitivity to all evaluated molecules, particularly **III.5b (16 mm; MIC = 62.5 µg/mL)**, **III.5a (15 mm)**, and **III.5c (13 mm)**. Conversely, *Candida tropicalis* exhibited resistance to all tested compounds, with the exception of **III.5c (14 mm** inhibition zone**; MIC= 500 µg/mL)** and the AM-B antifungal control **(20 mm; MIC = 250 µg/mL)**.

Table IV.6. Results of the evaluation of the antibacterial activity of the compounds **(III.5a- III.5f).**

	Compounds						**Treatment**		
	Diameter zone of inhibition (mm)								
Strains	**III.5b**	**III.5a**	**III.5c**	**III.5d**	**III.5f**	**III.5e**	**AK10**	**AMC30**	**AM-B**
Klebsiella pneumoniae	13	12	13.5	18	15	17	R	R	/
Pseudomonas aeruginosa	12	R	R	R	R	R	19	25	/
Staphylococcus aureus	R	R	R	R	R	R	R	R	/
Staphylococcus epidermidis	12	12	R	R	R	R	R	R	/
Candida albicans	16	15	13	13	12	12	/	/	R
Candida tropicalis	R	R	14	R	R	R	/	/	20
Minimimal inhibitory concentration (µg/ml)									
Klebsiella pneumoniae	500	1000	250	125	500	62.5	R	R	/
Pseudomonas aeruginosa	500	R	R	R	R	R	250	125	/
Staphylococcus aureus	R	R	R	R	R	R	R	R	/

Staphylococcus epidermidis	1000	500	R	R	R	R	R	R	/
Candida albicans	62,5	125	500	250	250	500	/	/	R
Candida tropicalis	R	R	500	R	R	R	/	/	250

In this work, we assessed the impact of these chemicals on biofilm formation by the microorganisms examined. The outcomes of biofilm inhibition are depicted in **figure IV.7**.

The effect of the compounds on biofilm formation was also studied. The results obtained by the crystal violet staining method, illustrated in **figure IV.7**, showed significant inhibition of biofilm formation in both bacterial and fungal strains exposed to the compounds. Inhibition rates for bacterial biofilms ranged from **55.34%** to **75.33%**, while those for fungal biofilms varied from **58.24%** to **71.28%**. These values exceeded those of the reference treatments, amikacin and amphotericin B, which showed inhibition rates of **45.90%** and **50.65%,** respectively.

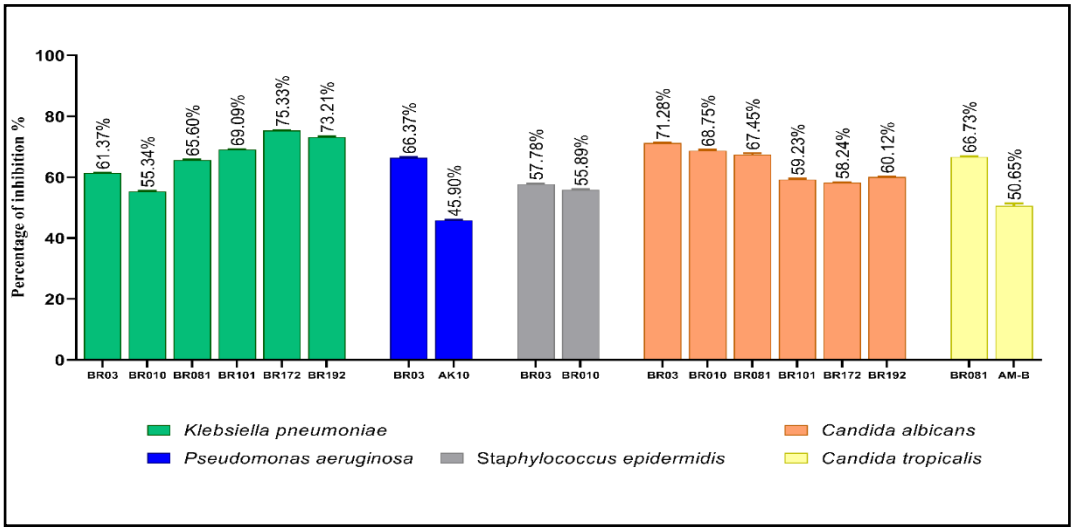

Figure IV.7. Inhibition of the biofilm formation

In light of the promising *in vitro* results obtained for the antibacterial activity of the synthesized 1,2-oxaphospholane-2-oxides, which were notably more encouraging than their antioxidant potential, we proceeded with molecular docking studies to further investigate their mechanism of action. This computational approach aimed to establish a correlation between the experimental findings and the theoretical interactions of the most active compounds with potential bacterial targets. Specifically, docking simulations were conducted to explore the binding mode of these derivatives within the active site of dihydropteroate synthase **(DHPS)**, an enzyme implicated in microbial viability and used here as a representative antibacterial target. For this purpose, the crystal structure of dihydropteroate synthase in complex with sulfamethoxazole **(PDB :** 3TZF **[235])** was selected as the docking model. The obtained

results, summarized in **table IV.8,** provide valuable insights into the molecular interactions that may underlie the observed antibacterial effects.

Table IV.8. Docking scores of 1,2-oxaphospholane-2-oxides.

Compound	Docking score ($kcal.mol^{-1}$)
Sulfamethoxazole	-6.80
III.5a	-4.96
III.5b	-5.77
III.5c	-5.67
III.5d	**-6.25**
III.5e	-5.92
III.5f	-6.14

The synthesized 1,2-oxaphospholane-2-oxides were subjected to molecular docking studies to evaluate their binding affinity toward the active site of the enzyme dihydropteroate synthase **(DHPS)**. The results revealed binding scores ranging from **-4.96** to **-6.25** $kcal.mol^{-1}$.

Among all tested compounds, derivative **III.5d** exhibited the most favourable docking score, indicating a strong affinity for the enzyme dihydropteroate synthase **(DHPS)** cavity.

This compound also demonstrated notable antibacterial activity, with an inhibition zone diameter of **18 mm**, as well as significant efficacy in inhibiting biofilm formation by *Klebsiella pneumoniae*, showing the highest inhibition rate among the evaluated derivatives. In parallel, antioxidant assays confirmed its potent radical scavenging ability, with a DPPH inhibition percentage of **68.10 ± 0.01%** and an **IC_{50}** value of **23.91 ± 0.05 µg/mL**. Altogether, these findings suggest that compound **III.5d** is a promising bioactive molecule with remarkable antioxidant, antibacterial, and antibiofilm properties.

Several significant interactions were observed between the docked compounds and the active site of dihydropteroate synthase **(DHPS)**, notably hydrogen bonds involving key residues such as **Arg235 (Figure IV.8)**. The functional groups participating in these interactions primarily include the carbonyl moiety, which acted as a hydrogen bond acceptor interacting with amino acid residues within the enzymatic cavity. In addition, PI-PI stacking interactions were identified between the aromatic rings of the ligands and aromatic residues of the active site, such as **Phe23**, further contributing to the stabilization of the ligand-enzyme complex.

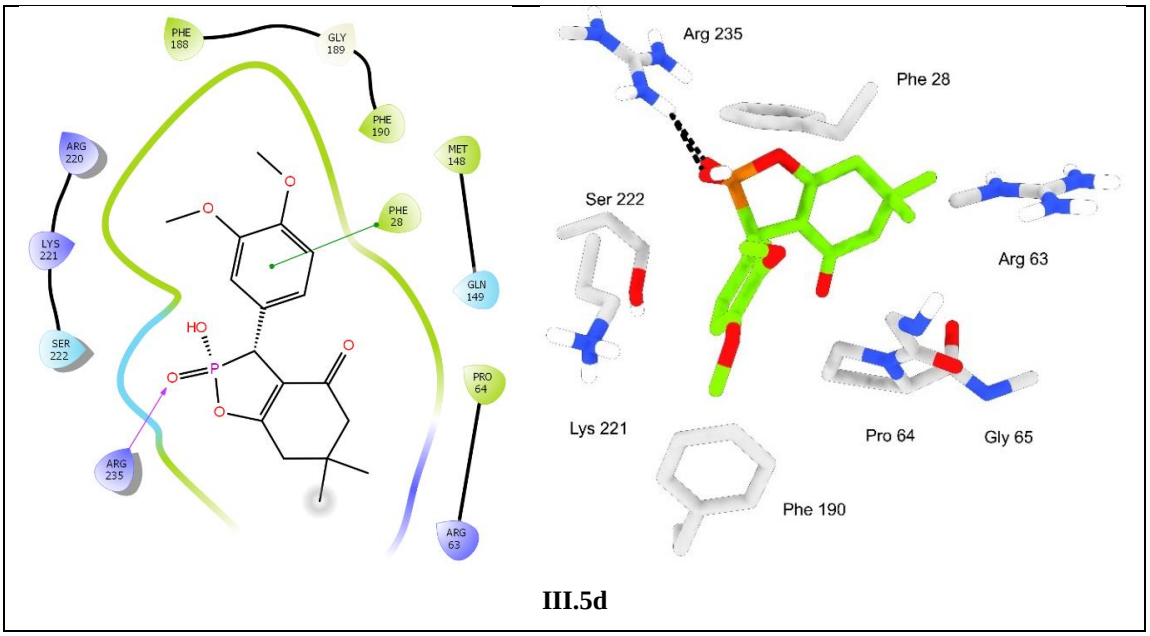

Figure IV.8. 2D and 3D representations of compound III.5d docked into the active site of DHPS.

2.3. ADME prediction

The pharmacokinetic properties of the synthesized 1,2-oxaphospholane-2-oxide analogues were assessed using the SwissADME platform, as presented in **table IV.9**. All examined compounds complied with Lipinski's rule of five, suggesting a high likelihood of good oral bioavailability. Their molecular weights, ranging from **280.21** to **371.16** g.mol^{-1}, fall within the optimal range for effective diffusion across biological membranes.

Structural analysis revealed that these molecules contain between **0** and **1** hydrogen bond donors, **4** to **6** hydrogen bond acceptors, and between **1** and **5** rotatable bonds key parameters that directly influence conformational flexibility and molecular recognition. The predicted lipophilicity, expressed as **Log P**, ranged from **1.76** to **3.33**, indicating a physicochemical profile consistent with that of drug-like molecules.

In addition, crucial properties such as aqueous solubility **(Log S)** and skin permeability **(Log Kp)** were estimated to evaluate the compounds' behavior in physiological environments. The predicted values ranged from **-2.78** to **-3.81** for **Log S**, and from **-6.22** to **-7.39 cm/s** for **Log Kp**, reflecting an adequate capacity to cross biological barriers while maintaining moderate solubility.

Table IV.9. Predicted ADME Properties of 1,2-Oxaphospholane-2-Oxide Analogues Obtained Using the SwissADME Tool

Properties	Molecular weight (g/mole)	Rotatable bonds	H-bond donor	H-bond acceptor	Log Po/W iLogP	Log S ESOL	Log Kp	Bioavailability Score	TPSA (˚A)
III.5a	292.27	1	1	4	1.76	-2.78	-6.75	0.85	73.41
III.5b	326.71	1	1	4	2.06	-3.38	-6.28	0.85	73.41
III.5c	306.29	1	1	4	2.05	-3.09	-6.81	0.85	73.41
III.5d	352.32	3	1	6	2.12	-2.95	-7.39	0.56	91.87
III.5e	371.16	1	1	4	2.17	-3.70	-6.97	0.85	73.41
III.5f	348.37	5	0	4	3.33	-3.81	-6.22	0.85	62.41

The analysis of the bioavailability radar plots **(Figure IV.9)** provided valuable insights into the alignment of the physicochemical properties of the studied derivatives with the requirements for favorable pharmacokinetic behavior. Overall, all compounds displayed values within the optimal ranges for the six key parameters namely lipophilicity, molecular size, polarity, solubility, conformational flexibility, and saturation. When these properties fall within the target intervals (represented by the pink area of the radar plot), they are typically associated with satisfactory oral bioavailability. Consequently, the results suggest that the compounds exhibit physicochemical characteristics consistent with those generally expected of promising drug candidates.

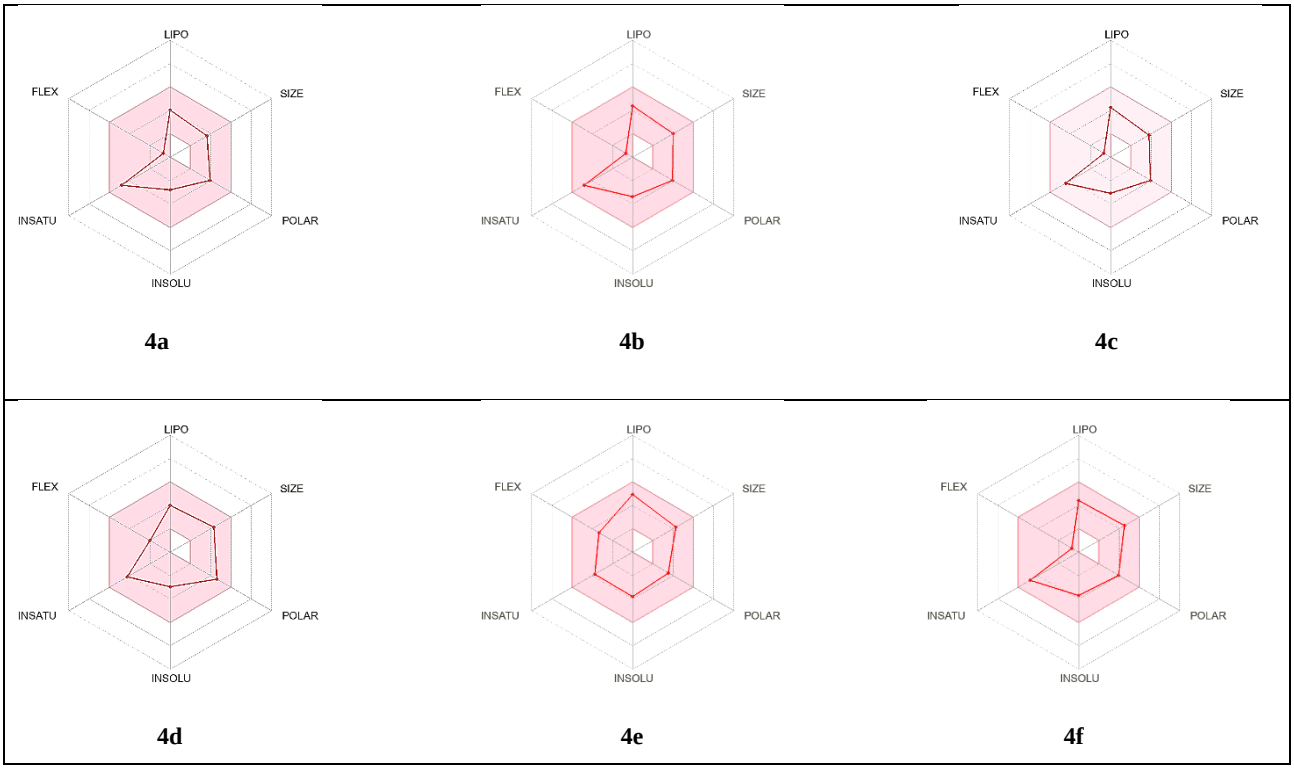

Figure IV.9. Bioavailability radars for 1,2-oxaphospholane-2-oxide synthesized derivatives.

2.4. Density functional theory

A comprehensive DFT study was carried out on a series of 1,2-oxaphospholane-2-oxide analogues in the gas phase using Gaussian 09 software. Geometry optimizations and electronic property calculations were performed at the **B3LYP/6-31G(d,p)** level of theory. Initial 3D structures were generated using ChemDraw 3D, converted to Mol **(MDL)** format, and processed with GaussView 06. Dipole moment analysis revealed a wide range of polarity values (**2.7901** to **4.9029** D), depending on the nature of the substituents. The HOMO–LUMO energy gaps, ranging from **4.5214** to **5.2186** eV, provided insights into the relative electronic stability of the compounds, with derivative **III.5** identified as the most stable.

The spatial distribution of the frontier molecular orbitals **(HOMO** and **LUMO)** was also examined to assess the electronic reactivity and stability of the compounds. As illustrated in **figure IV.11**, red and green isosurfaces represent areas of high and low electron density, respectively. Numerical values of $\mathbf{E_{HOMO}}$, $\mathbf{E_{LUMO}}$, **ΔE**, total dipole moment $\mathbf{(\mu_{total})}$, and total energy are summarized in **table IV.10**. Significant variations were observed across the series, with increasing energy gap values in the following order: **III.5d**<**III.5** a< **III.5**b.

Table IV.10. Molecular descriptors and parameters of studied 1,2-oxaphospholane-2-oxide derivatives

Entry	μ (D)	E_{HOMO} (eV)	E_{LUMO} (eV)	ΔEgap	(η)	(S)	(μ)	(χ)	(ω)
III.5a	3.1183	-6.4096	-1.2778	5.1318	2.5659	0.3897	-3.8437	3.8437	2.8790
III.5b	4.4068	-6.5803	-1.3617	5.2186	2.6093	0.3832	-3.9710	3.9710	3.0216
III.5c	2.7901	-6.3343	-1.2539	5.0804	2.5402	0.3937	-3.7941	3.7941	2.8335
III.5d	4.9029	-5.7530	-1.2316	4.5214	2.2607	0.4423	-3.4923	3.4923	2.6974
III.5e	3.6845	-6.4105	-1.4082	5.0023	2.5011	0.3998	-3.9093	3.9093	3.0552

Table IV.11. Optimized structures and HOMO/LUMO orbitals of studied 1,2-oxaphospholane-2-oxide.

Code	Optimized structure	HOMO	LUMO
III.5a	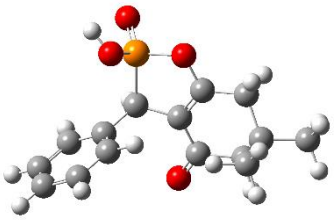	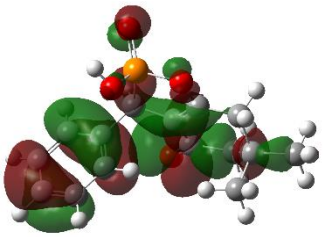	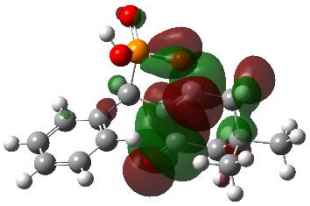
III.5b	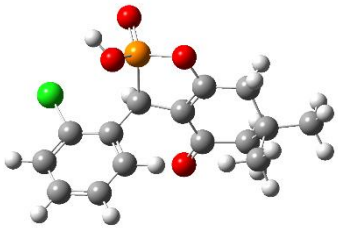	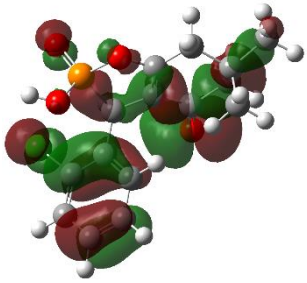	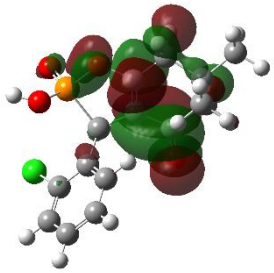
III.3c	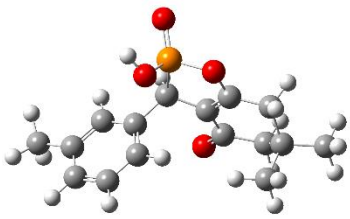	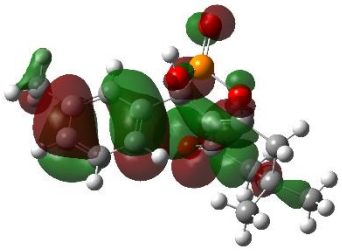	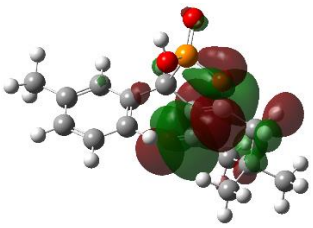
III.3d	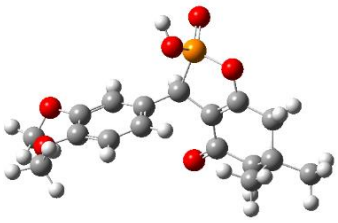	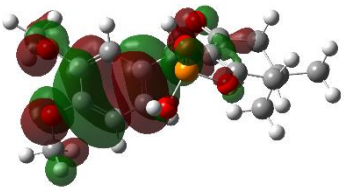	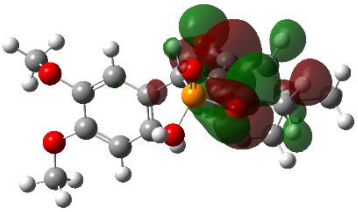
III.3e	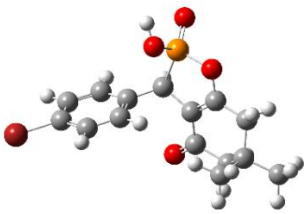	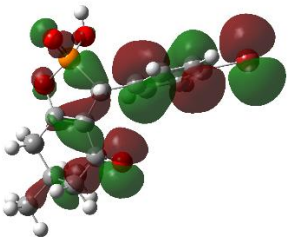	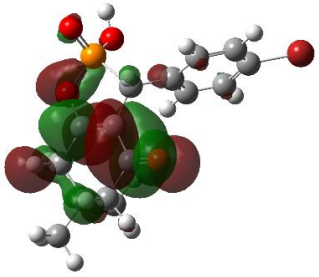

3. *In vitro* and *in silico* assessment of *N*-2-chloroetylcarbamate derivatives

3.1. Evaluation of antimicrobial efficacy using *in vitro* assays and docking simulations

Using the same method described previously, the antimicrobial activities of the chemical compounds were evaluated against a panel of pathogenic microorganisms, including two Gram-negative bacteria (*Klebsiella pneumoniae* and *Pseudomonas aeruginosa*), two Gram-positive bacteria (*Staphylococcus aureus* and *Staphylococcus epidermidis*), and two *Candida* yeast species (*Candida albicans* and *Candida tropicalis*). The data indicated a variable response of the strains to the ten compounds tested.

For antibacterial activity, inhibition zone diameters ranged from **12 to 32.5 mm**, with minimum inhibitory concentrations **(MICs)** between **1000 and 31.25 µg/mL**. Among the tested compounds, **III.8f** exhibited the highest activity against all bacterial strains.

Concerning antifungal activity, **III.8g** was the only compound to show notable efficacy against both yeast strains, with inhibition zone diameters of **30 mm** and **35 mm**, and MICs values ranging from **7.81 to 15.62 µg/mL**.

Additionally, control tests revealed that the strains displayed a multidrug resistance profile. The antimicrobial activities of the studied compounds are summarized in **Table IV.12**.

Table IV.12. Antimicrobial activity results

Strains	Molecules					Antibiotic / Antifungal		
	Inhibition Zone Diameters (IZD) in mm							
	III.8a	**III.8f**	**III.8e**	**III.8g**	**III.8h**	**AK10**	**AMC30**	**AM-B**
Klebsiella pneumoniae	R	22	12	14	R	R	R	/
Pseudomonas aeruginosa	R	26	R	12	14	19	25	/
Staphylococcus aureus	20	32.5	12	20	R	R	R	/
Staphylococcus epidermidis	R	31	R	R	R	R	R	/
Candida albicans	R	R	R	35	R	/	/	R
Candida tropicalis	R	R	R	30	R	/	/	20
Minimum Inhibitory Concentrations (MIC) in µg/ml								
Klebsiella pneumoniae	R	62.5	1000	500	R	R	R	/
Pseudomonas aeruginosa	R	31.25	R	500	125	250	125	/
Staphylococcus aureus	125	31.25	500	62.5	R	R	R	/
Staphylococcus epidermidis	R	31.25	R	R	R	R	R	/
Candida albicans	R	R	R	7.81	R	/	/	R
Candida tropicalis	R	R	R	15.62	R	/	/	250

The effect of the compounds on biofilm formation was also investigated. The results obtained using the crystal violet staining method, as illustrated in **figure IV.10**, revealed a significant

inhibition of biofilm formation in both bacterial and fungal strains exposed to the compounds. The inhibition rates for bacterial biofilms ranged from **56.18% to 88.33%**, while those for fungal biofilms were **89.59%** and **90.18%** for *Candida albicans* and *Candida tropicalis*, respectively. These values surpassed those of the reference treatments, such as **amikacin** and **amphotericin B**, which exhibited inhibition rates of **45.90%** and **50.65%**, respectively.

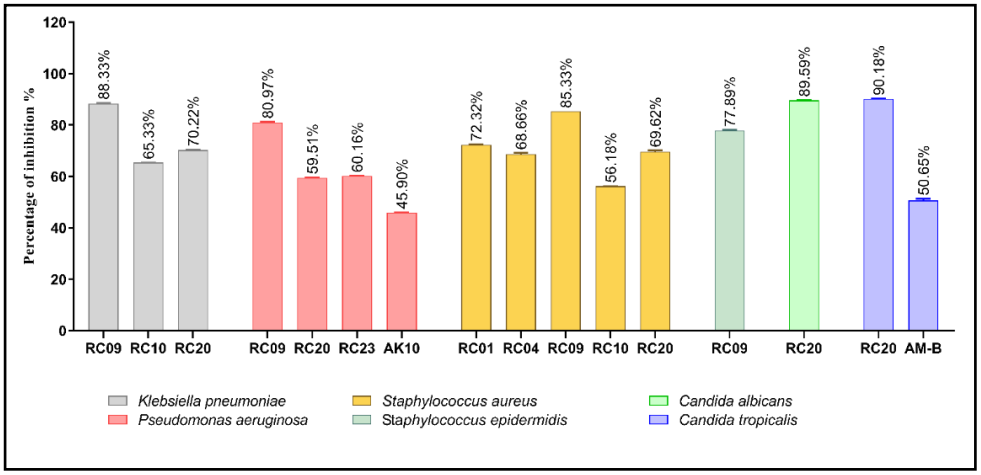

Figure IV.10. Inhibition of microbial biofilm formation by chemical compound

To further investigate the observations obtained from the *in vitro* tests**,** a molecular docking study was carried out to better understand the molecular interactions underlying the antibacterial activity of the studied compounds. This *in silico* analysis provided deeper insight into the binding modes of the compounds within the active site of the dihydropteroate synthase **(DHPS)**.

The complex formed between the ligand and dihydropteroate synthase **(DHPS)** (**PDB:**3TZF**[235]**) exhibited good binding affinity, with docking scores ranging from **-4.77 to -6.12 kcal/mol**, indicating satisfactory molecular stability **(table IV.13)**. The molecular interaction analysis revealed several specific contacts between the ligands and residues within the enzyme's active site. Notably, hydrogen bonds were formed with **Thr62**, **Gly189**, and **Arg235**. In addition, π-π stacking interactions were observed with **Phe28** and **Phe190**. Furthermore, cation-π interactions were identified between **Lys221** and the aromatic rings of the compounds, contributing to the stabilization of the ligand-enzyme complex **(Figure IV.11)**.

Table IV.12. Docking scores of *N*-2-chloroetylcarbamate derivatives.

Compound	Docking score (kcal.mol^{-1})
Sulfamethoxazole	-6.80
III.8a	-5.07
III.8b	-6.08
III.8c	--4.98
III.8d	-5.11
III.8e	-5.77
III.8f	**-6.12**
III.8g	-4.77
III.8h	-6.02

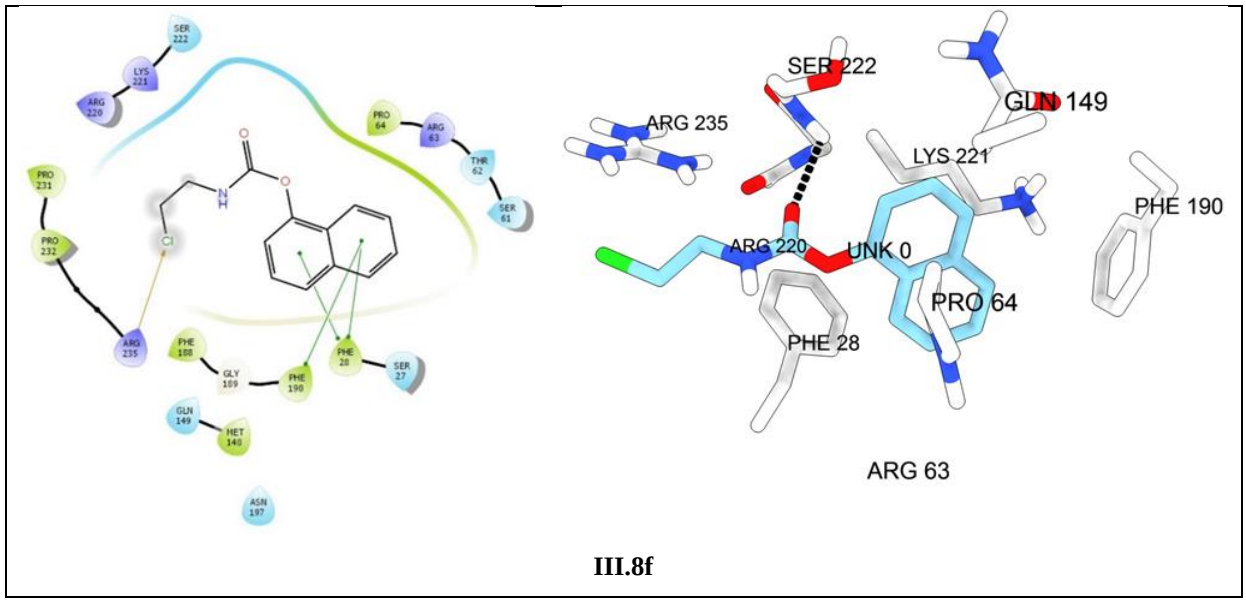

III.8f

Figure IV.11. 2D and 3D representation of compound **III.8f** docked with DHPS.

3.2. Combined *in vitro* and *in silico* approaches for evaluating antioxidant properties

The antioxidant potential of the synthesized *N*-2-chloroetylcarbamate compounds was assessed by determining their half-maximal inhibitory concentration **(IC_{50})** values**.** These values indicate the concentration of each compound required to scavenge **50%** of the DPPH (2,2-diphenyl-1-picrylhydrazyl) radicals in the reaction medium. Ascorbic acid was used as a reference standard. The IC_{50} values of the tested compounds and the standard are summarized in **Table IV.13**.

The tested compounds exhibited varying degrees of antioxidant activity. Among them, **III8f** and **III8a** stood out due to their notable radical scavenging capacity, with IC_{50} values of **12.24 ± 1.06 µg/mL** and **13.17 ± 1.76 µg/mL**, respectively. These values are comparable to that of

the reference standard, ascorbic acid (**IC_{50}: 11.31 ± 0.32 µg/mL**), indicating a strong free radical scavenging ability.

Other compounds, such as **III8c** and **III8d**, also demonstrated moderate antioxidant activity, with **IC_{50}** values of **20.23 ± 1.18 µg/mL** and **18.81 ± 1.09 µg/mL**, respectively. In contrast, **III8e**, **III8h** and **III8j** exhibited significantly weaker activity, with **IC_{50}** values of **27.41 ± 0.93 µg/mL**, **25.36 ± 0.15 µg/mL**, **39.21 ± 1.26 µg/mL**, **26.43 ± 0.96 µg/mL**, and **60.02 ± 1.44 µg/mL**, respectively. These results indicate a lower antioxidant efficacy compared to the other compounds tested.

In terms of DPPH inhibition percentage, **III8f** achieved the highest value (**88.84 ± 0.30%**), followed closely by **III8a (84.17 ± 0.92%)**. Conversely, **III8g** displayed the lowest inhibition percentage **(46.48 ± 0.11%)**, confirming its weak antioxidant potential.

To support the experimental data and elucidate the underlying molecular interactions, a molecular docking study was conducted on xanthine oxidase in complex with hypoxanthine **(PDB:** 3NRZ **[236]),** selected as a reference antioxidant target. This *in silico* approach enabled the investigation of the binding modes of the newly synthesized N-(2-chloroethyl) carbamate derivatives. The docking results, summarized in **table IV.13**, revealed varying binding affinities depending on the structural features of the compounds. Notably, compound **III8f** exhibited the highest docking score, indicating strong interactions within the xanthine oxidase active site. This result is consistent with **its lowest IC_{50} value**, reflecting a potent inhibitory effect. Furthermore, regarding antioxidant activity assessed by the DPPH assay, **III8f** also achieved the highest inhibition percentage**,** further confirming its promising profile as an antioxidant agent.

Table IV.13. IC_{50} values of the synthesized compounds and ascorbic acid.

Molecules	IC_{50} (µg/mL)	DPPH inhibition percentage	Docking score (kcal.mol^{-1})
Ascorbic acid	11,31 ± 0,32	94,39± 0,18	/
III8a	13,17 ± 1,76	84,17± 0,92	-5.60
III8c	20,23 ± 1,18	79,98 ± 0,13	-5.12
III8d	18,81 ± 1,09	81,02±0,88	-5.89
III8e	25,36 ± 0,15	63,13± 0,94	-6.04
III8f	12,24 ± 1,06	88,84± 0,30	**-6.20**
III8g	39,21 ± 1,26	46,48± 0,11	-5.70
III8h	60,02 ± 1,44	23,16±0,75	-6.12

In this study, docking scores ranging from **-5.12** to **-6.20** kcal/mol were obtained for the series of *N*-(2-chloroethyl) carbamate derivatives. The predicted binding modes were stabilized by

key molecular interactions within the enzyme xanthine oxidase active site, notably hydrogen bonds involving critical residues such as **Glu802** and **Lys771**, as well as non-covalent interaction including Pi–stacking. Structurally, specific functional groups particularly the carbonyl group of the carbamate moiety played a central role as hydrogen bond acceptors. This ability to specifically interact with residues within the enzymatic pocket highlights their significant contribution to molecular recognition, the stability of the ligand-receptor complex, and consequently, the biological potential of the studied compounds.

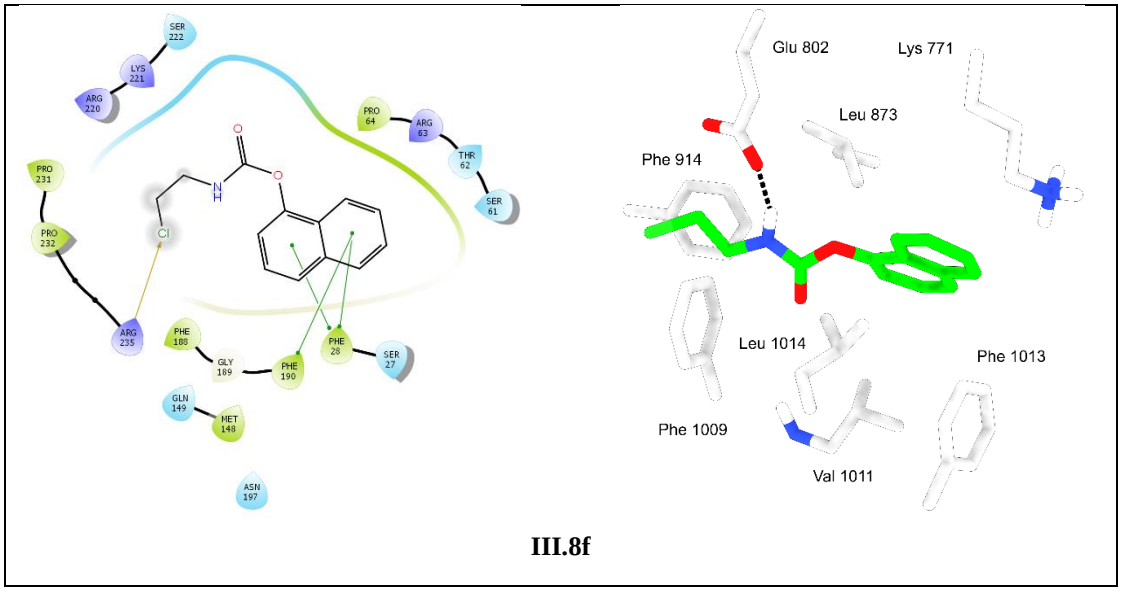

Figure IV.12. 2D and 3D molecular docking illustrations of compound III.8f interacting with XO.

3.3. ADME prediction

In order to assess the drug-likeness and pharmacokinetic behaviour of the synthesized *N*-(2-chloroetyl) carbamate compounds, a comprehensive *in silico* ADME analysis was conducted using the SwissADME online platform. This tool allowed the prediction of essential parameters related to absorption and distribution, including molecular weight, lipophilicity **(Log P)**, water solubility **(Log S)**, skin permeability **(Log Kp)**, hydrogen bond donors and acceptors, and rotatable bonds. All synthesized compounds were found to fully comply with Lipinski's rule of five, suggesting good potential for oral bioavailability. The obtained results are summarized in **table IV.14**.

Table IV.14. Predicted ADME properties of synthesized N-2-chloroetylcarbamate using the SwissADME tool

Properties	Molecular weight (g/mole)	Rotatable bonds	H-bond donor	H-bond acceptor	Violations	Log Po/W iLogP	Log S ESOL	Log Kp	Bioavailability Score	TPSA (˚A)
III.8a	199.63	5	1	2	0	2.01	-2.41	-6.03	0.55	38.33
III.8b	278.53	5	1	2	0	2.47	-3.31	-6.03	0.55	38.33
III.8c	217.62	5	1	3	0	2.20	-2.56	-6.07	0.55	38.33
III.8d	229.66	6	1	3	0	2.31	-2.46	-6.24	0.55	47.56
III.8e	283.79	7	1	2	0	3.17	-4.11	-4.94	0.55	38.33
III.8f	249.69	5	1	2	0	2.45	-3.35	-5.73	0.55	38.33
III.8g	255.70	1	1	3	0	2.35	-2.64	-6.26	0.55	55.40
III.8h	331.79	6	1	3	0	3.25	-4.22	-5.70	0.55	47.56

Additionally, the bioavailability radars **(figure IV.13)** provide a visual overview of the physicochemical properties of the compounds across six critical dimensions: lipophilicity, molecular size, polarity, solubility, flexibility, and saturation. These computational results offer a valuable preliminary indication of the compounds' suitability as orally administered drug candidates.

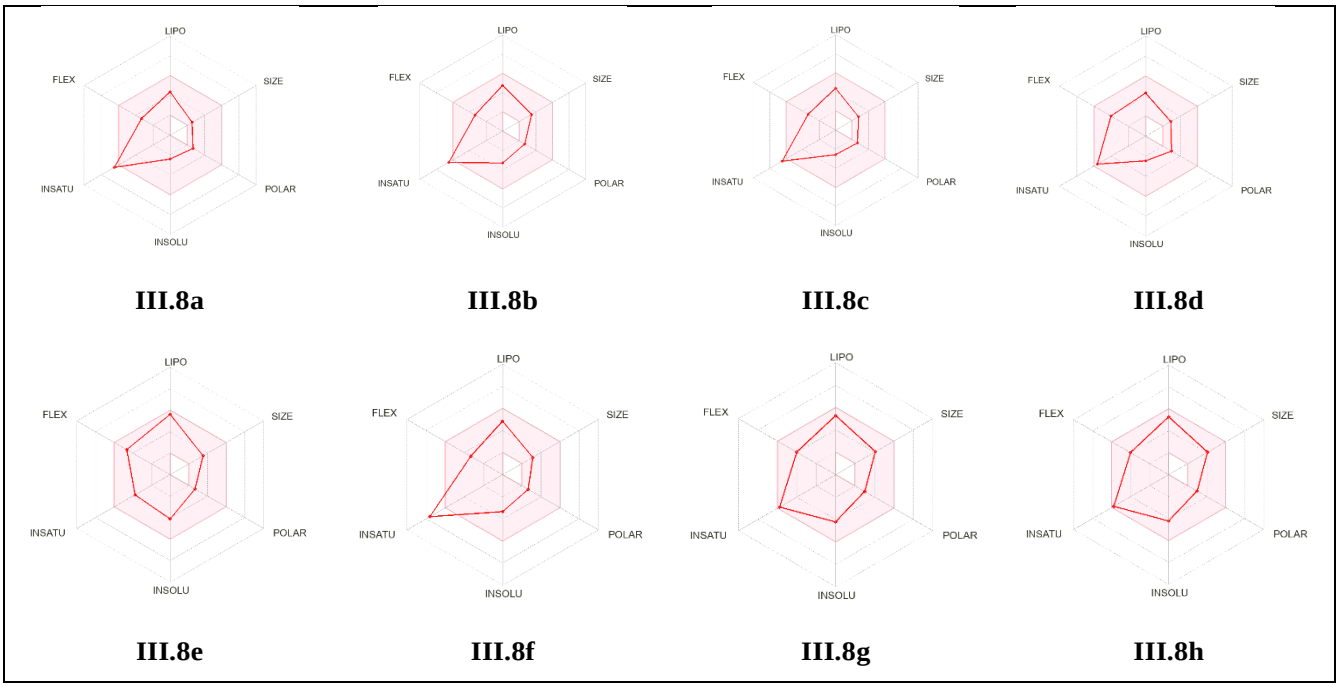

Figure IV.13. Bioavailability radars for *N*-2-chloroetylcarbamate derivatives.

3.4. Density functional theory

A computational analysis based on density functional theory (DFT) was conducted on all synthesized compounds to evaluate their fundamental electronic properties. Quantum parameters were obtained at the B3LYP/6-31G(d,p) level using the Gaussian 09 software, allowing the estimation of dipole moments, frontier molecular orbital energies **(HOMO–LUMO)**, and the corresponding energy gaps. The dipole moments of the studied *N*-2-

chloroethylcarbamate analogues ranged from **0,6562** to **4,5585** D, reflecting a broad polarity variation influenced by the nature of the substituents. The HOMO–LUMO energy gap values were found to lie within the range of **4,7005** to **6,1890** eV, indicating different degrees of electronic stability across the series. Compound **III.8** was identified as the most stable, exhibiting the highest energy gap. Detailed results, including orbital representations and numerical descriptors, are presented in the corresponding tables **(Table IV.15** and **Table IV.16).**

Table IV.15. Molecular descriptors and parameters of studied *N*-2-chloroetylcarbamate derivatives

Entry	μ (D)	E_{HOMO} (eV)	E_{LUMO} (eV)	ΔEgap	(η)	(S)	(μ)	(χ)	(ω)
III.8a	0,6562	-6,4575	-0,2686	6,1890	3,0945	0,3232	-3,3631	3,3631	1,8275
III.8b	2,0924	-6,4241	-0,3720	6,0521	3,0260	0,3305	-3,3980	3,3980	1,9079
III.8c	2,8545	-5,8232	-0,1404	5,6828	2,8414	0,3519	-2,9818	2,9818	1,5646
III.8d	2,5742	-6,3933	-0,4591	5,9343	2,9671	0,3370	-3,4262	3,4262	1,9781
III.8e	0.9427	-5,7509	-1,0504	4,7005	2,3502	0,4255	-3,4006	3,4006	2,4602
III.8f	4,5585	-6,6254	-1,3706	5,2548	2,6274	0,3806	-3,9980	3,9980	3,0418
III.8g	2,4506	-5,9868	-0,2754	5,7114	2,8557	0,3502	-3,1311	3,1311	1,7165

Table IV.16. Optimized structures and HOMO/LUMO orbitals of studied *N*-2-chloroetylcarbamate.

Code	Optimized structure	HOMO	LUMO
III.8a	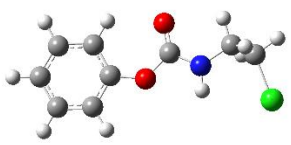	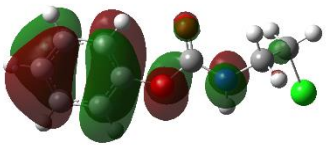	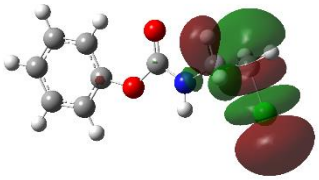
III.8b	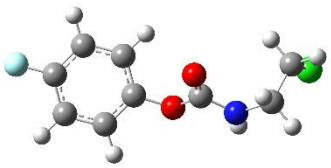	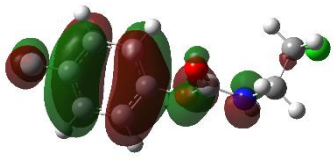	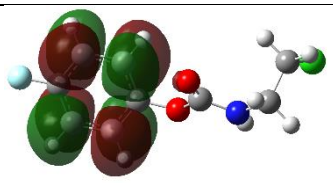
III.8c	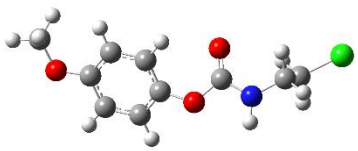	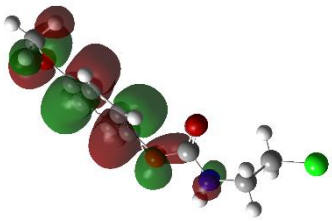	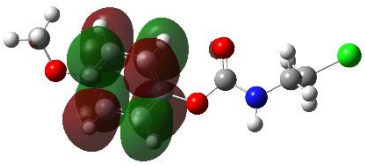

III.8d	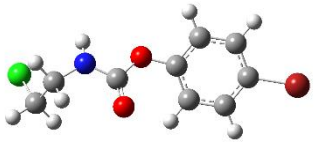	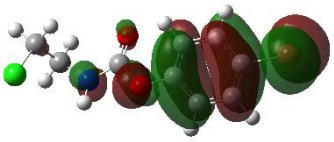	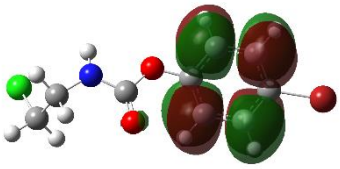
III.8e	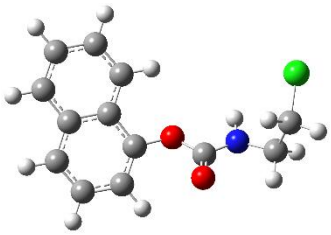	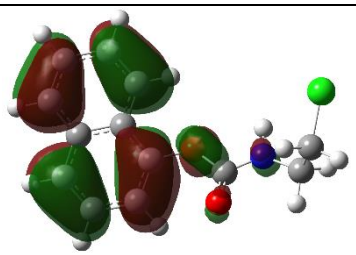	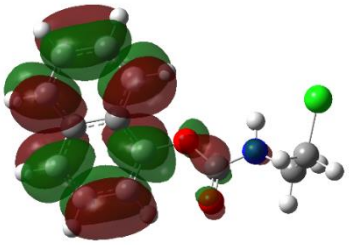
III.8f	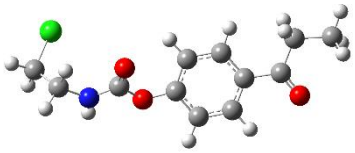	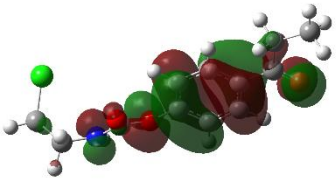	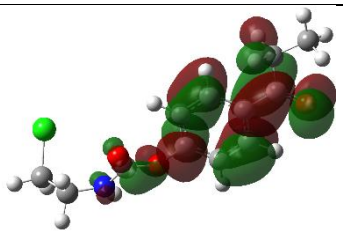
III.8g	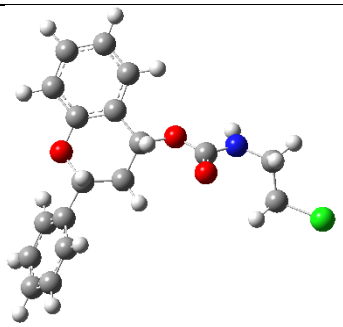	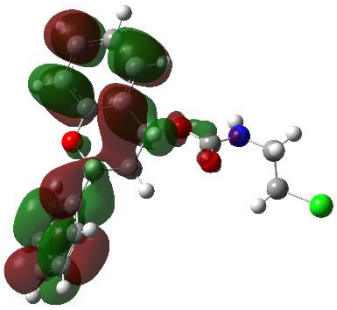	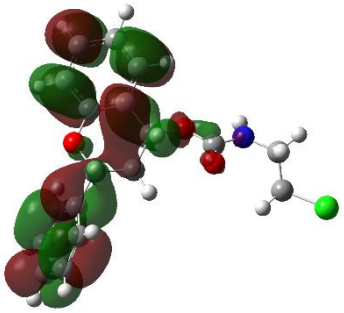

The molecular electrostatic potential (MEP) maps of the studied compounds were generated using a color scale ranging from deep red, indicating regions with high electron density (nucleophilic) to deep blue highlighting electron-deficient (electrophilic) areas, as shown in **figure IV.14**. In most cases, red regions were predominantly located on the carbonyl groups of the carbamate moiety, suggesting a strong ability of these sites to engage in intermolecular interactions by acting as proton acceptors in hydrogen bond formation. This assumption is supported by molecular docking results, where these same carbonyl groups were involved in hydrogen bonding interactions with the active site of xanthine oxidase. Additionally, the blue regions, indicative of low electron density, were mainly observed around the hydrogen atoms of the NH groups. This distribution reflects a significant electronegativity difference between the bonded atoms, implying a high lability of these hydrogen atoms and a pronounced ability to serve as hydrogen bond donors an observation also corroborated by docking study.

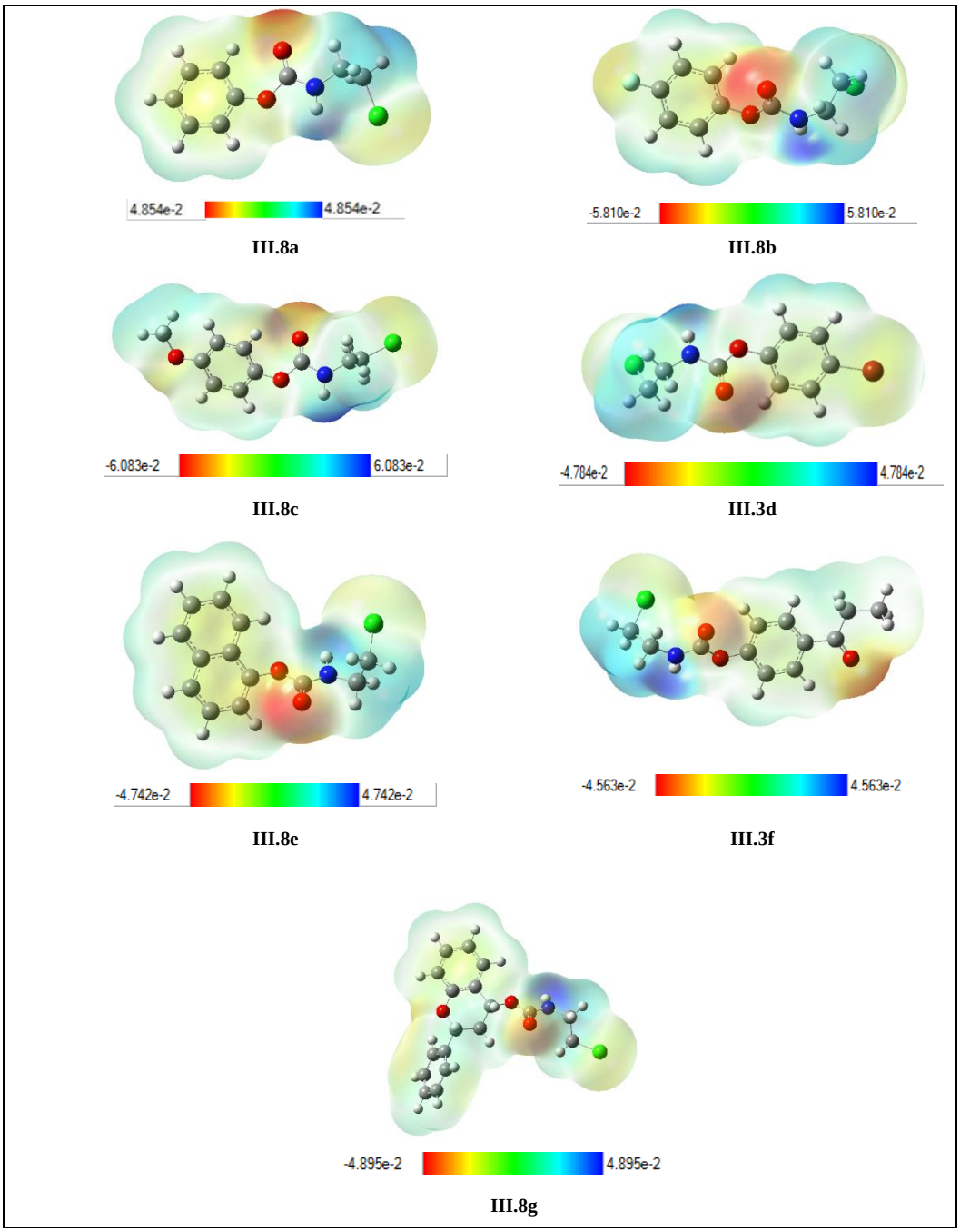

Figure IV.14. MEP maps of synthesized *N*-2-chloroetylcarbamate derivatives.

4. Conclusion

In this chapter, both *in silico* and *in vitro* studies were carried out to evaluate the biological potential of the synthesized compounds. Molecular docking investigations were conducted on the xanthene derivatives to assess their inhibitory potential toward VEGFR-2. The results revealed satisfactory interactions within the active site of the enzyme, highlighting their potential as VEGFR-2 inhibitors. In addition, a detailed study of their chemical reactivity was performed using DFT calculations, allowing the identification of the most reactive molecular regions. ADME predictions were also carried out to evaluate the pharmacokinetic properties and drug-likeness of the tested compounds.

The antimicrobial activity of 1,2-oxaphospholane-2-oxide derivatives was tested against a panel of pathogenic microorganisms. Promising results were observed, especially against *K. pneumoniae*, *C. albicans*, and in inhibiting biofilm formation. However, the compounds showed limited efficacy against *P. aeruginosa* and *S. aureus*, suggesting that further structural modifications are needed to broaden their antimicrobial spectrum.

Encouraging antibacterial activity was also found in the synthesized *N*-(2-chloroethyl) carbamate derivatives, with inhibition zones ranging from **12** to **32.5** mm and MIC values between **1000** and **31.25 µg/mL**. Among these, compound **III.8f** exhibited remarkable efficacy against all tested bacterial strains. Regarding antifungal activity, only compound **III.8g** demonstrated significant inhibition against both tested yeast strains, with inhibition zones reaching up to **35 mm** and MIC values as low as **7.81–15.62 µg/mL**.

Furthermore, the anti-biofilm evaluation revealed impressive inhibition rates, ranging from **56.18%** to **88.33%** against bacterial biofilms and up to **90.18%** against fungal biofilms. These values exceeded those of the reference drugs, such as amikacin and amphotericin B, underscoring the promising anti-infective potential of these compounds.

The antioxidant activities of the 1,2-oxaphospholane-2-oxide derivatives varied significantly, with compound **III.5d** standing out as the most potent, followed by **III.5b.** The remaining compounds showed limited radical scavenging abilities, suggesting that the scaffold may be less favourable for antioxidant purposes. In contrast, several *N*-(2-chloroethyl) carbamate derivatives displayed notable antioxidant potential. Compounds **III.8f** and **III.8a** showed excellent activity, with IC_{50} values comparable to that of ascorbic acid, while others demonstrated moderate effects.

A complementary *in silico* investigation, including molecular docking and DFT calculations, provided further insights into the interaction mechanisms and electronic properties of the

studied molecules. Finally, ADME predictions helped to evaluate the physicochemical behaviour and pharmacokinetic potential of these compounds, offering a basis for the future development of novel therapeutic agents.

Chapter V

Experimental data

1. Général Conditions

✓ Reagents and solvents

The starting reagents and solvents were purchased from standard commercial suppliers and used as received, without further purification or distillation. All solvents employed in the reactions and for the purification of the obtained derivatives were used directly, without any additional purification. The reactions were carried out under anhydrous conditions and monitored while maintaining under a nitrogen atmosphere.

✓ Chromatography

Thin-layer chromatography **(TLC)** was performed on aluminum plates coated with silica gel Merck **60 F254 (Ref. 5554)**. Reaction progress was monitored using this method, with product visualization under UV light at 254 nm for compounds containing chromophoric groups. Detection was further enhanced by spraying with a **10%** ninhydrin solution in ethanol, followed by heating to reveal amine functionalities. Column chromatography purification was carried out using silica gel **60 Å, 35-70 µm** (Carlo Erba) or silica gel **60 H** (Merck, Ref. 9385).

✓ Nuclear magnetic resonance (NMR)

Nuclear magnetic resonance **(NMR)** spectra were recorded using a Bruker spectrometer. ^{1}H NMR spectra were acquired at **400**, **500**, or **600 MHz**, and **^{13}C NMR** spectra at **100 MHz**. Chemical shifts are expressed in ***δ*** units **(ppm)** relative to tetramethylsilane **(TMS)** or the residual signals of deuterated solvents, such as **$CDCl_3$ (δ 77.0)** and **DMSO-d_6 (δ 39.0–40.0)**. Coupling constants **(*J*)** are reported in Hertz **(Hz)**, and signal multiplicities are denoted as follows: **s (singlet)**, **d (doublet)**, **t (triplet)**, **q (quartet)**, **m (multiplet)**, **dd (doublet** of **doublets)**. All spectra were recorded with high sensitivity and resolution, ensuring precise analysis of the synthesized molecules. The NMR data provided detailed structural information for all products and intermediates in the study.

✓ Ultra-high performance liquid chromatography (uHPLC/MS)

The analysis by **uHPLC/MS** was performed using an Agilent 1290 system equipped with a **ZORBAX** Eclipse Plus **C18** column **(2.1 mm × 50 mm, 1.8 µm)**. Elution was carried out in gradient mode, with a mobile phase ranging from **H_2O/CH_3CN (90:10)** to **H_2O/CH_3CN (10:90)**, each containing **0.1%** formic acid, at a constant flow rate of **0.5 mL/min.** UV detection was conducted at 254 nm over a total analysis time of **10 min**.

✓ **Infrared (IR)**

Infrared **(IR)** spectra were recorded on a Perkin Elmer FT-600 spectrometer. Solid samples were prepared as **KBr** pellets under pressure, and characteristic band positions are reported in wavenumbers **(cm^{-1})**.

✓ **Melting points**

Melting points for all final products were determined using open capillary tubes on a Büchi B-545 apparatus.

✓ **Ultrasound**

Reactions conducted under ultrasound were carried out using an ultrasonic bath **(FUNGILAB model**, **40 kHz**, **250 W)**. The reactions were performed in open glass tubes with a diameter of **25 mm**, a thickness of **1 mm**, and a volume of **20 mL**.

✓ **Microwave**

Reactions were performed under microwave irradiation in a domestic microwave oven **(Condor CMW-M2005W / M2005W, 700 W, 230 V ~ 50 Hz)**.

2. X-ray crystallography

Crystallographic data for compounds **III.3r** and **III.8a** were collected using a **SuperNova Dual, Cu at home/near, AtlasS2** four-circle diffractometer equipped with an **AtlasS2 CCD detector**. Data collection was carried out using **Cu Kα radiation (**micro-focus sealed tube, **λ = 1.54184 Å)**. The crystals were maintained at a constant temperature of **295 K** throughout data acquisition process.

The structure was solved using the **SHELXT-2014/5** program **[237]** through **Intrinsic Phasing**, with **Olex2 48 [238]** as the graphical user interface. Structural refinement was performed with **SHELXL-2018/3 [239]** using **full-matrix least-squares minimization** on F^2. Absorption corrections were applied using **CrysAlisPro 1.171.42.51a [240]**, employing **spherical harmonics** as implemented in the **SCALE3 ABSPACK** scaling algorithm. Crystal structure analysis and generation of packing diagrams were carried out using **Mercury 4.0** software **[241]**.

2.1. Structural Data for compound III.3r

Crystals **III.3r** for X-ray diffraction were obtained by crystallization from a **diethyl ether/*n*-hexane** mixture.

Crystallographic parameters and experimental details related to the structural analysis are

summarized in **Table IV.1**.

Supplementary crystallographic data for compound **III.3h** have been deposited under **CCDC Number: 2308384**, and can be obtained free of charge from the **Cambridge Crystallographic Data Centre** via the following link: www.ccdc.cam.ac.uk/data_request/cif

Table V.1. Crystallographic properties of compound III.3r.

Moiety formula	$C_{20}H_{20}O_3$	**Density (calculated) (g.cm^{-3})**	1.260
Sum formula	$C_{20}H_{20}O_3$	**Absorption coefficient (mm^{-1})**	0.670
Formula Weight (g.mol^{-1})	308.36	**F (000)**	656.0
Crystal habit, Color	Needle, colourless	**Crystal size (mm)**	0.22 × 0.04 × 0.02
Crystal system	Orthorhombic	**2θ range for data collection (°)**	9.606 to 149.024
Space group	$Pca2_1$	**Reflections collected**	6225
a (Å)	18.2645(5)	**Independent reflections**	2390
b (Å)	9.2078(2)	**R_{int}**	0.0363
c (Å)	9.6666(2)	**Number of parameters**	209
α (°)	90	**Goodness-of-fit on F^2**	1.045
β (°)	90	**Final R indices [I ≥ 2σ(*I*)]**	R_1 = 0.042, wR_2 = 0.1010
γ (°)	90	**R indexes [all data]**	R_1 = 0.0555, wR_2 = 0.1106
Volume (Å^3)	1625.69(7)	**Largest difference peak and hole (Å^3)**	0.13, -0.12
Z, Z'	4,0	**CCDC deposition no.**	CCDC 2308384

2.2. Crystallographic data for compound III.8a

Crystals of compound **III.8a** were obtained by recrystallization from a mixture of *n*-hexane and diethyl ether. The crystallographic parameters and experimental conditions for the structural analysis of compound **III.8a** are summarized in **table IV.2.**

CCDC 2448521, Supplementary crystallographic information for compound **III.8a** is available free of charge from the Cambridge Crystallographic Data Centre **(CCDC)** and can be accessed online at www.ccdc.cam.ac.uk/data_request/cif.

Table V.2. Crystallographic properties of compound **III.8a**.

Moiety formula	$C_9H_{10}ClNO_2$	**Density (calculated) (g.cm^{-3})**	1.340
Sum formula	$C_9H_{10}ClNO_2$	**Absorption coefficient (mm^{-1})**	3.168
Formula Weight (g.mol^{-1})	199.63	**F (000)**	416.0
Crystal habit, Color	Needle, colourless	**Crystal size (mm)**	0.2 × 0.12 × 0.05

Crystal system	monoclinic	**2θ range for data collection (º)**	8.514 to 145.422
Space group	P21/n	**Reflections collected**	7497
a (Å)	5.04220(10)	**Independent reflections**	1939
b (Å)	9.4482(3)	**R_{int}**	0.0245
c (Å)	20.7924(5)	**Number of parameters**	118
α (°)	90	**Goodness-of-fit on F^2**	1.058
β (°)	9 2.589(2)	**Final R indices [I ≥ 2σ(*I*)]**	R_1 = 0.0411, wR_2 =0.1181
γ (°)	90	**R indexes [all data]**	R_1 = 0.0439, wR_2 =0.1211
Volume (Å^3)	989.53(4)	**Largest difference peak and hole (Å^3)**	0.42/-0.35
Z, Z'	4, 0	**CCDC deposition no.**	CCDC 2448521

3. Preparation of xanthene derivatives

3.1. General Procedure

In a cylindrical open glass tube **(diameter: 25 mm; thickness: 1 mm; capacity: 20 mL),** a reaction mixture comprising dimedone **(2 mmol)** and a selected aromatic aldehyde **(1 mmol)** was subjected to ultrasonic irradiation for a specified duration. Zinc acetate dihydrate **($Zn(OAc)_2$)**, employed as a catalyst at **10 mol%**, was added to the system, with ethanol serving as the reaction medium. The reaction was conducted under ambient conditions; TLC monitored reaction progress on silica gel plates using a 9:1 dichloromethane/acetone mixture as the eluent.

Upon completion, as evidenced by the disappearance of starting materials on TLC, the heterogeneous catalyst was removed through filtration. The filtrate was then evaporated under reduced pressure to remove the solvent. For purification, the crude residue was treated with a diethyl ether/*n*-hexane solvent system **(6:4)** and allowed to stand at **6 °C** overnight. This induced crystallization of the final compound, which was subsequently isolated by filtration. This protocol was systematically applied for the synthesis and isolation of all derivatives in the study.

3.2. Physicochemical Properties

3,3,6,6-tetramethyl-9-phenyl-3,4,5,6,7,9-hexahydro-1H-xanthene-1,8(2H)-dione

$C_{23}H_{26}O_3$

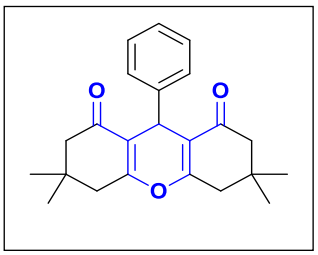

M = 350,19 **g/mol**

Aspect : white powder

M.p = 199-200 °C

R_f =0.71 **(DCM/Acetone : 9/1)**

Yield = 95%

IR (cm^{-1}): 1667 **(C=O)**, 1458 **(C=C)**.

^{1}H NMR (400 MHz, $CDCl_3$): δ 0.99 (s, 6H, 2C**H**$_3$), 1.10 (s, 6**H**, 2C**H**$_3$), 2.12-2.20 (q, $J_{H\text{-}H}$ =16.4 Hz, 4**H**, 2C**H**$_2$-C=C), 2.46 (s, 4**H**, 2C**H**$_2$-CO), 4.75 (s, 1**H**, *C**H**), 7.09 (t, $J_{H\text{-}H}$ =7.6 Hz, 1**H**, C**H**$_{Ar}$), 7.20 (t, $J_{H\text{-}H}$ =6.4 Hz, 2**H**, 2C**H**$_{Ar}$), 7.28 (t, $J_{H\text{-}H}$ =6.4 Hz, 2**H**, 2C**H**$_{Ar}$) ppm.

^{13}C NMR (100 MHz, $CDCl_3$): δ 27.5 (2**C**H$_3$), 29.4 (2**C**H$_3$), 31.9 (2**C**-(CH$_3$)$_2$), 32.3 (2**C**H$_2$-C=C), 41.0 (***C**H), 50.9 (2**C**H$_2$-CO), 115.8 (2**C**=CO), 126.4 (**C**H$_{Ar}$), 128.1 (**C**H$_{Ar}$), 128.5 (**C**H$_{Ar}$), 144.2 (**C**$_{Ar}$), 162.3 (2**C**-O), 196.4 (2**C**O) ppm.

9-(4-bromophenyl)-3,3,6,6-tetramethyl-3,4,5,6,7,9-hexahydro-1H-xanthene-1,8(2H)-dione

$C_{23}H_{23}O_3Br$

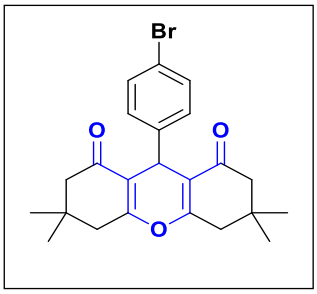

M = 428,10 **g/mol**

Aspect : white crystal

M.p = 227-229 °C

R_f =0.78 **(DCM/Acetone : 9/1)**

Yield = 93%

IR (cm^{-1}): 1662 **(C=O)**, 1469 **(C=C)**.

^{1}H NMR (400 MHz, $CDCl_3$): δ 0,98 (s, 6**H**, 2C**H**$_3$), 1.03 (s, 6**H**, 2C**H**$_3$), 2.08 (d, $J_{H\text{-}H}$ = 8.0 Hz, 2**H**, C**H**$_2$-C=C), 2.25 (d, $J_{H\text{-}H}$ = 8.0 Hz, 2**H**, C**H**$_2$-C=C), 2.50-2.56 (m, 4**H**, 2C**H**$_2$-CO), 4.50 (s, 1**H**, *C**H**), 7.20 (d, $J_{H\text{-}H}$ = 7.8 Hz, 2**H**, 2C**H**Ar), 7.28 (d, $J_{H\text{-}H}$ = 7.8, 2**H**, 2C**H**-Ar) ppm.

^{13}C NMR (100 MHz, $CDCl_3$): δ 26.9 (2**C**H$_3$), 29.0 (2**C**H$_3$), 31.4 (2**C**-(CH$_3$)$_2$), 32.3 (2**C**H$_2$-C=C), 40.6 (***C**H), 50.4 (2**C**H$_2$-CO), 114.4 (2**C**-CO), 128.3 (**C**H$_{Ar}$), 130.3 (**C**H$_{Ar}$), 134.7 (**C**$_{Ar}$-Br), 143.7 (**C**$_{Ar}$), 163.5 (2**C**-O), 196.5 (2**C**O) ppm.

9-(4-chlorophenyl)-3,3,6,6-tetramethyl-3,4,5,6,7,9-hexahydro-1H-xanthene-

$C_{23}H_{23}O_3Cl$

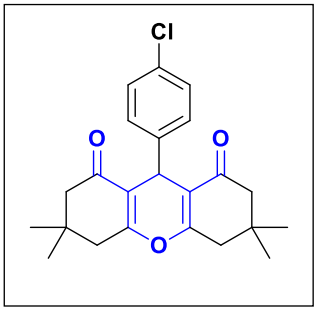

M = 384,69 **g/mol**

Aspect : white powder

M.p = 232-234°C

R_f =0.80 **(DCM/Acetone: 9/1)**

Yield = 94%

IR (cm^{-1}): 1665 (C=O), 1467 (C=C).

^{1}H NMR (400 MHz, $CDCl_3$): δ 0,99 (s, 6**H**, 2C**H**$_3$), 1.09 (s, 6**H**, 2C**H**$_3$), 2.12-2.25 (q, 4**H**, $J_{H-H=}$ 16.4 Hz, 2C**H**$_2$-C=C), 2.45 (s, 4**H**, 2C**H**$_2$-C=O), 4.66 (s, 1**H**, *C**H**), 6.53 (d, J_{H-H} =8.4 Hz, 2H, 2C**H**$_{Ar}$), 7.05 (d, J_{H-H} =8.0 Hz, 2**H**, 2C**H**$_{Ar}$) ppm.

^{13}C NMR (100 MHz, $CDCl_3$): δ 27.5 (2**C**H$_3$), 28.5 (2**C**H$_3$), 30.6 (2**C**-(CH$_3$)$_2$), 32.3 (2**C**H$_2$-C=C), 41.0 (***C**H), 49.2 (2**C**H$_2$-CO), 115.3 (2**C**-CO), 117.1 (2**C**H$_{Ar}$), 129.4 (2**C**H$_{Ar}$), 135.3 (**C**$_{Ar}$-Cl), 155.2 (**C**$_{Ar}$), 163.4 (**C**-O), 195.7 (2**C**O) ppm.

9-(4-fluorophenyl)-3,3,6,6-tetramethyl-3,4,5,6,7,9-hexahydro-1H-xanthene-1,8(2H)-dione

$C_{23}H_{23}O_3F$

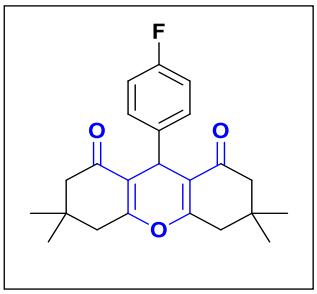

M = 368,18 **g/mol**

Aspect : white powder

M.p = 230-232°C

R_f =0.81 **(DCM/Acetone : 9/1)**

Yield = 92%

IR (cm^{-1}): 1659 **(C=O)**, 1507 **(C=C)**.

^{1}H NMR (400 MHz, $CDCl_3$): δ 0,94 (s, 6**H**, 2C**H**$_3$), 1.08 (s, 6**H**, 2C**H**$_3$), 2.00 (*d*, J_{H-H} =7.8 Hz, 2**H**, C**H**$_2$-C=C), 2.26 (*d*, J_{H-H} = 8.0 Hz, 2**H**, C**H**$_2$-C=C), 2.52-2.57 (m, 4**H**, 2C**H**$_2$-CO),4.51 (s, 1**H**, *C**H**), 7.01-7.15 (m, 2**H**, 2C**H**$_{Ar}$), 7.20-7.25 (m, 2H, 2C**H**$_{Ar}$) ppm.

9-(4-hydroxyphenyl)-3,3,6,6-tetramethyl-3,4,5,6,7,9-hexahydro-1H-xanthene-1,8(2H)-dione

$C_{23}H_{26}O_4$

M = 366,19 **g/mol**

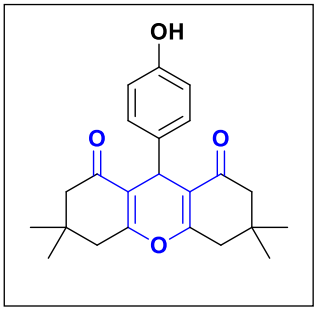

Aspect : white powder

M.p = 246-248 °C

R_f =0.80 **(DCM/Acetone : 9/1)**

Yield = 88%

IR (cm^{-1}): 3411 **(OH)**, 1659 **(C=O)**, 1512**(C=C)**.

^{1}H NMR (400 MHz, $CDCl_3$): ***δ*** 1,00 (s, 6**H**, 2C**H**$_3$), 1.09 (s, 6**H**, 2C**H**$_3$), 2.16-2.27 (q, 4**H**, $J_{H-H=}$ 16.4 Hz, 2C**H**$_2$-C=C), 2.45 (s, 4**H**, 2C**H**$_2$-CO), 4.67 (s, 1**H**, *C**H**), 6.29 (s, 1**H**, O**H**), 6.55 (d, J_{H-H} =8.8 Hz, 2**H**, 2C**H**$_{Ar}$), 7.06 (d, J_{H-H} =8.8 Hz, 2**H**, 2C**H**$_{Ar}$) ppm.

^{13}C NMR (100 MHz, $CDCl_3$): ***δ*** 26.8 (2**C**H$_3$), 29.3 (2**C**H$_3$), 31.9 (2**C**-(CH$_3$)$_2$), 33.0 (2**C**H$_2$-C=C), 41.0 (*C**H**), 50.9 (2**C**H$_2$-CO), 115.3 (2**C**-CO), 116.5 (**C**H$_{Ar}$), 130.3 (**C**H$_{Ar}$), 136.4 (**C**$_{Ar}$), 154.7 (**C**$_{Ar}$-OH), 162.9 (2**C**-O), 197.5 (2**C**O) ppm.

9-(naphthalen-1-yl)-3,3,6,6-tetramethyl-3,4,5,6,7,9-hexahydro-1H-xanthene-1,8(2H)-dione 1,8(2H)-dione

$C_{23}H_{28}O_3$

M = 400,20 **g/mol**

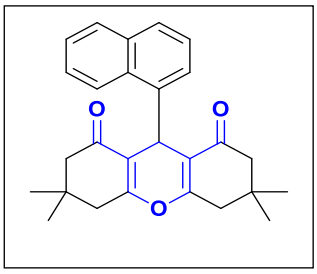

Aspect : white powder

M.p = 200-202 °C

R_f =0.70 **(DCM/Acetone : 9/1)**

Yield = 89%

IR (cm^{-1}): 1668 **(C=O)**, 1508 **(C=C)**.

^{1}H NMR (400 MHz, $CDCl_3$): ***δ*** 0,99 (s, 6**H**, 2C**H**$_3$), 1.11 (s, 6**H**, 2C**H**$_3$), 2.12-2.26 (q, 4**H**, $J_{H-H=}$ 16.4 Hz, 2C**H**$_2$-C=C), 2.50 (s, 4**H**, 2C**H**$_2$-CO), 4.92 (s, 1**H**, *C**H**), 7.34-7.46 (m, 3**H**, 3C**H**$_{Ar}$), 7.69-7.77 (m, 4**H**, 4C**H**$_{Ar}$) ppm.

^{13}C NMR (100 MHz, $CDCl_3$): ***δ*** 27.4 (2**C**H$_3$), 29.4 (2**C**H$_3$), 32.1 (2**C**-(CH$_3$)$_2$), 32.3 (**C**H$_2$-C=C), 41.1 (*C**H**), 50.9 (2**C**H$_2$-CO), 115.8 (2**C**-CO), 125.4 (**C**H$_{Ar}$), 125.7 (**C**H$_{Ar}$), 127.0 (**C**H$_{Ar}$), 127.2 (**C**H$_{Ar}$), 127.6 (**C**H$_{Ar}$), 127.8 (**C**H$_{Ar}$), 128.1 (**C**H$_{Ar}$), 132.5 (**C**$_{Ar}$), 133.5 (**C**$_{Ar}$), 141.7 (**C**$_{Ar}$), 162.4 (2**C**-O), 196.4 (2**C**O) ppm.

9-(3,4-dimethoxyphenyl)-3,3,6,6-tetramethyl-3,4,5,6,7,9-hexahydro-1H-xanthene-1,8(2H)-dione

$C_{25}H_{30}O_5$

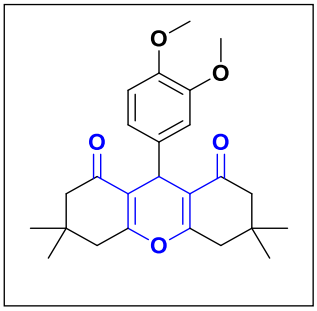

M = 410,21 **g/mol**

Aspect : white powder

M.p = 181-183°C

R_f =0.80 **(DCM/Acetone : 9/1)**

Yield = 86%

IR (cm^{-1}): 1644 **(C=O)**, 1514 **(C=C)**.

^{1}H NMR (400 MHz, $CDCl_3$): δ 0.97 (s, 6**H**, 2C**H**$_3$), 1.09 (s, 6**H**, 2C**H**$_3$), 2.11 (d, $J_{H\text{-}H}$ = 16.0 Hz, 2**H**, C**H**$_2$-C=C), 2.26 (d, $J_{H\text{-}H}$ = 16.2 Hz, 2**H**, C**H**$_2$-C=C), 2.55 (q, $J_{H\text{-}H}$ = 17.6 Hz, 4**H**, 2C**H**$_2$-CO), 3.72 (s, 6H, 2C**H**$_3$-O), 4.52 (s,1H, *C**H**), 6.94- 6.56 (m, 3**H**, 3C**H**$_{Ar}$) ppm.

^{13}C NMR (100 MHz, $CDCl_3$): δ 26.4 (2**C**H$_3$), 28.6 (2**C**H$_3$), 30.4 (2**C**-(CH$_3$)$_2$), 31.6 (2**C**H$_2$-C=C), 39.8 (***C**H), 49.5 (2**C**H$_2$-CO), 55.3 (2**C**H$_3$-O), 111.2 (**C**H$_{Ar}$), 111.8 (**C**H$_{Ar}$), 114.5 (2**C**-CO), 118.4 (**C**H$_{Ar}$), 136.7 (**C**$_{Ar}$), 147.1 (**C**$_{Ar}$-OCH$_3$) ,148.0 (**C**$_{Ar}$-OCH$_3$), 162.7 (2**C**-O), 196.7 (2**C**O) ppm.

3,3,6,6-tetramethyl-9-(*m*-tolyl)-3,4,5,6,7,9-hexahydro-1H-xanthene-1,8(2H)-dione 1,8(2H)-dione

$C_{24}H_{28}O_3$

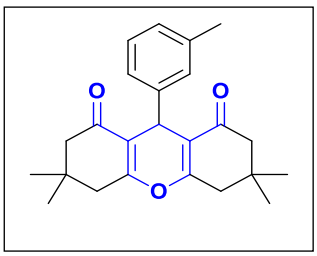

M = 364,20 g/mol

Aspect : white powder

M.p = 211-213°C

R_f =0.75 **(DCM/Acetone : 9/1)**

Yield = 89%

IR (cm^{-1}): 1667 **(C=O)**, 1463 **(C=C)**.

^{1}H NMR (400 MHz, $CDCl_3$): δ 0.99 (s, 6**H**, 2C**H**$_3$), 1.10 (s, 6**H**, 2C**H**$_3$), 2.14-2.24 (q, 4**H**, $J_{H\text{-}H}$ =16.2 Hz ,C**H**$_2$-C=C), 2.28 (s, 3**H**, C**H**$_3$), 2.46 (s, 4**H**, 2C**H**$_2$-CO), 4.71 (s, 1**H**, *C**H**), 6.89 (d, $J_{H\text{-}H}$ = 7.2 Hz, 1**H**, C**H**$_{Ar}$), 7.01 (d, $J_{H\text{-}H}$ =8.0 Hz, 1**H**, C**H**$_{Ar}$), 7.06-7.13 (m, 2**H**, 2C**H**$_{Ar}$) ppm.

^{13}C NMR (100 MHz, $CDCl_3$): δ 21.6 (**C**H$_3$-Ar), 27.5 (2**C**H$_3$), 29.4 (2**C**H$_3$), 31.9 (2**C**-(CH$_3$)$_2$), 32.4 (2**C**H$_2$-C=C), 41.1 (***C**H), 51.0 (2**C**H$_2$-CO), 116.0 (2**C**-CO), 125.4 (**C**H$_{Ar}$),

127.5 (**C**H_{Ar}), 128.1 (**C**H_{Ar}), 129.6 (**C**H_{Ar}), 137.6 (**C**$_{Ar}$-CH_3), 144.2 (**C**$_{Ar}$), 162.4 (2**C**-O), 197.0 (2**C**O) ppm.

9-(2-chlorophenyl)-3,3,6,6-tetramethyl-3,4,5,6,7,9-hexahydro-1H-xanthene-1,8(2H)-dione

$C_{23}H_{23}O_3Cl$

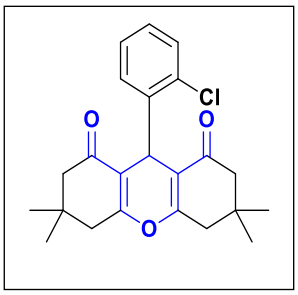

M = 384,69 **g/mol**

Aspect : white powder

M.p = 227-229°C

R_f =0.80 **(DCM/Acetone : 9/1)**

Yield = 87%

IR (cm^{-1}): 1665 **(C=O)**, 1467 **(C=C)**.

^{1}H NMR (400 MHz, $CDCl_3$): ***δ*** 1,01 (s, 6**H**, 2C**H**$_3$), 1.09 (s, 6**H**, 2C**H**$_3$), 2.13-2.24 (q, 4H, J_{H-H} =16.4 Hz, 2C**H**$_2$-C=C), 2.42 (s, 4**H**, 2C**H**$_2$-C=O), 4.99 (s, 1**H**, *C**H**), 7.05 (t, 1**H**, J_{H-H} =7.6 Hz, C**H**$_{Ar}$), 7.16 (t, 1**H**, J_{H-H} =7.6 Hz, C**H**$_{Ar}$), 7.21 (d, 1**H**, J_{H-H} =7.6 Hz, C**H**$_{Ar}$), 7.42 (d, 1**H**, J_{H-H} =7.6 Hz, C**H**$_{Ar}$) ppm.

^{13}C NMR (100 MHz, $CDCl_3$): ***δ*** 27.5 (2**C**H_3), 29.4 (2**C**H_3), 31.8 (2**C**-$(CH_3)_2$), 32.8 (2**C**H_2-C=C), 40.9 (*C**H**), 50.8 (2**C**H_2-CO), 113.8 (2**C**-CO), 126.4 (**C**H_{Ar}), 128.5 (**C**H_{Ar}), 129.2 (**C**H_{Ar}), 130.3 (**C**H_{Ar}), 132.5 (**C**$_{Ar}$-Cl), 140.1 (**C**$_{Ar}$), 163.0 (2**C**-O), 196.1 (2**C**O) ppm.

9-(2-hydroxyphenyl)-3,3,6,6-tetramethyl-3,4,5,6,7,9-hexahydro-1H-xanthene-1,8(2H)-dione

$C_{23}H_{26}O_4$

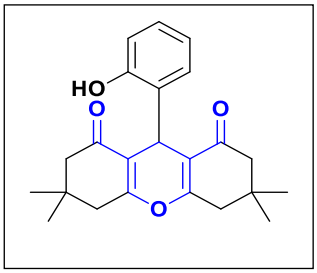

M = 366,19 **g/mol**

Aspect : white powder

M.p = 246-248 °C.

R_f =0.80 **(DCM/Acetone : 9/1)**

Yield = 84%

IR (cm^{-1}): 3400 **(OH)**, 1637 **(C=O)**, 1458**(C=C)**.

^{1}H NMR (400 MHz, $CDCl_3$): ***δ*** 0,99 (s, 6H, 2C**H**$_3$), 1.03 (s, 3H, C**H**$_3$), 1.12 (s, 3H, C**H**$_3$), 1.90-2.00 (q, 2**H**, J_{H-H} =16.4 Hz, C**H**$_2$-C=C), 2.33 (s, 2**H**, C**H**$_2$-C=C), 2.35-2.61 (q, 4**H**, J_{H-H} =17.6 Hz, 2C**H**$_2$-C=O), 4.76 (s, 1**H**, *C**H**), 6.95-7.07 (m, 3**H**, C**H**$_{Ar}$), 7.11-7.19 (m, 1**H**, C**H**$_{Ar}$), 10.44 (s, 1**H**, O**H**) ppm.

^{13}C NMR (100 MHz, $CDCl_3$): δ 27.3 (**C**H_3), 27.9 (**C**H_3), 29.2 (**C**H_3), 29.9 (**C**H_3), 31.1 (2**C**-$(CH_3)_2$), 32.4 (2**C**H_2-C=C), 41.7 (2**C**H_2-C=C), 50.0 (*C**H**), 50.8 (2**C**H_2-CO), 111.2 (2**C**-CO), 115.9 (**C**H_{Ar}), 124.7 (**C**H_{Ar}), 127.6 (**C**H_{Ar}), 128.1 (**C**H_{Ar}), 151.2 (**C**$_{Ar}$), 169.2 (2**C**-O), 170.7 (**C**-OH), 201.0 (**C**O) ppm.

9-(4-chlorophenyl)-3,4,5,6,7,9-hexahydro-1H-xanthene-1,8(2H)-dione

$C_{19}H_{17}O_3Cl$

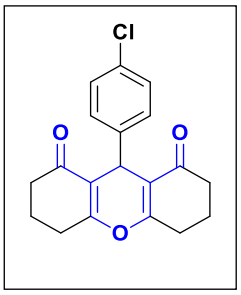

M = 328,09 **g/mol**

Aspect : white powder

M.p = 225-227 °C

R_f =0.74 **(DCM/Acetone : 9/1)**

Yield = 93%

IR (cm^{-1}): 1665 **(C=O)**, 1467 **(C=C)**.

^{1}H NMR (400 MHz, $CDCl_3$): δ 1,01 1.83-1.96 (m, 4**H**, 2C**H**$_2$-CH_2), 2.23-2.30 (m, 4**H**, 2C**H**$_2$-C=C), 2.60-2.68 (m, 4**H**, 2C**H**$_2$-CO), 4.50 (s, 1**H**, *C**H**), 6.58 (d, $J_{H\text{-}H}$ =8.0 Hz, 2**H**, 2C**H**$_{Ar}$), 6.97 (d, $J_{H\text{-}H}$ =8.0 Hz, 2**H**, 2C**H**$_{Ar}$) ppm.

^{13}C NMR (100 MHz, $CDCl_3$): δ 20.6 (2**C**H_2-CH_2), 26.3 (2**C**H_2-C=C), 30.9 (2**C**H_2-CO), 35.3 (*C**H**), 113.9 (2**C**-CO), 117.1 (**C**H_{Ar}), 128.7 (**C**H_{Ar}), 135.7 (**C**-Cl), 157.1 (**C**$_{Ar}$), 163.9 (2**C**-O), 196.2 (2**C**O) ppm.

9-(4-fluorophenyl)-3,4,5,6,7,9-hexahydro-1H-xanthene-1,8(2H)-dione

$C_{19}H_{17}O_3F$

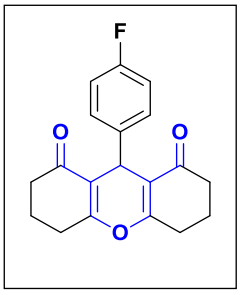

M = 312,12 **g/mol**

Aspect : white powder

M.p = 228-230 °C

R_f =0.75 **(DCM/Acetone : 9/1)**

Yield = 92%

IR (cm^{-1}): 1656 **(C=O)**, 1501 **(C=C)**.

^{1}H NMR (400 MHz, $CDCl_3$): δ 1.82-1.89 (m, 2**H**, C**H**$_2$-CH_2), 1.91-2.00 (m, 2**H**, C**H**$_2$-CH_2), 2.25-2.33 (m, 4**H**, 2C**H**$_2$-C=C), 2.53-2.69 (m, 4**H**, 2C**H**$_2$-C=C), 4.57 (d, $J_{H\text{-}F}$ = 11.9 Hz, 1**H**,

*C**H**), 6.94 (t, J_{H-H} = 8.6 Hz, 1**H**, C**H**$_{Ar}$), 7.15 (d, J_{H-H} = 8.0 Hz, 1**H**, C**H**$_{Ar}$), 7.24 (t, J_{H-H} = 6.0 Hz, 1**H**, C**H**$_{Ar}$), 7.33 (d, J_{H-H} = 8.0 Hz, 1**H**, C**H**$_{Ar}$) ppm.

^{13}C NMR (100 MHz, CDCl$_3$): δ 20.7 (2**C**H$_2$-CH$_2$), 26.9 (2**C**H$_2$-C=C), 34.2 (2**C**H$_2$-CO), 50.7 (***C**H), 112.9 (2**C**-CO), 114.1 (**C**H$_{Ar}$), 115.0 (**C**H$_{Ar}$), 116.0 (**C**H$_{Ar}$), 129.5 (**C**H$_{Ar}$),130.5 (**C**$_{Ar}$),163.9 (2**C**-O), 164.5 (**C**-F), 195.8 (**C**O), 205.6 (**C**O)ppm.

9-(4-hydroxyphenyl)-3,4,5,6,7,9-hexahydro-1H-xanthene-1,8(2H)-dione

C$_{19}$H$_{18}$O$_4$

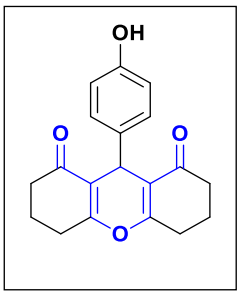

M = 310,12 **g/mol**

Aspect : white powder

M.p = 243-245 °C

R$_f$ =0.85 **(DCM/Acetone : 9/1)**

Yield = 89%

IR (cm^{-1}): 3353 **(OH)**, 1644 **(C=O)**, 1512 **(C=C)**.

^{1}H NMR (400 MHz, CDCl$_3$): δ 1.79-1.98 (m, 4**H**, 2C**H**$_2$-CH$_2$), 2.21-2.30 (m, 4**H**, 2C**H**$_2$-C=C), 2.54-2.69 (m, 4**H**, 2C**H**$_2$-CO), 4.49 (s, 1**H**, *C**H**), 6.57 (d, J_{H-H} =8.0 Hz, 2**H**, 2C**H**$_{Ar}$), 6.95 (d, J_{H-H} =8.0 Hz, 2**H**, 2C**H**$_{Ar}$), 9.09 (s, 1**H**, O**H**) ppm.

^{13}C NMR (100 MHz, CDCl$_3$): δ 19.8 (2**C**H$_2$-CH$_2$), 26.3 (2**C**H$_2$-C=C), 29.7 (2**C**H$_2$-CO), 36.0 (***C**H), 114.6 (2**C**-CO), 116.9 (**C**H$_{Ar}$), 128.7 (**C**H$_{Ar}$), 135.6 (**C**-Cl), 155.9 (**C**$_{Ar}$), 163.6 (2**C**-O), 195.8 (2**C**O) ppm.

9-(4-(trifluoromethyl) phenyl)-3,4,5,6,7,9-hexahydro-1H-xanthene-1,8(2H)-dione

C$_{24}$H$_{25}$O$_3$F$_3$

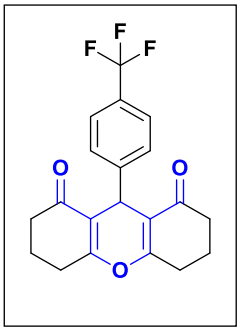

M = 362,11 **g/mol**

Aspect : white powder

M.p = 222-225 °C

R$_f$ =0.73 **(DCM/Acetone : 9/1)**

Yield = 90%

IR (cm^{-1}): 1663 **(C=O)**, 1420 **(C=C)**.

^{1}H NMR (400 MHz, $CDCl_3$): δ 1.96-2.11 (m, 4H, 2C**H**$_2$-CH_2), 2.27-2.42 (m, 4**H**, 2C**H**$_2$-C=C), 2.54-2.74 (m, 4**H**, 2C**H**$_2$-CO), 4.85 (s, 1**H**, *C**H**), 7.41 (d, J_{H-H} = 8.2 Hz, 2**H**, 2C**H**$_{Ar}$), 7.47 (d, J_{H-H}= 8.2 Hz, 2**H**, 2C**H**$_{Ar}$) ppm.

^{13}C NMR (100 MHz, $CDCl_3$): δ 20.4 (2**C**H_2-CH_2), 27.2 (2**C**H_2-C=C), 33.0 (2**C**H_2-CO), 37.0 (*C**H**), 116.4 (2**C**-CO), 125.2 (**C**F_3), 130.1 (**C**-CF_3), 128.9 (**C**H_{Ar}), 149.3 (**C**$_{Ar}$), 164.4 (2**C**-O), 196.5 (2**C**O) ppm.

9-(3,4-dimethoxyphenyl)-3,4,5,6,7,9-hexahydro-1H-xanthene-1,8(2H)-dione

$C_{21}H_{22}O_5$

M = 354,15 **g/mol**

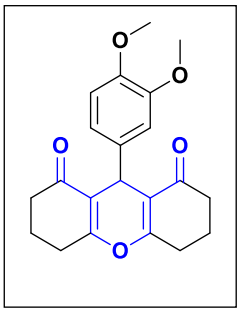

Aspect : white powder

M.p = 93-95 °C

R_f =0.82 **(DCM/Acetone : 9/1)**

Yield = 85%

IR (cm^{-1}): 1668 **(C=O)**, 1512 **(C=C)**.

^{1}H NMR (400 MHz, $CDCl_3$): δ 1.81-1.99 (m, 4**H**, 2C**H**$_2$-CH_2), 2.24-2.39 (m, 4**H**, 2C**H**$_2$-C=C), 2.54-2.69 (m, 4**H**, 2C**H**$_2$-CO), 3.67 (s, 3**H**, O-C**H**$_3$), 3.69 (s, 3**H**, O-C**H**$_3$), 4.54 (s, 1**H**, *C**H**), 6.63 (d, J_{H-H} =6.0 Hz, 1**H**, C**H**$_{Ar}$), 6.76 (J_{H-H} =7.6 Hz, 2**H**, 2C**H**$_{Ar}$) ppm.

^{13}C NMR (100 MHz, $CDCl_3$): δ 19.8 (2**C**H_2-CH_2), 26.3 (2**C**H_2-C=C), 29.6 (2**C**H_2-CO), 37.6 (*C**H**), 56.7 (2**C**H_3-O), 111.6 (**C**H_{Ar}), 113.3 (**C**H_{Ar}), 115.9 (**C**H_{Ar}), 119.6 (2**C**-CO), 137.1 (**C**$_{Ar}$), 146.9 (**C**-OCH_3), 148.1 (**C**-OCH_3), 165.9 (2**C**-O), 197.1 (2**C**O) ppm.

9-(*m*-tolyl)-3,4,5,6,7,9-hexahydro-1H-xanthene-1,8(2H)-dione

$C_{20}H_{20}O_3$

M = 3018,14 **g/mol**

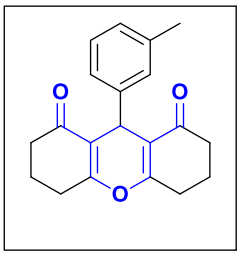

Aspect : white powder

M.p = 209-211°C

R_f =0.77 **(DCM/Acetone : 9/1)**

Yield = 87%

IR (cm^{-1}): 1665 **(C=O)**, 1486 **(C=C)**.

^{1}H NMR (400 MHz, $CDCl_3$): ***δ*** 1.94 –2.05 (m, 4**H**, 2C**H**$_2$-CH_2), 2.25-2.38 (m, 4**H**, 2C**H**$_2$-C=C), 2.28 (s, 3**H**, C**H**$_3$), 2.50-2.66 (m, 4**H**, 2C**H**$_2$-CO), 4.77 (s, 1**H**, *C**H**), 6.91 (d, J_{H-H} =7.6 Hz, 1**H**, C**H**$_{Ar}$), 7.02 (d, J_{H-H} =8.0 Hz, 1**H**, C**H**$_{Ar}$), 7.07 (d, J_{H-H}=7.6 Hz, 1**H**, C**H**$_{Ar}$), 7.12 (s, 1**H**, C**H**$_{Ar}$) ppm.

^{13}C NMR (100 MHz, $CDCl_3$): ***δ*** 20.4 (2**C**H_2-CH_2), 21.5 (**C**H_3), 27.2 (2**C**H_2-C=C), 31.6 (2**C**H_2-CO), 37.0 (*C**H**), 117.1 (2**C**-CO), 125.3 (**C**H_{Ar}),127.9 (**C**H_{Ar}), 128.0 (**C**H_{Ar}),129.4 (**C**H_{Ar}), 137.5 (**C**-CH_3), 143.6 (**C**$_{Ar}$), 163.94 (2**C**-O), 196.53 (2**C**O) ppm.

4. Preparation of 1,2-oxaphospholane 2-oxide derivatives

4.1. General procedure

A mixture of aldehyde **(1 mmol)**, dimedone **(1 mmol)**, and diethylphosphite **(1 mmol)** was dissolved in 1 mL of ethanol and subjected to microwave irradiation in a microwave reactor for **2** minutes. The reaction progress was monitored by thin-layer chromatography **(TLC)**. Once complete, the obtained derivatives were purified by column chromatography using ethyl acetate/ petroleum ether **(6:4)** as eluent. The combined pure fractions were concentrated under reduced pressure.

4.2. Physicochemical properties

2-hydroxy-6,6-dimethyl-3-phenyl-3,6,7-trihydrobenzo [1,2] oxaphosphol-4(5H)-one 2-oxide

$C_{20}H_{20}O_3$

M = 308,14 **g/mol**

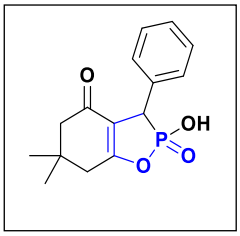

Aspect : Brown oil

R_f =0.44 **(ethyl acetate /petroleum ether :6/4)**

Yield = 87%

IR (cm^{-1}): 3302 **(OH)**, 1667 **(C=O)**, 1196 **(P=O)**, 1002 **(P-O)**.

^{1}H NMR (400 MHz, DMSO-d_6): δ 0.92 (s, 6**H**, 2C**H**$_3$), 2.24 (s,4**H**, 2C**H**$_2$-C=C),4.76 (d, J_{H-P} = 27.12 Hz, 1**H**, *C**H**), 7.51 (s, 5H, 5C**H**$_{Ar}$) ppm.

^{13}C NMR (100 MHz, DMSO-d_6): δ 18.9 (2**C**H$_3$),32.5 (**C**-(CH$_3$)$_2$), 40.5 (***C**H),56.4 (**C**H$_2$-C), 61.2 (**C**H$_2$-CO), 108.8 (**C**-CO), 119.2 (3**C**H$_{Ar}$),128.5 (2**C**H$_{Ar}$),139.5 (**C**$_{Ar}$),182.3 (**C**=C), 198.8 (**C**O) ppm.

^{31}P NMR (MHz, DMSO-d_6): δ 21.24 ppm.

3-(2-chlorophenyl) -2-hydroxy-6,6-dimethyl-3,6,7-trihydrobenzo [1,2] oxaphosphol-4(5H)-one 2-

$C_{17}H_{20}ClO_4P$

M = 326,05 **g/mol**

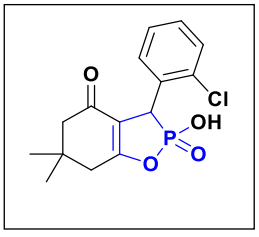

Aspect: Brown oil

R_f =0.45 **(ethyl acetate /petroleum ether :6/4)**

Yield = 78%

IR (cm^{-1}): 3382 **(OH)**, 1677 **(C=O)**, 1212 **(P=O)**, 1048 **(P-O)**.

^{1}H NMR (400 MHz, DMSO-*d*$_6$): ***δ*** 0.93 (s, 6**H**, 2C**H**$_3$), 2.24 (s,4**H**, 2C**H**$_2$-C), 4.67 (d, J_{H-H} = 27.24 Hz,1**H**, *C**H**), 7.10- 7.13 (m, 3**H**, 3C**H**$_{Ar}$),7.51 (s, 1**H**, 1C**H**$_{Ar}$) ppm

^{13}C NMR (100 MHz, DMSO-*d*$_6$): ***δ*** 18.5 (2**C**H$_3$), 31.1 (**C**-(CH$_3$)$_2$), 40.3 (***C**H),56.0 (2**C**H$_2$-C), 110.0 (**C**-CO), 125.5 (**C**H$_{Ar}$),126.3 (**C**H$_{Ar}$), 127.4 (**C**H$_{Ar}$),129.3 (**C**H$_{Ar}$),136.4 (**C**$_{Ar}$), 137.9 (**C**$_{Ar}$),182.3 (**C**=C), 194.8 (**C**O) ppm.

^{31}P NMR (MHz, DMSO-*d*$_6$): ***δ*** 26.86 ppm**.**

2-hydroxy-6,6-dimethyl-3-(m-tolyl)-3,6,7-trihydrobenzo [1,2] oxaphosphol-4(5H)-one

C$_{18}$H$_{22}$O$_4$P

M = 306,10 **g/mol**

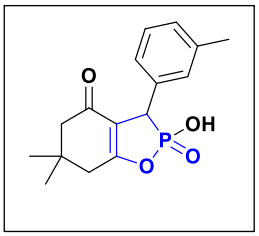

Aspect : Brown oil

R$_f$ =0.46 **(ethyl acetate /petroleum ether :6/4)**

Yield = 80%

IR (cm^{-1}): 3380 **(OH)**, 1727 **(C=O)**, 1198 **(P=O)**, 1023 **(P-O)**.

^{1}H NMR (400 MHz, DMSO-*d*$_6$): ***δ*** 0.92 (s, 6H, 2C**H**$_3$), 2.20 (s,4H, 2C**H**$_2$-C), 2.51 (s, 3**H**, C**H**$_3$), 4.72 (d, J_{H-P} = 26.52 Hz,1**H**, *C**H**), 7.70- 7.74 (m, 3**H**, 3C**H**$_{Ar}$),7.51 (m, 1**H**, 1C**H**$_{Ar}$) ppm

^{13}C NMR (100 MHz, DMSO-*d*$_6$): ***δ*** 18.9 (2**C**H$_3$), 25.4 (**C**H$_3$), 31.6 (**C**-(CH$_3$)$_2$), 40.6 (***C**H), 56.4 (2**C**H$_2$-C), 110.2 (C-CO), 125.3 (**C**H$_{Ar}$),125.9 (**C**H$_{Ar}$), 126.9 (**C**H$_{Ar}$),127.8 (**C**H$_{Ar}$),133.2 (**C**$_{Ar}$), 137.7 (**C**$_{Ar}$),178.4 (**C**=C), 194.5 (**C**O) ppm.

^{31}P NMR (MHz, DMSO-*d*$_6$): ***δ*** 22.55 ppm.

3-(3,4-dimethoxyphenyl)-2-hydroxy-6,6-dimethyl-3,6,7-trihydrobenzo[1,2]oxaphosphol-4(5H)-one 2-oxide

C$_{17}$H$_{21}$O$_6$P

M = 352,11 **g/mol**

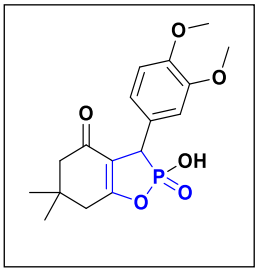

Aspect : Brown oil

R$_f$ =0.43 **(ethyl acetate /petroleum ether :6/4)**

Yield = 82%

IR (cm^{-1}): 3425 **(OH)**, 1650 **(C=O)**, 1146 **(P=O)**, 1021 **(P-O)**.

^{1}H NMR (400 MHz, DMSO-*d*$_6$): *δ* 0.93 (s, 6**H**, 2C**H**$_3$), 2.20 (s,4**H**, 2C**H**$_2$-C), 3.68 (s, 6**H**, 2OC**H**$_3$), 4.55 (d, J_{H-P} = 26.88 Hz,1**H**, *C**H**), 6.79 (s, 2H, 2C**H**$_{Ar}$),7.50 (m, 1**H**, 1C**H**$_{Ar}$) ppm

^{13}C NMR (100 MHz, DMSO-d_6): δ 24.9 (**C**H_3), 27.7 (**C**H_3), 31.1 (**C**-$(CH_3)_2$), 42.2 (*__C__H), 55.3 (**C**H_2-C), 57.0 (**C**H_2-C), 64.9 (2 O**C**H_3), 94.4 (**C**-CO),111.4 (**C**H_{Ar}), 113.3 (**C**H_{Ar}),115.4 (**C**H_{Ar}),131.9 (**C**$_{Ar}$), 138.9 (2**C**$_{Ar}$),189.9 (**C**=C), 196.6 (**C**O) ppm.

^{31}P NMR (MHz, DMSO-d_6): δ 26.85 ppm.

3-(4-bromophenyl)-2-ethoxy-6,6-dimethyl-3,6,7-trihydrobenzo[1,2] oxaphosphol-4(5H)-one2-oxide

$C_{15}H_{16}BrO_4P$

M = 370,00 **g/mol**

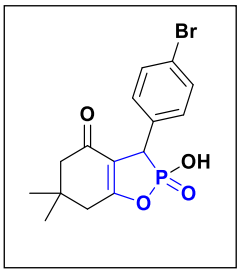

Aspect : Yellow oil

R_f =0.47 **(ethyl acetate /petroleum ether :6/4)**

Yield = 76%

IR (cm^{-1}): 3383 **(OH)**, 1711 **(C=O)**, 1149 **(P=O)**, 1014 **(P-O)**.

^{1}H NMR (400 MHz, DMSO-d_6): δ 0.92 (s, 6H, 2C**H**$_3$), 2.24 (s,4**H**, 2C**H**$_2$-C), 3.68 (s, 6**H**, 2OC**H**$_3$), 4.91 (d, J_{H-P} = 27.04 Hz,1**H**, *C**H**), 7.49 (d, J_{H-H} = 8.8 Hz, 1**H**, 2C**H**), 7.72 (d, J_{H-H} =8.8 Hz, 2**H**, 2C**H**) **ppm**.

^{13}C NMR (100 MHz, DMSO-d_6): δ 18.7 (2**C**H_3), 31.3 (**C**-$(CH_3)_2$), 41.2 (*__C__H), 49.6 (**C**H_2-C), 56.2 (**C**H_2-C), 127.4 (**C**H_{Ar}),129.3 (**C**H_{Ar}),130.9 (**C**$_{Ar}$), 157.5 (**C**$_{Ar}$),166.4 (**C**=C), 192.1 (**C**O) **ppm**.

^{31}P NMR (MHz, DMSO-d_6): δ 21.41 ppm.

5. Preparation of 2-chloroethyl carbamates derivatives

5.1. General procedure

Aromatic alcohol (**1** equivalent) was dissolved in **10** mL of anhydrous dichloromethane (**DCM**) along with triethylamine (**1.2** equivalents) in a **25** mL two-necked flask. The resulting solution was stirred under cooling at 0 °C After **30** minutes, a solution of 2-chloroethyl isocyanate (**1** equivalent) in **10** mL of anhydrous DCM was introduced dropwise using a bromine addition funnel. The reaction was maintained with stirring for 1h at **0**°C. Thin-layer chromatography **(TLC)** on silica gel plates, with an eluent system of dichloromethane and petroleum ether **(8:2)**, was used to monitor the reaction progress. Once complete, the mixture was concentrated under reduced pressure to remove the solvent. For purification, diethyl ether and *n*-hexane **(1:1)** were added to the concentrated residue to induce crystallization of the target compound.

5.2. Physicochemical properties

Phenyl (2-chloroethyl) carbamate

$C_9H_{10}ClNO_2$

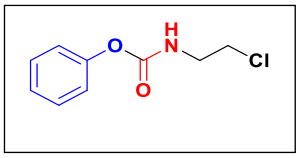

M = 199.04 **g/mol**

Aspect : White powder

M.p = 125-127 °C

R_f =0.57 **(DCM/ Petroleum ether: 8/2)**

Yield = 89%

IR (cm^{-1}): 3302 **(NH)** ,1707 **(C=O)**.

^{1}H NMR (400 MHz, $CDCl_3$): ***δ*** 3.70 (t, J_{H-H} =6.3 Hz, 2**H**, C**H**$_2$-N), 4.16 (t, J_{H-H} =6.3Hz, 2**H**, C**H**$_2$-Cl), 7.10 (d, J_{H-H} =7.5 Hz, 1**H**, C**H**$_{Ar}$), 7.20 (t, J_{H-H} =6.8 Hz, 2**H**, 2C**H**$_{Ar}$), 7.38 (d, J_{H-H} =7.5 Hz, 2**H**, 2C**H**$_{Ar}$), 8.00 (s, 1**H**, N**H**) **ppm**.

^{13}C NMR (100 MHz, $CDCl_3$): ***δ*** 42.5 (**C**H$_2$-Cl), 43.3(**C**H$_2$-N), 121.7 (2**C**-Ar), 125.0 (**C**-Ar), 129.3 (**C**-Ar), 150.9 (**C**=O), 154.5 (**C**-O-CO) ppm.

4-bromophenyl (2-chloroethyl) carbamate

$C_9H_{10}BrClNO_2$

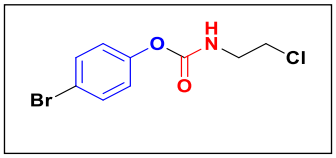

M = 276.95 **g/mol**

Aspect : White powder

M.p = 128-130°C

R_f =0.5 **(DCM/ Petroleum ether : 8/2)**

Yield = 92%

IR (cm^{-1}): 3287 **(NH)**,1703 **(C=O)**.

^{1}H NMR (400 MHz, $CDCl_3$): ***δ*** 3.40 (t, J_{H-H} =6.3 Hz ,2**H**, C**H**$_2$-N), 3.67 (t, J_{H-H} =6.3Hz ,2**H**, C**H**$_2$-Cl), 7.10 (d, J_{H-H} =8 Hz, 1**H**, C**H**$_{Ar}$), 7.56 (d, J_{H-H} =7.9 Hz, 2**H**, 2C**H**$_{Ar}$), 8.08 (s, 1**H**, N**H**) **ppm**.

^{13}C NMR (100 MHz, $CDCl_3$): ***δ*** 40.1(**C**H$_2$-Cl), 41.9 (**C**H$_2$-N), 123.9 (2**C**H-Ar), 132.7 (2**C**H-Ar), 149.4 (**C**-Br), 151.7 (**C**-O-CO), 156.7 (**C**=O) ppm.

4-fluorophenyl (2-chloroethyl) carbamate

$C_9H_{10}ClFNO_2$

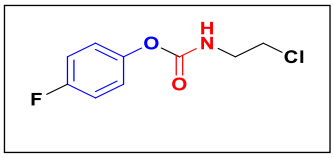

M = 217.03 **g/mol**

Aspect : White powder

M.p = 126 -128 °C

R_f =0.55 **(DCM/ Petroleum ether : 8/2)**

Yield = 95%

IR (cm^{-1}): 3285 **(NH)**, 1704 **(C=O)**.

^{1}H NMR (400 MHz, $CDCl_3$): ***δ*** 3.40 (t, J_{H-H} =6.3 Hz ,2**H**, C**H**$_2$-N), 3.67 (t, J_{H-H} =6.3Hz ,2**H**, C**H**$_2$-Cl), 7.18 (m, J_{H-H} =8 Hz, 1**H**, C**H**$_{Ar}$), 8.08 (s, 1**H**, N**H**) **ppm**.

^{13}C NMR (100 MHz, $CDCl_3$): ***δ*** 39.9 (**C**H$_2$-Cl), 41.9(**C**H$_2$-N), 116.3 (2**C**H-Ar), 123.6 (2**C**H-Ar), 152.0 (**C**-F), 159.1(**C**=O), 161.1 (**C**-O-CO) ppm.

4-methoxyphenyl (2-chloroethyl) carbamate

$C_{10}H_{12}ClNO_3$

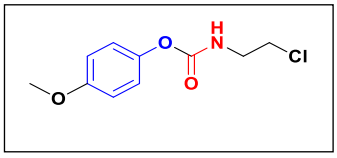

M = 229.05 **g/mol**

Aspect : White crystal

M.p = 121-123 °C

R_f =0.4 **(DCM/ Petroleum ether : 8/2)**

Yield = 90%

IR (cm^{-1}): 3294 **(NH)**, 1703 **(C=O)**.

^{1}H NMR (400 MHz, $CDCl_3$): δ 3.38-3.40 (q, J_{H-H} =6.0 Hz, 2**H**, C**H**$_2$-N), 3.66 (t, J_{H-H} =6.1Hz, 2**H**, C**H**$_2$-Cl), 3.74 (s, 3**H**, OC**H**$_3$), 6.90-7.03 (m, J_{H-H} =8 Hz, 4**H**, C**H**$_{Ar}$), 7.91 (t, J_{H-H}=5,7 *Hz*, 1**H**, N**H**) **ppm**.

^{13}C NMR (100 MHz, $CDCl_3$): δ 42.5 (**C**H$_2$-Cl), 43.3 (**C**H$_2$-N), 55.3 (O-**C**H$_3$), 114.2 (2**C**H-Ar), 122.5 (2**C**H-Ar), 144.3(**C**=O), 154.8 (**C**-O-CO), 156.3 (**C**-OCH$_3$) ppm.

2,6-diisopropylphenyl (2-chloroethyl) carbamate

$C_{15}H_{22}ClNO_2$

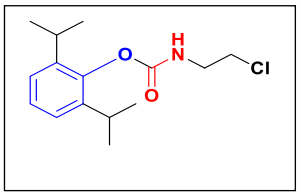

M = 283.13 **g/mol**

Aspect : Yellow powder

M.p = 130-132°C

R_f =0.59 **(DCM/ Petroleum ether : 8/2)**

Yield = 91%

IR (cm^{-1}): 3315 **(NH)**, 1703 **(C=O)**.

^{1}H NMR (400 MHz, $CDCl_3$): δ 1,13 (d, J_{H-H}= 6,0 *Hz*, **12H, 4(**C**H**$_3$)$_2$-CH), 2.95-3.03 (m, 2**H**, 2C**H**-(CH$_3$)$_2$), 3.41 (t, 2**H**, J_{H-H} =6 Hz, 2C**H**$_2$- CI), 3.67 (t, 2**H**, J_{H-H} = 5.8 Hz, 2C**H**$_2$- NH) 7.13-7.18 (m, 3**H**, 3C**H**$_{Ar}$), 7.9 (t, J_{H-H}=5,6 *Hz*, 1**H**, N**H**) **ppm**.

^{13}C NMR (100 MHz, $CDCl_3$): δ 23.1 (**C**H), 26.7 (4**C**H$_3$), 42.4 (**C**H$_2$-Cl), 43.5 (**C**H$_2$-N), 123.6 (**C**H-Ar), 125.9 (**C**H-Ar), 140.9 (**C**-Ar), 145.3 (**C**=O), 154.8 (**C**-O-CO) ppm.

Naphthalen(2-chloroethyl) carbamate

$C_{13}H_{12}ClNO_2$

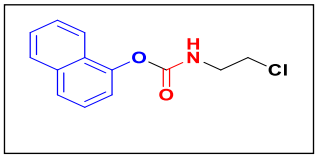

M = 249.05 **g/mol**

Aspect : White powder

M.p = 120-122 °C

R_f =0.58 **(DCM/ Petroleum ether: 8/2)**

Yield = 89%

IR (cm^{-1}): 3327 **(NH)**, 1718 **(C=O)**.

^{1}H NMR (400 MHz, $CDCl_3$): δ 3.43 (t, J_{H-H} =6.4 Hz ,2**H**, C**H**$_2$-Cl), 3.72-3.68 (q, J_{H-H} = 5.2 Hz, 2H, C**H**$_2$-NH), 7.46-7.54 (m, 2**H**, 2C**H**$_{Ar}$), 7.20 (s,1H, 1C**H**$_{Ar}$), 7.88-7.93 (m,3**H**, 3C**H**$_{Ar}$), 8.00 (t, J_{H-H} = 5.6 Hz, 1**H**, N**H**) **ppm**.

^{13}C NMR (100 MHz, $CDCl_3$): δ 42.7 (**C**H$_2$-Cl), 43.4 (**C**H$_2$-N), 118.3 (**C**H-Ar), 121.9 (**C**H-Ar), 125.6 (**C**H-Ar), 126.7 (**C**H-Ar), 127.5 (**C**H-Ar), 127.7 (CH-Ar), 130.8 (**C**-Ar), 133.6 (**C**-Ar), 148.8 (**C**=O), 154.7 (**C**-O-CO) ppm.

4-acetylphenyl (2-chloroethyl) carbamate

$C_{11}H_{12}ClNO_3$

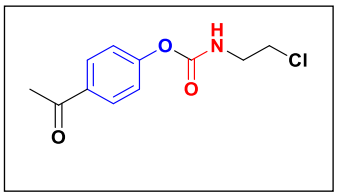

M = 241.05 **g/mol**

Aspect : White powder

M.p = 131-133 °C

R_f =0.58 **(DCM/ Petroleum ether: 8/2)**

Yield = 95%

IR (cm^{-1}): 3326 **(NH)**, 1714 **(C=O)**.

^{1}H NMR (400 MHz, $CDCl_3$): δ 2.57 (**s**, 3**H,** C**H**$_3$), 3.40-3.43 (q, J_{H-H} = 6.0 Hz, 2H, C**H**$_2$-NH), 3.69 (t, J_{H-H} =6.1 Hz, 2**H**, C**H**$_2$-Cl), 7.25-7.28 (m, 2**H**, 2C**H**$_{Ar}$), 7.97-8.00 (m, 2H, 2C**H**$_{Ar}$), 8.20 (t, J_{H-H} = 5.8 Hz 1H, N**H**) **ppm**.

^{13}C NMR (100 MHz, $CDCl_3$): δ 27.2 (**C**H$_3$), 43.6 (**C**H$_2$-Cl), 46.2 (**C**H$_2$-N), 122.5 (2**C**H-Ar), 130.2 (2**C**H-Ar), 131.1 (**C**=C), 134.1 (**C**-Ar), 154.7 (**C**-O-CO), 170.4 (**C**=O), 197.2 (**C**=O) ppm.

4-propionylphenyl (2-chloroethyl) carbamate

$C_{12}H_{14}ClNO_3$

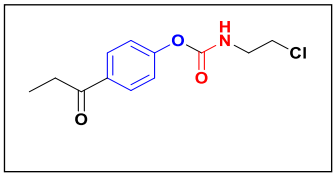

M = 255.01 **g/mol**

Aspect: White powder

M.p = 132 -134 °C

R_f =0.52 **(DCM/ Petroleum ether: 8/2)**

Yield = 92%

IR (cm^{-1}): 3326 **(NH)**, 1714 **(C=O)**.

^{1}H NMR (600 MHz, DMSO-*d6*): ***δ*** 1.07 (t, 3**H,** *J* = 7.2 Hz, C**H**$_3$), 3.05-3.02 (q, J_{H-H} = 7.2 Hz, 2H, C**H**$_2$), 3.43-3.39 (q, J_{H-H} = 7.2 Hz, 2H, C**H**$_2$), 3.69 (t, 2**H**, J_{H-H} =6.1 Hz, CH_2- Cl), 7.27-7.24 (m, 2H, 2C**H**), 8.00-7.98 (m, 2H, 2C**H**), 8.20 (t, 2**H**, J_{H-H} = 6 Hz, N**H**) **ppm**.

^{13}C NMR (151 MHz, DMSO-*d6*): ***δ*** 8.1 (**C**H_3), 31.1 (**C**H_2-CH_3), 42.5 (**C**H_2-Cl), 43.3 (**C**H_2-N), 121.6 (2**C**H-Ar), 129.4 (2**C**H-Ar),153.8 (2**C**-Ar), 154.5 (**C**=O), 169.8 (**C**-O-CO), 199.3 (**C**=O) ppm.

2-phenylchroman-4-yl (2-chloroethyl) carbamate

$C_{18}H_{18}ClNO_3$

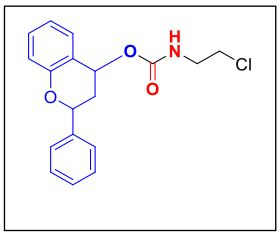

M = 331.10 **g/mol**

Aspect: White powder

M.p = 127-129°C

R_f =0.57 **(DCM/ Petroleum ether: 8/2)**

Yield = 89%

IR (cm^{-1}): 3327 **(NH)**, 1687 **(C=O)**.

^{1}H NMR (600 MHz, DMSO-*d6*): ***δ*** 2.04-2.10 (q, J_{H-H} =11.8 Hz ,1**H**, C**H**), 3.36-3.39 (q, J_{H-H} = 6.1 Hz , 2**H**, C**H**), 3.57 (t, $\boldsymbol{J_{H-H}}$ = 6.2 Hz ,1**H**, C**H**), 3.66 (dt, $\boldsymbol{J_{H-H}}$ =*J* = 7.3, 3.7 Hz, 2**H**, C**H**$_2$), 5.36 (d, J_{H-H} =11.8 Hz, 1**H**, C**H**), 6.09-6.12 (dd, J_{H-H} = 10.6, 6.5 Hz, 1**H**, C**H**), 6.86 (d, J_{H-H} =8 Hz, 1**H**, 1C**H**$_{Ar}$), 6.95 (t, J_{H-H} = 7.56 Hz, 1**H**, C**H**$_{Ar}$), 7.20-7.22 (m, 2**H**, 2C**H**$_{Ar}$), 7.36 (t, J_{H-H} =7.4 Hz, 1**H**, 1C**H**$_{Ar}$), 7.41 (t, J_{H-H} =7.5 Hz, 2**H**, 2C**H**$_{Ar}$), 7.49 (d, J_{H-H} = 7.8 Hz, 2**H**, 2C**H**$_{Ar}$), 8.00 (t, J_{H-H} =6 Hz, 1**H**, N**H**) **ppm**.

^{13}C NMR (151 MHz, DMSO-*d6*): *δ* 35.6 (**C**H_2), 41.4 (**C**H_2-Cl), 39.6 (**C**H_2-N), 42.4 (**C**H_2), 43.3 (**C**H), 75.9 (**C**H), 116.4 (**C**H_{Ar}), 120.5 (**C**H_{Ar}), 122.5 (**C**H_{Ar}), 126.2 (**C**H_{Ar}), 127.0 (**C**H_{Ar}), 128.1 (**C**H_{Ar}), 128.4 (**C**H_{Ar}), 129.0 (**C**H_{Ar}), 154.7 (**C**=O), 156.3 (**C**-O-CO) ppm.

2,6-di-*tert*-butyl-4-methylphenyl (2-chloroethyl)carbamate

$C_{18}H_{28}ClNO_2$

M = 325.18 **g/mol**

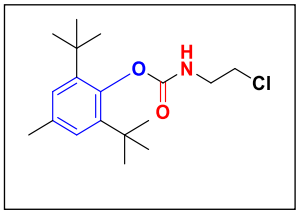

Aspect: White powder

M.p = 136-138°C

R_f =0.5 **(DCM/ Petroleum ether: 8/2)**

Yield = 91%

IR (cm^{-1}): 3320 **(NH)**, 1718 **(C=O)**.

^{1}H NMR (600 MHz, DMSO-*d6*): *δ* 1.28 (s, 18**H**, 6C**H**$_3$), 2.26 (s, 3**H**, 1C**H**$_3$), 3.36-3.39 (q, J_{H-H} =6 Hz, 2**H**, CH_2-N), 3.63 (t, ***J*$_{H-H}$** =6 Hz, 2**H**, CH_2-Cl), 7.10 (s, 1H, 1C**H**$_{Ar}$), 8.10 (s, J_{H-H} =5.8 Hz, 1H, N**H**) **ppm**.

^{13}C NMR (151 MHz, DMSO-*d6*): *δ* 21.0 (**C**H_3), 31.1 (6**C**H_3), 34.9 (**C**H), 42.5 (**C**H_2Cl), 43.1 (**C**H_2N), 42.4 (**C**H_2), 43.3 (**C**H), 126.2 (2**C**H_{Ar}), 133.2 (**C**$_{Ar}$), 142.4 (**C**$_{Ar}$), 145.9 (**C**-O-CO), 155.5 (**C**=O) **ppm.**

6. Preparation of 2-chloroethyl (nitroso)carbamates derivatives

6.1. General procedure

The synthesis was performed in a **25 mL** reaction vessel, where one equivalent of alkyl 2-chloroethyl carbamate was dissolved in **2.5 mL** of dry dichloromethane, followed by the addition of formic acid **(10 eq).** Sodium nitrite **(10 eq)** was then added gradually in small portions at **30 second** intervals, maintaining the temperature strictly at **0 °C**. The reaction mixture was stirred for 2 hours, with the internal temperature maintained between **-10** to **0 °C**. Progress of the transformation was followed by thin-layer chromatography **(TLC)** on silica gel plates using a mixture of dichloromethane and petroleum ether **(9:1)** as the developing solvent. Once the conversion was complete, the reaction mixture was evaporated under reduced pressure. The crude product was then subjected to column chromatography using a dichloromethane/petroleum ether **(8:2)** system to afford the purified compound. This synthetic approach was employed for the preparation and isolation of all target derivatives.

6.2. Physicochemical properties

Phenyl (2-chloroethyl)(nitroso) carbamate

$C_9H_9ClN_2O_3$

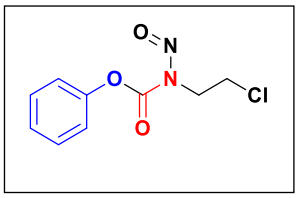

M = 228.03 **g/mol**

Aspect: Yellow oil

R_f =0.74 **(DCM/ Petroleum ether: 8/2)**

Yield = 43%

IR (cm^{-1}): 1707 **(C=O)**, 1537 **(N=O)**.

^{1}H NMR (400 MHz, DMSO-d_6): δ 3.71 (t, J_{H-H} =6.3 Hz ,2**H**, C**H**$_2$-N), 4.16 (t, J_{H-H} =6.3Hz, 2**H**, C**H**$_2$-Cl), 7.40 (m, J_{H-H} =6.8 Hz, 2**H**, 2C**H**$_{Ar}$), 7.53 (m, J_{H-H} =7.5 Hz, 2**H**, 2C**H**$_{Ar}$) **ppm**.

^{13}C NMR (100 MHz, DMSO-d_6): δ 42.5 (**C**H$_2$-Cl), 43.3 (**C**H$_2$-N), 121.5 (2**C**H-Ar), 126.7 (2**C**H-Ar), 129.8 (**C**H-Ar), 150.1 (**C**-O-CO), 151.9 (**C**=O) ppm.

4-bromophenyl (2-chloroethyl) (nitroso) carbamate

$C_9H_9BrClN_2O_3$

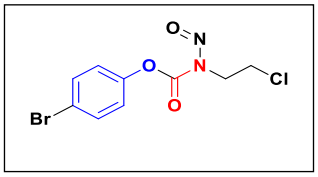

M = 305.94 **g/mol**

Aspect : Yellow oil

R_f =0.65 **(DCM/ Petroleum ether : 8/2)**

Yield = 32%

IR (cm^{-1}): 1703 **(C=O),** 1564 **(N=O)**.

^{1}H NMR (400 MHz, DMSO-d_6): δ 3.40 (t, J_{H-H} =6.3 Hz, 2**H**, C**H**$_2$-N), 3.67 (t, J_{H-H} =6.3 Hz, 2**H**, C**H**$_2$-Cl), 7.10 (d, J_{H-H} =8 Hz, 1**H**, C**H**$_{Ar}$), 7.56 (d, J_{H-H} =7.9 Hz, 2**H**, 2C**H**$_{Ar}$), 8.08 (s, 1**H**, N**H**) **ppm**.

^{13}C NMR (100 MHz, DMSO-d_6): δ 40.1 (**C**H$_2$-Cl), 41.9 (**C**H$_2$-N), 123.9 (2**C**H-Ar), 132.7 (2**C**H-Ar), 149.4 (**C**-Br), 151.7 (**C**-O-CO), 156.7 (**C**=O) ppm.

4-fluorophenyl (2-chloroethyl) (nitroso) carbamate

$C_9H_{10}ClFN_2O_3$

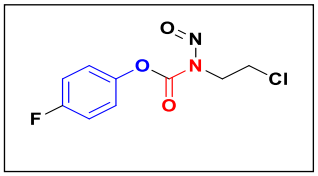

M = 246.02 **g/mol**

Aspect: Yellow oil

R_f =0.7 **(DCM/ Petroleum ether: 8/2)**

Yield = 35%

IR (cm^{-1}): 1722 **(C=O)**, 1567 **(N=O)**.

^{1}H NMR (400 MHz, DMSO-*d*$_6$): ***δ*** 3.96 (t, J_{H-H} =6.3 Hz, 2**H**, C**H**$_2$-N), 4.15 (t, J_{H-H} =6.3Hz, 2**H**, C**H**$_2$-Cl), 7.40 (m, 2**H**, C**H**$_{Ar}$), 7.56 (m, 2**H**, C**H**$_{Ar}$) **ppm**.

^{13}C NMR (100 MHz, DMSO-*d6*): ***δ*** 39.9 (**C**H$_2$-Cl), 41.9 (**C**H$_2$-N), 116.5 (2**C**H-Ar), 123.5 (2**C**H-Ar), 152.0 (**C**-F), 159.1 (**C**=O), 161.0 (**C**-O-CO) ppm.

4-methoxyphenyl (2-chloroethyl) (nitroso) carbamate

$C_{10}H_{11}Cl\ N_2O_4$

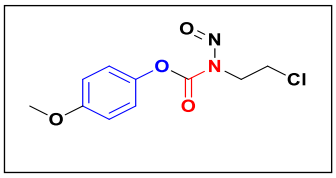

M = 258.04 **g/mol**

Aspect: Yellow oil

R_f =0.4 **(DCM/ Petroleum ether: 8/2)**

Yield = 90%

IR (cm^{-1}): 1703 **(C=O) ,** 1545 **(N=O)**.

^{1}H NMR (400 MHz, DMSO-*d*$_6$): ***δ*** 3.38 (q, J_{H-H} =6.0 Hz ,2**H**, C**H**$_2$-N), 3.66 (t, J_{H-H} =6.1Hz ,2**H**, C**H**$_2$-Cl), 3.74 (s, 3**H**, OC**H**$_3$), 6.90-7.03 (m, J_{H-H} =8 Hz, 4**H**, C**H**$_{Ar}$), 7.91 (t, J_{H-H}=5,7 *Hz*,1**H**, N**H**) **ppm**.

^{13}C NMR (100 MHz, DMSO-*d6*): ***δ*** 42.5 (**C**H$_2$-Cl), 43.3(**C**H$_2$-N), 55.3 (O-**C**H$_3$), 114.2 (2**C**H-Ar), 122.5 (2**C**H-Ar), 144.3 (**C**=O), 154.8 (**C**-O-CO), 156.3 (**C**-OCH$_3$) ppm.

2,6-diisopropylphenyl (2-chloroethyl) (nitroso) carbamate

$C_{15}H_{21}ClN_2O_3$

M = 312.12 **g/mol**

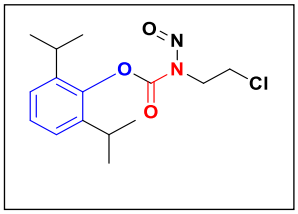

Aspect: Yellow oil

R_f =0.72 **(DCM/ Petroleum ether: 8/2)**

Yield = 40**%**

IR (cm^{-1}): 1738 **(C=O)**, 1531 **(N=O)**.

^{1}H NMR (400 MHz, DMSO-d_6): δ 1.17 (d, J_{H-H}= 6.8 *Hz*, **12H, 4(**C**H**$_3$$)_2$-CH), 3.07 (s**p**, J_{H-H} =6.8 Hz, 2**H**, 2C**H**-$(CH_3)_2$), 3.75 (t, 2**H**, J_{H-H} =5.8 Hz, 2C**H**$_2$-Cl), 4.21 (t, 2**H**, J_{H-H} = 5.8 Hz, 2C**H**$_2$-N), 7.29-7.35 (m, 3**H**, 3C**H**) ppm.

^{13}C NMR (151 MHz, DMSO-d_6): δ: 23.0 (4**C**H_3), 42.6 (**C**H_2-Cl), 43.7 (**C**H_2-N), 124.5 (2**C**H-Ar), 1**C**H-Ar (126.0), 2**C**-Ar (145.4), **C**=O (152.3), **C**-O-CO (154.9) ppm.

Naphthalen(2-chloroethyl) (nitroso) carbamate

$C_{13}H_{11}ClN_2O_2$

M = 278.05 **g/mol**

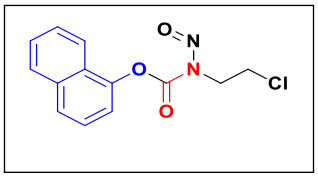

Aspect: Yellow oil

R_f =0.72 **(DCM/ Petroleum ether: 8/2)**

Yield = 49%

IR (cm^{-1}): 1712 **(C=O)**, 1530 **(N=O)**.

^{1}H NMR (600 MHz, DMSO-d_6): δ 3.74 (t, J_{H-H} =6.4 Hz, 2**H**, C**H**$_2$-Cl), 4.20 (t, J_{H-H} = 6 Hz, 2**H**, C**H**$_2$-NH), 7.62-7.57 (m, 3**H**, 3C**H**$_{Ar}$), 7.97-8.03 (m, 3**H**, 3C**H**$_{Ar}$), 8.08 (*d*, 1**H**, J_{H-H} =6 Hz, C**H**$_{Ar}$) **ppm**.

^{13}C NMR (151 MHz, DMSO- d_6): δ 42.7 (**C**H_2-Cl), 43.4 (**C**H_2-N), 118.6 (**C**H-Ar), 120.9 (**C**H-Ar), 126.3 (**C**H-Ar), 127.0 (**C**H-Ar), 127.8 (**C**H-Ar), 129.8 (**C**H-Ar), 133.2 (**C**-Ar), 147.7 (**C**-Ar), 152.2 (**C**=O), 169.9 (**C**-O-CO) ppm.

4-acetylphenyl (2-chloroethyl) (nitroso) carbamate

$C_{11}H_{12}ClN_2O_4$

M = 270.04 **g/mol**

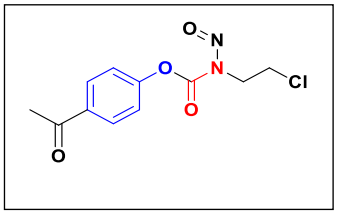

Aspect : Yellow oil

R_f =0.73 **(DCM/ Petroleum ether: 8/2)**

Yield = 95%

IR (cm^{-1}): 1605 **(C=O)**, 1727 **(C=O)**, 1536 **(N=O)**.

^{1}H NMR (600 MHz, DMSO-d_6): δ 2.57 (**s**, 3**H,** C**H**$_3$), 3.75 (t, J_{H-H} = 6.0 Hz, 2**H**, C**H**$_2$-NH), 4.20 (t, J_{H-H} =6.1 Hz, 2**H**, C**H**$_2$-Cl), 7.55-7.60 (m, 2**H**, 2C**H**$_{Ar}$), 8.01-8.05 (m, 2**H**, 2C**H**$_{Ar}$) **ppm**.

^{13}C NMR (151 MHz, DMSO-d_6): δ 27.3 (**C**H$_3$), 43.7 (**C**H$_2$-Cl), 46.3 (**C**H$_2$-N), 126.0 (2**C**H-Ar), 127.9 (2**C**H-Ar), 131.2 (**C**=C), 134.3 (**C**-Ar), 155.1 (**C**-O-CO), 170.3 (**C**=O), 197.3 (**C**=O)

ppm.

4-propionylphenyl (2-chloroethyl) (nitroso) carbamate

$C_{12}H_{13}ClNO_4$

M = 284.06 **g/mol**

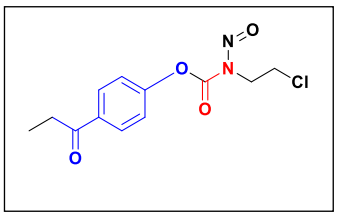

Aspect: Yellow oil

R_f =0.72 (DCM/ Petroleum ether: 8/2)

Yield = 40%

IR (cm^{-1}):1602 **(C=O)**, 1728 **(C=O)**, 1536 **(N=O)**.

^{1}H NMR (400 MHz, DMSO-$_{d6}$): δ 1.08 (t, 3**H,** J = 7.2 Hz, C**H**$_3$), 3.05-3.02 (q, J_{H-H} = 7.2 Hz, 2**H**, C**H**$_2$), 3.39-3.43 (q, J_{H-H} = 7.2 Hz, 2**H**, C**H**$_2$),3.69 (t, 2**H**, J_{H-H} =6.1 Hz, C**H**$_2$- CI), 7.24-7.27 (m, 2**H**, 2C**H**), 7.98-8.00 (m, 2**H**, 2C**H**) **ppm**.

^{13}C NMR (151 MHz, DMSO-d_6): δ 8.1 (**C**H$_3$), 31.1 (**C**H$_2$-CH$_3$), 42.5 (**C**H$_2$-Cl), 43.3 (**C**H$_2$-N), 121.5 (2**C**H-Ar), 129.4 (2**C**H-Ar),133.6 (2**C**-Ar), 153.8 (**C**=O), 154.6 (**C**-O-CO), 199.3 (**C**=O) ppm.

2-phenylchroman-4-yl (2-chloroethyl) (nitroso) carbamate

$C_{18}H_{18}ClNO_3$

M = 331.10 **g/mol**

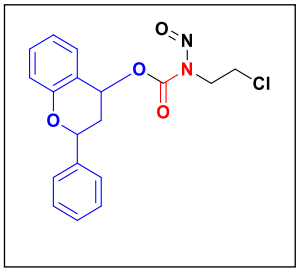

Aspect: Yellow oïl

R_f =0.7 **(DCM/ Petroleum ether: 8/2)**

Yield = 89%

IR (cm^{-1}): 1728 **(C=O)**, 1537 **(N=O)**.

^{1}H NMR (400 MHz, DMSO-d_6): δ 3.65-3.58 (m, 2**H**, 2C**H**$_2$), 4.56 (td, J_{H-H} = 10.9, 4.4 Hz, 2**H**), 4.63 (t, J_{H-H} = 3.1 Hz, 1**H**, C**H**) , 5.26-5.14 (m, 1H,C**H**) , 7.03-6.90 (m, 1**H,** C**H**), 6.85 (dd, J_{H-H} = 8.3, 1.2 Hz, 1**H,** C**H**), 7.23-7.16 (m, 1**H,** C**H**), 7.32 (dd, J_{H-H} = 7.6, 1.7 Hz, 1**H**, C**H**), 7.39-7.34 (m, 1**H**, C**H**), 7.50 (hept, J_{H-H} = 4.1 Hz, 2**H,** 2C**H**) **ppm**.

^{13}C NMR (151 MHz, DMSO-d_6): δ 38.7 (CH2), 40.0 (CH2-Cl), 47.0 (CH2-N), 61.3 (CH-O), 73.0 (CH-Ph), 116.7 **(**C**H$_{Ar}$)**, 128.8 (**2**C**H$_{Ar}$), 127.9 (**2**C**H$_{Ar}$), 126.2 (C**H$_{Ar}$), 128.8 (C**H$_{Ar}$), 129.6 (**2**C**H$_{Ar}$),**130.7** (C**H$_{Ar}$), **141.1** (C$_{Ar}$), 153.7 (C-O-**CO)**, 170.3 (C=O) **ppm**.

2,6-di-*tert*-butyl-4-methylphenyl (2-chloroethyl) (nitroso)carbamate

$C_{18}H_{28}ClN_2O_5$

M = 373.10 **g/mol**

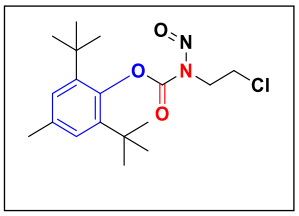

Aspect : Yellow oïl

R_f =0.73 **(DCM/ Petroleum ether: 8/2)**

Yield = 39%

IR (cm^{-1}): 1730 **(C=O)**, 1534 **(N=O)**.

^{1}H NMR (600 MHz, DMSO-d_6): δ 1.28 (s, 18**H**, 6C**H**$_3$), 2.25 (s, 3**H**, 1C**H**$_3$), 3.76 (t, J_{H-H} =6.3 Hz, 2**H**, C**H**$_2$-N), 4.10 (t, J_{H-H} =6.3Hz, 2**H**, C**H**$_2$-Cl),7.04 (s, 2**H**, 2C**H**$_{Ar}$) ppm.

^{13}C NMR (151 MHz, DMSO-d_6): δ 21.5 (C**H**$_3$), 31.6 (6C**H**$_3$), 35.4 (C**H**), 43.2 (C**H**$_2$-Cl), 48.7 (C**H**$_2$-N), 126.7 (2C**H**$_{Ar}$), 133.7 (C$_{Ar}$), 146.4 (C$_{Ar}$), 153.4 (C-O-CO), 156.0 (C=O) ppm.

7. Preparation of diethoxy phosphoryl (alkyl)methyl(2-chloroethyl) carbamate derivatives

7.1. General procedure

In a **100 mL** round-bottom flask, 1 eq **(500 mg, 2.05 mmol)** of α-hydroxyphosphonate was dissolved in **10 mL** of anhydrous dichloromethane **(DCM)**. The reaction mixture was cooled to **0°C** using an ice bath, followed by the slow, dropwise addition of 1.1 eq **(313 µL, 2.25 mmol)** of triethylamine **(TEA)**. The resulting solution was stirred under an inert atmosphere for 30 min to ensure thorough mixing before the gradual addition of 1.2 eq **(200 µL, 2.46 mmol)** of 2-chloroethyl isocyanate via a dropping funnel over a two-hour period. The reaction was periodically monitored by thin-layer chromatography (TLC), indicating the formation of a new product, less polar product compared to α-hydroxyphosphonate, detected using ninhydrin staining.

7.2. Work-up

Upon completion of the **2h** reaction period, the mixture was diluted with dichloromethane **(DCM)** and subjected to successive washes with **0.1 N** hydrochloric acid until the aqueous layer exhibited an acidic pH. This was followed by washing with distilled water until neutrality was achieved. The organic phase was then dried over anhydrous sodium sulfate. Concentration of the solution under reduced pressure afforded the crude product, which was purified by recrystallization from a diethyl ether/hexane solvent mixture, yielding the target ((diethoxyphosphoryl)(alkyl)methyl(2-chloroethyl)) carbamate.

7.3. Physicochemical properties

(diethoxyphosphoryl)(phenyl)methyl (2-chloroethyl) carbamate

$C_{14}H_{21}ClNO_5P$

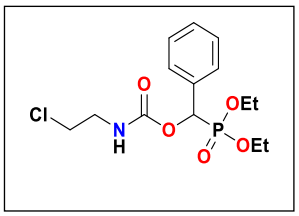

M = **349.75 g/mol**

Aspect: White powder

M.p = 60-62 °C

R_f =0.86 **(DCM/MeOH : 94/6)**

Yield = 80%

IR (cm^{-1}): 3342 **(NH)**, 1735 **(C=O)**, 1225 **(P=O)**, 1075 **(P-O).**

MS (ESI^+) : m/z = 372.1 $[M+Na]^+$.

^{1}H NMR (400 MHz, $CDCl_3$) : δ 1.17 (t, J_{H-H} = 7.2Hz, 3**H**, C**H**$_3$), 1.29 (t, J_{H-H} = 6.6Hz, 3**H**, C**H**$_3$), 3.50-3.65 (m, 4**H**, 2C**H**$_2$Cl), 3.81-3.95 (m, 1**H**, CH_2C**H**$_3$), 4.00-4.12 (m, 3**H**, CH_2C**H**$_3$), 5.48 (brs, 1**H**, N**H**), 6.10 (d,J_{H-P} = 14.1Hz, 1**H**, C**H***), 7.32-7.36 (m, 3**H**, **H**-Ar), 7.46-7.51 (m, 2H, **H**-Ar) **ppm**.

^{13}C NMR (100 MHz, $CDCl_3$): δ 42.5 (**C**H_2-Cl), 43.3 (**C**H_2-N), 121.7 (2**C**-Ar), 125.0 (**C**-Ar), 129.3 (**C**-Ar), 150.9 (**C**=O), 154.5 (**C**-O-CO) ppm.

8. Preparation of diethoxyphosphoryl (alkyl)methyl(2-chloroethyl) (nitroso)carbamate derivatives

8.1. General procedure

In a **25 mL** round-bottom flask, equimolar amounts **(200 mg, 0.57 mmol)** of (diethoxyphosphoryl)(phenyl)methyl(2-chloroethyl) were dissolved in **10 mL** of anhydrous dichloromethane **(DCM)** under an ice bath at **0°C**. To this stirred solution, formic acid **(HCOOH) (215.05 µL, 5.7 mmol, 10 eq)** and sodium nitrite **($NaNO_2$) (393.24 mg, 5.7 mmol, 10 eq)** were carefully added dropwise over a 2-hour period to ensure controlled reaction kinetics. The reaction's progression was regularly monitored via thin-layer chromatography **(TLC)** using a dichloromethane/methanol **(94:6)** solvent system as the mobile phase.

8.2. Work-up

The reaction mixture was subsequently diluted by slow addition into **100 mL** of chilled distilled water. Following this, the pH was carefully adjusted by the gradual introduction of **20 mL** of a **5%** sodium bicarbonate solution. The resulting aqueous layer was then subjected to two consecutive extractions using dichloromethane **(DCM)**. The combined organic extracts were washed with **15 mL** of a saturated sodium chloride solution to remove residual aqueous impurities. The organic phase was then dried over anhydrous sodium sulfate, filtered to remove the drying agent, and finally concentrated under reduced pressure by rotary evaporation to afford the crude product.

8.3. Physicochemical properties

(diethoxyphosphoryl)(phenyl)methyl (2-chloroethyl) carbamate

$C_5H_9Cl_2NO_2$

M = 185.00 **g/mol**

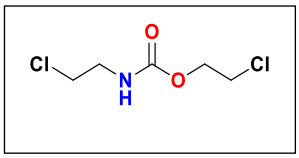

Aspect: Yellow oil

R_f =0.86 **(DCM/MeOH: 94/6)**

Yield = 80%

IR (cm^{-1}): 3292 **(NH)**, 1735 **(C=O)**,

^{1}H NMR (600 MHz, DMSO-d_6): δ 3.60-3.64 (m, 4**H**, 2C**H**$_2$Cl), 3.76 (t, J_{H-H} =6.51Hz, 2**H**, C**H**$_2$), 4.10 (t, J_{H-H} =6.5 Hz, 2**H**, C**H**$_2$), 8.92 (t, J_{H-H} =6.0 Hz, 1**H**, N**H**) **ppm**.

^{13}C NMR (151 MHz, DMSO-d_6): δ 42.6 (2**C**H$_2$Cl), 43.2 (2**C**H$_2$), 153.4 (**C**=O) **ppm.**

9. Biological evaluation methods

9.1. DPPH radical scavenging assay

The antioxidant capacity of the synthesized compounds was investigated using the DPPH (2,2-diphenyl-1-picrylhydrazyl) free radical scavenging assay, following the methodology adapted from by Benzaid et *al*. **[242]** . A stock solution of **DPPH** at **0.1 mM** was freshly prepared by dissolving 4 mg of the radical in **100** mL of methanol, and the solution was kept protected from light. For the assay, **200** µL of each test compound, prepared at different concentrations, was combined with **800** µL of the DPPH solution in clean glass tubes. Ascorbic acid, prepared under identical conditions, served as a reference antioxidant, while the negative control consisted of solvent mixed with DPPH solution. All reaction mixtures were incubated in the dark at room temperature for **30 min**. Absorbance was then recorded at **517 nm** using a UV–Vis spectrophotometer, with methanol used as the blank. Each experiment was performed in triplicate to ensure reproducibility. The percentage inhibition of the DPPH radical was calculated using the following equation:

%= [(OD Negative Control - OD Sample) /OD Negative Control)] x 100

IC_{50} values, indicating the concentration required to inhibit 50% of the DPPH radicals, were determined from the dose-response curves generated from the inhibition percentages.

9.2. Antimicrobial activity evaluation

The antimicrobial potential of the synthesized compounds was evaluated using the agar well diffusion technique, following a modified protocol based on the method described by Toty et *al*. **[243]** The assay was carried out against a representative panel of microbial strains, comprising two Gram-negative bacteria (*Klebsiella pneumoniae* and *Pseudomonas aeruginosa*), two Gram-positive bacteria (*Staphylococcus aureus* and *Staphylococcus epidermidis*), as well as two yeast species (*Candida albicans* and *Candida tropicalis*). Microbial suspensions were adjusted to an optical density **(OD)** between 0.08 and 0.1 at 600 nm to ensure standard inoculum concentration. The tested compounds were prepared in dimethyl sulfoxide **(DMSO)** at a final concentration of 4 mg/mL. DMSO alone was used as a negative control, while amoxicillin-clavulanic acid **(AMC30)** and amikacin **(AK10)** were used as reference antibacterial agents, and amphotericin **B (AM-B)** served as the positive control for antifungal activity. Following incubation **24** hours at **37 °C** for bacterial strains and 48 hours for yeasts the antimicrobial efficacy was determined by measuring the diameter of the inhibition zones (DIZ) surrounding each well.

9.2.1. Determination of Minimum Inhibitory Concentrations (MICs)

Minimum inhibitory concentrations (MICs) were assessed in accordance with the methodology reported by Toty et *al*.**[243]**, starting from an initial concentration of 4 mg/mL. A serial dilution series was prepared using the following dilution factors: 1/2, 1/4, 1/8, 1/16, 1/32, 1/64, 1/128, and 1/256.

Each tube corresponding to a dilution level was inoculated with 1 mL of the microbial suspension and 1 mL of the compound solution. The tubes were incubated under the same conditions described above.

The minimum inhibitory concentration **(MIC)** was determined as the lowest concentration of the tested compound that completely inhibited visible microbial growth under macroscopic observation. Standard antibiotics and antifungal agents, known to be effective against the tested strains, were employed as positive controls.

9.2.2. Biofilm formation inhibition

The antibiofilm potential of the synthesized compounds was assessed through the crystal violet (CV) staining assay, performed in 96-well microtiter plates. The experiments were conducted at concentrations equivalent to the previously established minimum inhibitory

concentrations (MICs), allowing for the quantification of biofilm biomass in response to treatment. **[244],[245]**.

After the incubation period, biofilm structures were stained with crystal violet, followed by careful washing of the wells to remove excess dye. The retained stain, indicative of biofilm biomass, was quantified by measuring absorbance at 570 nm using a microplate reader. The extent of biofilm inhibition was expressed as a percentage, calculated according to the following formula.:

% = [(OD of the negative control − OD of the test) / OD of the negative control] × 100

10. *In silico* methods

10.1. Molecular docking studies

The X-ray crystal structures of 4-amino-furo[2,3-d]pyrimidine bound to VEGFR-2 (**PDB:** 1YWN) **[224]**, xanthine oxidase with hypoxanthine (**PDB:**3NRZ) [236] and dihydropteroate synthase with a sulfonamide drug **(DHPS)** (**PDB**:3TZF) **[235]** . were retrieved from the RCSB Protein Data Bank. Protein structures were prepared using the Protein Preparation Wizard module in the Schrödinger Suite. The three-dimensional structures of the synthesized derivatives were built using Maestro and subsequently optimized with LigPrep, applying the OPLS3e force field.**[246]** The finalized PDB files of both protein targets and ligands were then utilized for molecular docking simulations. Docking experiments were performed with Glide software in standard precision mode.**[247]** The resulting ligand–protein complexes, particularly those involving VEGFR-2, were analyzed and visualized using Chimera X. **[229]**

10.2. DFT study

Quantum chemical studies were conducted using the **Gaussian 09** suite of programs. **[248]** . The molecular geometries of the synthesized compounds were optimized in the gas phase employing Density Functional Theory **(DFT)** at the **B3LYP** level with the **6-31G(d,p)** basis set. Initial three-dimensional structures were constructed using **ChemDraw 3D**, converted into MDL Mol format, and then visualized with **GaussView 06** prior to optimization. Furthermore, calculations of Frontier Molecular Orbitals **(FMOs)**, namely the Highest Occupied Molecular Orbital **(HOMO)** and the Lowest Unoccupied Molecular Orbital **(LUMO)**, were performed to estimate the HOMO–LUMO energy gap and to derive global reactivity parameters..**[249]** All quantum chemical calculations were consistently carried out at the **DFT/B3LYP/6-31G(d,p**) level.

Conclusion

In light of the limited efficacy of current therapies and the increasing complexity of diseases, the development of new biologically active compounds has become a pressing scientific priority. This thesis contributes to this effort by proposing innovative, rational, and efficient synthetic strategies to access pharmacologically significant molecular frameworks.

Emphasis was placed on heterocycles due to their pivotal role in medicinal chemistry. The first chapter presented a critical overview of synthetic approaches, focusing on oxygen-containing and oxygen–phosphorus heterocycles as promising scaffolds for new bioactive entities. This theoretical groundwork underpinned a structure-activity relationship (*SAR*)-based design, explored in the second chapter, targeting carbonyl analogues of carmustine. Pharmacophoric modifications, particularly through the introduction of carbamate moieties, were proposed to enhance the therapeutic profile of nitrosoureas while mitigating their associated toxicity.

From a methodological perspective, the third chapter detailed the development of heterocyclic compounds using efficient and environmentally sustainable synthetic strategies. Specifically, twenty oxygenated xanthene derivatives were synthesized using zinc acetate under an ultrasound-assisted protocol, highlighting the advantages of this technique in terms of reduced reaction time and improved yield. Concurrently, seven O,P-hybrid 1,2-oxaphospholane-2-oxides were obtained *via* the Phospha-Michael addition combined with microwave-assisted synthesis, demonstrating the effectiveness of microwave irradiation in promoting reaction efficiency and selectivity.

In parallel, the chapter aimed to expand on the laboratory's prior work on structural analogues of nitrosoureas. Within this framework, nine nitrosocarbamate derivatives, designed as analogues of carmustine, were successfully synthesized through a concise two-step sequence. Moreover, preliminary efforts to prepare carbamate analogues of fotemustine from hydroxyphosphonate precursors were undertaken. However, these efforts were thwarted by competing rearrangement reactions, which impeded the formation of the desired target molecules, highlighting the synthetic challenges inherent in this class of compounds.

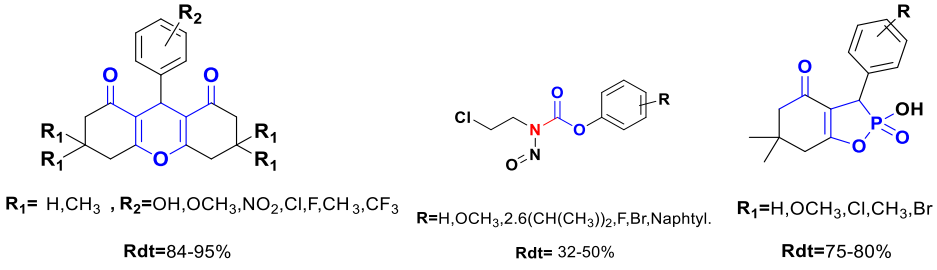

Figure VI.1. Synthesized derivatives of xanthenes, 1,2-oxaphospholanes-2-oxides and *N*-(2-chloroethyl)nitroso carbamates.

The experimental evaluation of the synthesized compounds highlighted their promising pharmacological potential. The 1,2-oxaphospholane-2-oxide derivatives exhibited notable antimicrobial activity, as well as an ability to inhibit biofilm formation. In parallel, the *N*-(2-chloroethyl)carbamate derivatives showed broad-spectrum antibacterial and antifungal activity, in some cases surpassing conventional therapeutic standards, thereby underscoring their potential as innovative anti-infective agents.

In addition, the antioxidant evaluation revealed variability among the compounds: while some 1,2-oxaphospholane-2-oxide derivatives showed modest activity, the *N*-(2-chloroethyl) carbamate derivatives demonstrated stronger antioxidant potential, with some matching the efficacy of standard references like ascorbic acid.

Although this work has yielded promising results, the subject remains only partially explored, revealing several research avenues that deserve further investigation. In this context, and in light of the data obtained, it would be appropriate to consider continuing these studies along the following lines:

- ✓ The synthesis of new 1,2-oxaphospholane-2-oxide derivatives by exploring various structural modifications of aldehydes.
- ✓ In light of literature data highlighting the therapeutic potential of nitrosoureas in the treatment of various cancer pathologies, it would be particularly relevant to consider evaluating the anticancer activity of the synthesized compounds from the *N*-(2-chloroethyl) nitroso-carbamate series.
- ✓ The series of nitroso-carbamate derivatives could undergo in-depth theoretical investigations, including density functional theory (DFT) calculations, molecular docking studies, and ADME property predictions. Molecular dynamics simulations, particularly for the most active compounds, could further complement these approaches by providing deeper insights into their atomic-level interactions and pharmacological potential.
- ✓ A rigorous optimization of the reaction conditions for the synthesis of fotemustine carbamate analogues would be required in order to improve the selectivity and yield of the synthetic processes.
- ✓ After a molecular docking study on carbamate derivatives analogous of carmustine, based on aliphatic alcohols, high docking scores were obtained compared to previously synthesized compounds. In this perspective, expanding this series by exploring additional aliphatic alcohols would be a promising approach to enhance the pharmacological potential of these analogues.

References

References

1. Nicolaou, K., *Advancing the drug discovery and development process.* Angewandte Chemie, 2014. **126**(35): p. 9280-9292.
2. Taylor, A.P., et al., *Modern advances in heterocyclic chemistry in drug discovery.* Organic & Biomolecular Chemistry, 2016. **14**(28): p. 6611-6637.
3. Larrosa, I., P. Romea, and F. Urpí, *Synthesis of six-membered oxygenated heterocycles through carbon-oxygen bond-forming reactions.* Tetrahedron, 2008. **64**(12): p. 2683-2724.
4. Keglevich, G., *Organophosphorus Chemistry: Novel Developments*2018: De Gruyter.
5. Sheng, X.C., et al., *Discovery of novel phosphonate derivatives as hepatitis C virus NS3 protease inhibitors.* Bioorganic & Medicinal Chemistry Letters, 2009. **19**(13): p. 3453-3457.
6. Ran, X.-Y., et al., *Xanthene-based NIR organic phototheranostics agents: design strategies and biomedical applications.* Journal of Materials Chemistry B, 2025.
7. Song, Y., et al., *Synthesis and Cytotoxicity of N-Substituted Dibenzo [a, j] xanthene-3, 11-dicarboxamide Derivatives.* Molecules, 2017. **22**(4): p. 517.
8. Yunnikova, L., et al., *Synthesis and antimicrobial activity of amines with azaxanthene fragments.* Pharmaceutical Chemistry Journal, 2013. **47**: p. 139-141.
9. Kancheva, V., et al., *Antiradical and antioxidant activities of new bio-antioxidants.* Biochimie, 2012. **94**(2): p. 403-415.
10. Hafez, H., et al., *A facile regioselective synthesis of novel spiro-thioxanthene and spiro-xanthene-9', 2-[1, 3, 4] thiadiazole derivatives as potential analgesic and anti-inflammatory agents.* Bioorganic & Medicinal Chemistry Letters, 2008. **18**(16): p. 4538-4543.
11. Brewster, R., M.C. Vandergeten, and F. Montel, *Syntheses of Heteraphosphacyclanes: Follow the Guide!* European Journal of Organic Chemistry, 2014. **2014**(5): p. 905-917.
12. Ali, T.E., M.A. Ibrahim, and S.M. El-Edfawy, *Synthesis and cytotoxicity evaluation of some novel chromone annulated phosphorus heterocycles.* Phosphorus, Sulfur, and Silicon and the Related Elements, 2017. **192**(7): p. 819-826.
13. Li, Z., et al., *Nitrobenzocyclophosphamides as potential prodrugs for bioreductive activation: synthesis, stability, enzymatic reduction, and antiproliferative activity in cell culture.* Bioorganic & Medicinal Chemistry, 2003. **11**(19): p. 4171-4178.
14. Wang, Y. and J. Wang, *Modelling and prediction of global non-communicable diseases.* BMC public health, 2020. **20**: p. 1-13.
15. Tarin, D., *Causes of Cancer and Mechanisms of Carcinogenesis*, in *Understanding Cancer: The Molecular Mechanisms, Biology, Pathology and Clinical Implications of Malignant Neoplasia*, D. Tarin, Editor 2023, Springer International Publishing: Cham. p. 229-279.
16. Kaur, R., A. Bhardwaj, and S. Gupta, *Cancer treatment therapies: traditional to modern approaches to combat cancers.* Molecular Biology Reports, 2023. **50**(11): p. 9663-9676.
17. Montgomery, J.A. and T.P. Johnston, *Nitrosoureas*, in *The Chemistry of Antitumour Agents*, D.E.V. Wilman, Editor 1990, Springer Netherlands: Dordrecht. p. 131-158.
18. Lemoine, A., C. Lucas, and R. Ings, *Metabolism of the chloroethylnitrosoureas.* Xenobiotica, 1991. **21**(6): p. 775-791.
19. Alvarez-Builla, J. and J. Barluenga, *Heterocyclic compounds: An introduction.* Modern heterocyclic chemistry, 2011: p. 1-9.
20. Saini, M.S., et al., *A review: biological significances of heterocyclic compounds.* Int. J. Pharm. Sci. Res, 2013. **4**(3): p. 66-77.

References

21. Al-Mulla, A., *A review: biological importance of heterocyclic compounds.* Der Pharma Chem, 2017. **9**(13): p. 141-147.
22. Arora, P., et al., *Importance of heterocyclic chemistry: A review.* International Journal of Pharmaceutical Sciences and Research, 2012. **3**(9): p. 2947.
23. Brugnatelli, G., *V. Observations on the various changes which take place on treating uric with nitrous acid, and on a new acid callea "erythric" thence produced.* The Philosophical Magazine, 1818. **52**(243): p. 30-47.
24. Döbereiner, J., *Ueber die medicinische und chemische Anwendung und die vortheilhafte Darstellung der Ameisensäure.* Annalen der Pharmacie, 1832. **3**(2): p. 141-146.
25. Campaigne, E., *Adrien Albert and the rationalization of heterocyclic chemistry.* Journal of Chemical Education, 1986. **63**(10): p. 860.
26. Dua, R., et al., *Pharmacological significance of synthetic heterocycles scaffold: a review.* Advances in Biological Research, 2011. **5**(3): p. 120-144.
27. Chen, C.-J., et al., *Synthesis and antifungal activities of 5-(3,4,5-trimethoxyphenyl)-2-sulfonyl-1,3,4-thiadiazole and 5-(3,4,5-trimethoxyphenyl)-2-sulfonyl-1,3,4-oxadiazole derivatives.* Bioorganic & Medicinal Chemistry, 2007. **15**(12): p. 3981-3989.
28. Chandra, T., et al., *Synthesis of substituted acridinyl pyrazoline derivatives and their evaluation for anti-inflammatory activity.* European Journal of Medicinal Chemistry, 2010. **45**(5): p. 1772-1776.
29. Banday, M.R., R.H. Mattoo, and A. Rauf, *Synthesis, characterization and anti-bacterial activity of 5-(alkenyl)-2-amino-and 2-(alkenyl)-5-phenyl-1, 3, 4-oxadiazoles.* Journal of chemical sciences, 2010. **122**: p. 177-182.
30. Zarghi, A., et al., *Synthesis and anticonvulsant activity of new 2-substituted-5-(2-benzyloxyphenyl)-1,3,4-oxadiazoles.* Bioorganic & Medicinal Chemistry Letters, 2005. **15**(7): p. 1863-1865.
31. Kok, S.H.L., et al., *Synthesis and anti-cancer activity of benzothiazole containing phthalimide on human carcinoma cell lines.* Bioorganic & Medicinal Chemistry, 2008. **16**(7): p. 3626-3631.
32. Kunied, T. and H. Mutsanga, *The chemistry of heterocyclic compounds.* Palmer (B), 2002. **175**.
33. Majumdar, P., et al., *Acid Hydrazides, Potent Reagents for Synthesis of Oxygen-, Nitrogen-, and/or Sulfur-Containing Heterocyclic Rings.* Chemical Reviews, 2014. **114**(5): p. 2942-2977.
34. Eftekhari-Sis, B., M. Zirak, and A. Akbari, *Arylglyoxals in Synthesis of Heterocyclic Compounds.* Chemical Reviews, 2013. **113**(5): p. 2958-3043.
35. Paul, S., et al., *Microwave assisted synthesis of 1, 5-disubstituted hydantoins and thiohydantoins in solvent-free conditions.* Synthesis, 2002. **2002**(01): p. 0075-0078.
36. Makhova, N.N., et al., *Progress in the chemistry of nitrogen-, oxygen-and sulfur-containing heterocyclic systems.* Russian Chemical Reviews, 2020. **89**(1): p. 55.
37. Wieczorkiewicz, P.A., T.M. Krygowski, and H. Szatylowicz, *Substituent effects and electron delocalization in five-membered N-heterocycles.* Physical Chemistry Chemical Physics, 2024. **26**(28): p. 19398-19410.
38. Sunbal, et al., *Chemical insights into the synthetic chemistry of five-membered saturated heterocycles—a transition metal–catalyzed approach.* Frontiers in Chemistry, 2023. **11**: p. 1185669.
39. Aggarwal, V., et al., *Diazinon—chemistry and environmental fate: a California perspective.* Reviews of environmental contamination and toxicology Volume 223, 2013: p. 107-140.

References

40. Heeres, J., et al., *Antimycotic imidazoles. Part 4. Synthesis and antifungal activity of ketoconazole, a new potent orally active broad-spectrum antifungal agent.* Journal of Medicinal Chemistry, 1979. **22**(8): p. 1003-1005.
41. Amin, A., et al., *A review on the medicinal and industrial applications of N-containing heterocycles.* The Open Medicinal Chemistry Journal, 2022. **16**(1).
42. Katritzky, A.R., et al., *Handbook of heterocyclic chemistry*2010: Elsevier.
43. García-Valverde, M. and T. Torroba, *Sulfur-nitrogen heterocycles*, 2005, MDPI. p. 318-320.
44. Garrett, R. and C.M. Grisham, *Biochemistry*, *Cengage Learning.* Inc, Bost, 2016.
45. Davies, M.B., D.A. Partridge, and J. Austin, *Vitamin C: its chemistry and biochemistry*2007: royal society of chemistry.
46. Kaur, P., R. Arora, and N. Gill, *Review on oxygen heterocycles.* Indo American J of Pharmaceutical Research, 2013. **3**: p. 9067-9084.
47. Min, L., et al., *Strategies and Lessons Learned from Total Synthesis of Taxol.* Chemical Reviews, 2023. **123**(8): p. 4934-4971.
48. Cossy, J. and A. Guérinot, *Chapter Five - Natural Products Containing Oxygen Heterocycles—Synthetic Advances Between 1990 and 2015*, in *Advances in Heterocyclic Chemistry*, E.F.V. Scriven and C.A. Ramsden, Editors. 2016, Academic Press. p. 107-142.
49. Antus, S., et al., *Synthesis of naturally occurring o-heterocyclic compounds of biological activity.* Pure and Applied Chemistry, 2004. **76**(5): p. 1025-1032.
50. Singh, P.K. and O. Silakari, *The current status of O-heterocycles: A synthetic and medicinal overview.* ChemMedChem, 2018. **13**(11): p. 1071-1087.
51. Krygowski, T.M. and M.K. Cyranski, *Aromaticity in heterocyclic compounds*. Vol. 19. 2008: Springer.
52. Jassas, R.S., et al., *Current status of N-, O-, S-heterocycles as potential alkaline phosphatase inhibitors: a medicinal chemistry overview.* RSC Advances, 2023. **13**(24): p. 16413-16452.
53. Eicher, T., S. Hauptmann, and A. Speicher, *The chemistry of heterocycles: structures, reactions, synthesis, and applications*2013: John Wiley & Sons.
54. Nylund, K. and P. Johansson, *Heterocyclic compounds: synthesis, properties, and applications*2010: Nova Science Publishers.
55. Bellina, F., et al., *Selective synthesis of natural and unnatural 5,6-disubstituted 2(2H)-pyranones via iodolactonization of 5-substituted (Z)-2-en-4-ynoic acids.* Tetrahedron, 2001. **57**(14): p. 2857-2870.
56. Douglas, C.J., et al., *Synthesis and UV Studies of A Small Library of 6-Aryl-4-hydroxy-2-pyrones. A Relevant Structural Feature for the Inhibitory Property of Arisugacin Against Acetylcholinesterase.* Tetrahedron, 1999. **55**(48): p. 13683-13696.
57. Evidente, A., et al., *Viridepyronone, a New Antifungal 6-Substituted 2H-Pyran-2-one Produced by Trichoderma viride.* Journal of Agricultural and Food Chemistry, 2003. **51**(24): p. 6957-6960.
58. JAIN, R. and M. BANSAL, *A fascile synthesis and central nervous system activities of fluorine containing spiro-[3H-indole-3, 4'(4H)-pyran]-2 (1H)-ones.* Pharmazie, 1995. **50**(3): p. 224-225.
59. McCORD, R.S., M.K. Breinig, and P.S. Morahan, *Antiviral effect of pyran against systemic infection of mice with herpes simplex virus type 2.* Antimicrobial Agents and Chemotherapy, 1976. **10**(1): p. 28-33.

References

60. Grover, P., et al., *Current developments in the pyran-based analogues as anticancer agents.* Anti-Cancer Agents in Medicinal Chemistry-Anti-Cancer Agents), 2022. **22**(19): p. 3239-3268.
61. Almalki, F.A., *An overview of structure-based activity outcomes of pyran derivatives against Alzheimer's disease.* Saudi Pharmaceutical Journal, 2023. **31**(6): p. 998-1018.
62. Hatakeyma, S., et al., *A Concise Enantioselective Route to (-)-Kainic acid from (S)-2-(6 enzyloxymethyl) oxirane.* J. Chem. Soc. Chem. Commun, 1988. **17**: p. 1200-1202.
63. Taghartapeh, M.R., et al., *Synthesis, spectroscopic and photophysical studies of xanthene derivatives.* Journal of molecular structure, 2017. **1149**: p. 862-873.
64. Chaudhary, A. and J.M. Khurana, *Advances in the synthesis of xanthenes: an overview*. Current Organic Synthesis, 2018. **15**(3): p. 341-369.
65. Burange, A.S., et al., *Green synthesis of xanthene and acridine-based heterocycles of pharmaceutical importance: a review.* Environmental Chemistry Letters, 2021. **19**(4): p. 3283-3314.
66. Herole, R., R.K. Jat, and R.D. Dighe, *A review on acridine, xanthene and its derivatives: Synthesis, physical and pharmacological properties.* Tropical Journal of Pharmaceutical and Life Sciences, 2022. **9**(6): p. 01-12.
67. Noroozi Pesyan, N., et al., *Two Independent Intermolecular 1D-Polymeric H-Bonds between Each Enantiomer in Octahydro-1H-Xanthene-1, 8 (2H)-Diones and Bis-Xanthen Analogues: Synthesis and Crystal Structure.* Organic Chemistry Research, 2020. **6**(1): p. 100-120.
68. Shabir, G., A. Saeed, and P. Ali Channar, *A review on the recent trends in synthetic strategies and applications of xanthene dyes.* Mini-Reviews in Organic Chemistry, 2018. **15**(3): p. 166-197.
69. Naseem, S., et al., *Synthesis, structural, DFT studies, docking and antibacterial activity of a xanthene based hydrazone ligand.* Journal of molecular structure, 2017. **1143**: p. 235-244.
70. Shchekotikhin, Y.M. and T. Nikolaeva, *Transformations of sym-octahydroxanthene-1, 8-diones and 1, 8-dioxo-sym-octahydroxanthylium salts in recyclization under the influence of amines.* Chemistry of Heterocyclic Compounds, 2006. **42**: p. 28-33.
71. Abdel-Galil, F.M., et al., *ACTIVATED NITRILES IN HETEROCYCLIC SYNTHESIS: A NOVEL SYNTHESIS OF 4-AZOLOYL-2-AMINOQUINOLINES.* Chemistry Letters, 2006. **11**(8): p. 1123-1126.
72. Callan, J.F., A.P. de Silva, and D.C. Magri, *Luminescent sensors and switches in the early 21st century*. Tetrahedron, 2005. **61**(36): p. 8551-8588.
73. Sirkecioglu, O., N. Talinli, and A. Akar, *Chemical aspects of santalin as a histological stain.* J Chem Res (s), 1995. **502**.
74. Poupelin, J., et al., *H4SiW12O40 catalyzed one-Pot synthesis of 12-Aryl-8, 9, 10, 12-tetrahydrobenzo [a] xanthen-11-ones under solvent-free conditions.* Eur. J. Med. Chem, 1978. **13**: p. 67.
75. Banerjee, A. and A.K. Mukherjee, *Chemical Aspects of Santalin as a Histological Stain.* Stain Technology, 1981. **56**(2): p. 83-85.
76. Banik, B., *Green Approaches in Medicinal Chemistry for Sustainable Drug Design: Applications*. Vol. 1. 2024: Elsevier.
77. Marco-Contelles, J., et al., *Recent Advances in the Friedländer Reaction.* Chemical Reviews, 2009. **109**(6): p. 2652-2671.
78. Sato, S., et al., *Synthesis and evaluation of a new water-soluble fluorescent red dye, xanthene bis-C-glycoside.* Journal of Heterocyclic Chemistry, 2020. **57**(9): p. 3342-3349.

79. Maia, M., et al., *Xanthenes in Medicinal Chemistry – Synthetic strategies and biological activities.* European Journal of Medicinal Chemistry, 2021. **210**: p. 113085.
80. Ghahsare, A.G., Z.S. Nazifi, and S.M. Nazifi, *Structure-bioactivity relationship study of xanthene derivatives: a brief review.* Current Organic Synthesis, 2019. **16**(8): p. 1071-1077.
81. Kurniawan, Y.S., et al., *An update on the anticancer activity of xanthone derivatives: A review.* Pharmaceuticals, 2021. **14**(11): p. 1144.
82. Giri, R., et al., *Synthesis and cancer cell cytotoxicity of substituted xanthenes.* Bioorganic & Medicinal Chemistry, 2010. **18**(4): p. 1456-1463.
83. Richardson, S.N., et al., *Antimicrobial dihydrobenzofurans and xanthenes from a foliar endophyte of Pinus strobus.* Phytochemistry, 2015. **117**: p. 436-443.
84. Yunnikova, L.P. and É.V. Voronina, *Synthesis of xanthene and thioxanthene derivatives and study of their antimicrobial activity.* Pharmaceutical Chemistry Journal, 1996. **30**(11): p. 695-696.
85. Carr, A.A., et al., *Bis-basic-substituted polycyclic aromatic compounds. A new class of antiviral agents. 7. Bisalkamine esters of 9-oxoxanthene-2,7-dicarboxylic acid, 3,6-bis-basic ethers of xanthen-9-one, and 2,7-bis(aminoacyl)xanthen-9-ones, -xanthenes, and -thioxanthenes.* Journal of Medicinal Chemistry, 1976. **19**(9): p. 1142-1148.
86. Chibale, K., et al., *Exploring the potential of xanthene derivatives as trypanothione reductase inhibitors and chloroquine potentiating agents.* Tetrahedron, 2003. **59**(13): p. 2289-2296.
87. Wu, C.-P., et al., *Reversal of chloroquine resistance in Plasmodium falciparum by 9H-xanthene derivatives.* International Journal of Antimicrobial Agents, 2005. **26**(2): p. 170-175.
88. Banerjee, A.G., et al., *A facile microwave assisted one pot synthesis of novel xanthene derivatives as potential anti-inflammatory and analgesic agents.* Arabian Journal of Chemistry, 2016. **9**: p. S480-S489.
89. Naya, A., et al., *Design, Synthesis, and Discovery of a Novel CCR1 Antagonist.* Journal of Medicinal Chemistry, 2001. **44**(9): p. 1429-1435.
90. Jiang, B.-C., T. Liu, and Y.-J. Gao, *Chemokines in chronic pain: cellular and molecular mechanisms and therapeutic potential.* Pharmacology & Therapeutics, 2020. **212**: p. 107581.
91. Kwon, Y., et al., *Xanthene derivatives increase glucose utilization through activation of LKB1-dependent AMP-activated protein kinase.* PLoS One, 2014. **9**(9): p. e108771.
92. Yamamura, T., et al., *Chain-breaking fused heterocyclic antioxidants: Antioxidant activities of 9H-xanthene-2, 7-diols and α-tocopherol upon liposomal membranes.* Journal of the American Oil Chemists' Society, 1997. **74**(6): p. 739-744.
93. Kancheva, V.D., et al., *Antiradical and antioxidant activities of new bio-antioxidants.* Biochimie, 2012. **94**(2): p. 403-415.
94. Chauhan, D., H.K. Chopra, and S.K. Nayak, *Solvent-Free, Microwave-Assisted Sr (Clo4) 2 Catalyzed Highly Efficient One-Pot Synthesis of Xanthene Derivatives.* Available at SSRN 4066985.
95. Kaiser, C., et al., *Analogs of phenothiazines. 4. Effect of structure upon neuropharmacological activity of some chlorpromazine analogs of the diphenylmethane type.* Journal of Medicinal Chemistry, 1972. **15**(6): p. 665-673.
96. Rahmati, A., *A rapid and efficient method for the synthesis of 14H-dibenzo[α.j] xanthenes, aryl-5H-dibenzo [b.i]xanthene-5,7,12,14-(13H)-tetraone and 1,8-dioxo-octahydroxanthenes by acidic ionic liquid.* Chinese Chemical Letters, 2010. **21**(7): p. 761-764.

97. Sen, R.N. and N.N. Sarkar, *THE CONDENSATION OF PRIMARY ALCOHOLS WITH RESORCINOL AND OTHER HYDROXY AROMATIC COMPOUNDS.* Journal of the American Chemical Society, 1925. **47**(4): p. 1079-1091.
98. Darviche, F., et al., *Diammonium Hydrogen Phosphate as a Neutral and Efficient Catalyst for Synthesis of 1,8-Dioxo-octahydroxanthene Derivatives in Aqueous Media.* Synthetic Communications, 2007. **37**(7): p. 1059-1066.
99. Borah, R., P. Dutta, and P. Sarma, *Investigation of efficient synthesis of 1, 8-dioxo-octahydroxanthene derivatives under solvent-free grinding method.* Curr Chem Lett, 2013. **2**(4): p. 159-66.
100. Sivaguru, P. and A. Lalitha, *Ceric ammonium nitrate supported HY-zeolite: An efficient catalyst for the synthesis of 1,8-dioxo-octahydroxanthenes.* Chinese Chemical Letters, 2014. **25**(2): p. 321-323.
101. Verma, G.K., et al., *An efficient one-pot solvent-free synthesis and photophysical properties of 9-aryl/alkyl-octahydroxanthene-1,8-diones.* Tetrahedron, 2011. **67**(20): p. 3698-3704.
102. FAN, X.-S., et al., *FeCl3• 6H2O Catalyzed Con-densation of Aromatic Aldehydes with 5, 5-Dimethyl-1, 3-cyclohexanedione in Ionic Liquids.* Chinese Journal of Organic Chemistry, 2005. **25**(11): p. 1482.
103. Ma, J.-J., et al., *Condensation of aromatic aldehydes with 1, 3-cyclohexanedione catalyzed by NaHSO4 in ionic liquids.* Chinese Journal of Organic Chemistry, 2007. **27**(05): p. 640.
104. Karade, H.N., M. Sathe, and M. Kaushik, *An efficient synthesis of 1, 8-dioxo-octahydroxanthenes using tetrabutylammonium hydrogen sulfate.* Arkivoc, 2007. **13**: p. 252-258.
105. Seyyedhamzeh, M., P. Mirzaei, and A. Bazgir, *Solvent-free synthesis of aryl-14H-dibenzo[a,j]xanthenes and 1,8-dioxo-octahydro-xanthenes using silica sulfuric acid as catalyst.* Dyes and Pigments, 2008. **76**(3): p. 836-839.
106. John, A., P.J.P. Yadav, and S. Palaniappan, *Clean synthesis of 1,8-dioxo-dodecahydroxanthene derivatives catalyzed by polyaniline-p-toluenesulfonate salt in aqueous media.* Journal of Molecular Catalysis A: Chemical, 2006. **248**(1): p. 121-125.
107. Kantevari, S., R. Bantu, and L. Nagarapu, *HClO4–SiO2 and PPA–SiO2 catalyzed efficient one-pot Knoevenagel condensation, Michael addition and cyclo-dehydration of dimedone and aldehydes in acetonitrile, aqueous and solvent free conditions: Scope and limitations.* Journal of Molecular Catalysis A: Chemical, 2007. **269**(1): p. 53-57.
108. Jin, T.S., et al., *Solid-State Condensation Reactions Between Aldehydes and 5,5-Dimethyl-1,3-cyclohexanedione by Grinding at Room Temperature.* Synthetic Communications, 2005. **35**(17): p. 2339-2345.
109. Das, B., et al., *Amberlyst-15: An efficient reusable heterogeneous catalyst for the synthesis of 1,8-dioxo-octahydroxanthenes and 1,8-dioxo-decahydroacridines.* Journal of Molecular Catalysis A: Chemical, 2006. **247**(1): p. 233-239.
110. Song, G., et al., *Fe3+-montmorillonite as a cost-effective and recyclable solid acidic catalyst for the synthesis of xanthenediones.* Catalysis Communications, 2007. **8**(4): p. 673-676.
111. Pramanik, A. and S. Bhar, *Alumina-sulfuric acid catalyzed eco-friendly synthesis of xanthenediones.* Catalysis Communications, 2012. **20**: p. 17-24.
112. Rashedian, F., D. Saberi, and K. Niknam, *Silica-bonded N-propyl sulfamic acid: a recyclable catalyst for the synthesis of 1, 8-dioxo-decahydroacridines, 1,*

8-dioxo-octahydroxanthenes and quinoxalines. Journal of the Chinese Chemical Society, 2010. **57**(5A): p. 998-1006.

113. Sunkara, J.R. and S.M. Botsa, *Facile Synthesis of 1, 8-dioxooctahydro Xanthenes by Reusable Zinc Sulfide based Ternary Nanocomposite via Hydrothermal Route.* Current Catalysis, 2020. **9**(1): p. 72-79.
114. Srihari, P., et al., *Synthesis of 1,8-dioxo-octahydroxanthenes utilizing PMA-SiO2 as an efficient reusable catalyst.* Chinese Chemical Letters, 2008. **19**(7): p. 771-774.
115. Mahdavinia, G.H., *Clean synthesis of 1, 8-dioxo-octahydroxanthene derivatives using NBS as an efficient and almost neutral catalyst in aqueous media.* 2008.
116. Niknam, K. and M. Damya, *1-Butyl-3-methylimidazolium Hydrogen Sulfate [Bmim] HSO4: An Efficient Reusable Acidic Ionic Liquid for the Synthesis of 1, 8-Dioxo-Octahydroxanthenes.* Journal of the Chinese Chemical Society, 2009. **56**(3): p. 659-665.
117. Dabiri, M., M. Baghbanzadeh, and E. Arzroomchilar, *1-Methylimidazolium triflouroacetate ([Hmim]TFA): An efficient reusable acidic ionic liquid for the synthesis of 1,8-dioxo-octahydroxanthenes and 1,8-dioxo-decahydroacridines.* Catalysis Communications, 2008. **9**(5): p. 939-942.
118. Fang, D., K. Gong, and Z.-L. Liu, *Synthesis of 1,8-Dioxo-octahydroxanthenes Catalyzed by Acidic Ionic Liquids in Aqueous Media.* Catalysis Letters, 2009. **127**(3): p. 291-295.
119. Moosavi-Zare, A.R., et al., *Preparation, characterization and application of ionic liquid sulfonic acid functionalized pyridinium chloride as an efficient catalyst for the solvent-free synthesis of 12-aryl-8,9,10,12-tetrahydrobenzo[a]-xanthen-11-ones.* Journal of Molecular Liquids, 2013. **186**: p. 63-69.
120. Singh, H., S. Kumari, and J.M. Khurana, *A new green approach for the synthesis of 12-aryl-8,9,10,12-tetrahydrobenzo[a]xanthene-11-one derivatives using task specific acidic ionic liquid [NMP]H2PO4.* Chinese Chemical Letters, 2014. **25**(10): p. 1336-1340.
121. Gérard, E.M., et al., *Systematic study of a solvent-free mechanochemically induced domino oxa-Michael-aldol reaction in a ball mill.* Synlett, 2008. **2008**(17): p. 2702-2704.
122. Shaabani, A., et al., *A new one-pot three-component synthesis of 2, 4-diamino-5 H-chromeno [2, 3-b] pyridine-3-carbonitrile derivatives.* Molecular diversity, 2010. **14**: p. 179-182.
123. Narayana, V.R., Z. Pudukulathan, and R. Varala, *SO 4 2-/SnO 2-Catalyzed efficient one-pot synthesis of 7, 8-Dihydro-2H-Chromen-5-ones by formal [3+ 3] cycloaddition and 1, 8-Dioxo-octahydroxanthenes via a Knoevenagel condensation.* Organic communications, 2013. **6**(3): p. 110.
124. Bazgir, A., Z.N. Tisseh, and P. Mirzaei, *An efficient synthesis of spiro[dibenzo[b,i]xanthene-13,3'-indoline]-pentaones and 5H-dibenzo[b,i]xanthene-tetraones.* Tetrahedron Letters, 2008. **49**(35): p. 5165-5168.
125. Turhan, K., et al., *Novel benzo [b] xanthene derivatives: Bismuth (III) triflate-catalyzed one-pot synthesis, characterization, and acetylcholinesterase, glutathione S-transferase, and butyrylcholinesterase inhibitory properties.* Archiv der Pharmazie, 2020. **353**(8): p. 2000030.
126. Bansal, R.K. and J. Heinicke, *Anellated Heterophospholes and Phospholides and Analogies with Related Non-Phosphorus Systems.* Chemical Reviews, 2001. **101**(11): p. 3549-3578.

127. Simulescu, V., E. Crasmareanu, and G. Ilia, *Synthesis, properties and structures of phosphorus-nitrogen heterocycles.* Heterocycles, 2011. **83**(2): p. 275.
128. McReynolds, M.D., J.M. Dougherty, and P.R. Hanson, *Synthesis of Phosphorus and Sulfur Heterocycles via Ring-Closing Olefin Metathesis.* Chemical Reviews, 2004. **104**(5): p. 2239-2258.
129. Petkova, N.I., et al., *Synthesis of heterocyclic methylenebisphosphonates by 1,3-dipolar cycloaddition of ethyl diazoacetate to 1,2-benzoxaphosphorin-3-phosphonates.* Tetrahedron, 2009. **65**(8): p. 1639-1647.
130. MORITA, I., et al., *Synthesis and antihypertensive activities of 1, 4-dihydropyridine-5-phosphonate derivatives. II.* Chemical and pharmaceutical bulletin, 1987. **35**(10): p. 4144-4154.
131. Ruda, G.F., et al., *Aryl Phosphoramidates of 5-Phospho Erythronohydroxamic Acid, A New Class of Potent Trypanocidal Compounds.* Journal of Medicinal Chemistry, 2010. **53**(16): p. 6071-6078.
132. Point, V., et al., *Synthesis and Kinetic Evaluation of Cyclophostin and Cyclipostins Phosphonate Analogs As Selective and Potent Inhibitors of Microbial Lipases.* Journal of Medicinal Chemistry, 2012. **55**(22): p. 10204-10219.
133. Xu, J., *Synthesis of 1, 2-oxaphosphinane 2-oxides and 1, 2-oxaphosphinine 2-oxides: δ-phosphonolactones and δ-phosphinolactones.* New Journal of Chemistry, 2023. **47**(11): p. 5441-5469.
134. Xu, J., *Synthetic strategies for the preparation of γ-phostams: 1,2-azaphospholidine 2-oxides and 1,2-azaphospholine 2-oxides.* Beilstein Journal of Organic Chemistry, 2022. **18**: p. 889-915.
135. Ali, T.E., *Synthesis of Some New 1,3,2-Oxazaphosphinine, 1,3,2-Diazaphosphinine, Acyclic, and/or Cyclic α-Aminophosphonate Derivatives Containing the Chromone Moiety.* Phosphorus, Sulfur, and Silicon and the Related Elements, 2009. **185**(1): p. 88-96.
136. Abdou, W.M., A.A. Kamel, and A.A. Shaddy, *Use of phosphonyl carbanions in the synthesis of anti-inflammatory active phosphorus-containing fused heterocycles and relevance phosphonates.* European Journal of Medicinal Chemistry, 2010. **45**(11): p. 5217-5224.
137. Khidre, R.E., *Wafaa M. Abdou, Reham F. Barghash &.* Monatsh Chem, 2013. **144**: p. 1233-1242.
138. Berton, J.K., et al., *Fifty years of (benz) oxaphospholene chemistry.* Chemistry–A European Journal, 2017. **23**(69): p. 17413-17431.
139. Xu, Y., et al., *Phosphonothioate and Fluoromethylene Phosphonate Analogues of Cyclic Phosphatidic Acid: Novel Antagonists of Lysophosphatidic Acid Receptors.* Journal of Medicinal Chemistry, 2006. **49**(17): p. 5309-5315.
140. Zhang, A., et al., *Lanthanide-Catalyzed Selective Addition of Diethyl Phosphite to Chalcones.* Heteroatom Chemistry, 2013. **24**(5): p. 345-354.
141. Ageeva, A. and B. Ivanov, *Reaction of trialkyl phosphites with o-hydroxybenzyl alcohol and its derivatives.* Bulletin of the Academy of Sciences of the USSR. Division of Chemical Sciences, 1967. **16**(7): p. 1443-1446.
142. Miles, J.A., R.C. Grabiak, and C. Cummins, *Synthesis of novel phosphorus heterocycles: 1,3-dihydro-2,1-benzoxaphosphole 1-oxides.* The Journal of Organic Chemistry, 1982. **47**(9): p. 1677-1682.
143. López-Rodríguez, R., et al., *Pathways for N-Nitroso Compound Formation: Secondary Amines and Beyond.* Organic Process Research & Development, 2020. **24**(9): p. 1558-1585.

References

144. Hecht, S.S., *Tobacco carcinogens, their biomarkers and tobacco-induced cancer.* Nature Reviews Cancer, 2003. **3**(10): p. 733-744.
145. Williams, D.L.H., *Nitrosation reactions and the chemistry of nitric oxide*2004: Elsevier.
146. Andrés, C.M.C., et al., *Dual-Action Therapeutics: DNA Alkylation and Antimicrobial Peptides for Cancer Therapy.* Cancers, 2024. **16**(18): p. 3123.
147. Waziri, I., et al., *Synthesis, anti-microbial, toxicity and molecular docking studies of N-nitroso-N-phenylhydroxylamine (cupferron) and its derivatives.* Bioorganic & Medicinal Chemistry Letters, 2021. **52**: p. 128381.
148. Food, U. and D. Administration, *Control of nitrosamine impurities in human drugs: guidance for industry.* Center for Drug Evaluation and Research: Silver Spring, MD, USA, 2021.
149. Beard, J.C. and T.M. Swager, *An Organic Chemist's Guide to N-Nitrosamines: Their Structure, Reactivity, and Role as Contaminants.* The Journal of Organic Chemistry, 2021. **86**(3): p. 2037-2057.
150. Balayiannis, G.P. and H. Karasali, *N-Nitrosamine Impurities in Ethalfluralin: Determination of an Overlooked Deleterious Source in Pesticides.* Agriculture, 2023. **13**(5): p. 1104.
151. White, E.H., *The chemistry of the N-alkyl-N-nitrosoamides. I. Methods of preparation.* Journal of the American Chemical Society, 1955. **77**(22): p. 6008-6010.
152. Tanno, M. and S. SUEYOSHI, *Preparation and properties of 3-alkyl-1-arylnitrosoureas and related compounds.* Chemical and pharmaceutical bulletin, 1987. **35**(4): p. 1360-1371.
153. Garcia, J., et al., *Nitrosation of peptide bonds. Cleavage of nitrosated peptides by pyrrolidine and α-amino esters.* Tetrahedron, 1984. **40**(16): p. 3121-3127.
154. Moser, J., et al., *N-nitrosamine formation in pharmaceutical solid drug products: experimental observations.* Journal of Pharmaceutical Sciences, 2023. **112**(5): p. 1255-1267.
155. Rivière, J., *Détection de la présence de nitrosamines dans les médicaments: impact pour l'industrie pharmaceutique et gestion du risque*, 2022, Université de Lorraine.
156. Li, K., et al., *Estimated cancer risks associated with nitrosamine contamination in commonly used medications.* International journal of environmental research and public health, 2021. **18**(18): p. 9465.
157. Lijinsky, W., *N-Nitroso compounds in the diet.* Mutation Research/Genetic Toxicology and Environmental Mutagenesis, 1999. **443**(1): p. 129-138.
158. Magee, P.N., *Nitrosamines and human cancer: introduction and overview.* European Journal of Cancer Prevention, 1996. **5**: p. 7-10.
159. Qiu, Q., et al., *The combi-targeting concept: a novel 3,3-disubstituted nitrosourea with EGFR tyrosine kinase inhibitory properties.* Cancer Chemotherapy and Pharmacology, 2003. **51**(1): p. 1-10.
160. Hung, C.F., *Effects of carmustine and lomustine on arylamine N-acetyltransferase activity and 2-aminofluorene-DNA adducts in rat glial tumor cells.* Neurochemical research, 2000. **25**: p. 845-851.
161. Lin, K.-I., et al., *Carnosic acid impedes cell growth and enhances anticancer effects of carmustine and lomustine in melanoma.* Bioscience Reports, 2018. **38**(4): p. BSR20180005.
162. Mirvish, S.S., *N-nitroso compounds: Their chemical and in vivo formation and possible importance as environmental carcinogens.* Journal of Toxicology and Environmental Health, Part A Current Issues, 1977. **2**(6): p. 1267-1277.

References

163. Rose, U., *European Pharmacopoeia Activities on Control of Nitrosamines and other DNA-Reactive Impurities.* Journal of Pharmaceutical Sciences, 2023. **112**(5): p. 1163-1165.
164. Laihia, K., et al., *1H, 13C and 15N NMR study of 2-alkylnitrosoamino-4-nitropyridines and N-oxides: An example on restricted inversion of sp3 nitrogen.* Journal of molecular structure, 2007. **831**(1-3): p. 203-208.
165. Dyablo, O., et al., *Synthesis and investigation of the conformational mobility of certain (n-benzyl-n-nitrosoamino) azoles.* Chemistry of Heterocyclic Compounds, 2005. **41**: p. 329-339.
166. Austin, A.T., *NITROSATION IN ORGANIC CHEMISTRY.* Science Progress (1933-), 1961. **49**(196): p. 619-640.
167. Potturi, H.K., R.K. Gurung, and Y. Hou, *Nitromethane with IBX/TBAF as a Nitrosating Agent: Synthesis of Nitrosamines from Secondary or Tertiary Amines under Mild Conditions.* The Journal of Organic Chemistry, 2012. **77**(1): p. 626-631.
168. Ohwada, T., et al., *Structural Features of Aliphatic N-Nitrosamines of 7-Azabicyclo[2.2.1]heptanes That Facilitate N−NO Bond Cleavage.* Journal of the American Chemical Society, 2001. **123**(42): p. 10164-10172.
169. Teuten, E.L. and R.N. Loeppky, *The mechanistic origin of regiochemical changes in the nitrosative N-dealkylation of N,N-dialkyl aromatic amines.* Organic & Biomolecular Chemistry, 2005. **3**(6): p. 1097-1108.
170. Schirrmacher, R., et al., *Syntheses of novel N-([18F] fluoroalkyl)-N-nitroso-4-methyl-benzenesulfonamides and decomposition studies of corresponding 19F-and bromo-analogues: potential new compounds for the 18F-labelling of radiopharmaceuticals.* Journal of Labelled Compounds and Radiopharmaceuticals: The Official Journal of the International Isotope Society, 2003. **46**(10): p. 959-977.
171. Aouf, Z., et al., *An attempt to prepare sulfonyl analogues of fotemustine: unexpected rearrangement to sulfamate during nitrosation step.* RSC Advances, 2023. **13**(50): p. 35741-35754.
172. Rajni Gupta and Vandana Gupta, *Synthesis and Spectral studies of Nitrosourea derivatives of 3- Methyl - 5/7- Substituted -2- (3,4-dichloro) benzoyl-4H- 1,4-Benzothiazines as Bifunctional Anticancer Agents.* Heterocyclic Communications, 2010. **16**(1): p. 65-71.
173. Denmark, S.E., et al., *Development of Chiral Bis-hydrazone Ligands for the Enantioselective Cross-Coupling Reactions of Aryldimethylsilanolates.* The Journal of Organic Chemistry, 2015. **80**(1): p. 313-366.
174. Sather, A.C., et al., *Reactivity of N-nitrosoamides in confined spaces.* Tetrahedron Letters, 2011. **52**(17): p. 2100-2103.
175. Dewynter, G., et al., *Synthesis of n-sulfamoyloxazolidinones and -perhydrooxazinones reactivity and use as donors in the transsulfamoylation reaction; application to the preparation of 2-chloroethylnitrososulfamides. IV.* Tetrahedron, 1996. **52**(45): p. 14217-14224.
176. Domarkas, J., et al., *The Combi-Targeting Concept: Synthesis of Stable Nitrosoureas Designed to Inhibit the Epidermal Growth Factor Receptor (EGFR).* Journal of Medicinal Chemistry, 2006. **49**(12): p. 3544-3552.
177. Iglesias, E. and J. Casado, *Mechanisms of hydrolysis and nitrosation reactions of alkyl nitrites in various media.* International Reviews in Physical Chemistry, 2002. **21**(1): p. 37-74.

178. Challis, B.C. and T.I. Yousaf, *Facile formation of N-nitrosamines from bromonitromethane and secondary amines.* Journal of the Chemical Society, Chemical Communications, 1990(22): p. 1598-1599.
179. Demir, A.S., et al., *The Mild N-Nitrosation of Secondary Amines with Trichloro Nitromethane.* Synthetic Communications, 1992. **22**(18): p. 2607-2611.
180. Fan, T.Y., R. Vita, and D.H. Fine, *C-nitro compounds: A new class of nitrosating agents.* Toxicology Letters, 1978. **2**(1): p. 5-10.
181. Challis, B.C. and S.A. Kyrtopoulos, *The chemistry of nitroso compounds. Part 12. The mechanism of nitrosation and nitration of aqueous piperidine by gaseous dinitrogen tetraoxide and dinitrogen trioxide in aqueous alkaline solutions. Evidence for the existence of molecular isomers of dinitrogen tetraoxide and dinitrogen trioxide.* Journal of the Chemical Society, Perkin Transactions 2, 1978(12): p. 1296-1302.
182. Shiri, M., et al., *Advances in the application of N2O4/NO2 in organic reactions.* Tetrahedron, 2010. **66**(47): p. 9077-9106.
183. Ravindran, T., et al., *Chemistry of N-nitroso compounds. 1. Synthesis and stereodynamics of N-nitrosopiperidines and N-nitrosopiperidin-4-ones.* The Journal of Organic Chemistry, 1991. **56**(16): p. 4833-4840.
184. Dietrich, M., et al., *A review: dietary and endogenously formed N-nitroso compounds and risk of childhood brain tumors.* Cancer Causes & Control, 2005. **16**(6): p. 619-635.
185. Koestner, A., *Characterization of N-nitrosourea-induced tumors of the nervous system; their prospective value for studies of neurocarcinogenesis and brain tumor therapy.* Toxicologic pathology, 1990. **18**(1_part_2): p. 186-192.
186. Schepartz[1], S.A., *Early history and development of the nitrosoureas.* Cancer Treatment Reports, 1976. **60**(6): p. 647.
187. Mitchell, E.P. and P.S. Schein, *Contributions of nitrosoureas to cancer treatment.* Cancer Treat Rep, 1986. **70**(1): p. 31-41.
188. McKay, A.F., *A New Method of Preparation of Diazomethane.* Journal of the American Chemical Society, 1948. **70**(5): p. 1974-1975.
189. Skipper, H.E., et al., *Experimental evaluation of potential anticancer agents VI. Anatomical distribution of leukemic cells and failure of chemotherapy.* Cancer research, 1961. **21**(9): p. 1154-1164.
190. Johnston, T.P., G.S. McCaleb, and J.A. Montgomery, *The Synthesis of Antineoplastic Agents. XXXII. N-Nitrosoureas.1 I.* Journal of Medicinal Chemistry, 1963. **6**(6): p. 669-681.
191. Johnston, T.P., et al., *The Synthesis of Potential Anticancer Agents. XXXVI. N-Nitrosoureas.1 II. Haloalkyl Derivatives.* Journal of Medicinal Chemistry, 1966. **9**(6): p. 892-911.
192. Vavra, J.J., et al., *Streptozotocin, a new antibacterial antibiotic.* Antibiot Annu, 1959. **7**: p. 230-5.
193. Murray-Lyon, I.M., et al., *TREATMENT OF MULTIPLE-HORMONE-PRODUCING MALIGNANT ISLET-CELL TUMOUR WITH STREPTOZOTOCIN.* The Lancet, 1968. **292**(7574): p. 895-898.
194. Brakenhoff, J.P.G., et al., *Chemical and Glutathione Conjugation-Related Degradation of Fotemustine: Formation and Characterization of a Glutathione Conjugate of Diethyl (1-Isocyanatoethyl)phosphonate, a Reactive Metabolite of Fotemustine.* Chemical Research in Toxicology, 1994. **7**(3): p. 380-389.
195. Brandes, A.A., et al., *Nitrosoureas in the Management of Malignant Gliomas.* Current Neurology and Neuroscience Reports, 2016. **16**(2): p. 13.

196. Beall, H.D. and S. Winski, *Mechanisms of action of quinone-containing alkylating agents. I: NQO1-directed drug development.* Front Biosci, 2000. **5**: p. D639-48.
197. Montgomery, J.A., et al., *The Modes of Decomposition of 1,3-Bis(2-chloroethyl)-1-nitrosourea and Related Compounds.* Journal of Medicinal Chemistry, 1967. **10**(4): p. 668-674.
198. Yamada, S., et al., *In Vitro Metabolism Study of Carmustine, Active Pharmaceutical Ingredient of BCNU Implant, in Humans.*
199. Kann, H.E., Jr., K.W. Kohn, and J.M. Lyles, *Inhibition of DNA Repair by the 1,3-Bis(2-chloroethyl)-1-nitrosourea Breakdown Product, 2-Chloroethyl Isocyanate.* Cancer research, 1974. **34**(2): p. 398-402.
200. Gnewuch, C.T. and G. Sosnovsky, *A Critical Appraisal of the Evolution of N-Nitrosoureas as Anticancer Drugs.* Chemical Reviews, 1997. **97**(3): p. 829-1014.
201. Jaman, Z., et al., *Rapid On-Demand Synthesis of Lomustine under Continuous Flow Conditions.* Organic Process Research & Development, 2019. **23**(3): p. 334-341.
202. Dixon, W., et al. *A role for cysteine and other sulfhydryl compounds in controlling pigmentation and proliferation of transformed melanocytes*. in *JOURNAL OF INVESTIGATIVE DERMATOLOGY*. 1990. BLACKWELL SCIENCE INC 238 MAIN ST, CAMBRIDGE, MA 02142.
203. Gadjeva, V., *Structure-based design of nitrosoureas containing tyrosine derivatives as potential antimelanoma agents.* European Journal of Medicinal Chemistry, 2002. **37**(4): p. 295-300.
204. Pegg, A.E., *Multifaceted Roles of Alkyltransferase and Related Proteins in DNA Repair, DNA Damage, Resistance to Chemotherapy, and Research Tools.* Chemical Research in Toxicology, 2011. **24**(5): p. 618-639.
205. Sun, G., et al., *Synthesis and antitumor activity evaluation of a novel combi-nitrosourea prodrug: Designed to release a DNA cross-linking agent and an inhibitor of O6-alkylguanine-DNA alkyltransferase.* Bioorganic & Medicinal Chemistry, 2016. **24**(9): p. 2097-2107.
206. Wang, Y., et al., *Synthesis and Antitumor Activity Evaluation of a Novel Combi-nitrosourea Prodrug: BGCNU.* ACS Medicinal Chemistry Letters, 2017. **8**(2): p. 174-178.
207. Dewynter, G., et al., *Synthèse et structure de chloroéthylsulfonyl-et sulfoxylurees dérivées de l'isocyanate de chlorosulfonyle.* Phosphorus, Sulfur, and Silicon and the Related Elements, 1991. **61**(3-4): p. 223-237.
208. Abdaoui, M., et al., *A new family of potential oncostatics: 2-chloroethylnitrososulfamides (CENS)—I. Synthesis, structure, and pharmacological evaluation (preliminary results).* Bioorganic & Medicinal Chemistry, 1996. **4**(8): p. 1227-1235.
209. Winum, J.-Y., et al., *Synthesis and biological evaluation of Fotemustine analogues on human melanoma cell lines.* European Journal of Medicinal Chemistry, 2003. **38**(3): p. 319-324.
210. Zhao, L.J., X.Y. Ma, and R.G. Zhong, *A density functional theory investigation on the formation mechanisms of DNA interstrand crosslinks induced by chloroethylnitrosoureas.* International Journal of Quantum Chemistry, 2013. **113**(9): p. 1299-1306.
211. Nikolova, T., et al., *Chloroethylating nitrosoureas in cancer therapy: DNA damage, repair and cell death signaling.* Biochimica et Biophysica Acta (BBA) - Reviews on Cancer, 2017. **1868**(1): p. 29-39.

References

212. Beauchesne, P., *Fotemustine: A Third-Generation Nitrosourea for the Treatment of Recurrent Malignant Gliomas.* Cancers, 2012. **4**(1): p. 77-87.
213. Reynolds, R.C., et al., *Synthesis and evaluation of several new (2-chloroethyl) nitrosocarbamates as potential anticancer agents.* Journal of Medicinal Chemistry, 2000. **43**(8): p. 1484-1488.
214. Paradisi, M.P., G.P. Zecchini, and I. Torrini, *Selective acylations of aminophenols and hydroxyalkylphenols with 1-acetyl-v-triazolo [4, 5-b] pyridine.* Tetrahedron Letters, 1986. **27**(41): p. 5029-5032.
215. da Silva, M., *Teixeira RR de Azevedo Santos L. Martins FT Ramalho TC Arab.* J. Chem, 2020. **13**: p. 974-987.
216. Dadhania, A.N., V.K. Patel, and D.K. Raval, *Catalyst-free sonochemical synthesis of 1,8-dioxo-octahydroxanthene derivatives in carboxy functionalized ionic liquid.* Comptes Rendus Chimie, 2012. **15**(5): p. 378-383.
217. Walsh, C.T., *Chemical Biology of Phosphorus*. Vol. 13. 2020: Royal society of chemistry.
218. Kumar, A., J. Mukhopadhyay, and S. Bhagat, *Phosphorus Heterocycles and Their Biological Applications.* ChemistrySelect, 2024. **9**(45): p. e202404258.
219. Gagné-Boulet, M., *Conception, synthèse, caractérisation chimique et évaluation biologique de nouveaux agents anticancéreux ciblant les microtubules et les mécanismes de réparation et de réplication de l'ADN*, 2021, Université Laval.
220. Karati, D., et al., *Alkylating agents, the road less traversed, changing anticancer therapy.* Anti-Cancer Agents in Medicinal Chemistry-Anti-Cancer Agents), 2022. **22**(8): p. 1478-1495.
221. Faria, S., et al., *Computational investigation of the carmustine (BCNU) alkylation mechanism using the QTAIM, IQA, and NBO models.* Structural Chemistry, 2021. **32**(1): p. 79-96.
222. Listro, R., et al., *Urea-based anticancer agents. Exploring 100-years of research with an eye to the future.* Frontiers in Chemistry, 2022. **10**: p. 995351.
223. El-Helby, A.G.A., et al., *Design, synthesis, molecular docking, and anticancer activity of benzoxazole derivatives as VEGFR-2 inhibitors.* Archiv der Pharmazie, 2019. **352**(10): p. 1900113.
224. Miyazaki, Y., et al., *Novel 4-amino-furo[2,3-d]pyrimidines as Tie-2 and VEGFR2 dual inhibitors.* Bioorganic & Medicinal Chemistry Letters, 2005. **15**(9): p. 2203-2207.
225. Daina, A., O. Michielin, and V. Zoete, *Sci Rep 7, 42717.* 24-R. Dennington, T. Keith, J. Millam, GaussView, version 4.12 Semichem, 2017.
226. Waring, M.J., *Lipophilicity in drug discovery.* Expert opinion on drug discovery, 2010. **5**(3): p. 235-248.
227. Lipinski, C.A., *Lead-and drug-like compounds: the rule-of-five revolution.* Drug discovery today: Technologies, 2004. **1**(4): p. 337-341.
228. Halgren, J.J.K., et al., *Glide-related material.* J. Med. Chem, 2004. **47**: p. 1739-1749.
229. Pettersen, E.F., et al., *UCSF ChimeraX: Structure visualization for researchers, educators, and developers.* Protein science, 2021. **30**(1): p. 70-82.
230. Yu, J., N.Q. Su, and W. Yang, *Describing chemical reactivity with frontier molecular orbitalets.* JACS au, 2022. **2**(6): p. 1383-1394.
231. Sangwan, R., et al., *Synthesis of 1, 8-dioxooctahydroxanthene derivatives using ionic liquids, quantum chemical studies and anticancer activity.* Journal of molecular structure, 2020. **1208**: p. 127786.

References

232. Lakshminarayanan, S., et al., *Molecular electrostatic potential (MEP) surface analysis of chemo sensors: An extra supporting hand for strength, selectivity & non-traditional interactions.* Journal of Photochemistry and Photobiology, 2021. **6**: p. 100022.
233. Bentoumi, H., et al., *Theoretical investigations of some isolated compounds from Calophyllum flavoramulum as potential antioxidant agents and inhibitors of AGEs.* Journal of Biomolecular Structure and Dynamics, 2024: p. 1-27.
234. Blois, M.S., *Antioxidant determinations by the use of a stable free radical.* Nature, 1958. **181**(4617): p. 1199-1200.
235. Yun, M.-K., et al., *Catalysis and sulfa drug resistance in dihydropteroate synthase.* Science, 2012. **335**(6072): p. 1110-1114.
236. Cao, H., J.M. Pauff, and R. Hille, *Substrate orientation and catalytic specificity in the action of xanthine oxidase: the sequential hydroxylation of hypoxanthine to uric acid.* Journal of Biological Chemistry, 2010. **285**(36): p. 28044-28053.
237. Sheldrick, G., *SHELXL-2014.* University of Göttingen, Germany, 2014.
238. Dolomanov, O., et al., *_journal_name_full'American Mineralogist'_journal_year 2021 _journal_volume 106 _journal_page_first 1844 _journal_paper_doi 10.2138/am-2021-7785.* J. Appl. Cryst, 2009. **42**: p. 339-341.
239. Sheldrick, G.M., *SHELXT–Integrated space-group and crystal-structure determination.* Foundations of Crystallography, 2015. **71**(1): p. 3-8.
240. Oxford, R., *Diffraction CrysAlisPro Software System.* Rigaku Corporation: Wroclaw, Poland, 2019.
241. Macrae, C.F., et al., *Mercury 4.0: From visualization to analysis, design and prediction.* Applied Crystallography, 2020. **53**(1): p. 226-235.
242. Benzaid, C., et al., *Evaluation of the chemical composition, the antioxidant and antimicrobial activities of mentha× piperita essential oil against microbial growth and biofilm formation.* Journal of Essential Oil Bearing Plants, 2019. **22**(2): p. 335-346.
243. Toty, A.A., et al., *Évaluation in-vitro de l'activité antibactérienne de l'extrait aqueux de l'écorce de tronc de Harungana madagascariensis sur la croissance de souches multi-résistantes.* Bulletin de la société royale des sciences de Liège, 2013.
244. Christensen, G.D., et al., *Adherence of coagulase-negative staphylococci to plastic tissue culture plates: a quantitative model for the adherence of staphylococci to medical devices.* Journal of clinical microbiology, 1985. **22**(6): p. 996-1006.
245. Musk, D.J., D.A. Banko, and P.J. Hergenrother, *Iron salts perturb biofilm formation and disrupt existing biofilms of Pseudomonas aeruginosa.* Chemistry & biology, 2005. **12**(7): p. 789-796.
246. Release, S., *4: LigPrep, version 3.6.* Schrödinger, LLC, New York, NY, 2015.
247. Friesner, R., et al., *Mainz, MP Repasky, EH Knoll, M. Shelley, JK Perry, DE Shaw, P. Francis, PS Shenkin. Glide: A New Approach For Rapid, Accurate Docking And Scoring. 1. Method And Assessment Of Docking Accuracy.* Journal of Medicinal Chemistry, 2004. **47**: p. 1739-1750.
248. Frisch, M., *gaussian 09, Revision d. 01, Gaussian.* Inc, Wallingford CT, 2009. **201**.
249. Rachedi, K.O., et al., *DFT Study, POM analyses and molecular docking of novel oxazaphosphinanes: Identification of antifungal pharmacophore site.* Indonesian journal of chemistry, 2020. **20**(2): p. 440-450.

Appendix: Spectra

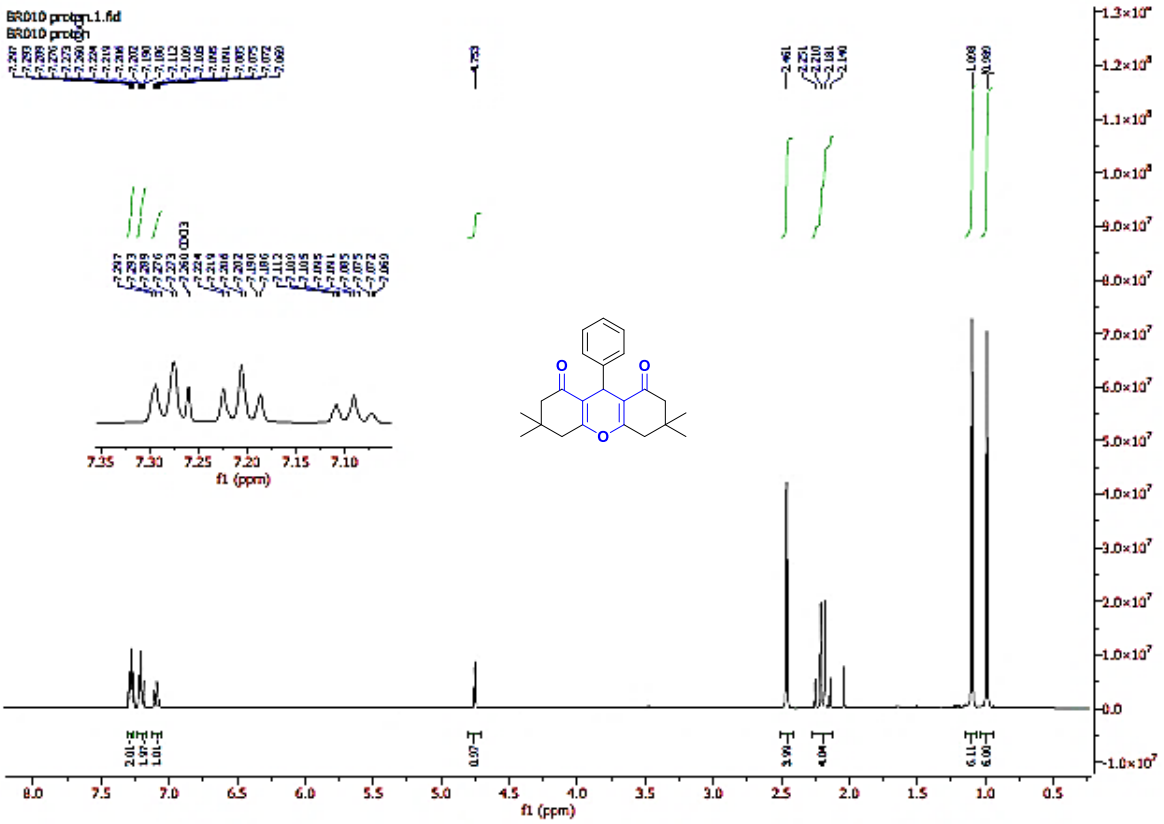

S1.[1]H NMR spectrum: 3,3,6,6-tetramethyl-9-phenyl-3,4,5,6,7,9-hexahydro-1H-xanthene-1,8(2H)-dione **(III.3a)**

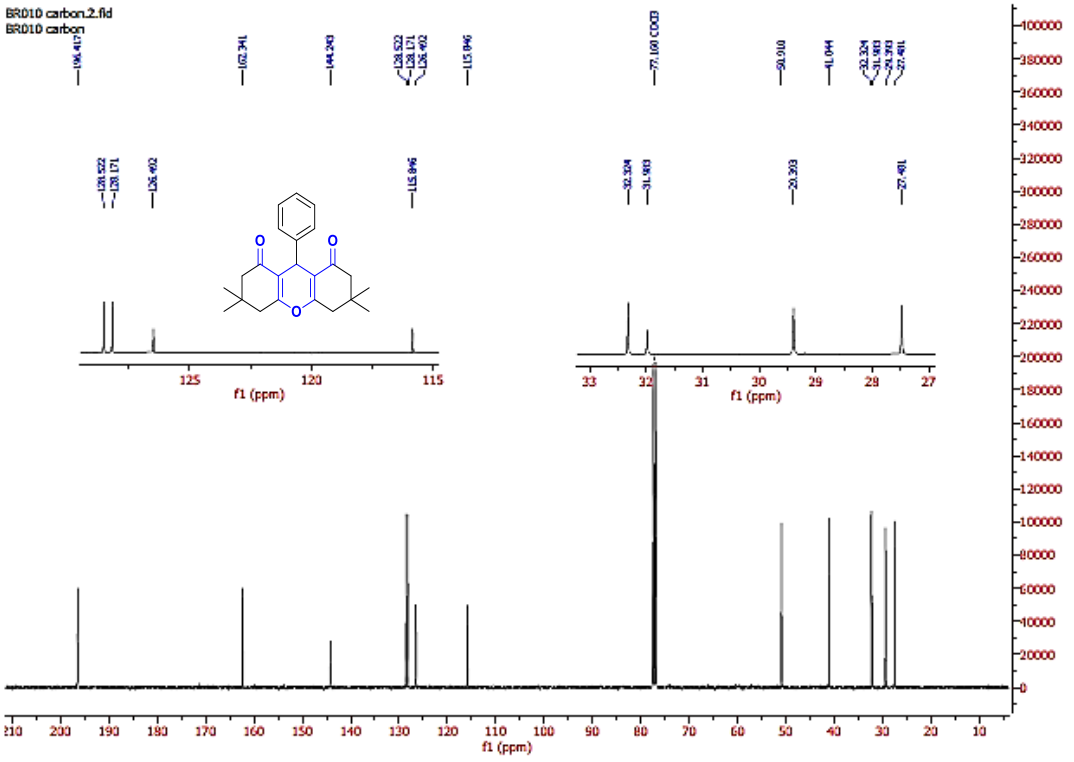

S2.[13]C NMR spectrum: 3,3,6,6-tetramethyl-9-phenyl-3,4,5,6,7,9-hexahydro-1H-xanthene-1,8(2H)-dione **(III.3a)**

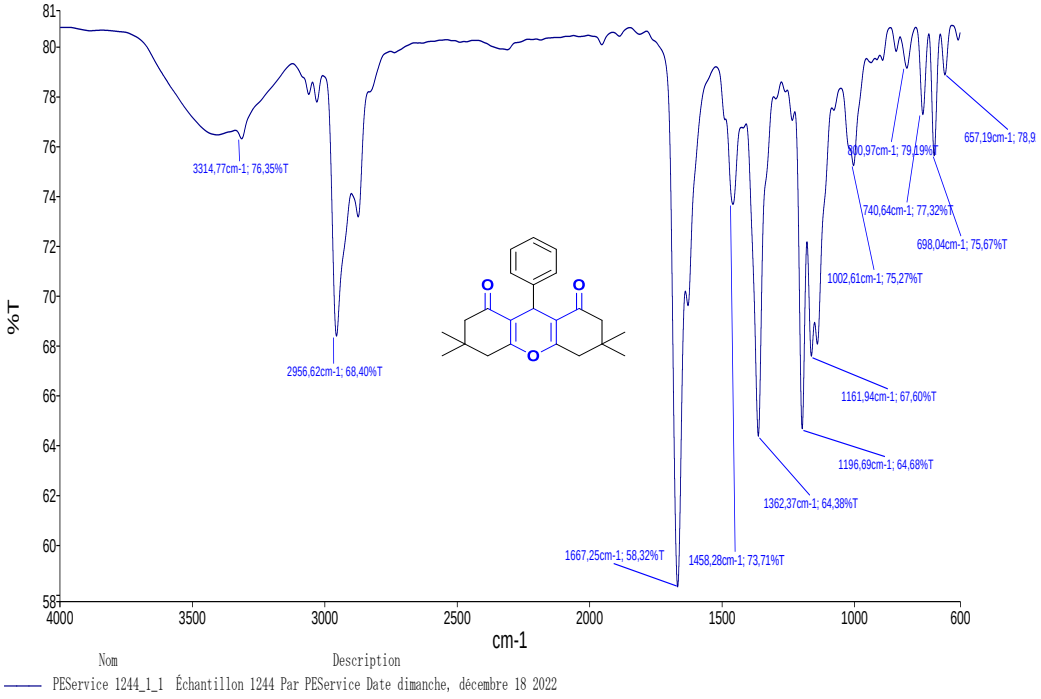

S3.IR spectrum: 3,3,6,6-tetramethyl-9-phenyl-3,4,5,6,7,9-hexahydro-1H-xanthene-1,8(2H)-dione **(III.3a)**

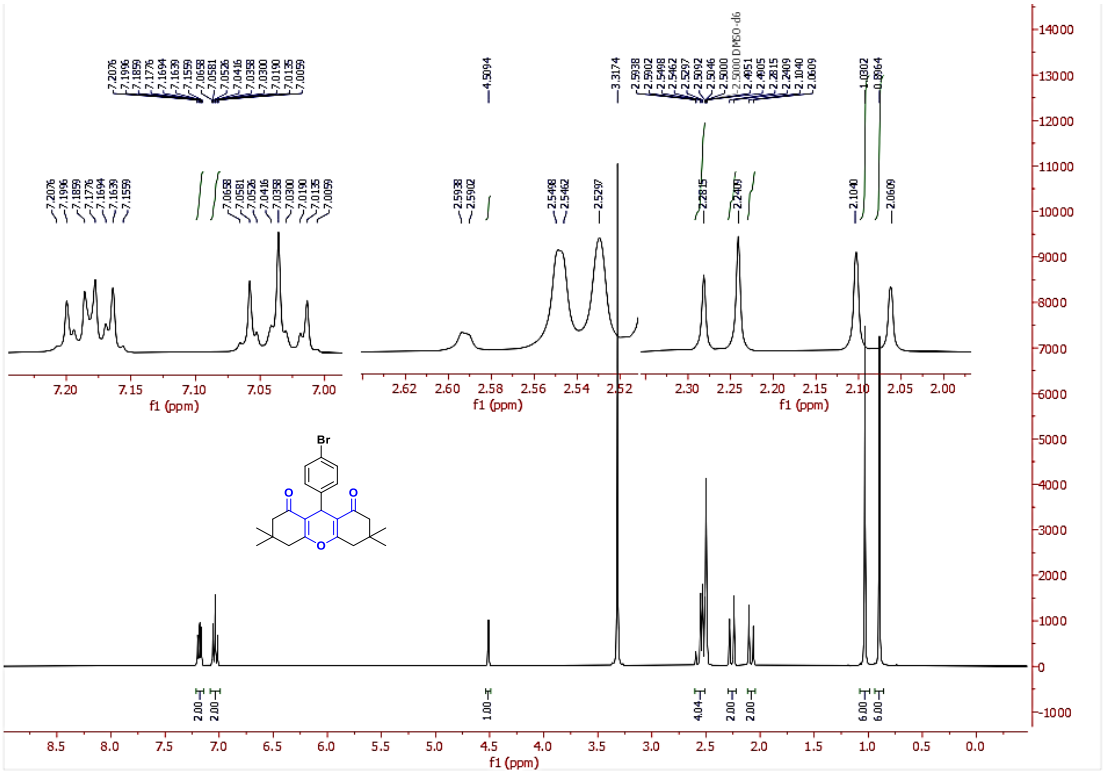

S4.^{1}H NMR spectrum: 9-(4-bromophenyl)-3,3,6,6-tetramethyl-3,4,5,6,7,9-hexahydro-1H-xanthene-1,8(2H)-dione **(III.3b)**

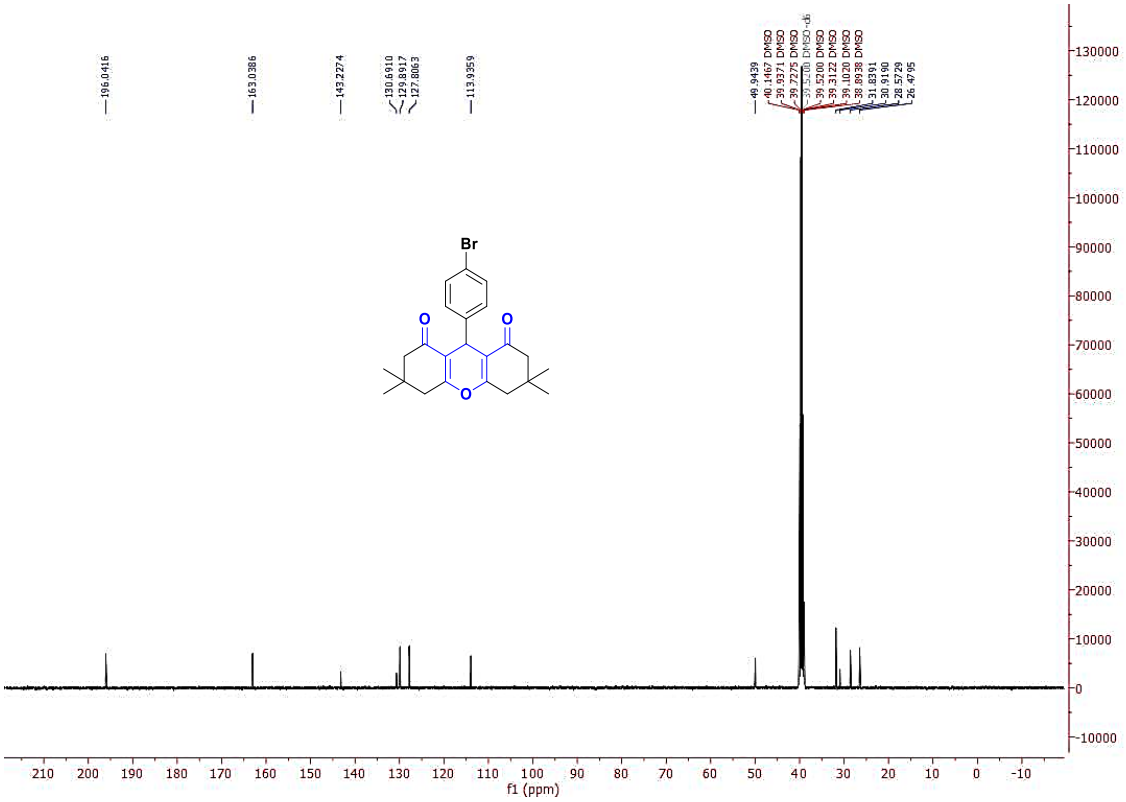

S5.^{13}C NMR spectrum: 9-(4-bromophenyl)-3,3,6,6-tetramethyl-3,4,5,6,7,9-hexahydro-1H-xanthene-1,8(2H)-dione **(III.3b).**

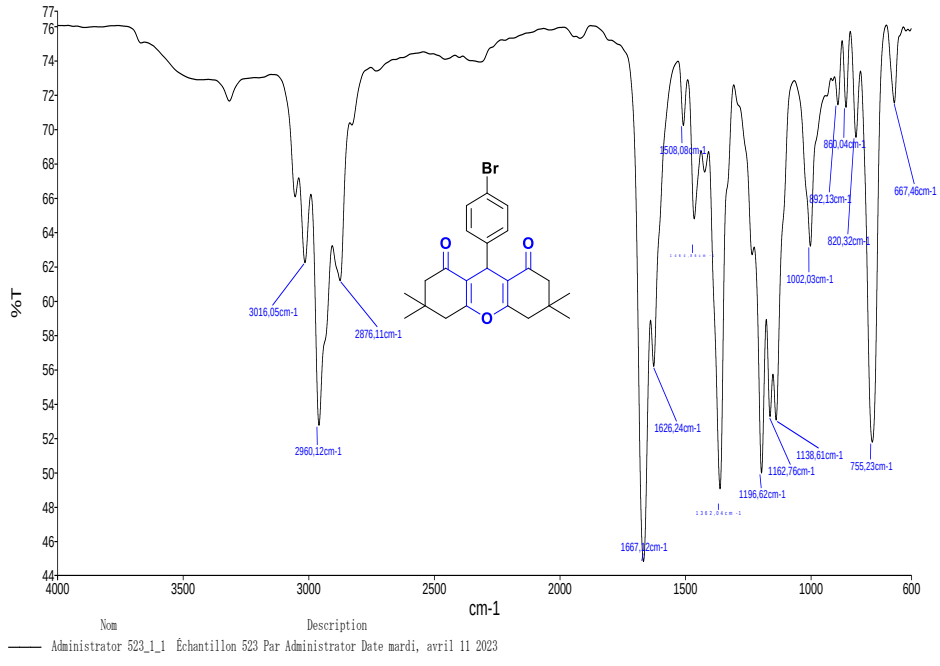

S6.IR spectrum: 9-(4-bromophenyl)-3,3,6,6-tetramethyl-3,4,5,6,7,9-hexahydro-1H-xanthene-1,8(2H)-dione **(III.3b)**

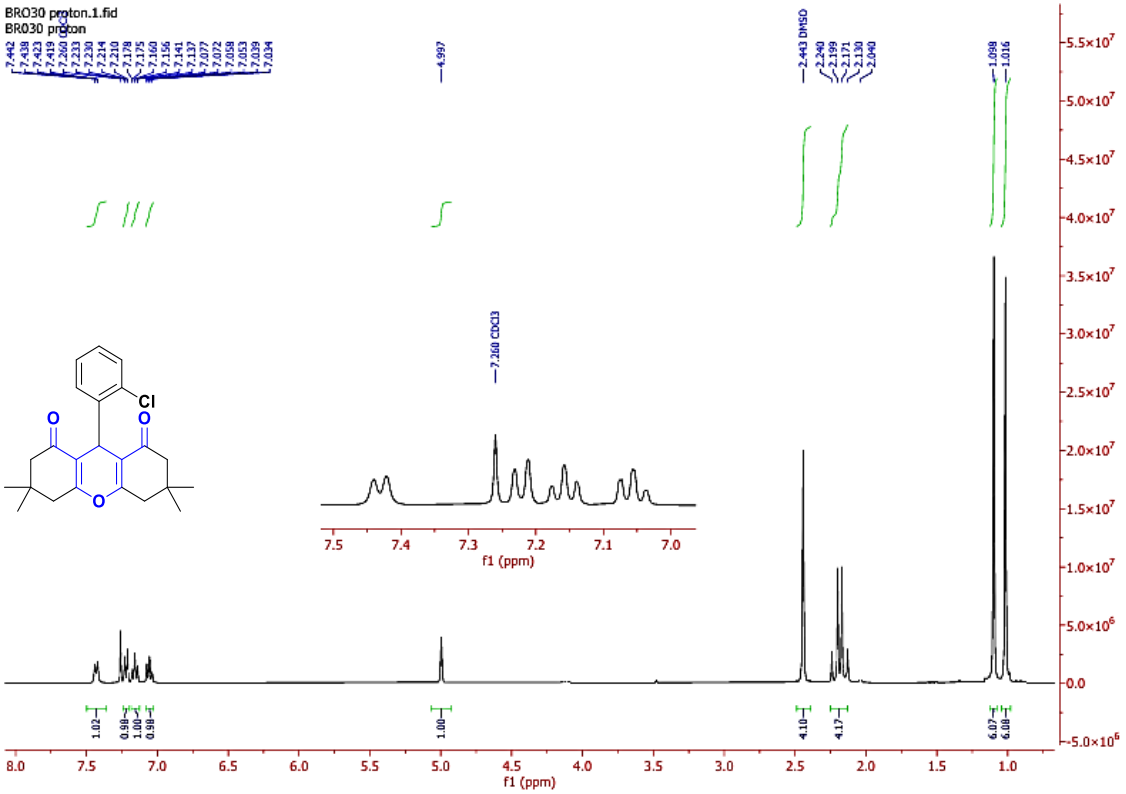

S7. ^{1}H NMR spectrum: 9-(4-chlorophenyl)-3,3,6,6-tetramethyl-3,4,5,6,7,9-hexahydro-1H-xanthene-1,8(2H)-dione (III.3c).

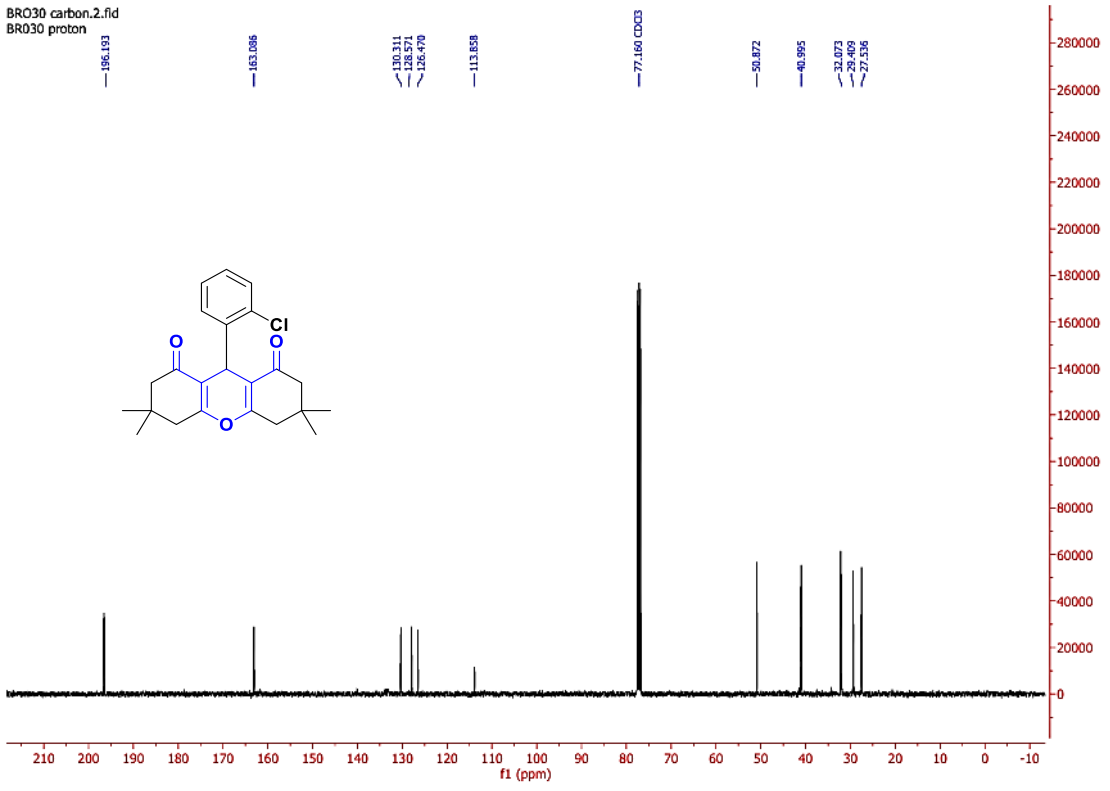

S8. ^{13}C NMR spectrum: 9-(4-chlorophenyl)-3,3,6,6-tetramethyl-3,4,5,6,7,9-hexahydro-1H-xanthene-1,8(2H)-dione **(III.3c)**

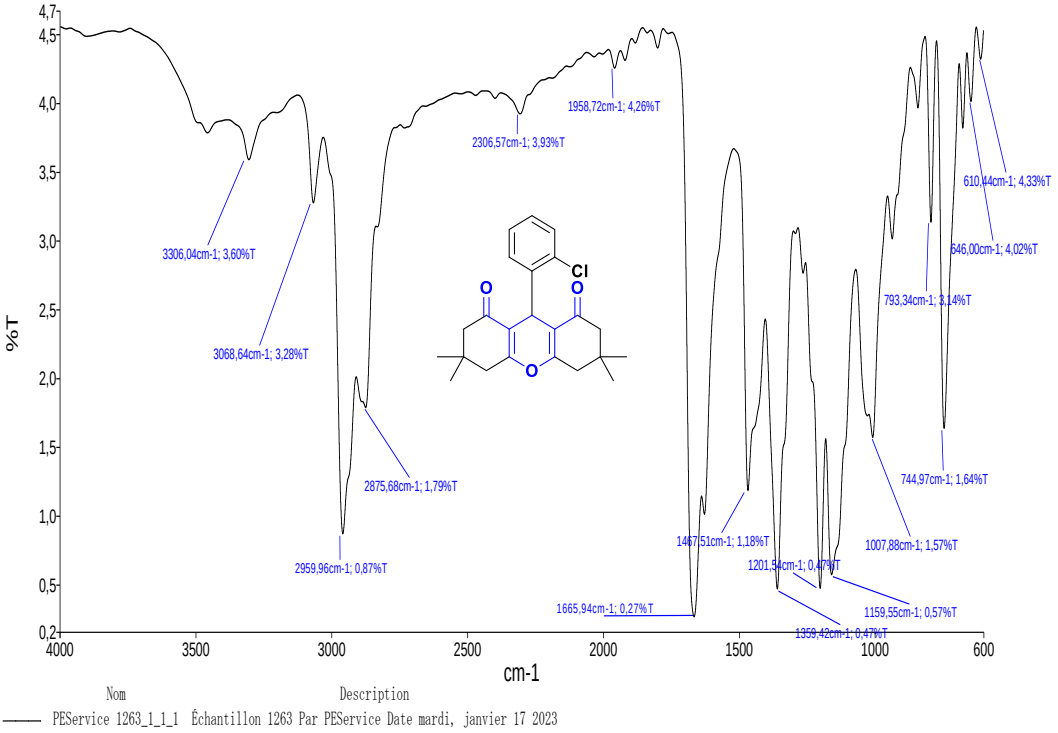

S9.IR spectrum: 9-(4-chlorophenyl)-3,3,6,6-tetramethyl-3,4,5,6,7,9-hexahydro-1H-xanthene-1,8(2H)-dione **(III.3c)**

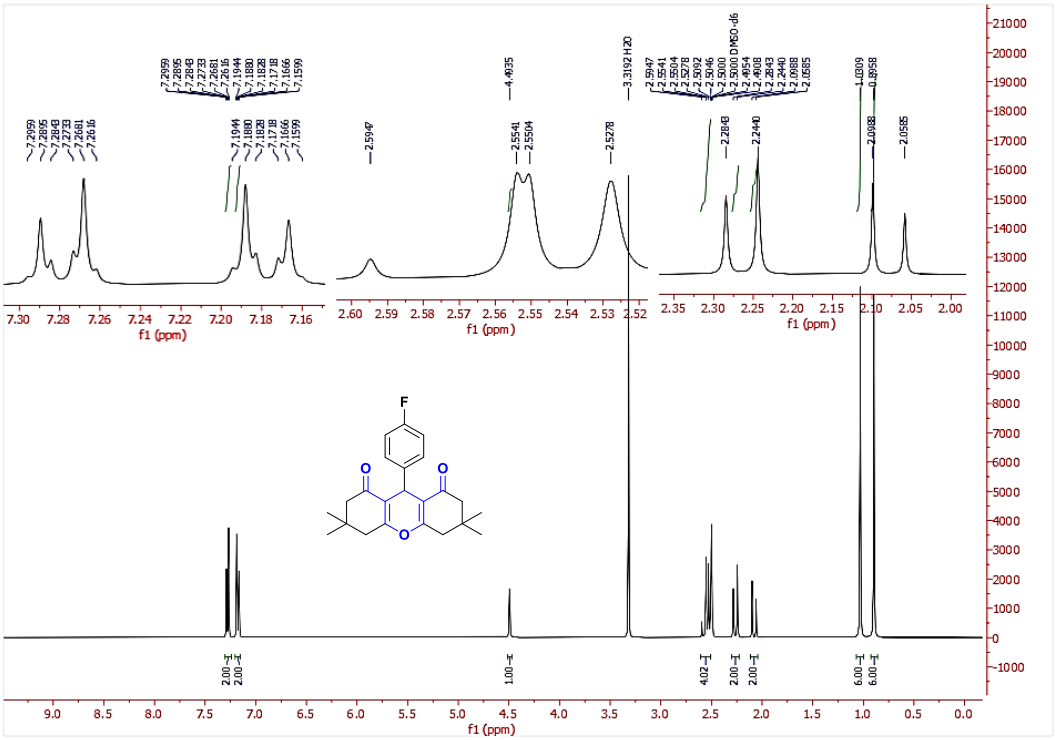

S10.^{1}H NMR spectrum: 9-(4-fluorophenyl)-3,3,6,6-tetrametyl-3,4,5,6,7,9-hexahydro-1H-xanthene-1,8(2H)-dione **(III.3d)**

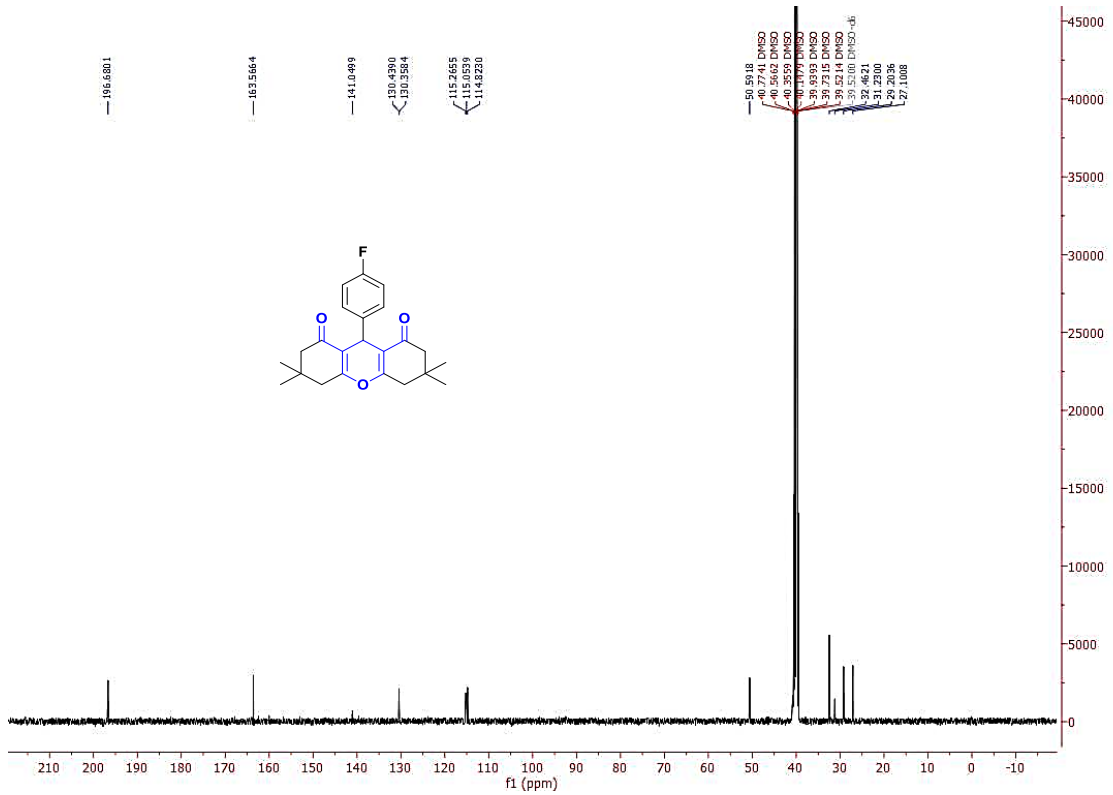

S11.^{13}C NMR spectrum: 9-(4-fluorophenyl)-3,3,6,6-tetrametyl-3,4,5,6,7,9-hexahydro-1H-xanthene-1,8(2H)-dione **(III.3d)**

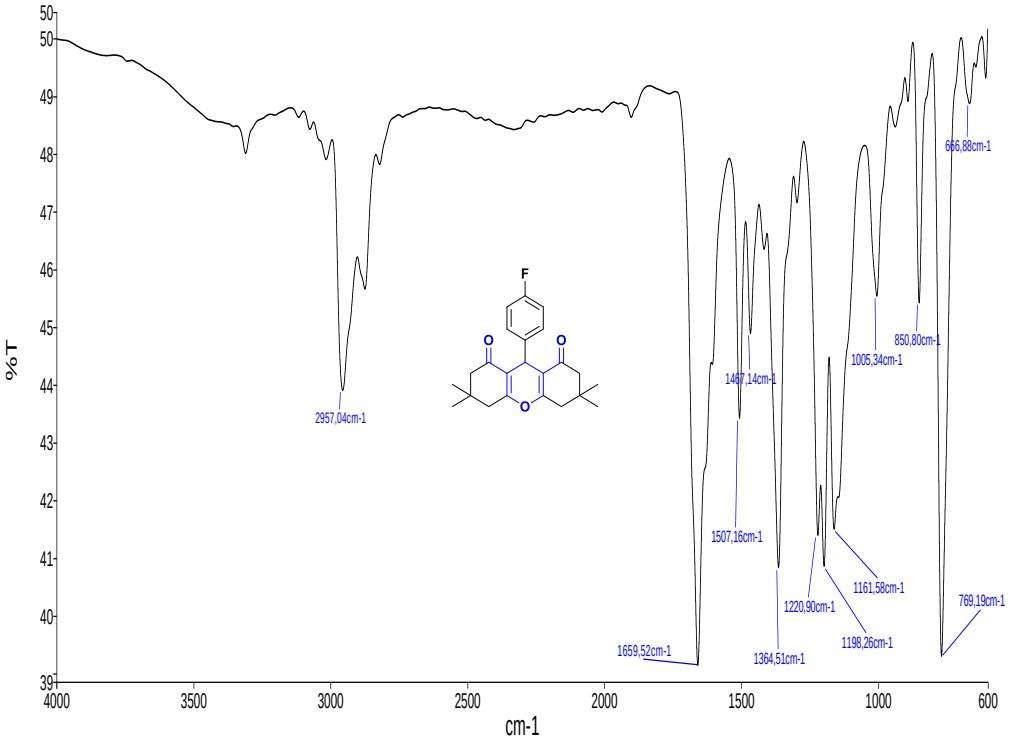

S12.IR spectrum: 9-(4-fluorophenyl)-3,3,6,6-tetrametyl-3,4,5,6,7,9-hexahydro-1H-xanthene-1,8(2H)-dione **(III.3d)**

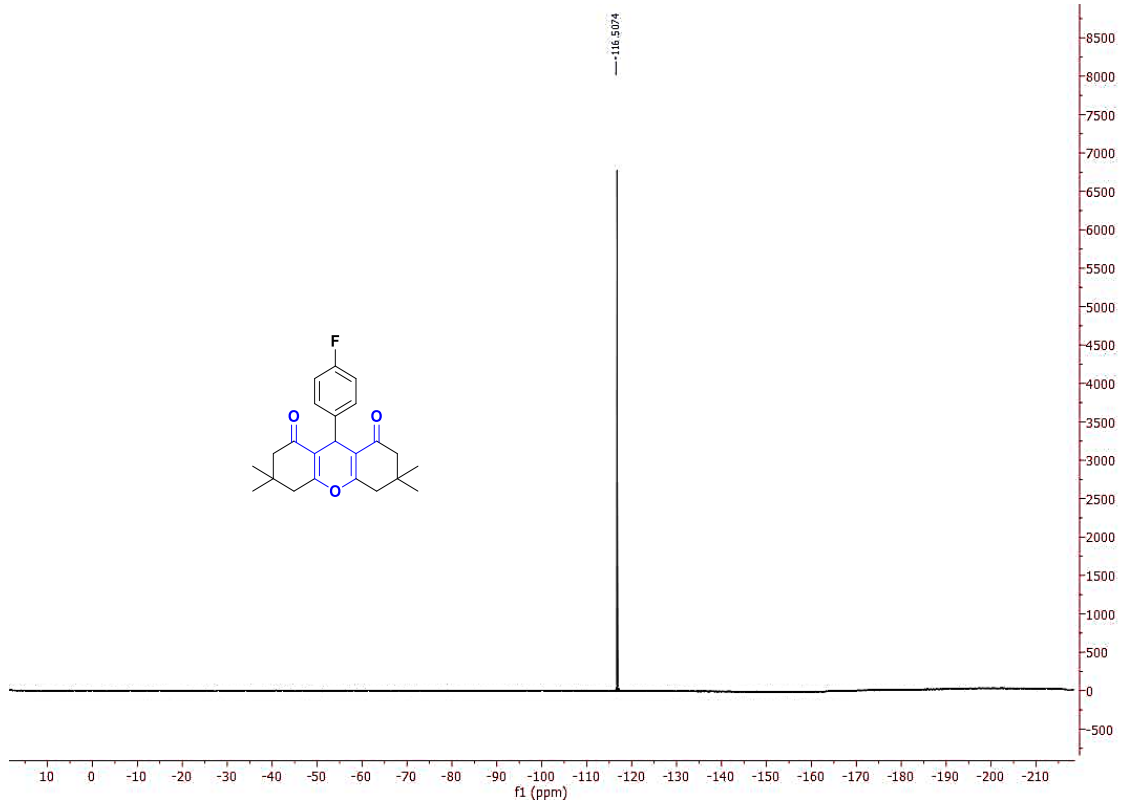

S13.^{19}F spectrum: 9-(4-fluorophenyl)-3,3,6,6-tetrametyl-3,4,5,6,7,9-hexahydro-1H-xanthene-1,8(2H)-dione **(III.3d)**

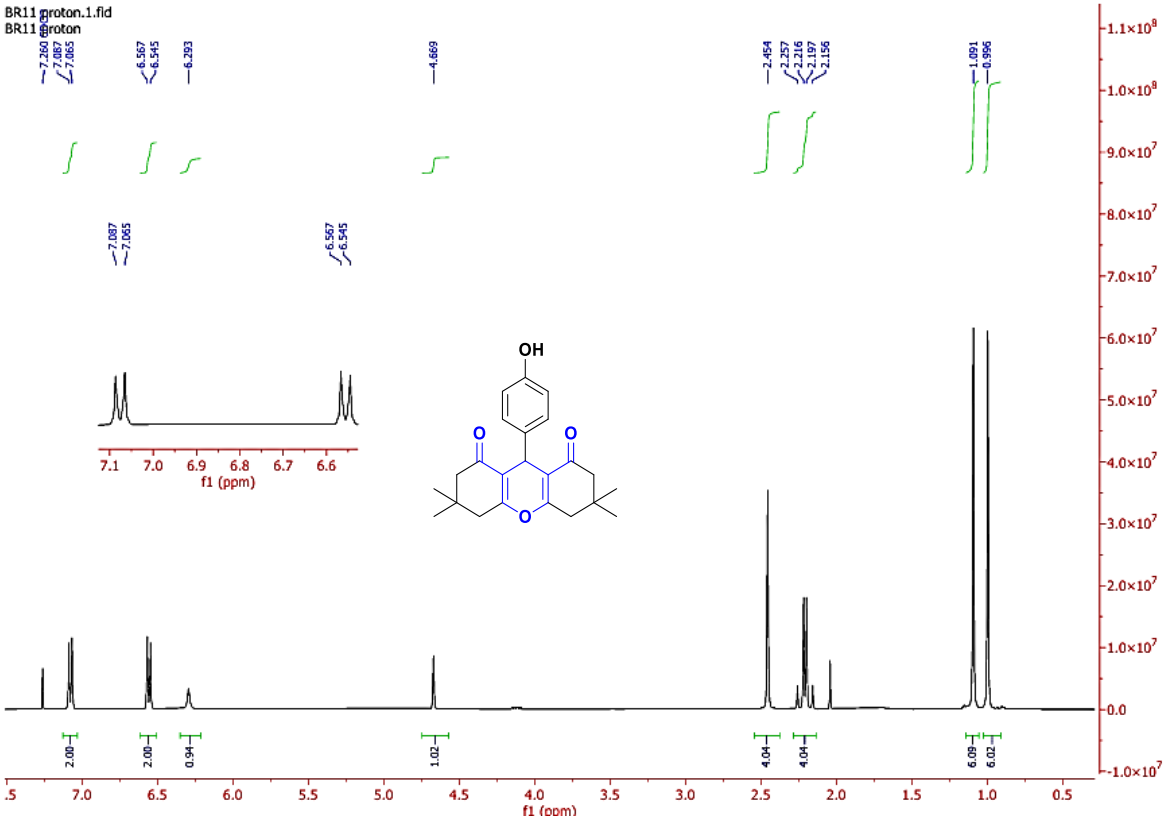

S14.^{1}H NMR spectrum: 9-(4-hydroxyphenyl)-3,3,6,6-tetramethyl-3,4,5,6,7,9-hexahydro-1H-xanthene-1,8(2H)-dione **(III.3e)**

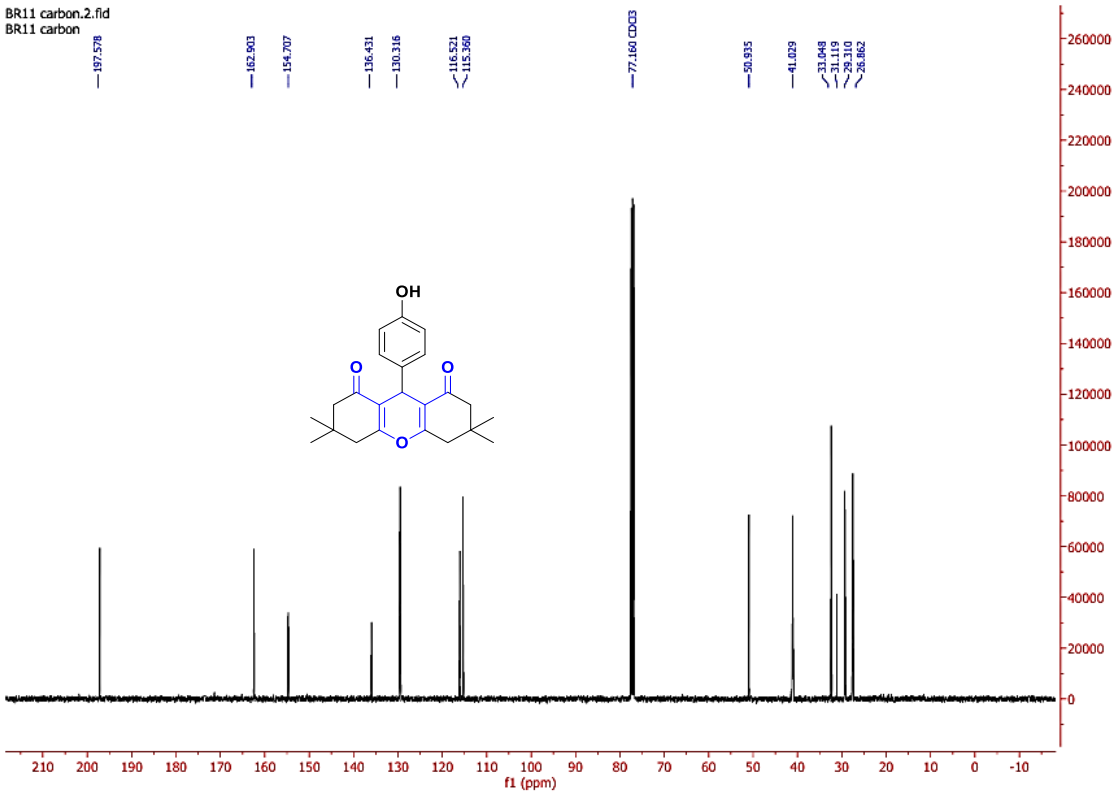

S15.^{13}C NMR spectrum: 9-(4-hydroxyphenyl)-3,3,6,6-tetramethyl-3,4,5,6,7,9-hexahydro-1H-xanthene-1,8(2H)-dione **(III.3e)**

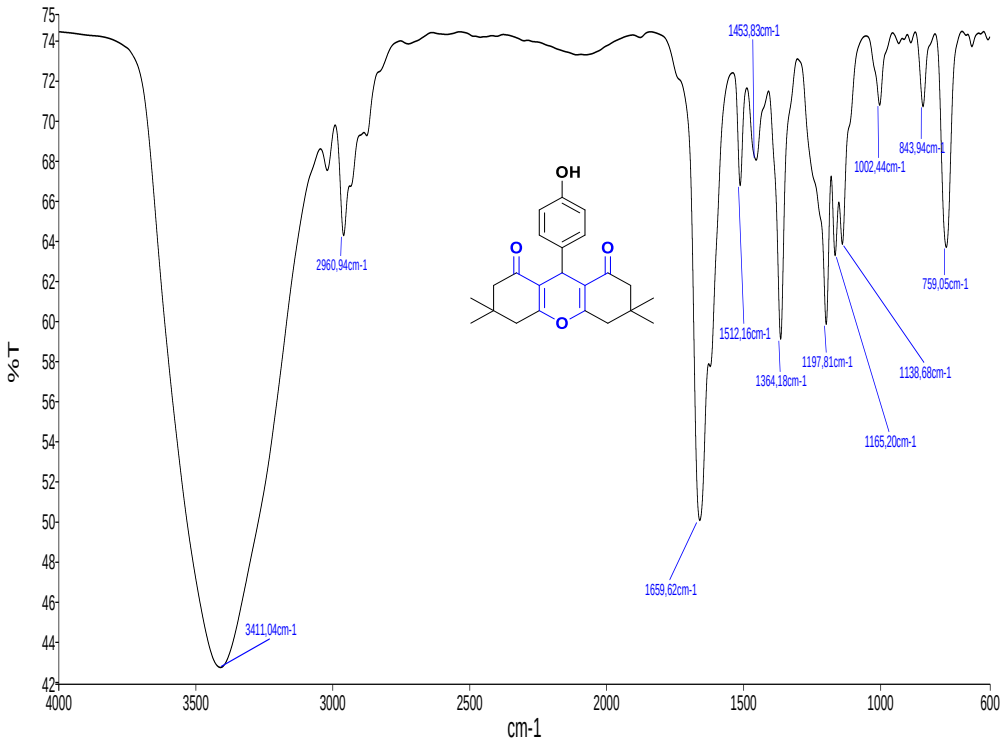

S16.IR spectrum: 9-(4-hydroxyphenyl)-3,3,6,6-tetramethyl-3,4,5,6,7,9-hexahydro-1H-xanthene-1,8(2H)-dione **(III.3e)**

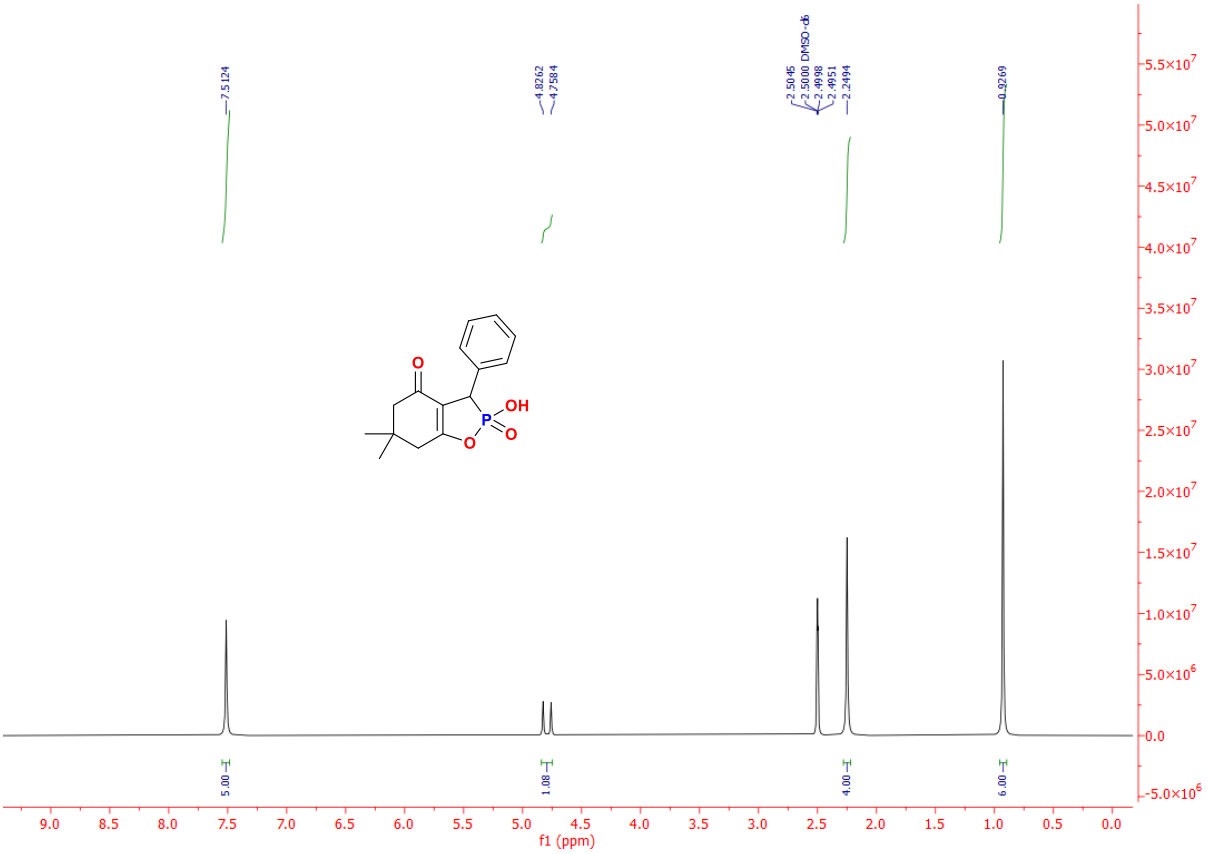

S17. [1]HNMR spectrum: 2-hydroxy-6,6-dimethyl-3-phenyl-3,6,7-trihydrobenzo[1,2]oxaphosphol-4(5H)-one 2-oxide **(III.5a).**

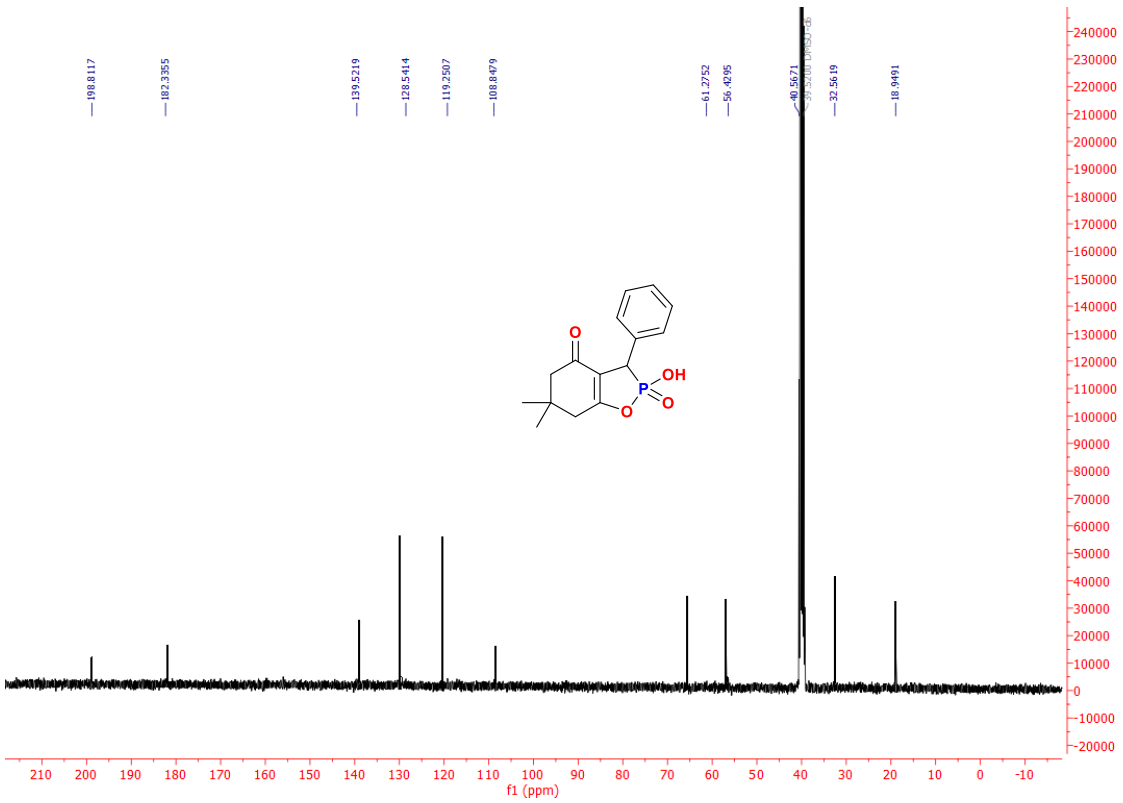

S18. [13]C NMR spectrum: 2-hydroxy-6,6-dimethyl-3-phenyl-3,6,7-trihydrobenzo [1,2]oxaphosphol-4(5H)-one 2-oxide **(III.5a).**

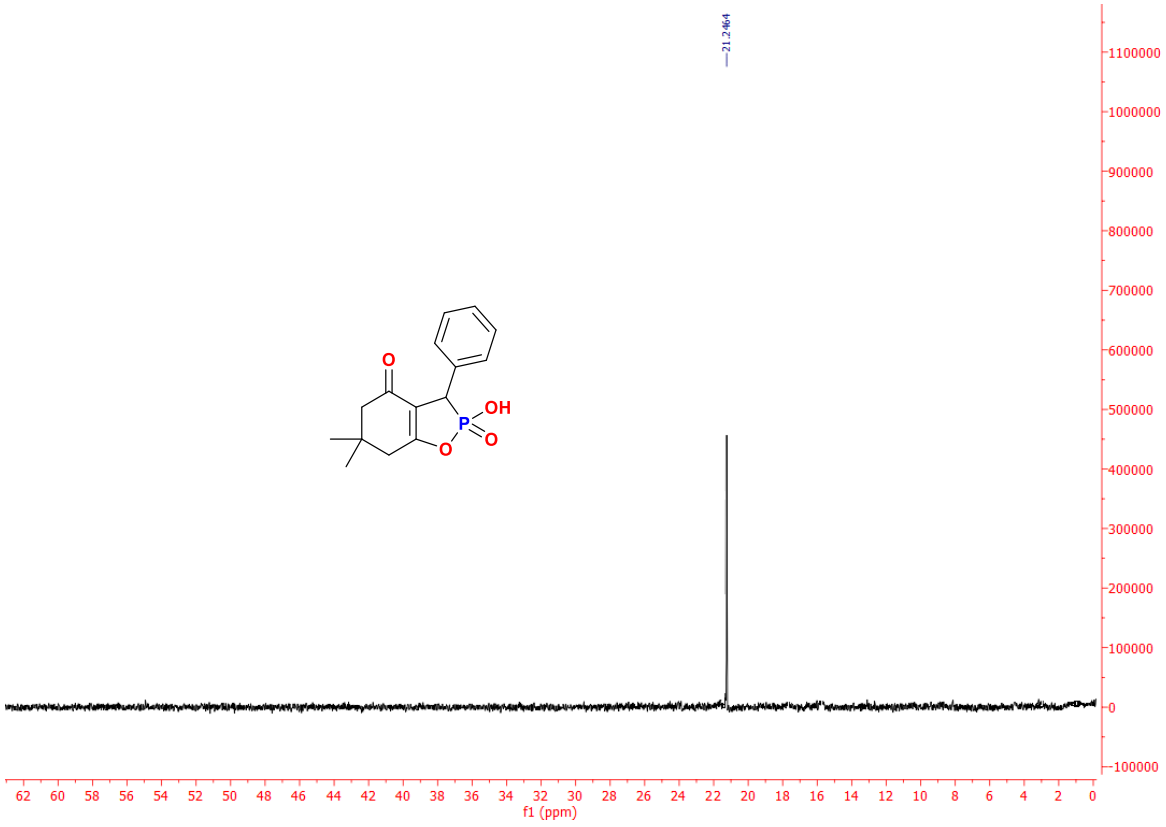

S19. ^{31}P NMR spectrum: 2-hydroxy-6,6-dimethyl-3-phenyl-3,6,7-trihydrobenzo [1,2]oxaphosphol-4(5H)-one 2-oxide **(III.5a)**

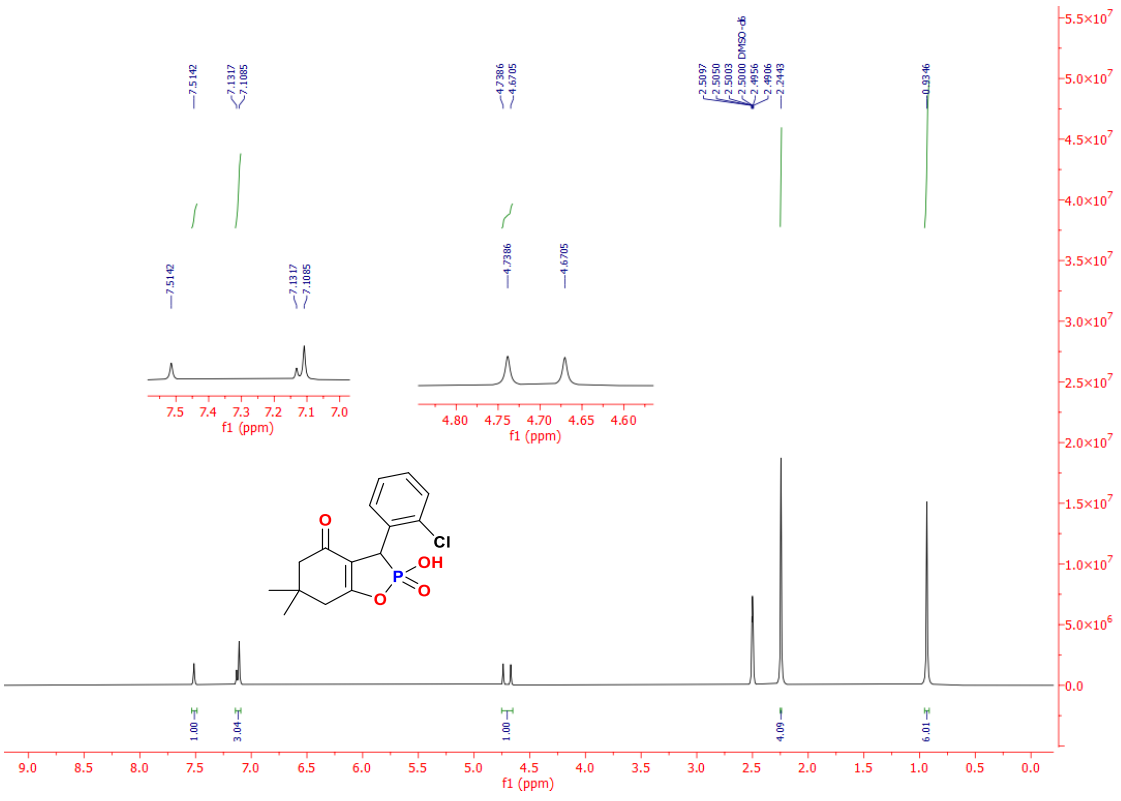

S20.^{1}H NMR spectrum: 3-(2-chlorophenyl)-2-hydroxy-6,6-dimethyl-3,6,7-trihydrobenzo[1,2]oxaphosphol-4(5H)-one 2-oxide **(III.5b)**.

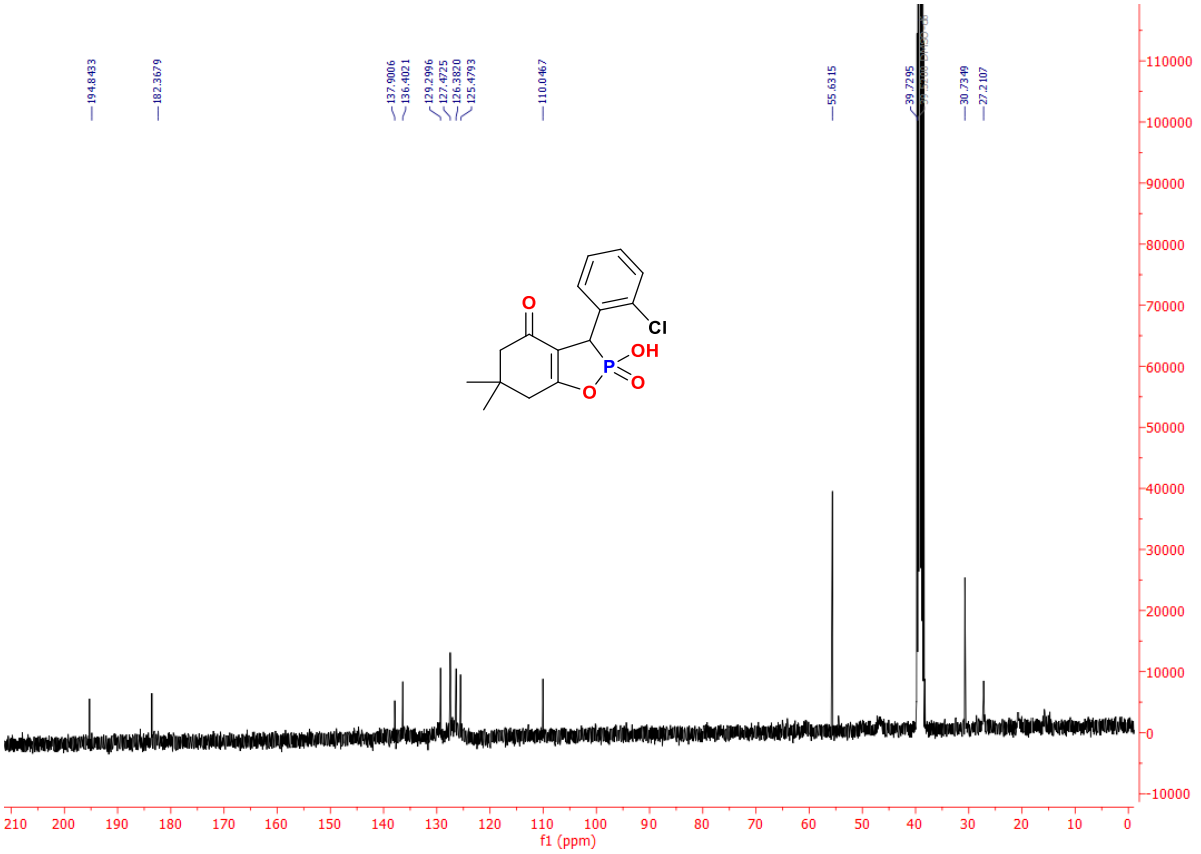

S21.[13]C NMR spectrum: 3-(2-chlorophenyl)-2-hydroxy-6,6-dimethyl-3,6,7-trihydrobenzo [1,2]oxaphosphol-4(5H)-one 2-oxide **(III.5b)**.

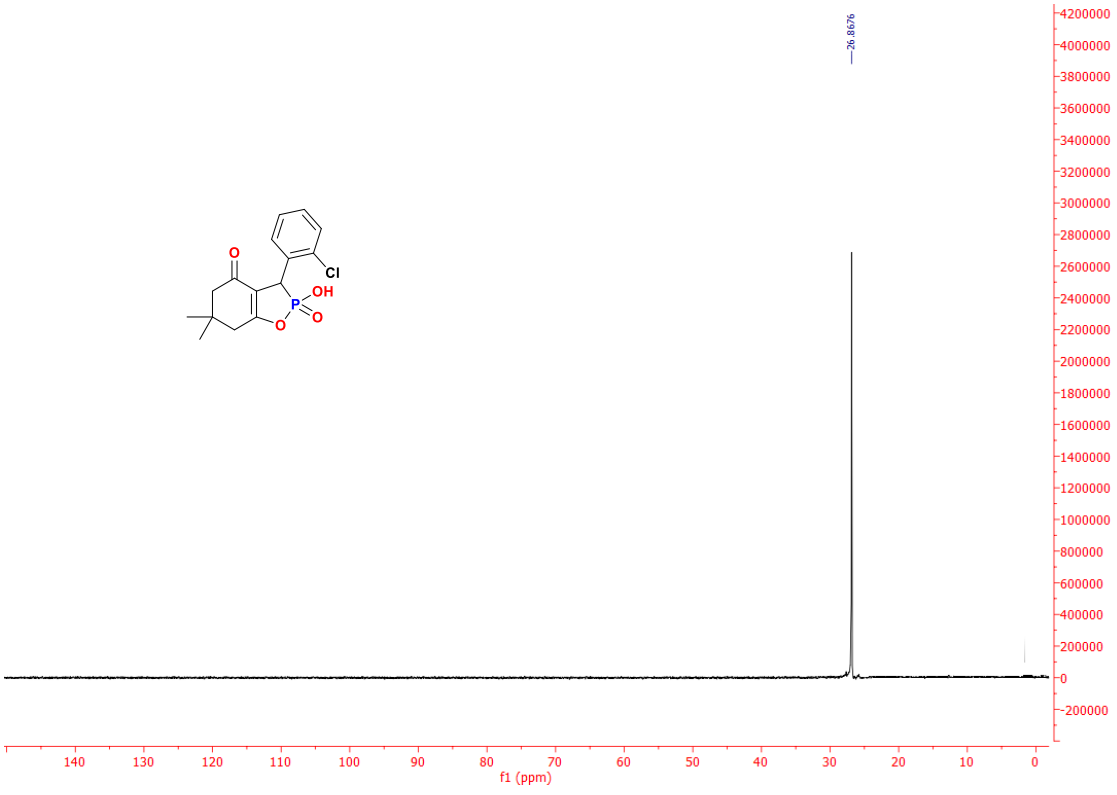

S22. [31]P NMR spectrum: 3-(2-chlorophenyl)-2-hydroxy-6,6-dimethyl-3,6,7-trihydrobenzo [1,2]oxaphosphol-4(5H)-one 2-oxide **(III.5b)**.

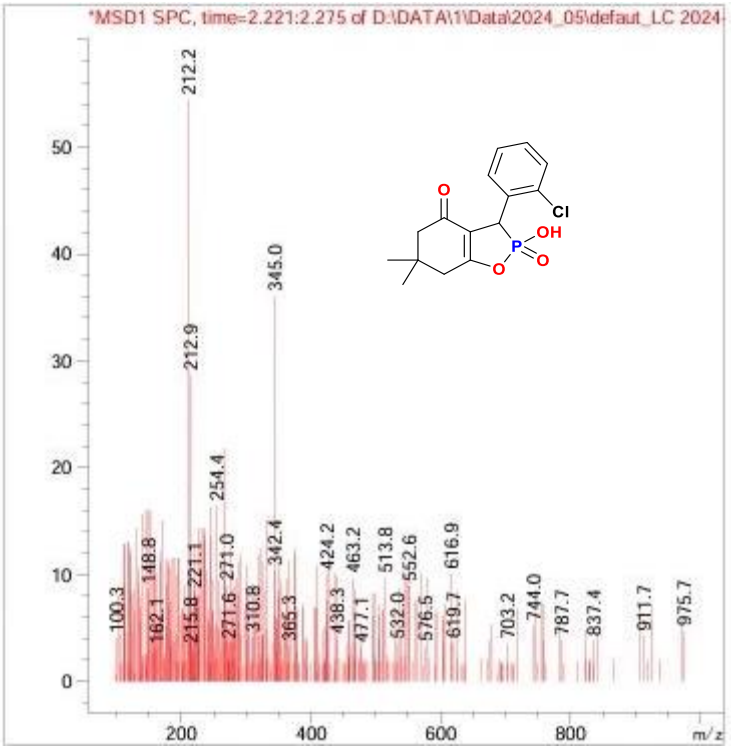

S23. Mass spectrum: 3-(2-chlorophenyl)-2-hydroxy-6,6-dimethyl-3,6,7-trihydrobenzo [1,2]oxaphosphol-4(5H)-one 2-oxide **(III.5b)**.

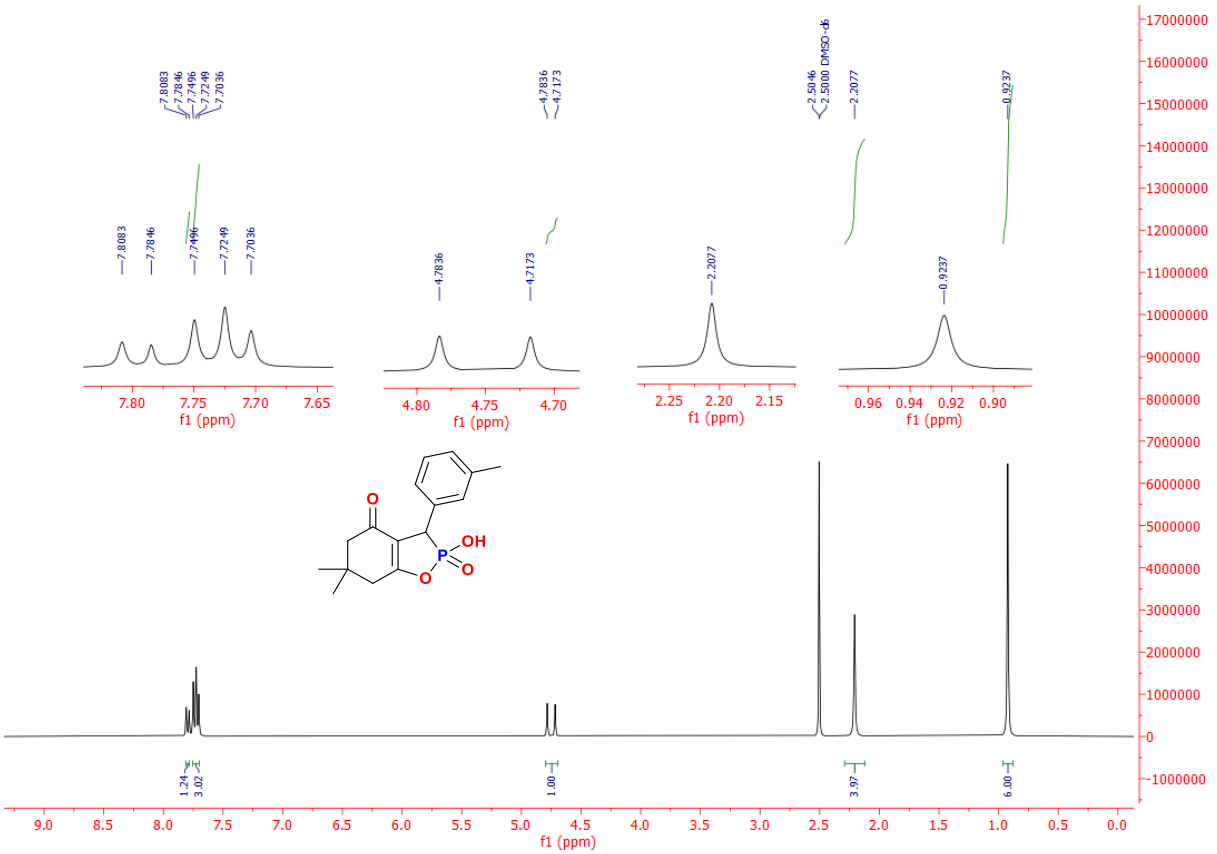

S24.[1]HNMR spectrum: 2-hydroxy-6,6-dimethyl-3-(m-tolyl)-3,6,7-trihydrobenzo [1,2] oxaphosphol-4(5H)-one 2-oxide **(III.5c).**

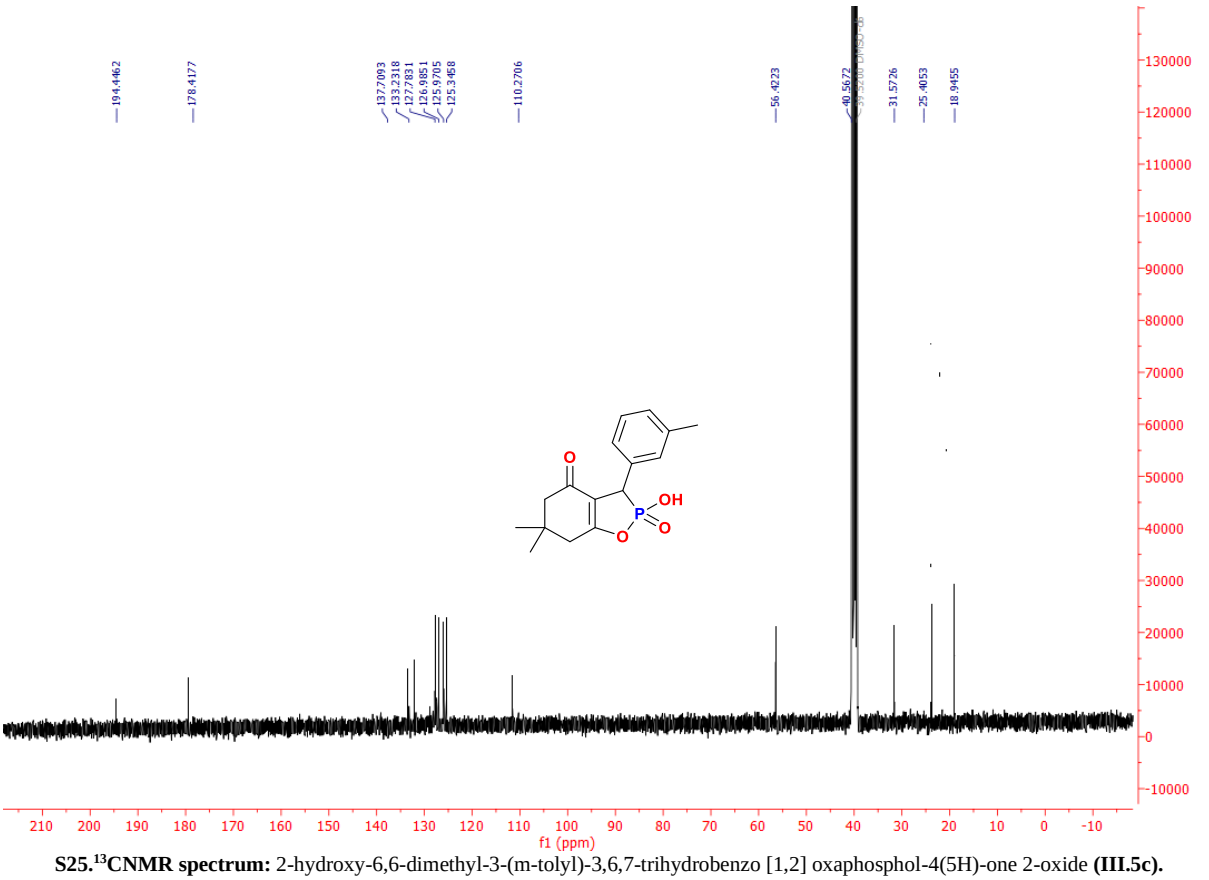

S25.[13]CNMR spectrum: 2-hydroxy-6,6-dimethyl-3-(m-tolyl)-3,6,7-trihydrobenzo [1,2] oxaphosphol-4(5H)-one 2-oxide **(III.5c).**

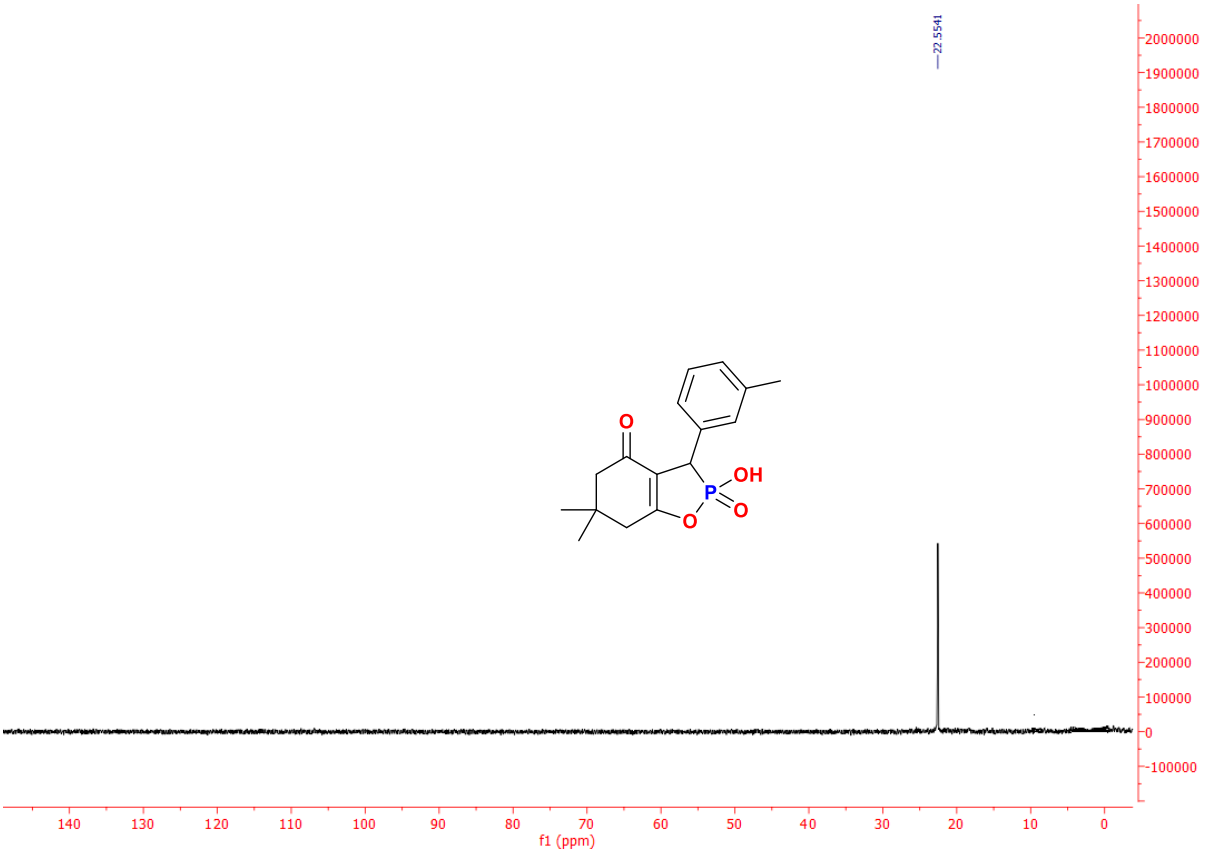

S26. [31]PNMR spectrum: 2-hydroxy-6,6-dimethyl-3-(m-tolyl)-3,6,7-trihydrobenzo [1,2] oxaphosphol-4(5H)-one 2-oxide **(III.5c).**

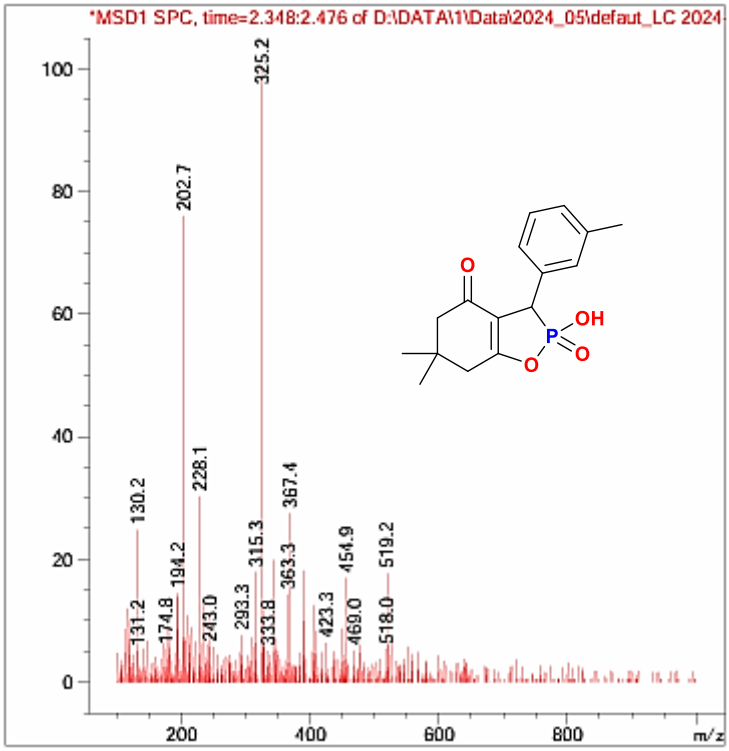

S27. Mass spectrum: 2-hydroxy-6,6-dimethyl-3-(m-tolyl)-3,6,7-trihydrobenzo [1,2] oxaphosphol-4(5H)-one 2-oxide **III.5c).**

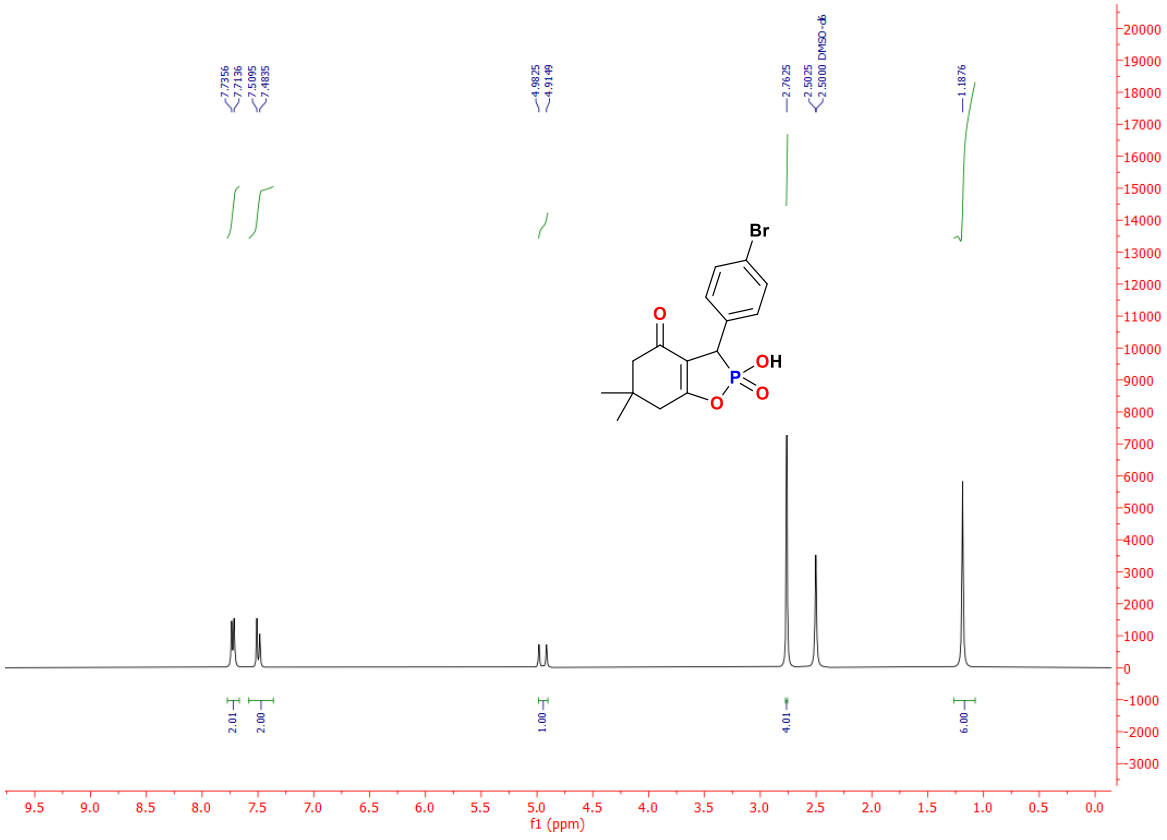

S28. ^{1}HNMR spectrum: 3-(4-bromophenyl)-2-hydroxy-6,6-dimethyl-3,6,7-trihydrobenzo[1,2]oxaphosphol-4(5H)-one 2-oxide**(III.5e).**

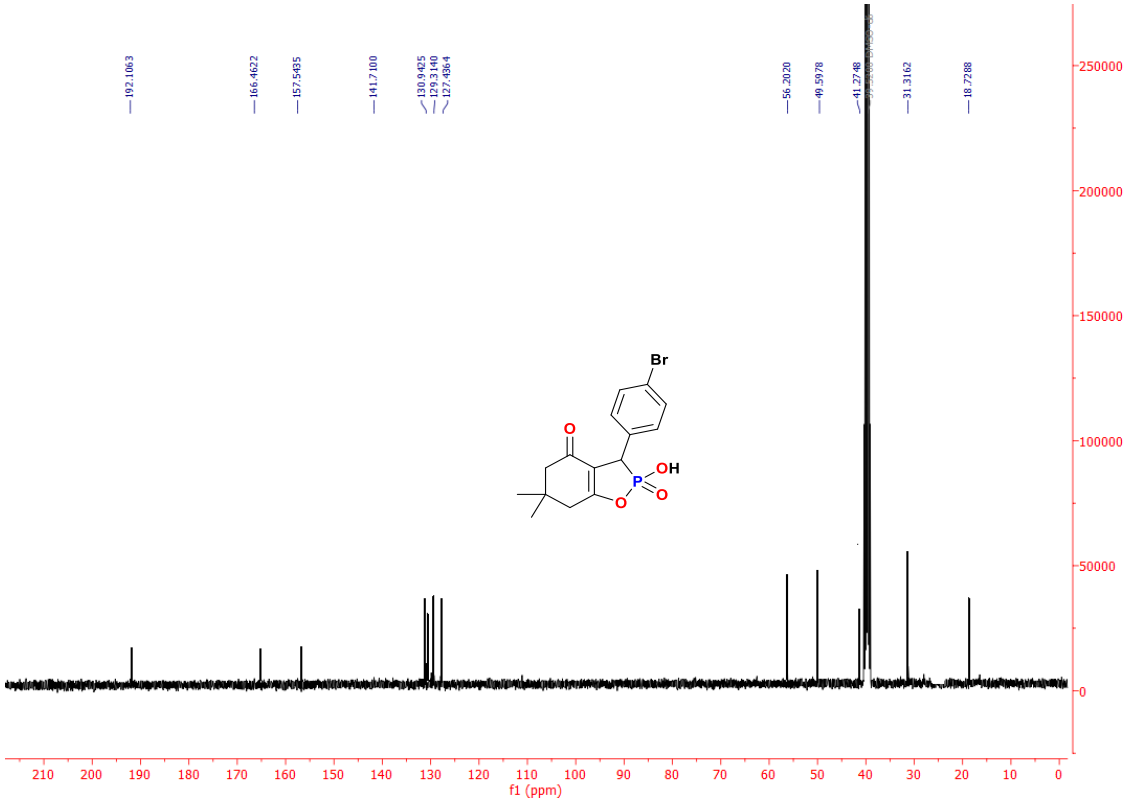

S29. ^{13}CNMR spectrum: 3-(4-bromophenyl)-2-hydroxy-6,6-dimethyl-3,6,7-trihydrobenzo[1,2]oxaphosphol-4(5H)-one 2-oxide**(III.5e).**

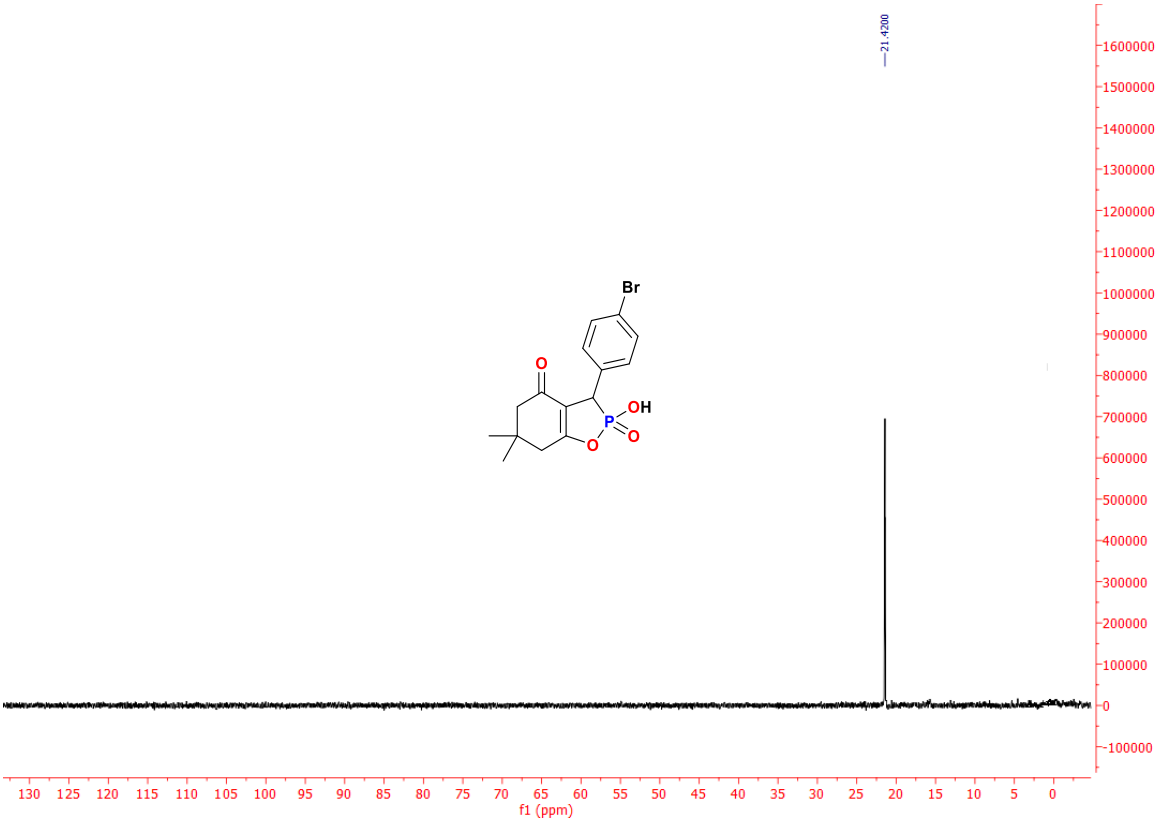

S30. ^{31}PNMR spectrum: 3-(4-bromophenyl)-2-hydroxy-6,6-dimethyl-3,6,7-trihydrobenzo[1,2]oxaphosphol-4(5H)-one 2-oxide**(III.5e).**

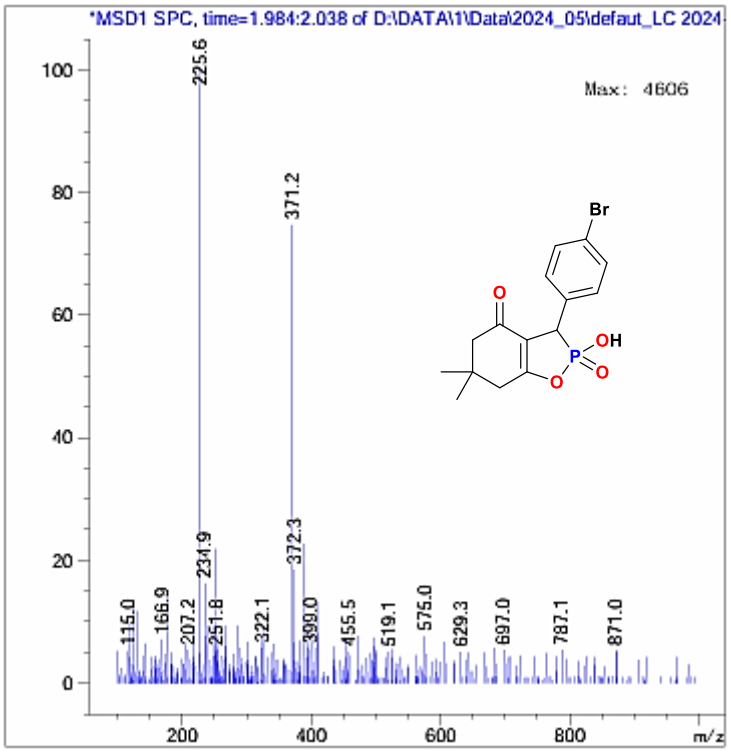

S31. Mass spectrum: 3-(4-bromophenyl)-2-hydroxy-6,6-dimethyl-3,6,7-trihydrobenzo[1,2]oxaphosphol-4(5H)-one 2-oxide**(III.5e).**

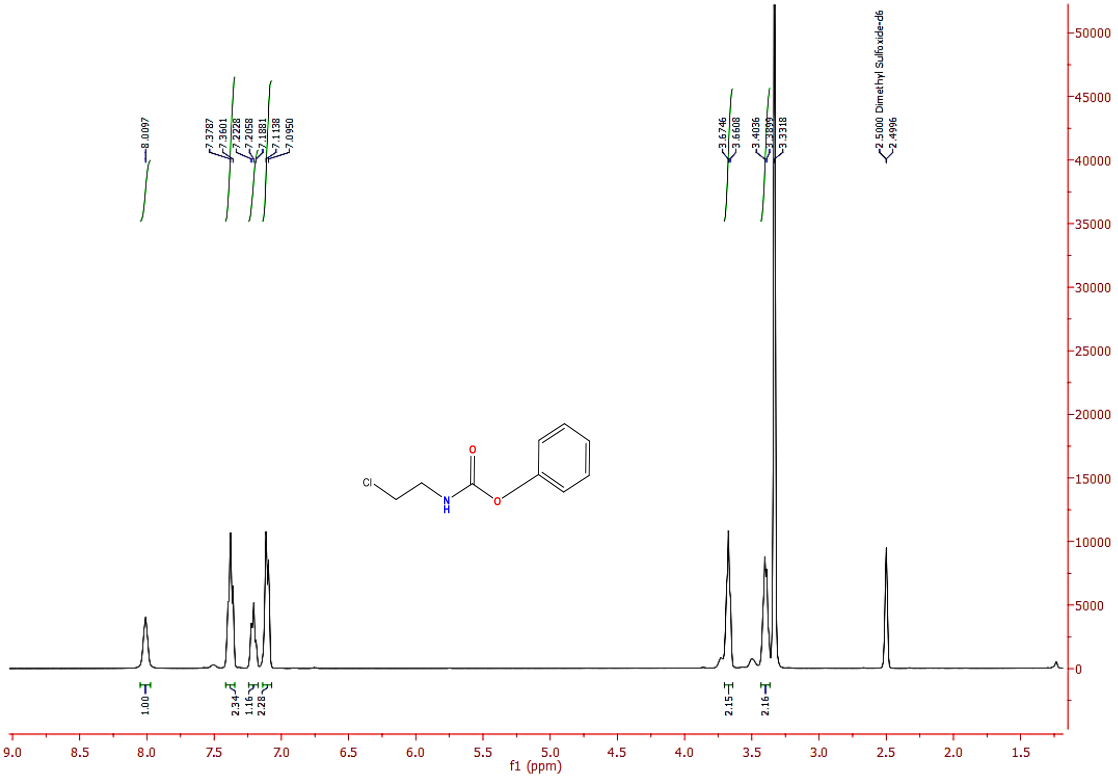

S32. ^{1}H NMR spectrum: Phenyl (2-chloroethyl) carbamate **(III.8a)**

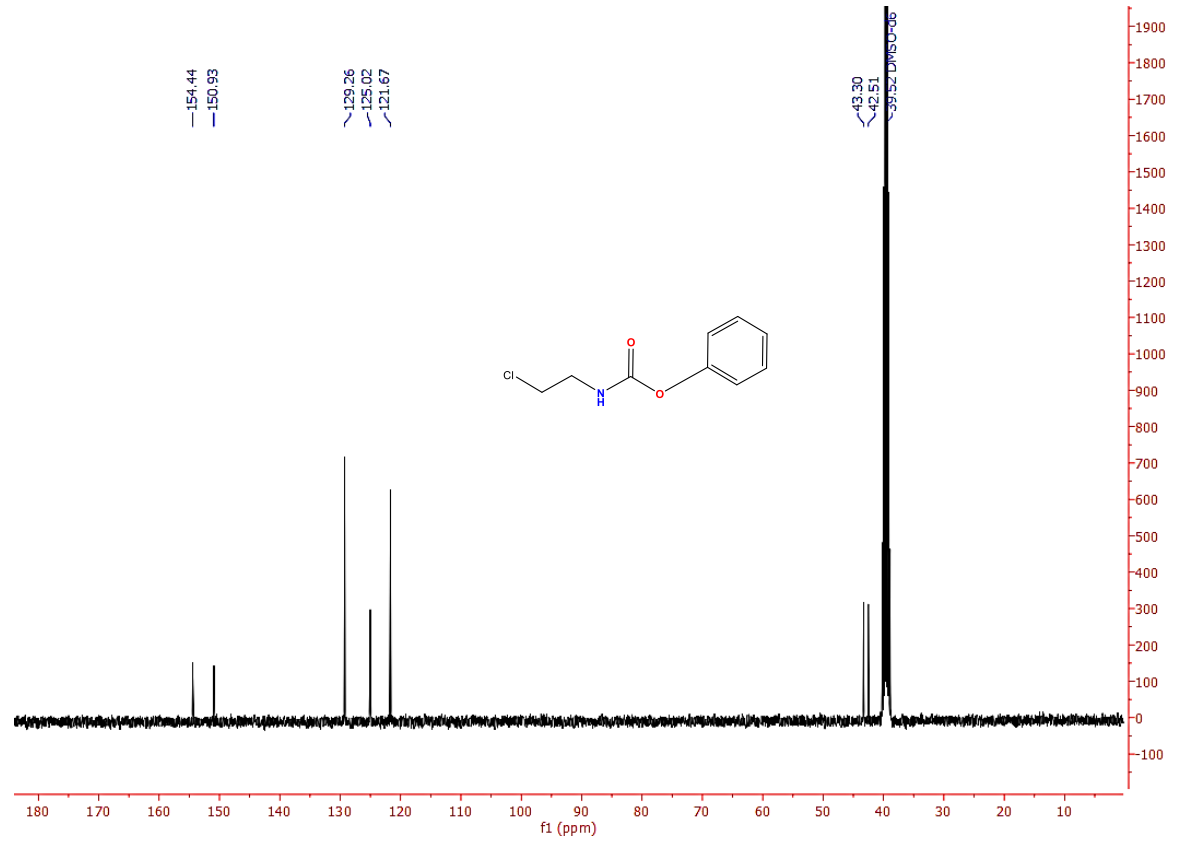

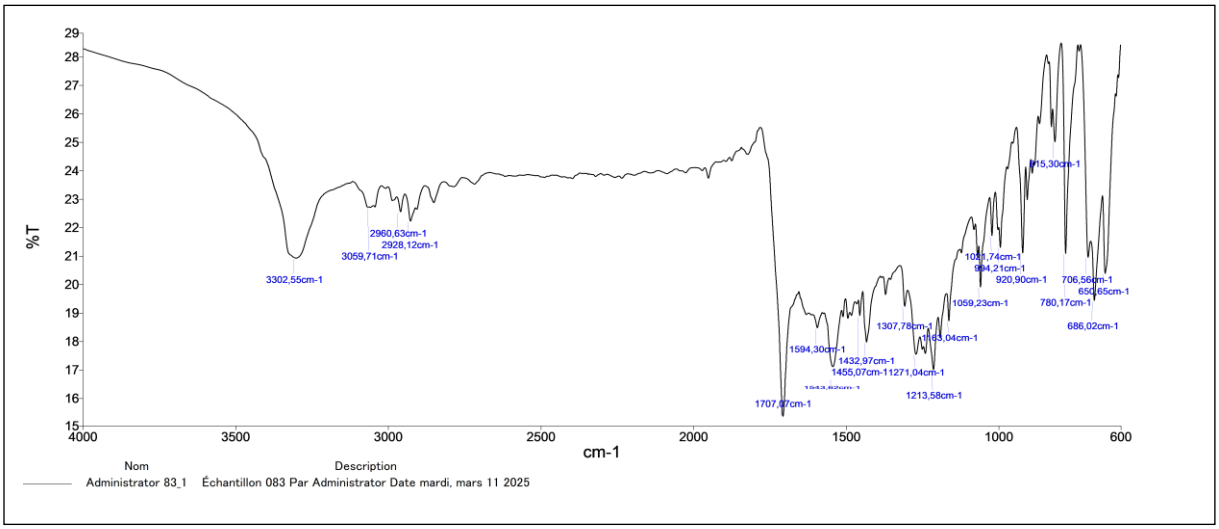

S33. ^{13}C NMR spectrum: Phenyl (2-chloroethyl)carbamate **(III.8a)**

S34. IR spectrum: Phenyl (2-chloroethyl)carbamate **(III.8a)**

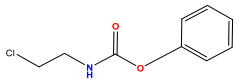

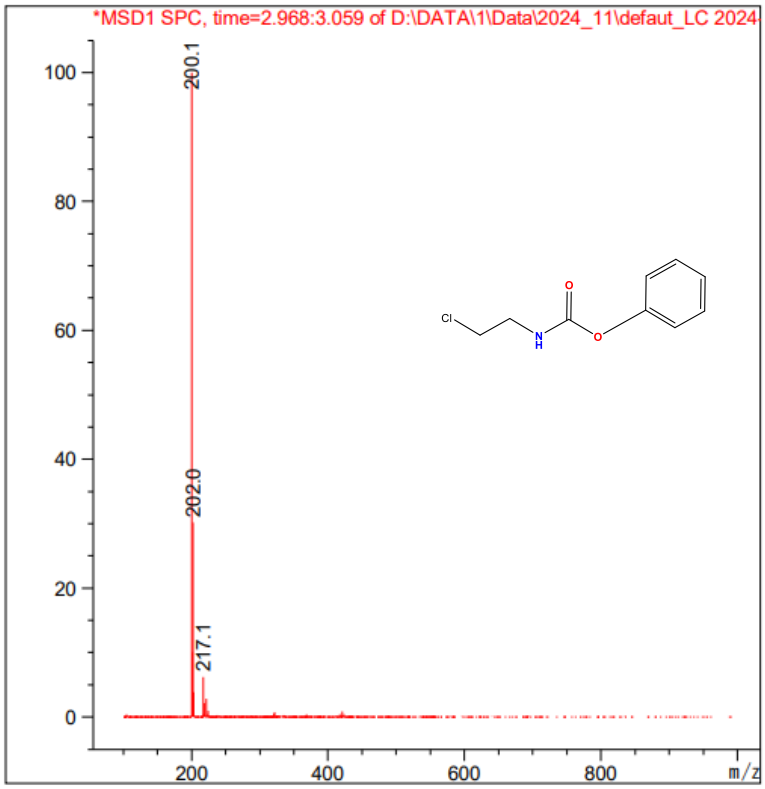

S35. Mass spectrum: Phenyl (2-chloroethyl) carbamate **(III.8a)**

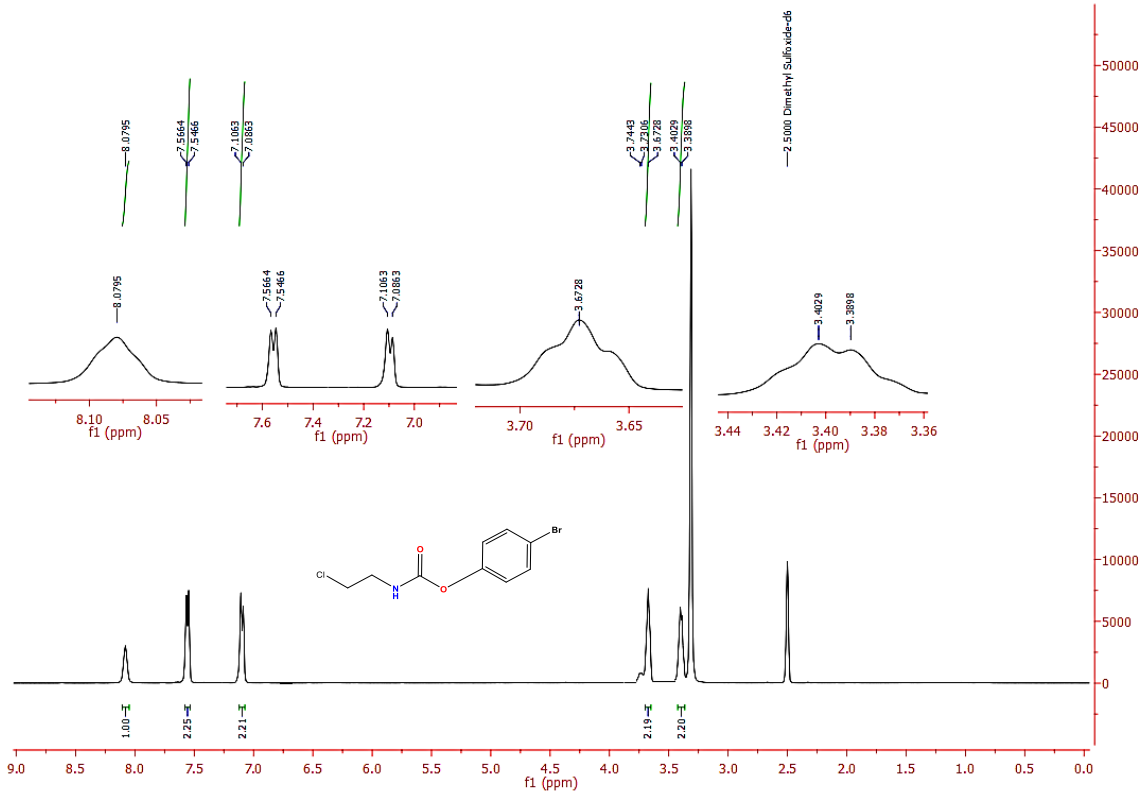

S36.^{1}H NMR spectrum: 4-bromophenyl (2-chloroethyl) carbamate **(III.8b)**

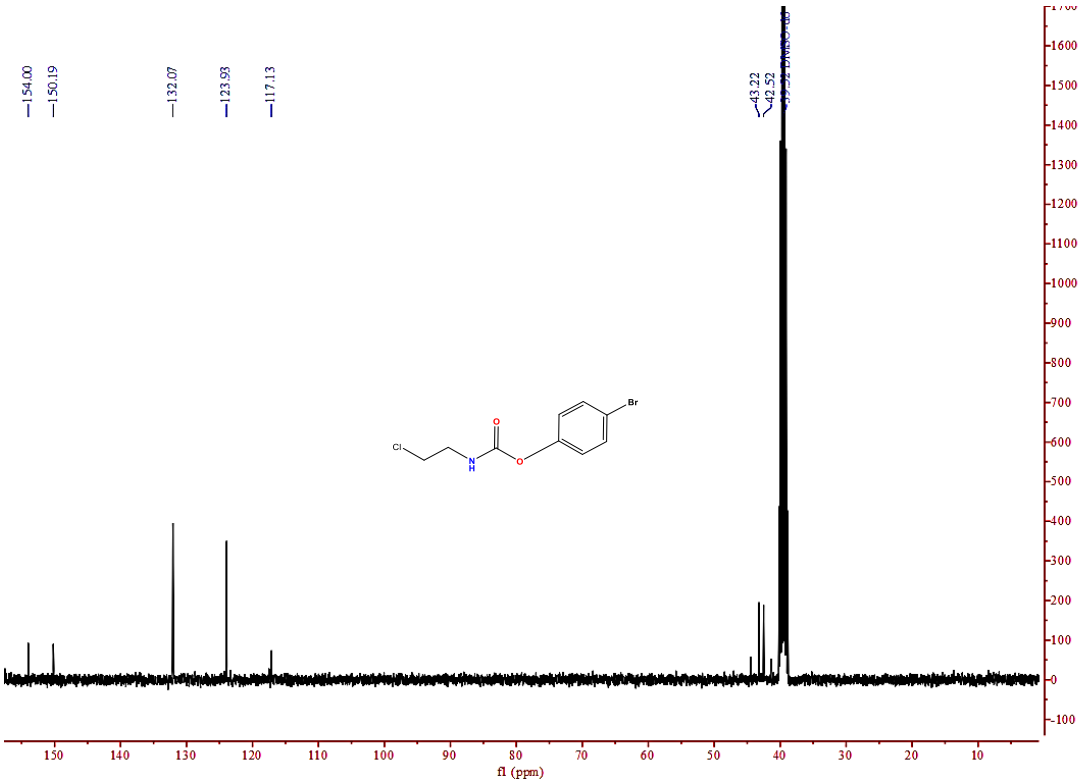

S37.^{13}CNMR spectrum: 4-bromophenyl (2-chloroethyl)carbamate **(III.8b)**

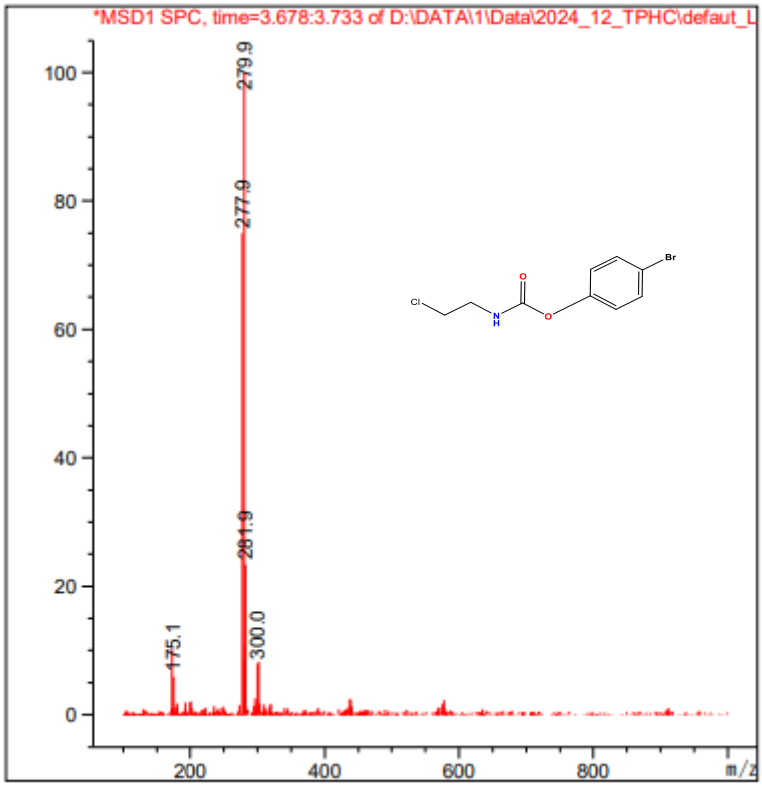

S38.Mass spectrum: 4-bromophenyl (2-chloroethyl)carbamate **(III.8b)**

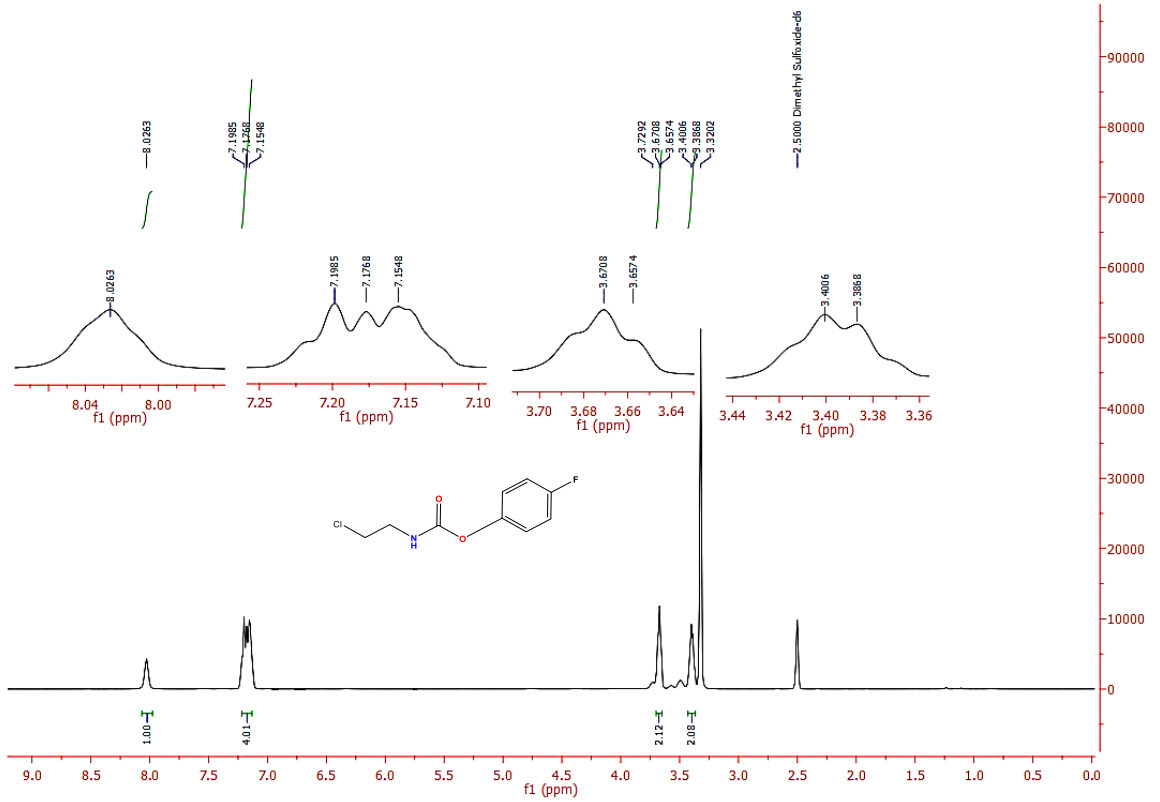

S39.^{1}H NMR spectrum: 4-fluorophenyl (2-chloroethyl)carbamate **(III.8c)**

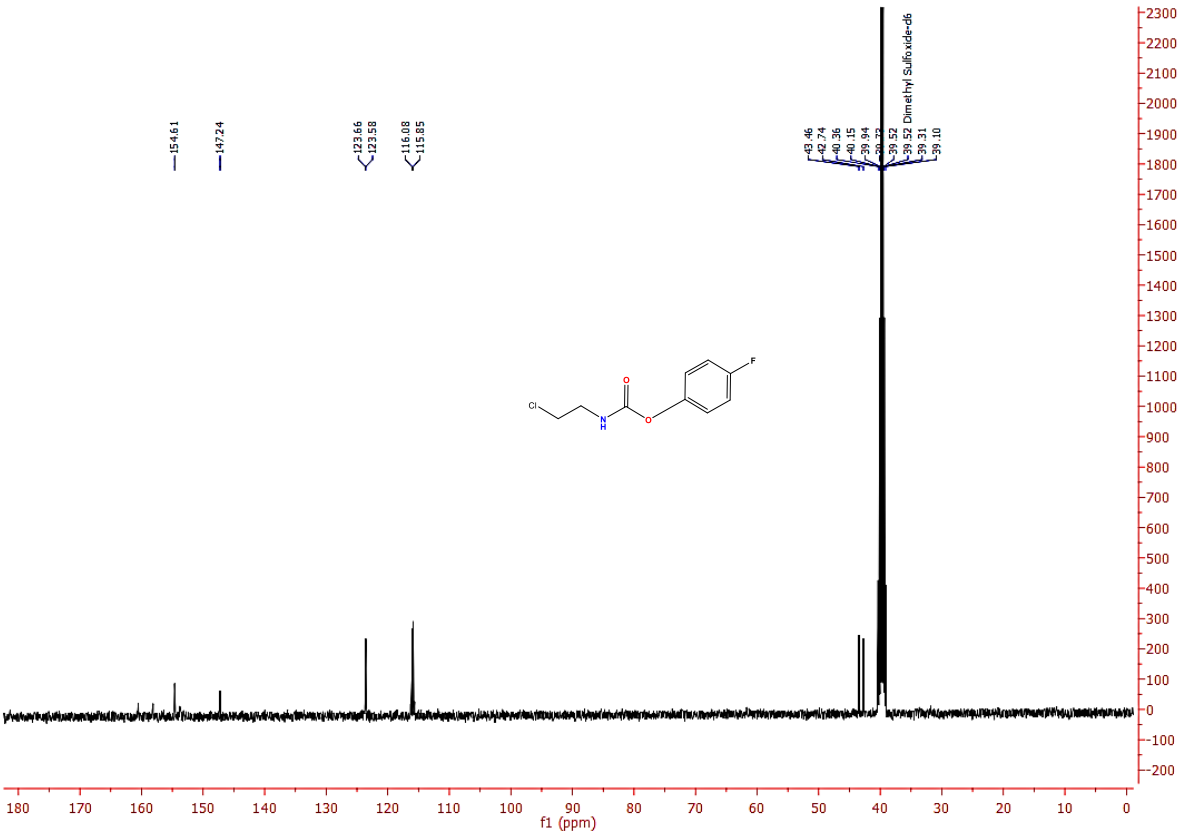

S40.^{13}C NMR spectrum: 4-fluorophenyl (2-chloroethyl)carbamate **(III.3c)**

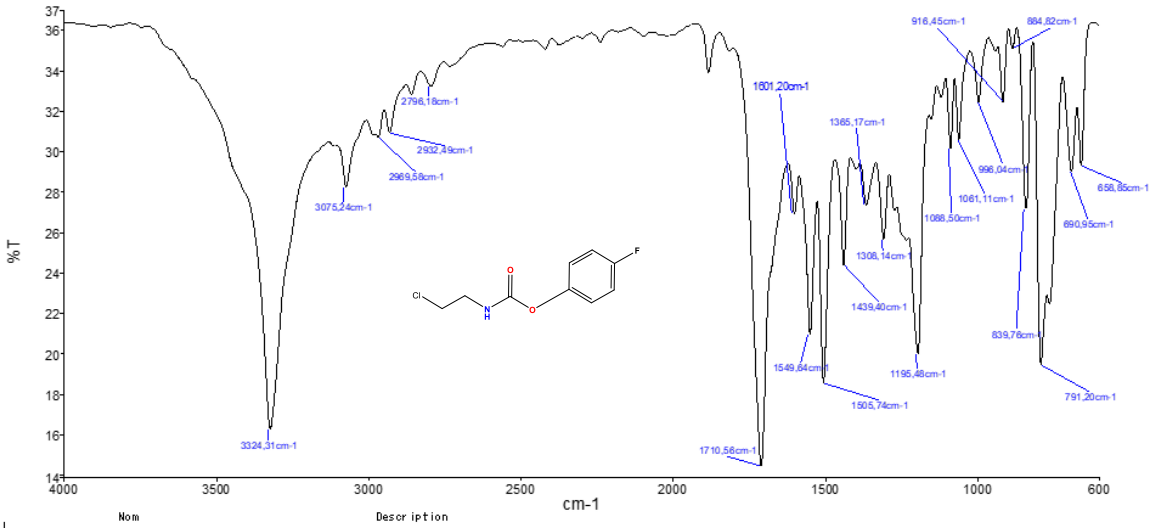

S41.IR spectrum: 4-fluorophenyl (2-chloroethyl)carbamate **(III.8c)**

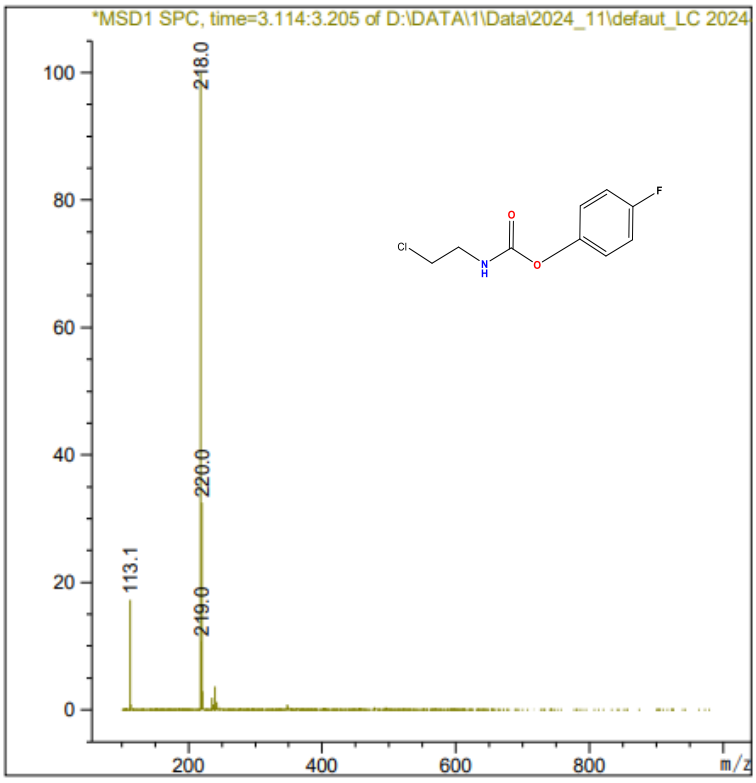

S42.Mass spectrum: 4-fluorophenyl (2-chloroethyl)carbamate **(III.8c)**

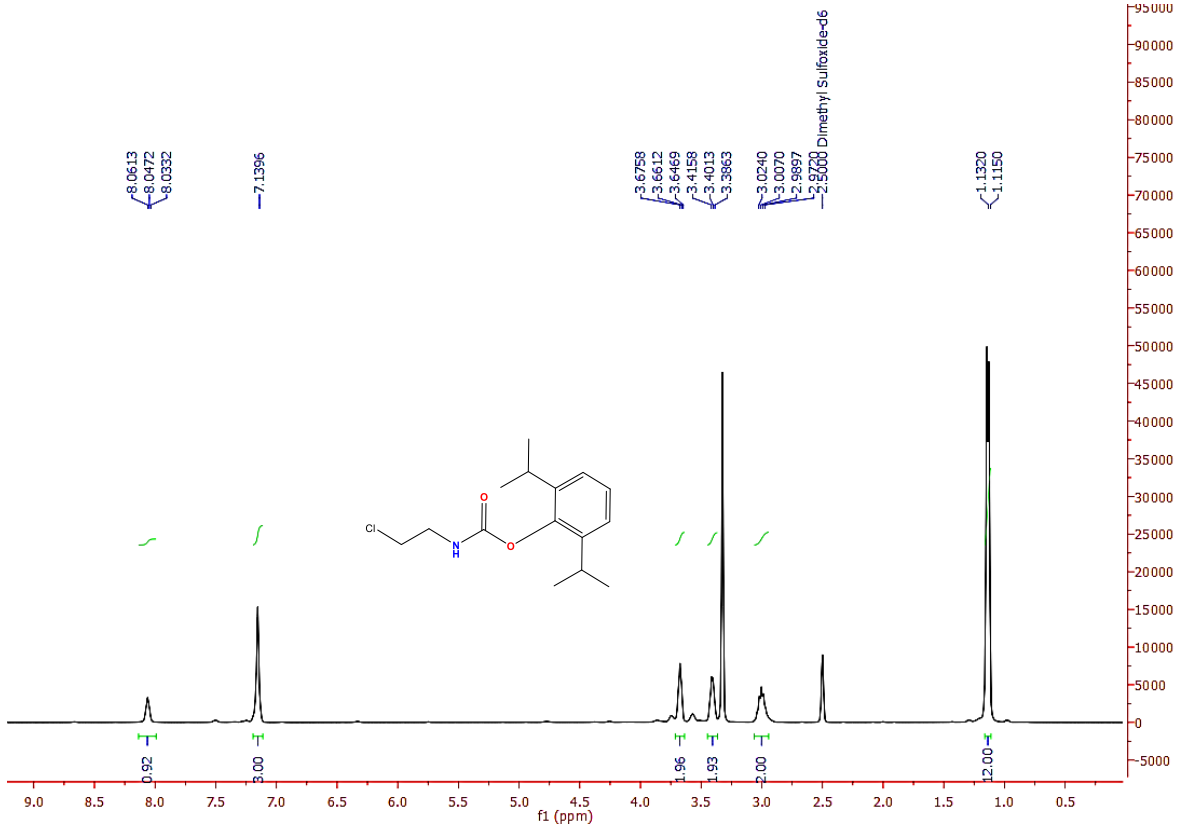

S43. ^{1}H NMR spectrum: 2,6-diisopropylphenyl (2-chloroethyl) carbamate **(III.8e)**

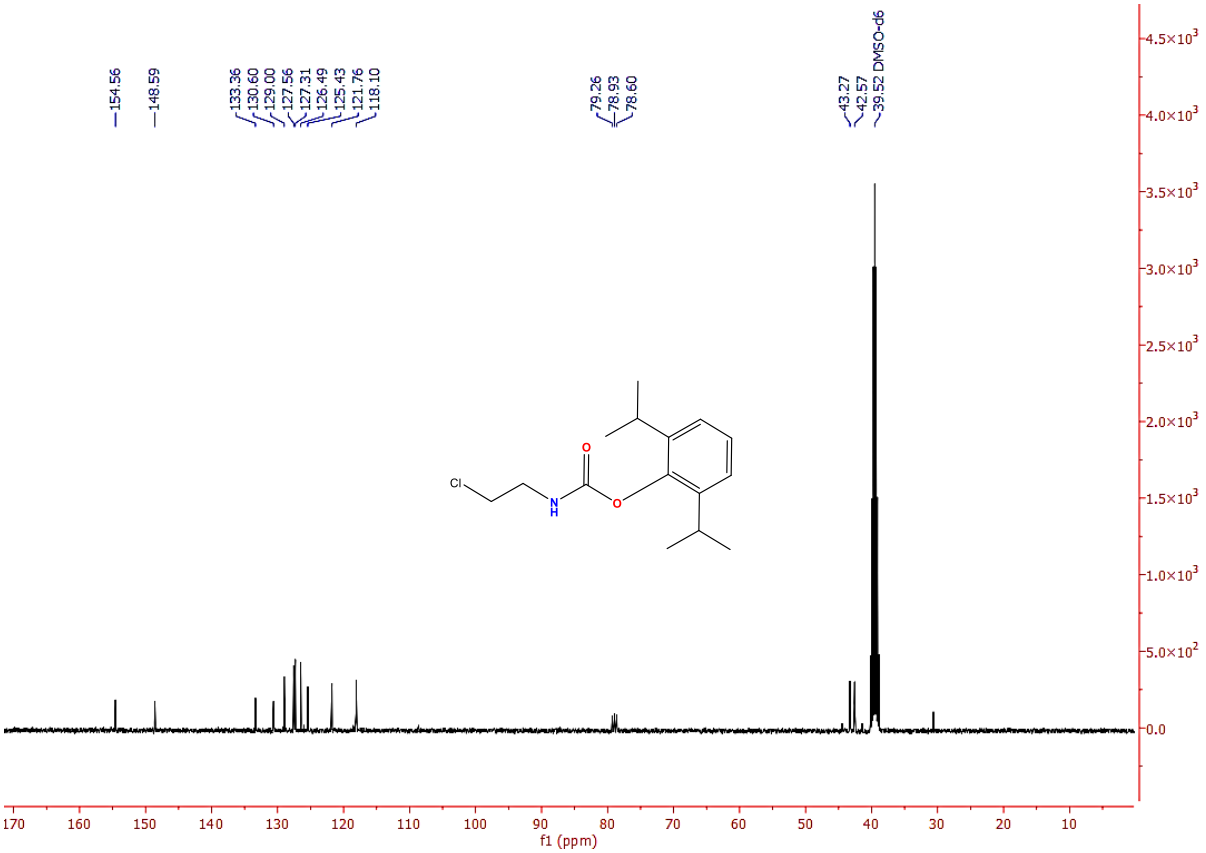

S44. ^{13}CNMR spectrum: 2,6-diisopropylphenyl (2-chloroethyl) carbamate **(III.8e)**

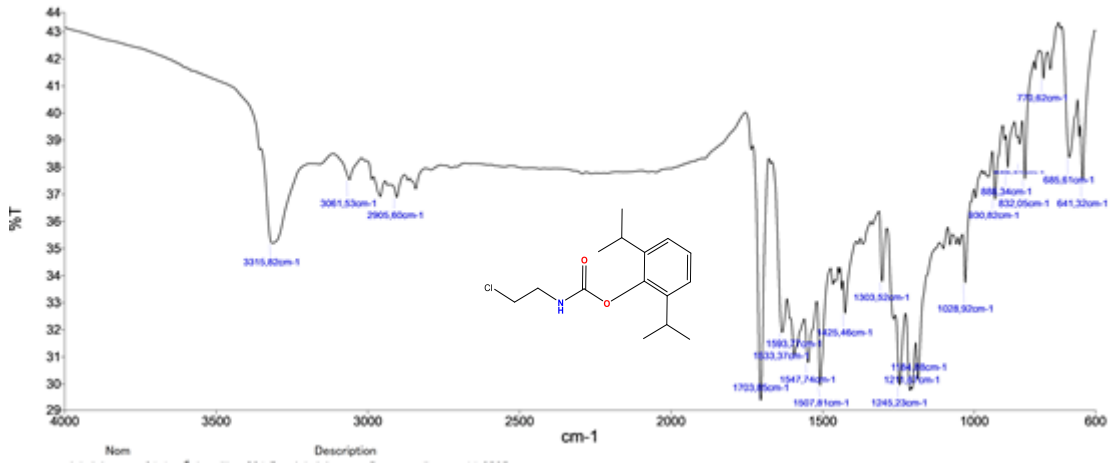

S45.IR spectrum: 2,6-diisopropylphenyl (2-chloroethyl) carbamate **(III.8e)**

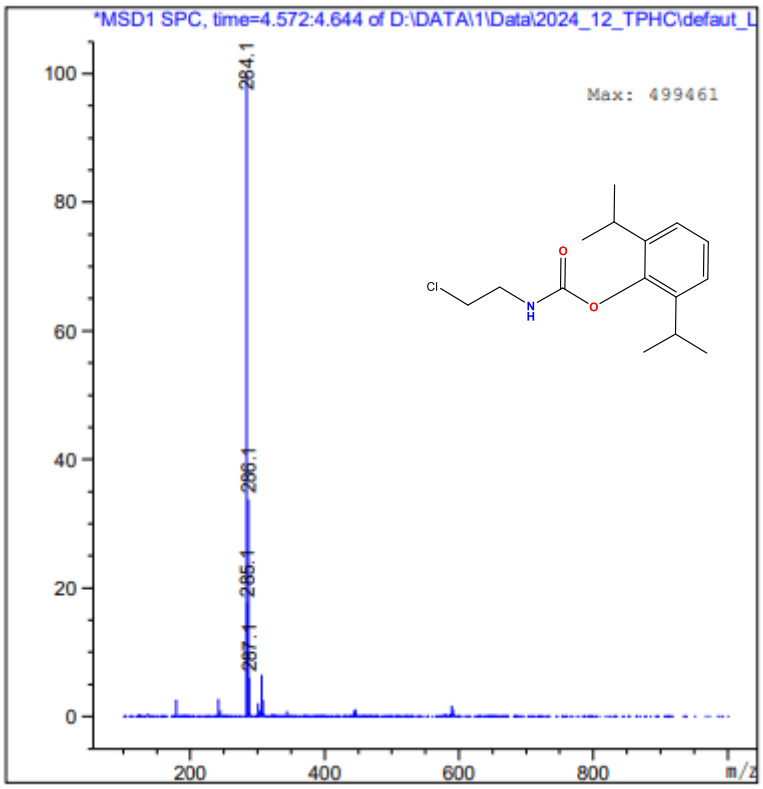

S46.Mass spectrum: 2,6-diisopropylphenyl (2-chloroethyl) carbamate **(III.8e)**

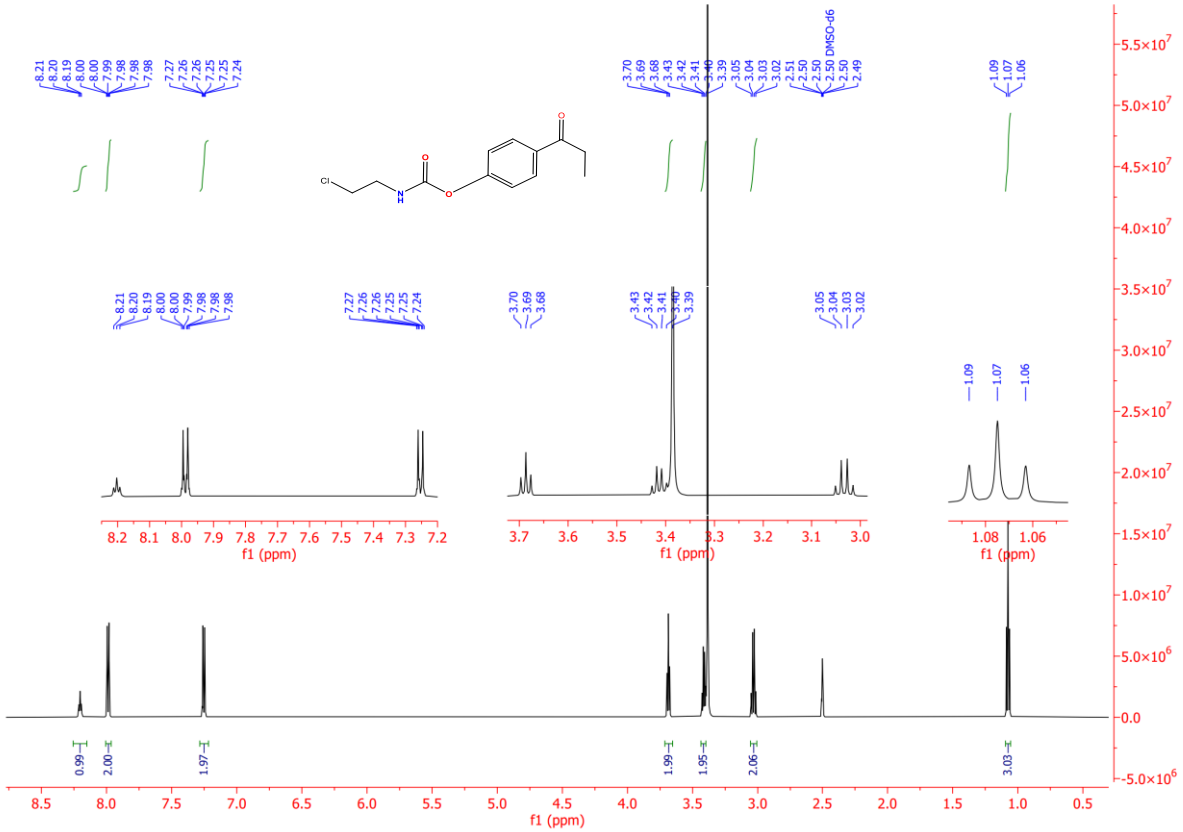

S47.^{1}H NMR spectrum: 4-propionylphenyl (2-chloroethyl)carbamate **(III.8j)**

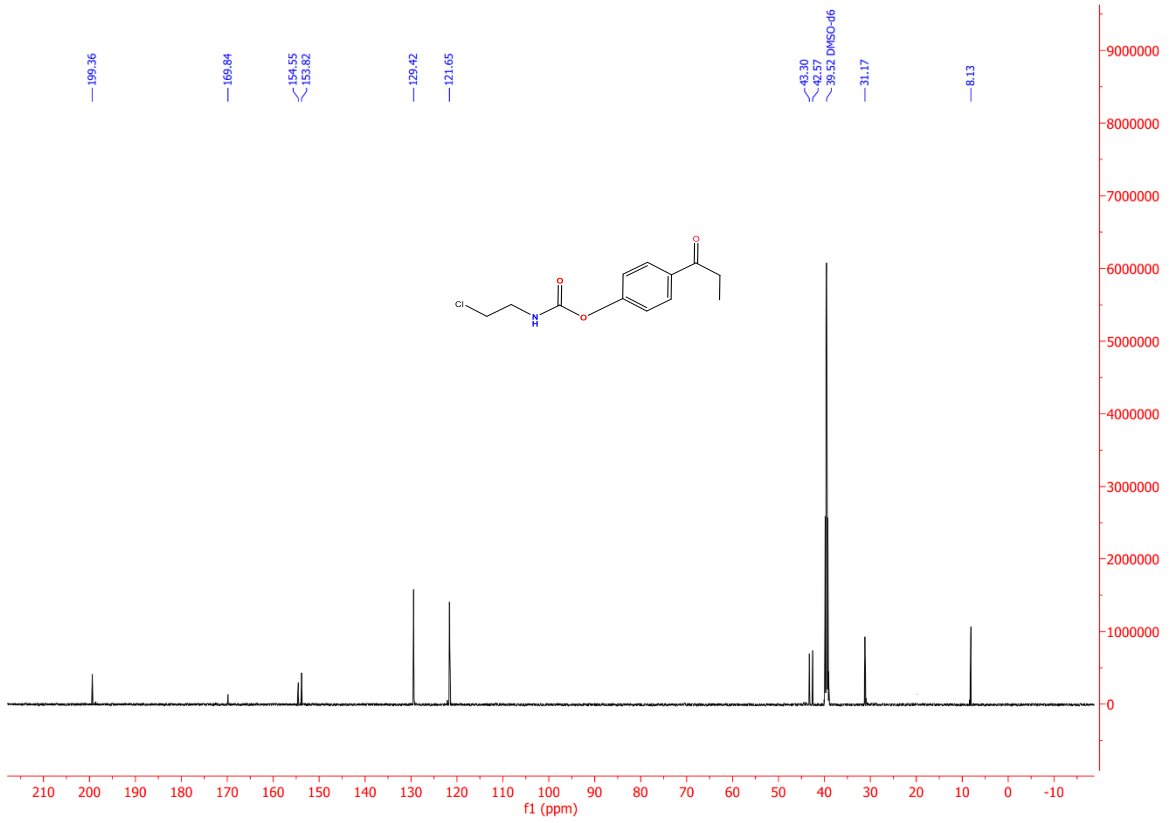

S48.^{13}C NMR spectrum: 4-propionylphenyl (2-chloroethyl) carbamate **(III.8j)**

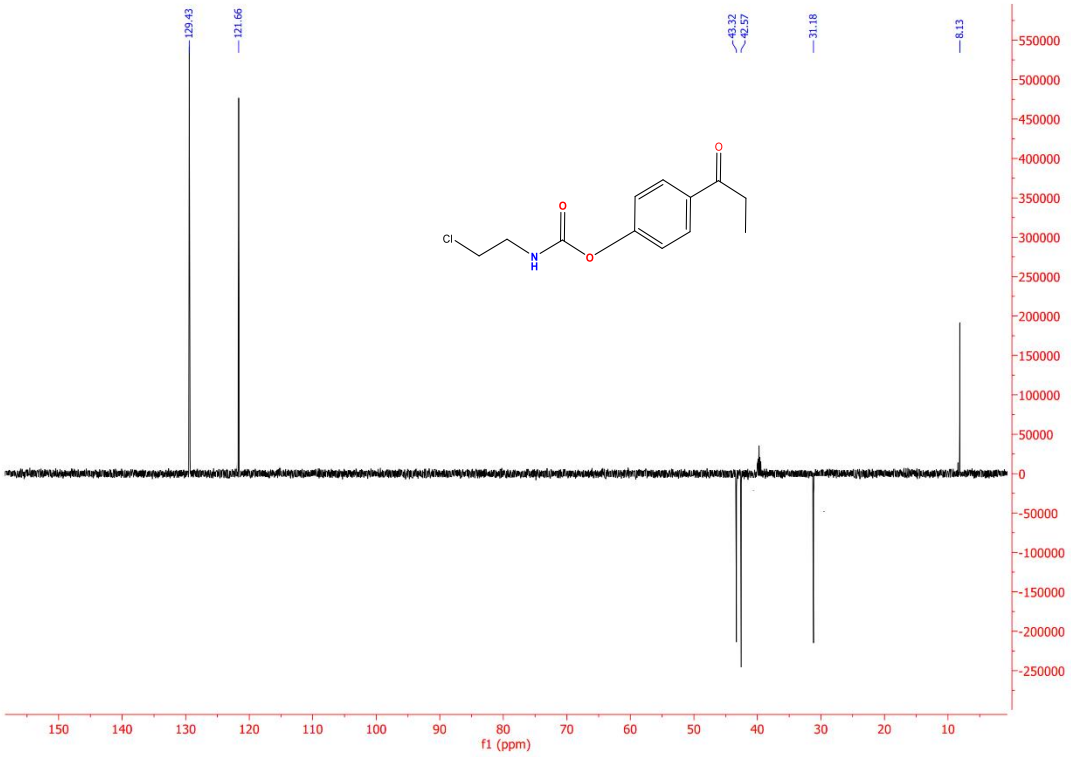

S49.DEPT spectrum: 4-propionylphenyl (2-chloroethyl) carbamate **(III.8j)**

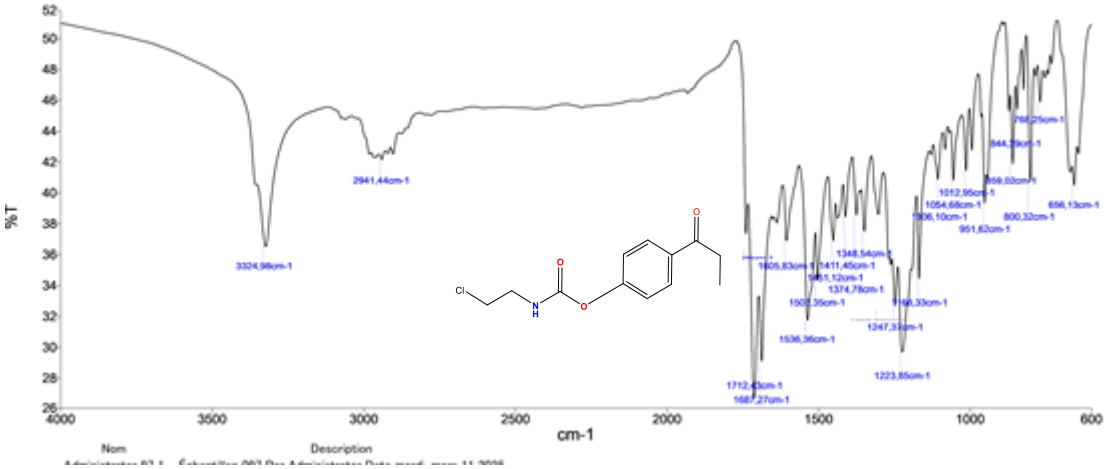

S50.IR spectrum: 4-propionylphenyl (2-chloroethyl) carbamate **(III.8j)**

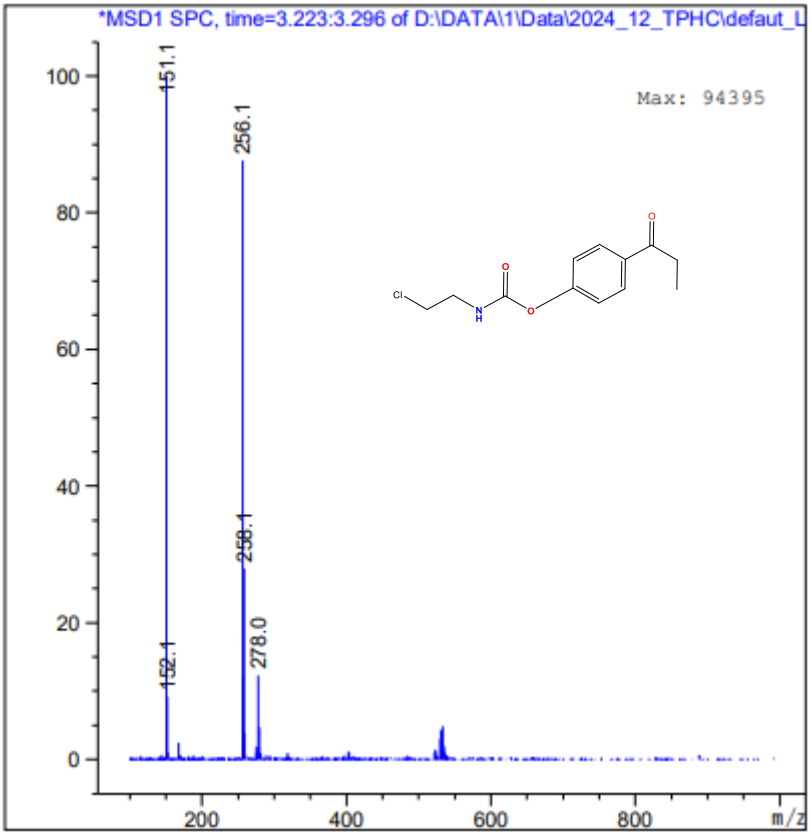

S51.Mass spectrum: 4-propionylphenyl (2-chloroethyl) carbamate **(III.8j)**

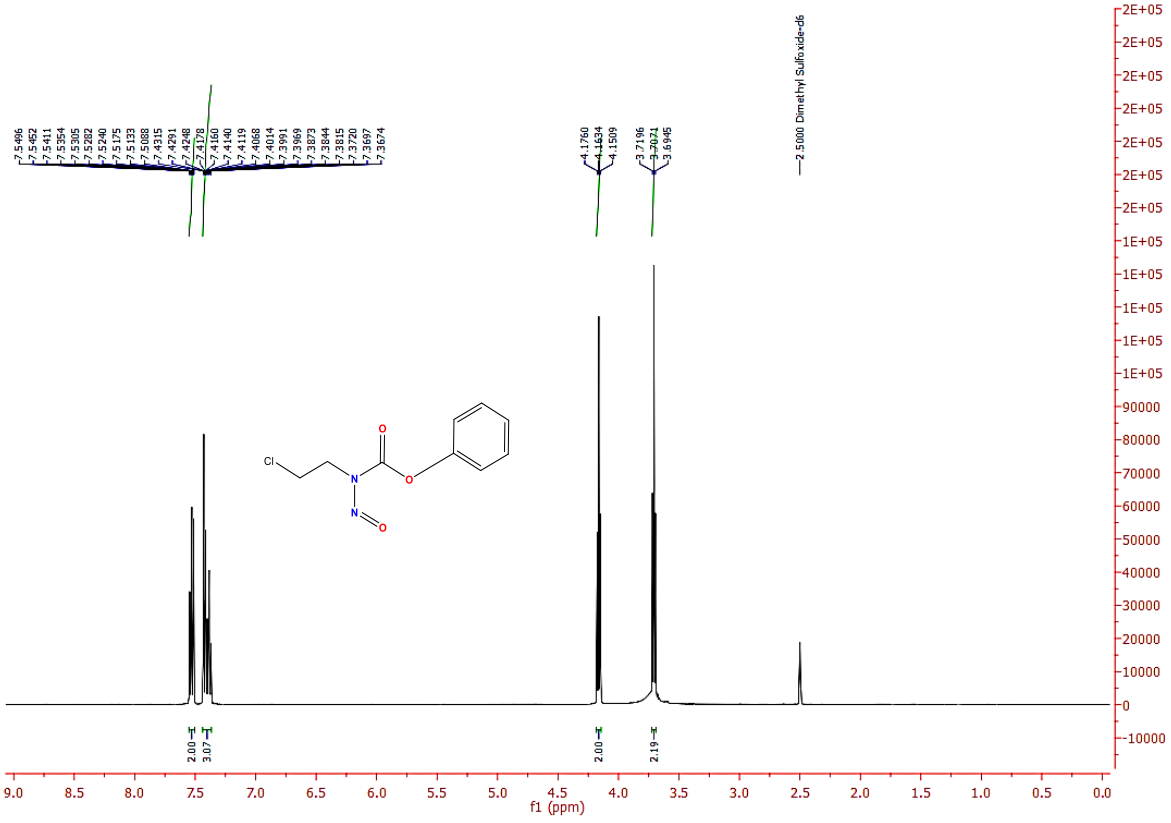

S52.^{1}H NMR spectrum: phenyl (2-chloroethyl)(nitroso)carbamate **(III.10a)**

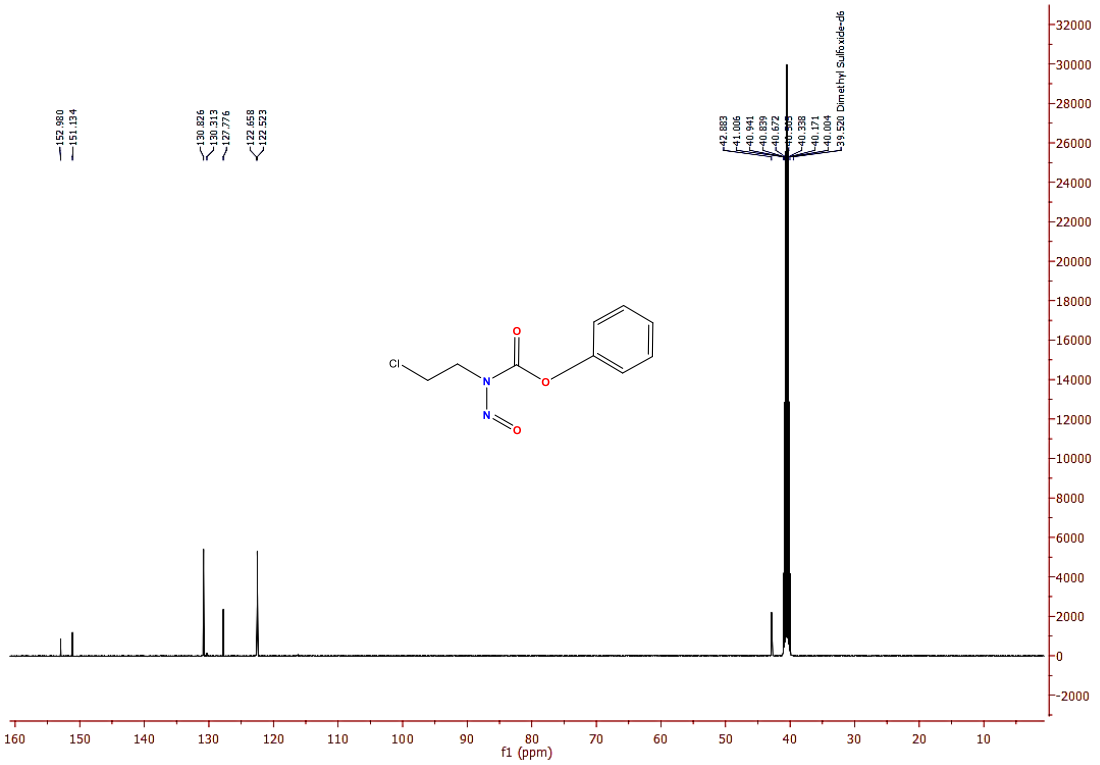

S53.^{13}CNMR spectrum: phenyl (2-chloroethyl)(nitroso)carbamate **(III.10a)**

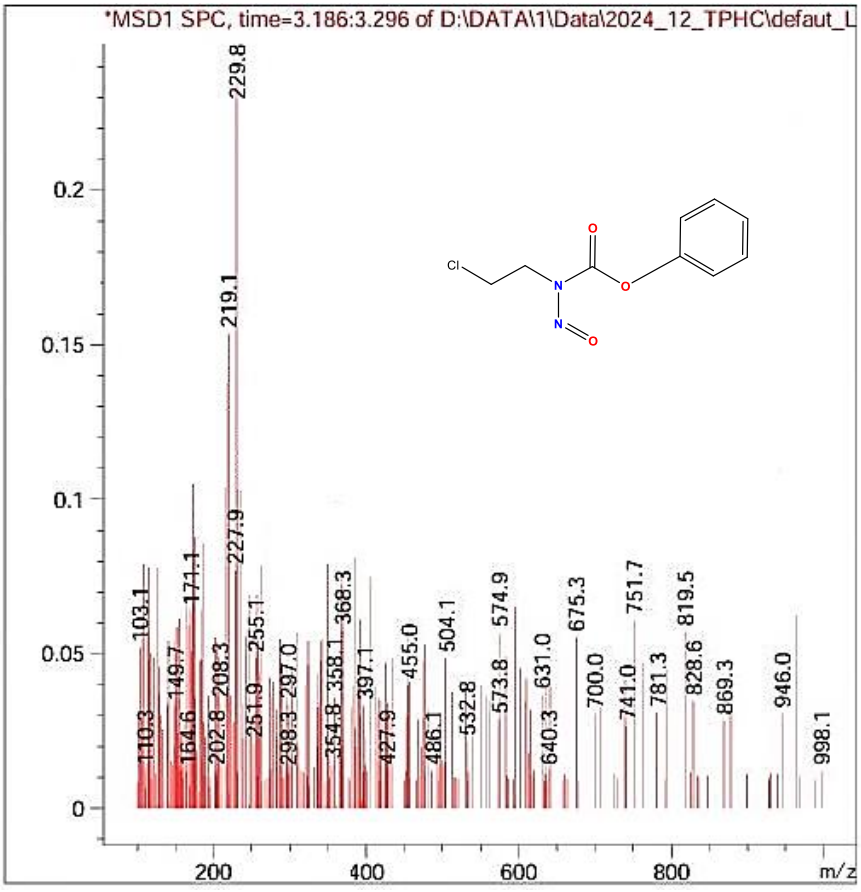

S44.Mass spectrum: phenyl (2-chloroethyl)(nitroso)carbamate **(III.10a)**

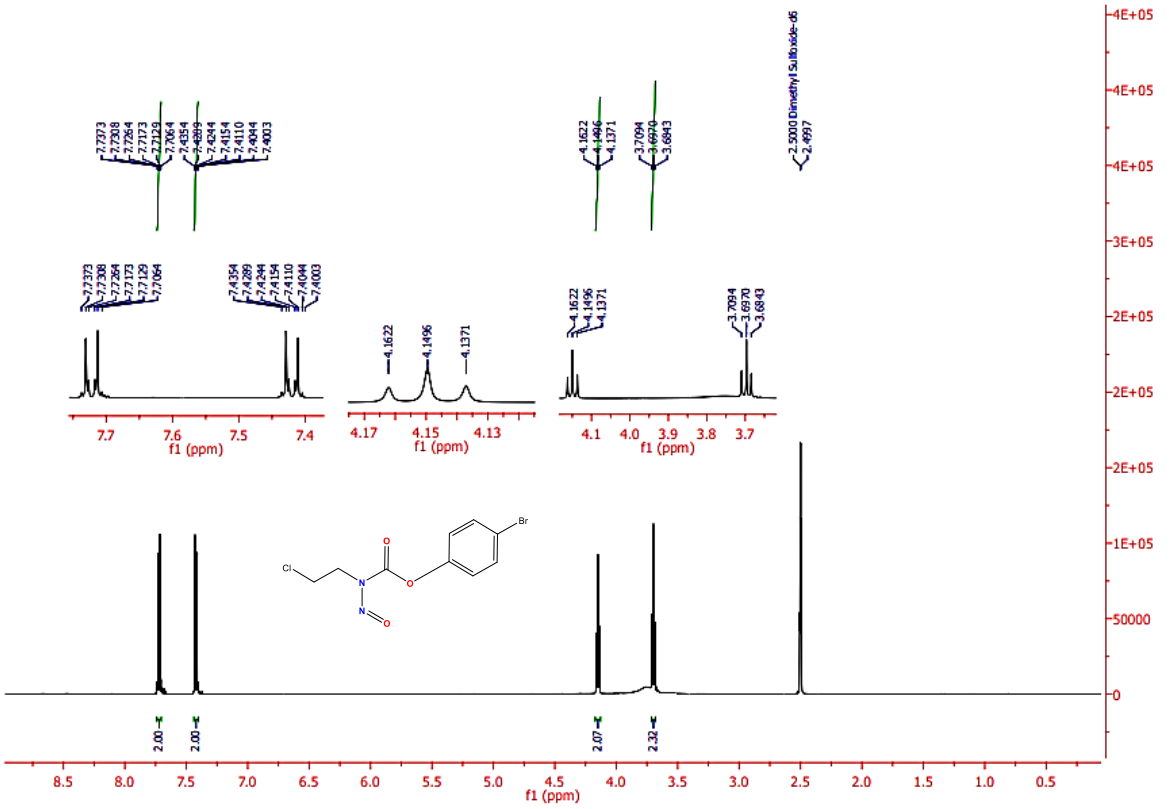

S45.^{1}H NMR spectrum: 4-bromophenyl (2-chloroethyl) (nitroso)carbamate **(III.10b)**

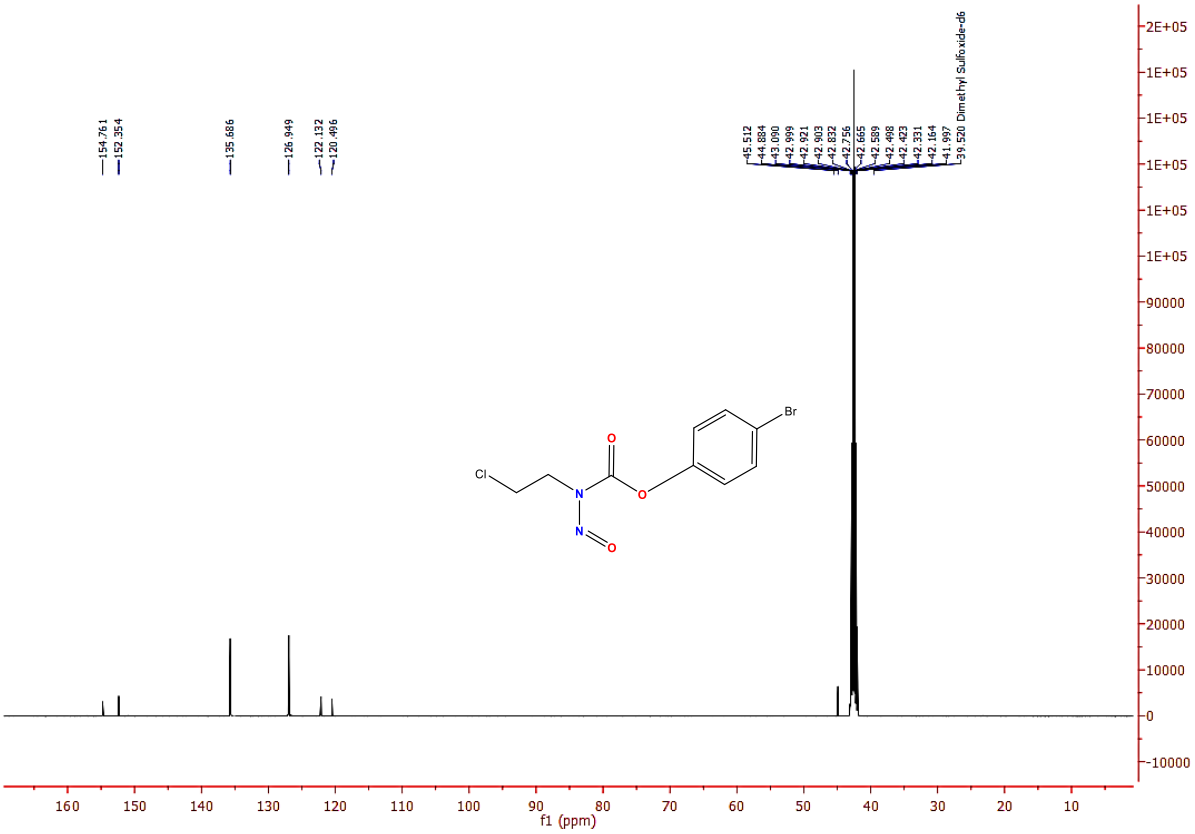

S46.^{13}C NMR spectrum: 4-bromophenyl (2-chloroethyl)(nitroso)carbamate **(III.10b)**

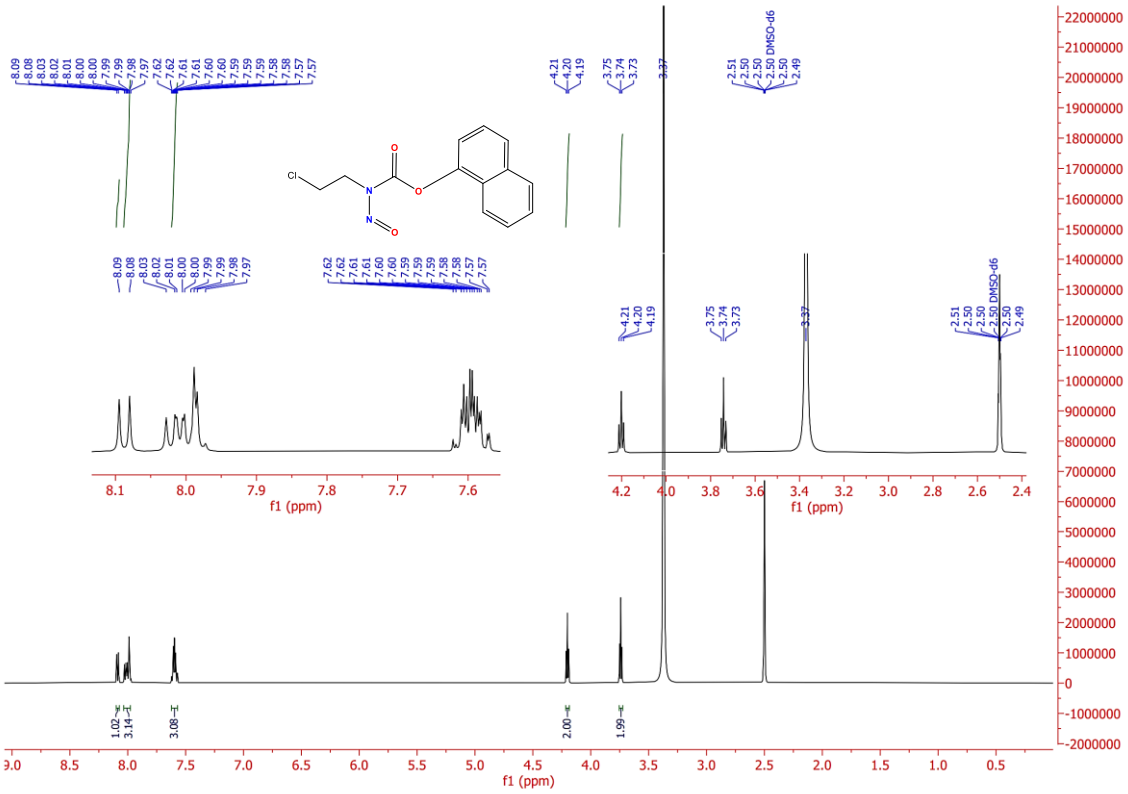

S47. ^{1}H NMR spectra of naphthalen-1-yl (2-chloroethyl) (nitroso)carbamate **(III.10f).**

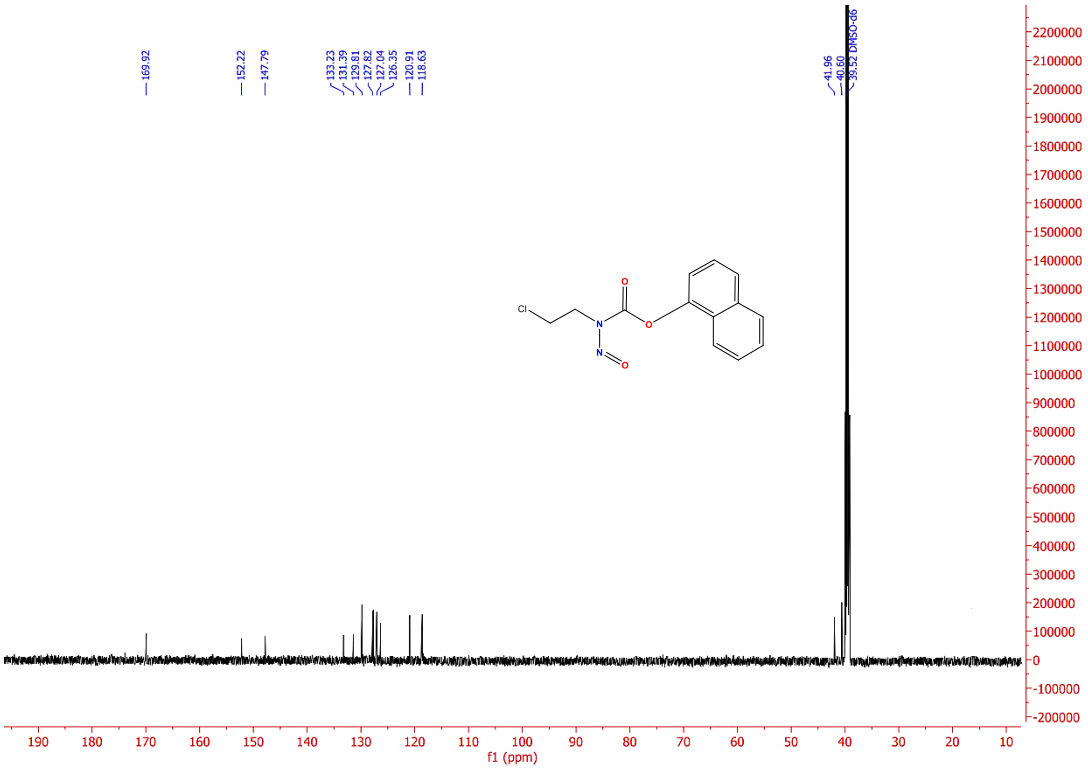

. S47. ^{13}C NMR spectra of naphthalen-1-yl (2-chloroethyl) (nitroso) carbamate **(III.10f)**.

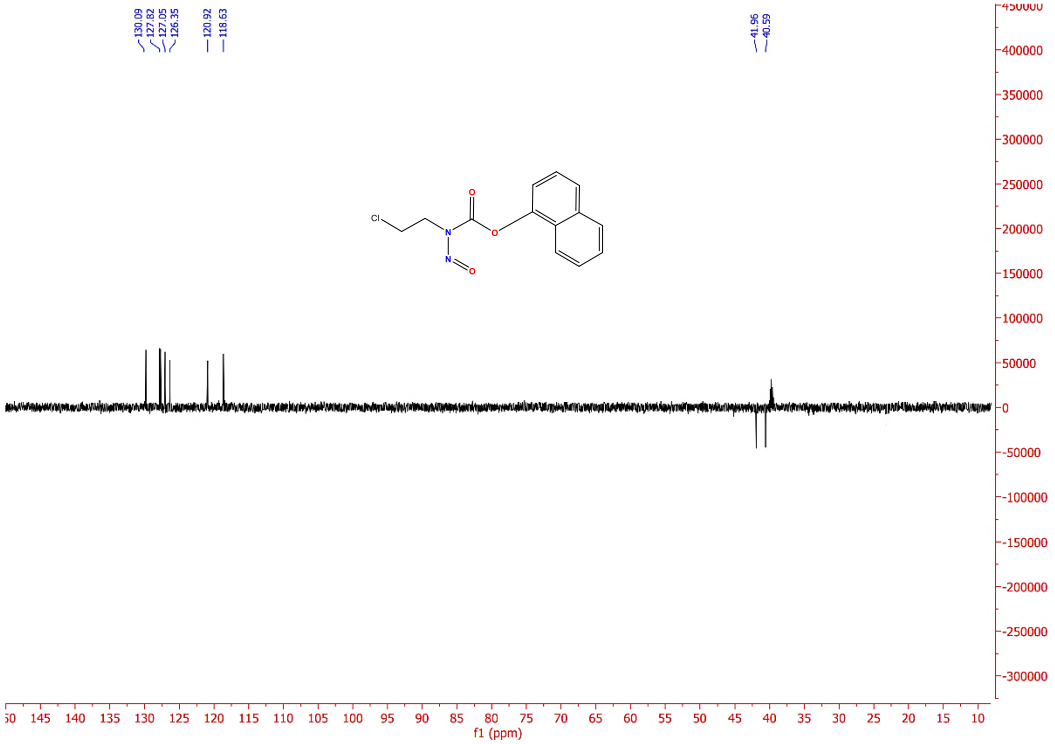

S47. DEPT spectrum naphthalen-1-yl (2-chloroethyl) (nitroso) carbamate **(III.10f)**.

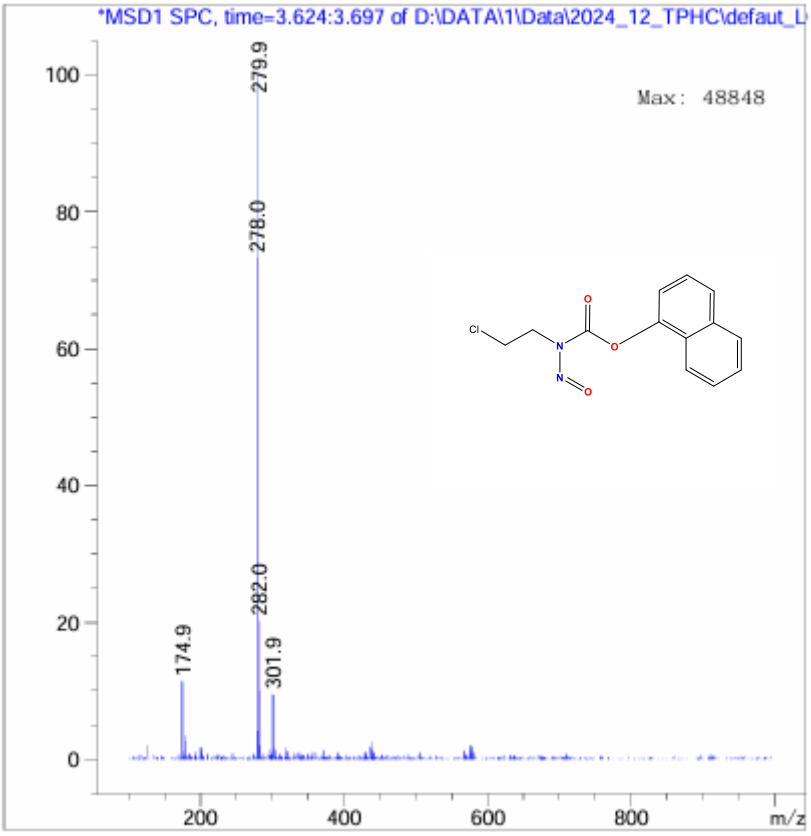

S47. Mass spectrum naphthalen-1-yl (2-chloroethyl) (nitroso) carbamate **(III.10f)**.

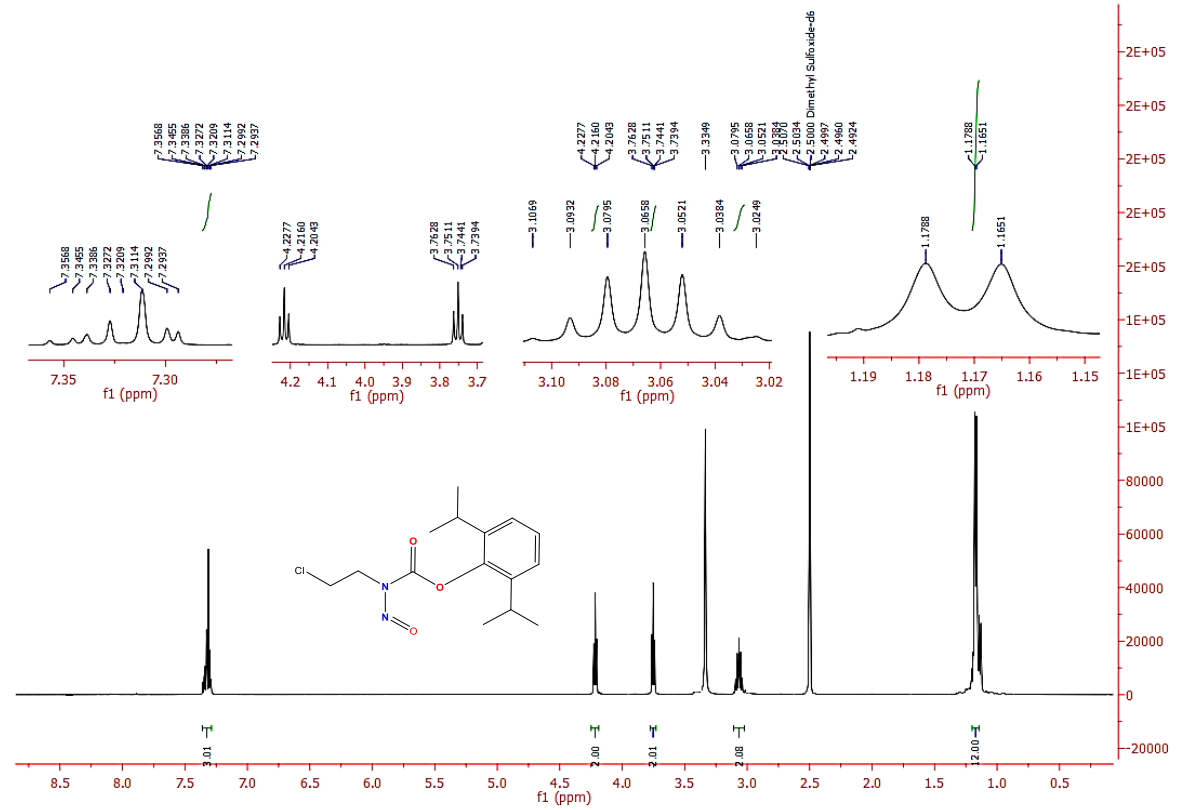

S49.^{1}H NMR spectrum: 2,6-diisopropylphenyl (2-chloroethyl)(nitroso)carbamate **(III.10e)**

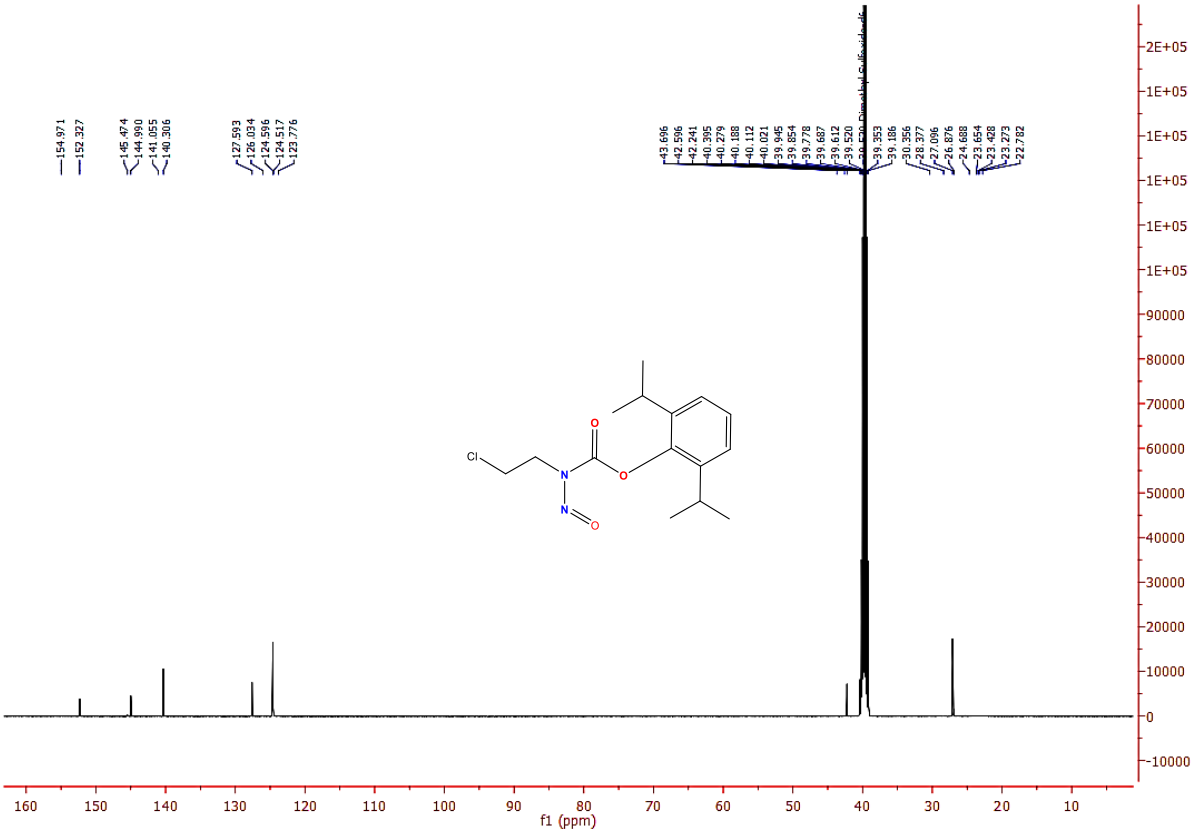

S50.^{13}C NMR spectrum: 2,6-diisopropylphenyl (2-chloroethyl)(nitroso)carbamate **(III. 10e)**

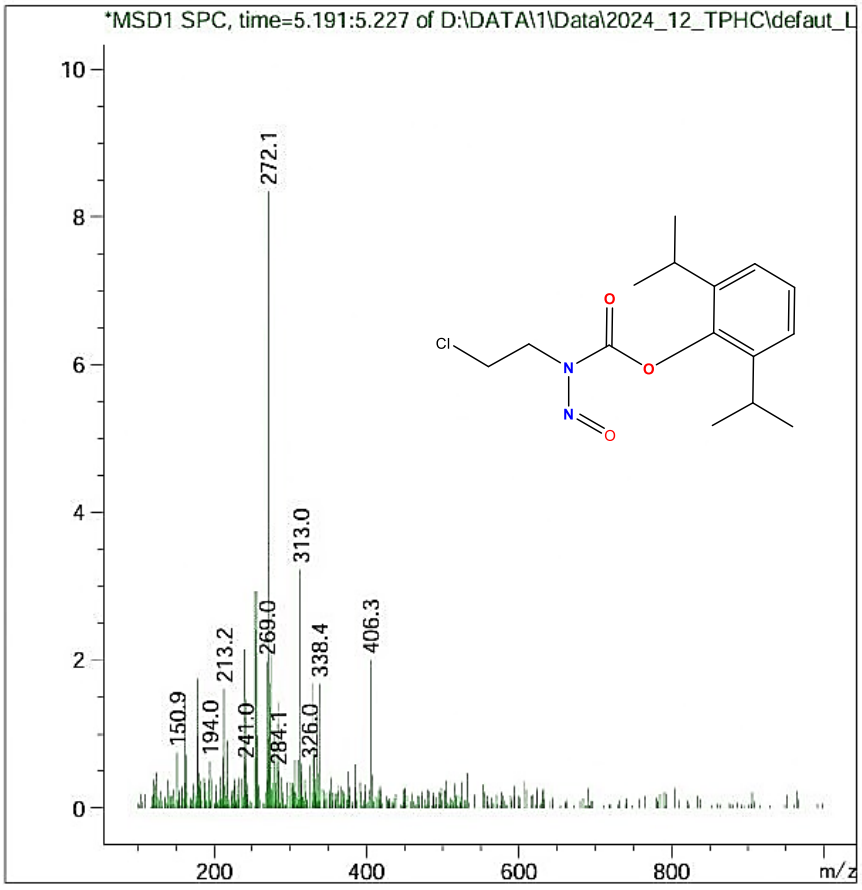

S51.Mass spectrum: 2,6-diisopropylphenyl (2-chloroethyl)(nitroso)carbamate **(III. 10e)**

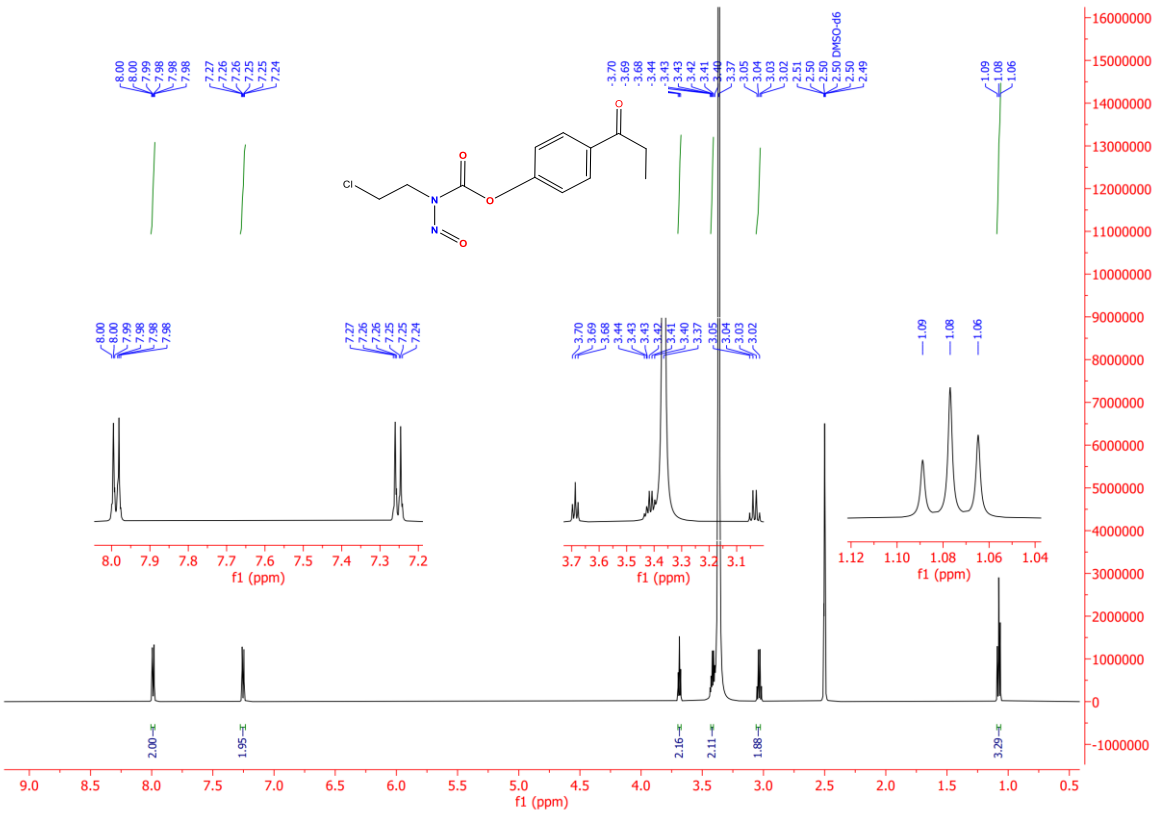

S52.^{1}H NMR spectrum: 4-propionylphenyl (2-chloroethyl) (nitroso) carbamate **(III.10j)**

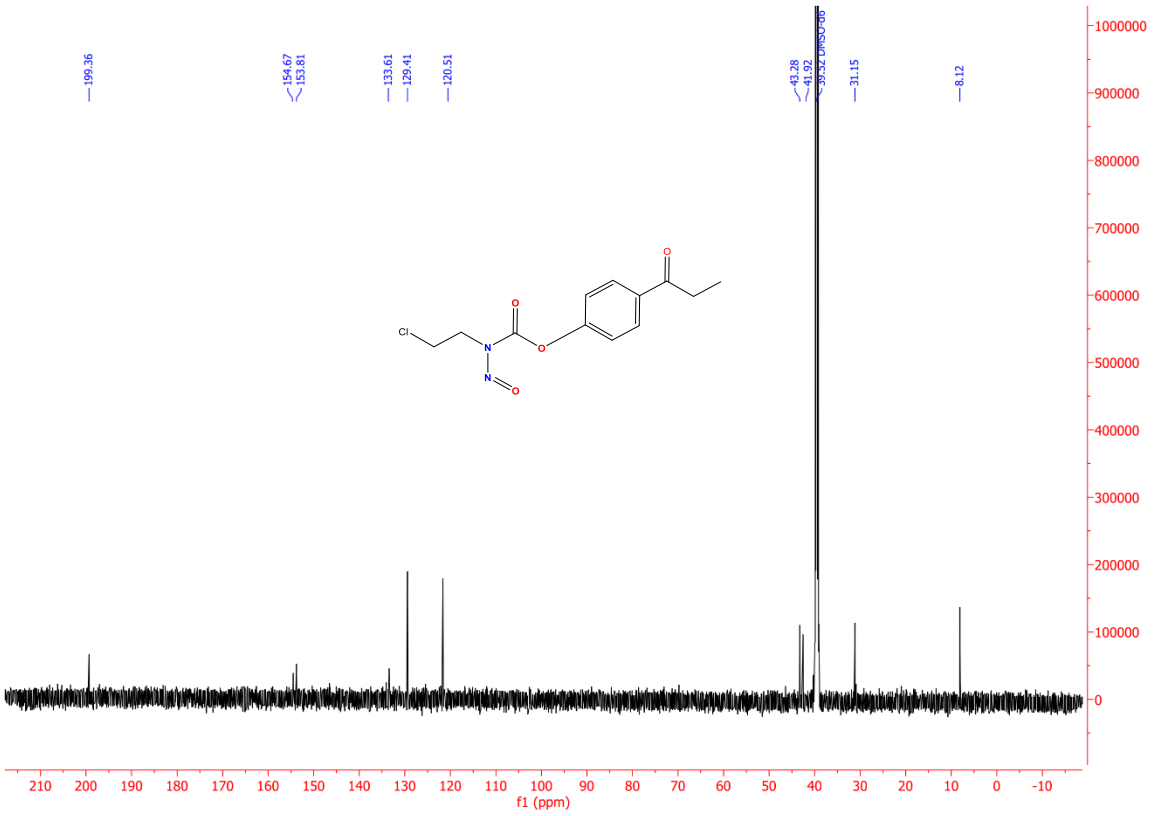

S53.^{13}C NMR spectrum: 4-propionylphenyl (2-chloroethyl) (nitroso) carbamate **(III.10j)**

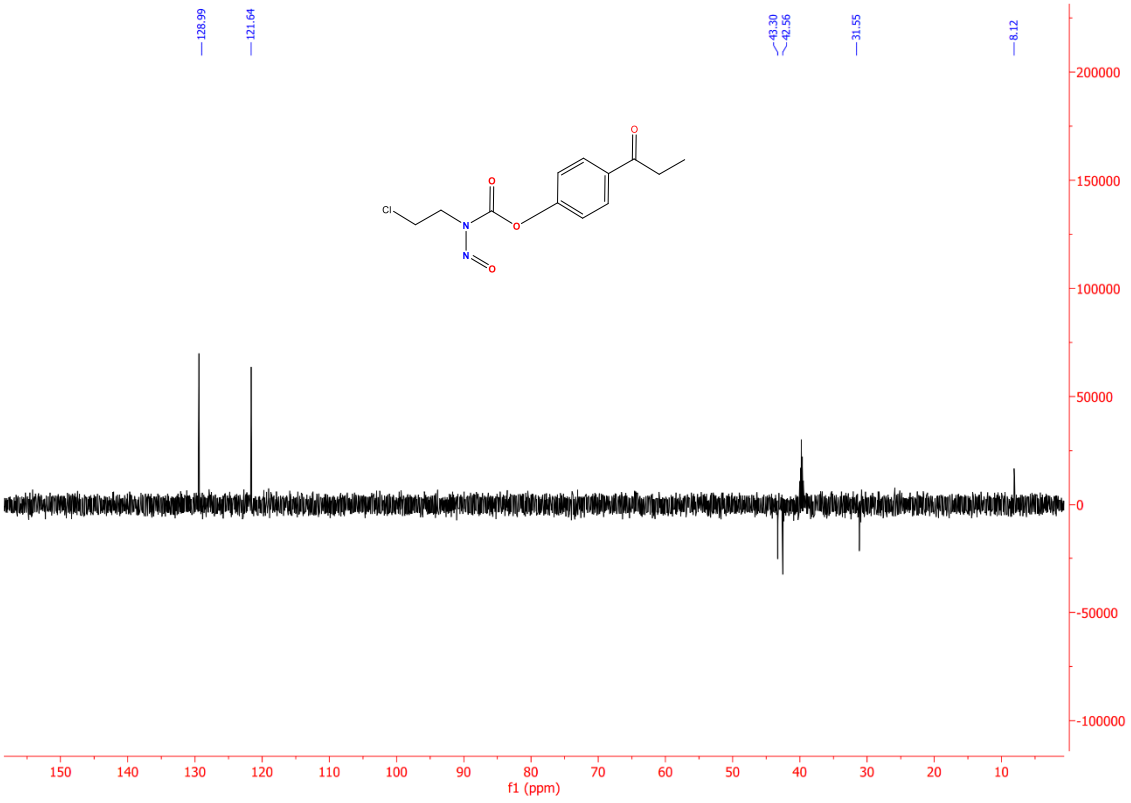

S54.DEPT spectrum: 4-propionylphenyl (2-chloroethyl) (nitroso) carbamate **(III.10j)**